DOCTOR OF PHILOSOPHY

Analysis of the function of Drop out, the single homologue of human MAST kinases, in Drosophila cellularisation

Sonnenberg, Hannah C.

Award date:
2016

University of Dundee
School of Life Sciences

Analysis of the function of Drop out, the single homologue of human MAST kinases, in *Drosophila* cellularisation

Hannah C. Sonnenberg

A thesis submitted for the degree of
Doctor of Philosophy

University of Dundee

September 2016

Parts of this thesis have been published with the following title:

D. Hain, A. Langlands, H.C. Sonnenberg, C. Bailey, S.L. Bullock, and H-A.J. Müller, `**The Drosophila MAST kinase Drop out is required to initiate membrane compartmentalisation during cellularisation and regulates dynein-based transport**' published in Development, 141(10), pp.2119-2130. doi:10.1242/dev.104711

Acknowledgements

I would like to thank my supervisor Dr. Arno Müller for the opportunity to do my PhD in his lab and for his help and guidance all along the way. It has been a pleasure to be part of the Drop out family for these few years of time and to learn so much. Thank you!

I want to thank Prof. Margarete Heck and Dr. Jens Januschke for taking the time and effort to read through and comment on this thesis.

A big thank you to all the staff of the Light Microscopy Facility, especially to Graeme Ball for helping me with image processing. Thank you as well to Central Technical Services, IT and the OMERO team for all their supporting work.

A further big thank you goes to current and former lab members of not only the HAM but also the JJ lab for their invaluable help and friendship throughout my PhD. I would like to thank Giuliana Clemente, Martina Lubach, Anne Ramat, Villo Muha, Ryan Webster, Daniel Mariyappa, Matthew Hannaford, Hamze Beati, Nicolas Loyer and Alistair Langlands for being amazing people! I hope we stay in contact throughout our future.

Additionally, I would like to thank all the great people I met during the past few years inside and outside of the School of Life Sciences for making me (and my boyfriend) feel at home.

Thanks to all of my family for looking after me, helping me to grow up and trying to support me always.

Last but not least, I want to thank my boyfriend Christian for following me into unknown territory, staying with me all the way, and not necessarily understanding but always supporting me. I love you and I hope we will always be together.

Declaration

I declare that the following thesis is based on the results of investigations conducted by myself, and that this thesis is of my own composition. Work other than my own is clearly indicated in the text by reference to the relevant researchers or to their publications. This dissertation has not in whole, or in part, been previously submitted for a higher degree.

Hannah Christine Sonnenberg

I certify that Hannah Christine Sonnenberg has spent the equivalent of at least nine terms in research work at the School of Life Sciences, University of Dundee, and that she has fulfilled the conditions of the Ordinance General No. 14 of the University of Dundee and is qualified to submit the accompanying thesis in application for the degree of Doctor of Philosophy.

Dr. Arno Müller

Drosophila life cycle

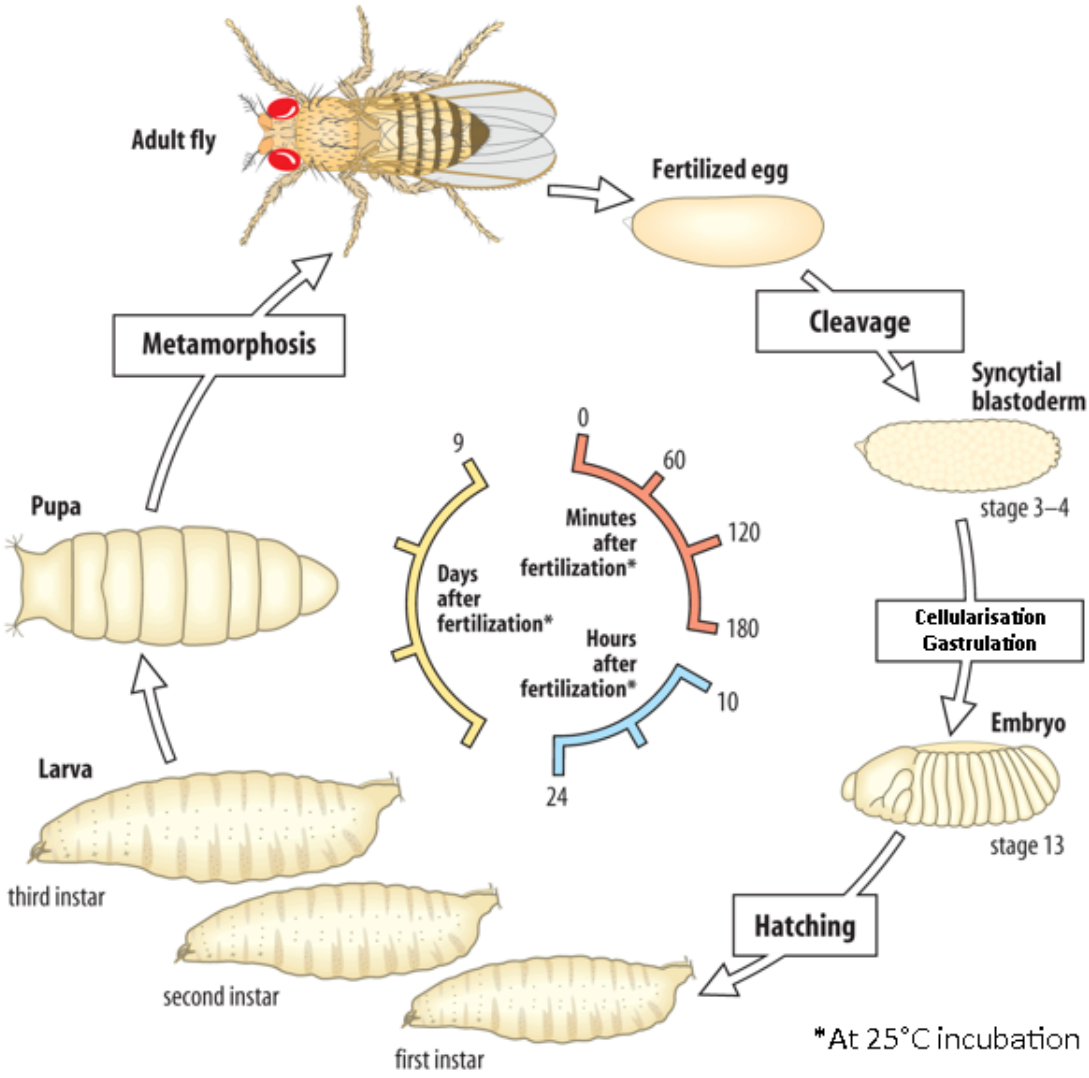

Adapted from and modified after Wolpert, L. and Tickle, C. Principles of Development, Fourth Edition.

Abbreviations

A	Alanine
aa	Amino acids
Amph	Amphiphysin
APC	Adenomatous polyposis coli
Arg	Arginine
Arm	Armadillo
ATP	Adenosine triphosphate
b	Base
Baz	Bazooka
BDSC	Bloomington Drosophila Stock Center
BJ	Basal junction
Bnk	Bottleneck
CAL	CFTR-associated ligand
CFTR	Cystic fibrosis transmembrane conductance regulator
Cnn	Centrosomin
D	Aspartic acid
Da	Dalton
Dah	Discontinuous actin hexagon
DAPI	4‘,6-Diamidino-2-phenylindole dihydrochloride
dH_2O	Distilled water
Dhc	Dynein heavy chain
Dia	Diaphanous
Dic	Dynein intermediate chain
Dlic	Dynein light intermediate chain
Dlg	Discs large
(h) Dmn	(human) Dynamitin
DMSO	Dimethyl sulfoxide
DNA	Deoxyribonucleic acid
Dop	Drop out
dsRNA	Double-stranded RNA
DUF	Domain of unknown function
E. coli	*Escherichia coli*
E-cadherin	Epithelial cadherin
EDTA	Ethylenediaminetetraacetic acid
EMS	Ethyl methane sulfonate
EMT	Epithelial to mesenchymal transition
Eps15	Epidermal growth factor receptor pathway substrate clone 15
ER	Endoplasmic reticulum
Fig.	Figure
F-actin	Filamentous actin
FITC	Fluorescein isothiocyanate
FLP	Flippase
FRT	Flippase recombination target
(e)GFP	(enhanced) Green fluorescent protein
GEF	Guanine nucleotide exchange factor
Gl	Glued
G	Glycine
g	Gram
glc	Germ line clones
gp120	Golgi protein 120 (kDa)
GRP1	General receptor for phosphoinositides-1

GTP	Guanosine triphosphate
HC	Heavy chain
Hrs	Hepatocyte growth factor-regulated tyrosine kinase substrate
hs	Heat shock
IBD	Inflammatory bowel disease
IC	Intermediate chain
k	Kilo-
Khc	Kinesin heavy chain
l	Litre
LB medium	Luria-Bertani medium
LIC	Light intermediate chain
LPS	Lipopolysaccharide
Lva	Lava lamp
Lys	Lysine
MAP	Microtubule associated protein
(h)MAST	(human) Microtubule-associated serine/threonine kinase
mat	Maternal
min	Minute
µ	Micro-
m	Milli-
	Metre
M	Molar
mol	Mole
mRNA	messenger RNA
MT	Microtubule
n	Nano-
	Number
NHE3	Na+/H+ exchanger 3
Nrt	Neurotactin
Nuf	Nuclear fallout
o/N	Over night
PBS	Phosphate-buffered saline
PCR	Polymerase chain reaction
PDZ	PSD-95, Discs large, ZO-1
p	Pico-
pH	Potential of hydrogen
$PI(3,4,5)P_3$	Phosphatidylinositol 3,4,5-triphosphate
$PI(4,5)P_2$	Phosphatidylinositol 4,5-bisphosphate
PI3K	Phosphoinositide 3-kinase
PI4K	Phosphoinositide 4-kinase
PTEN	Phosphatase and tensin homologue
RE	Recycling endosome
RNA	Ribonucleic acid
RNAi	RNA interference
S	Serine
S-phase	Synthesis phase
SILAC	Stable isotope labelling with amino acids in cell culture
Slam	Slow-as-molasses
SAJ	Spot adherens junction
sec	Second
SEM	Standard error of the mean
SJ	Septate junction
SNP	Single nucleotide polymorphism
sqh	*spaghetti squash* (promoter)

Sry-α	Serendipity-α
sw	*short wing*
t	Time
TLR	Toll-like receptor
TRAF6	TNF receptor-associated factor 6
U	Unit
UAS	Upstream activating sequence
ubi	*ubiquitin* (promoter)
UV	Ultraviolet
V	Volt
wt	*wild type*
ZA	Zonula adherens
°	Degrees
°C	Degree Celsius

Summary

The Drop out (Dop) kinase is the single homologue of the MAST kinase family in *Drosophila melanogaster*. Despite MAST kinases having been implicated in several human diseases such as breast cancer, neurodegenerative diseases, inflammatory bowel disease and cystic fibrosis, the biological role of this kinase family is still poorly understood. The study of Dop function in *Drosophila* is therefore of interest to elucidate the function of MAST kinases. Previous studies revealed that mutations in *dop* affect cellularisation, a process during early *Drosophila* embryogenesis which occurs after 13 syncytial divisions. Cellularisation establishes cells by invagination of membrane from the cortex to surround about 6000 nuclei, thereby forming polarised cells in a blastoderm epithelium. *dop* mutant embryos display defects in polarity establishment, furrow formation and the focussing of furrow canal proteins at the leading edge of the invaginating membrane. Additionally, several studies suggest that Dop affects phosphorylation of Dynein and Dynein-dependent transport processes. In this study, analysis of complete loss-of-function mutants for *dop* reveals that Dop function is specifically required for cellularisation, but is dispensable for syncytial divisions. The first protein defects are visible just prior to cellularisation affecting Slam and Eps15 protein focussing into furrow structures. In contrast, the first morphological defect occurs slightly later at onset of cellularisation affecting furrow canal formation. Membrane invagination is highly reduced in complete loss-of-function *dop* mutants and Golgi as well as recycling endosome localisation are affected, suggesting a function of Dop in membrane recruitment via both Dynein and Kinesin microtubule motors. Furthermore, the localisation of the Dynein subunit Dynein light intermediate chain (Dlic) displays only minor changes in *dop* mutants and is not altered expressing phospho-mutant versions of the candidate Dop substrate Dlic Serine 401. However, preliminary data suggest that a phospho-mimic version of Dlic Serine 401 can reduce lethality of *dop* mutant embryos. This thesis suggests, that Dop affects cellularisation by regulating membrane recruitment to the plasma membrane, likely by affecting Dynein- and possibly Kinesin-dependent microtubule transport.

Figures and Tables

Table of contents

1. Introduction

1.1 General introduction

This thesis was created during a three and a half year project to gain more insight into the mechanism of MAST kinase function. *Drosophila melanogaster* was used as model organism. In *Drosophila* only one MAST kinase homologue exists which was identified previously in our lab as a gene called *drop out* (*dop*). Mutations in this specific gene were identified in a screen for maternal effect loci by Galewsky and Schulz and show their strongest effects during cellularisation in *Drosophila melanogaster* embryogenesis (Galewsky & Schulz 1992). Maternal loss-of-function alleles like the mutant allele dop^{1} lead to severe defects during this stage of embryo development and to embryo lethality. Further work in our lab led to characterisation of Dop-dependent processes during cellularisation and identification of possible Dop targets (Hain 2010; Langlands 2012). Mutations in *dop* interfered with membrane growth and furrow canal formation. One important process also found to be disturbed by *dop* loss-of-function was the establishment of cell polarity in the newly forming cells of the blastoderm embryo. Several proteins important for polarity establishment were found to mislocalise within the new cell compartments (Hain 2010). Furthermore, some results suggested a possible involvement of Dop in Dynein-dependent transport processes, such as defects in lipid droplet clouding as well as mRNA transport (Hain et al. 2014; Meyer et al. 2006). Additionally, genetic interaction studies using mutant alleles of Dynein and Dynactin subunits showed enhanced *dop* phenotypes in combination with the dop^{1} mutant allele (Hain et al. 2014). Also biochemical studies found Dynein subunits as possible phosphorylation targets for Dop (Hain et al. 2014; Langlands 2012).

This thesis builds on the previous studies and aims to identify the Dop-dependent mechanism by which this protein kinase affects cellularisation. The results are grouped into three parts: The first part aims to identify the stage in *Drosophila* embryo development during which maternal Dop function is initially required using hypomorphic and complete loss-of-function mutants of *dop* in comparison; the second part focusses on transport pathways to elucidate a possible

mechanism controlled by Dop function affecting cellularisation processes; in the third part, analysis is set on exploring Dynein function and localisation in regard to Dynein as potential Dop target.

1.2 Cellularisation during *Drosophila* embryogenesis

After fertilisation, the *Drosophila melanogaster* embryo undergoes 13 rapid syncytial divisions. Each of these divisions involves duplication of DNA and nuclei but no cytokinesis. Thus, throughout these syncytial cycles the *Drosophila* embryo consists of only one cell with many nuclei, called a syncytium. The first 9 syncytial divisions take place in the interior of the embryo (Fig.1). However, between cycle 10 and 11, most nuclei migrate to the embryo cortex to form the syncytial blastoderm embryo. After 13 syncytial divisions, the embryo contains about 6000 nuclei that are aligned at the cortex. Subsequently, during interphase of cycle 14, these nuclei get surrounded by membrane invaginating from the cortex and, in the process, the first cells are formed. This process of cell formation, transforming a syncytial blastoderm into a cellular blastoderm, is called cellularisation (for review see (Mazumdar & Mazumdar 2002)).

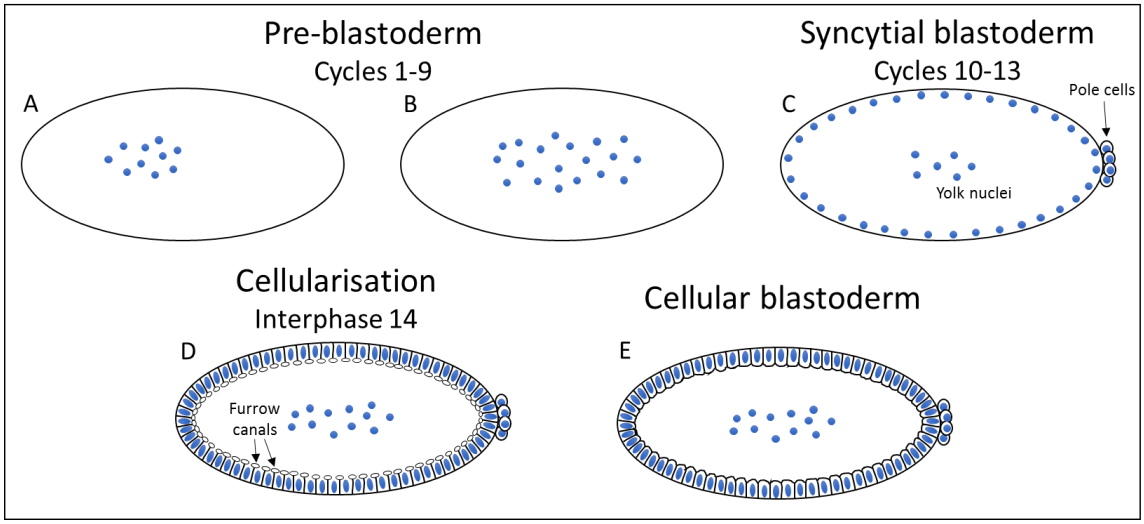

Figure 1 Nuclear cycles during early *Drosophila melanogaster* embryogenesis. In the *Drosophila* pre-blastoderm stage, syncytial (nuclear) divisions take place in the interior of the embryo (cycles 1-9). A: During cycles 1-3, nuclei divide in a sphere at the anterior of the embryo. B: Afterwards, during cycles 4-6, the nuclei spread out along the anterior-posterior axis in a process called axial expansion. C: Most nuclei migrate to the cortex during cycles 8-9 (nuclear migration), leaving behind yolk nuclei. During cycle 10, most nuclei have reached the cortex and,

subsequently, pole cells (the germline precursors) form at the posterior end. The other cortical nuclei undergo four more syncytial divisions (cycles 10-13) to form the syncytial blastoderm. D: At interphase of cycle 14, the plasma membrane invaginates, led by a structure called furrow canal, from the cortex between each nucleus in a process called cellularisation. E: By the end of cellularisation, a cellular blastoderm has formed containing approximately 6000 individual cells. Scheme based on and modified after (Mazumdar & Mazumdar 2002; Tram et al. 2002).

1.2.1 Acquisition of epithelial apico/basal polarity

Simultaneously with the formation of cells, also cell polarity is established in the embryo (reviewed in (Müller 2000; Müller 2001)). Establishment and maintenance of cell polarity is important for the function of most eukaryotic cells and tissues (Lo et al. 2012). The loss of polarity during epithelial to mesenchymal transition (EMT) enables tissue remodelling which is required for many developmental processes such as gastrulation. However, the same machinery that allows for EMT is also implicated in acquisition of invasiveness in tumours and, therefore, represents a key process in cancer development. *Drosophila melanogaster* is a widely used model system to elucidate how polarity is established and maintained in a genetically amenable system (reviewed in (Müller 2000; Müller 2001; Müller 2003).

Cell polarity in *Drosophila* embryos is established gradually and starts during syncytial divisions. When the nuclei first reach the cortex after syncytial cycle 9, they form already distinct compartments with equally distributed secretory systems and microtubule networks surrounding each nucleus (Frescas et al. 2006). Even though no separating membranes are present, not much exchange of neither vesicles nor proteins is visible between the different nuclear compartments. This compartmentalisation is further supported by the plasma membrane which is also already polarised at this stage (Mavrakis et al. 2009a; Mavrakis et al. 2009b). The plasma membrane above each nucleus has apical-like characteristics, whereas lateral membrane that is transiently invaginating during each division accumulates proteins that are specific for basolateral domains of polarised epithelial cells. Essential for this polarisation is the F-actin network that was shown to be required for the stable association of polarity proteins with the plasma membrane.

F-actin is also suggested as the main factor for compartmentalisation during cellularisation (Sokac & Wieschaus 2008a; Sokac & Wieschaus 2008b; Yan et al. 2013; Acharya et al. 2014; Figard et al. 2016). At onset of cellularisation, the plasma membrane invaginates between the nuclei at the cortex and forms a drop-like structure, called the furrow canal. This structure is formed when the membrane reaches about 5 µm into the embryo, about 5 to 8 min into cellularisation (Sokac & Wieschaus 2008b). Many proteins localise specifically to the furrow canal, such as F-actin, Rho1, Slow-as-molasses (Slam), RhoGEF2 and Diaphanous (Dia) (Acharya et al. 2014; Wenzl et al. 2010). As the furrow canal invaginates basally into the interior of the embryo, the lateral membrane is formed. The lateral membrane represents a compartment distinct from the furrow canal and several proteins that localise to the lateral membrane such as Discs large (Dlg) and Neurotactin (Nrt) are excluded from the furrow canal.

During the process of cellularisation, also epithelial polarity is established. One important aspect of epithelial polarity establishment is the formation of cell junctions (Müller 2000; Müller 2001). In contrast to vertebrates that contain three types of junctions in epithelial junctional complexes (zonula adherens (ZA), tight junctions and desmosomes), invertebrate epithelial junction complexes are composed of two junction types (ZA and septate junctions (SJs)). SJs are formed late during *Drosophila* embryogenesis (Müller 2000). In contrast, formation of so-called apical junctions (AJs) that give rise later on to ZA starts early during cellularisation with the formation of basal adherens junctions (BJs). These BJs are localised just apical to and move inward with the furrow canal as the lateral membrane elongates (Fig.2). The BJs provide a tight association of the opposing invaginating membranes. Proteins like Armadillo (Arm; *Drosophila* homologue of β-catenin), α-catenin as well as E-cadherin that localise and form apical spot adherens junctions (SAJs) are also involved in assembling the BJs (Hunter & Wieschaus 2000; Müller & Wieschaus 1996). SAJs form during mid-cellularisation as scattered protein accumulations distributed over the apical third of the newly forming lateral membranes (Fig.2). Whereas BJs dissolve at the end of cellularisation, the SAJs focus to the apical and basolateral border at this stage. Here, they begin to coalesce into incipient ZA during gastrulation and into a continuous ZA belt after

germband extension (Müller & Wieschaus 1996). Cadherins at the centre of ZA mediate cell-cell adhesions through their extracellular domains (Harris & Peifer 2004). With their intracellular domains, they bind to Arm/β-catenin which links the adhesions both to α-catenin and the F-actin network. ZA as well as AJs are required for intercellular adhesion and provide stability to the tissue which is particularly important during the extensive gastrulation movements (Müller 2001; Müller & Wieschaus 1996).

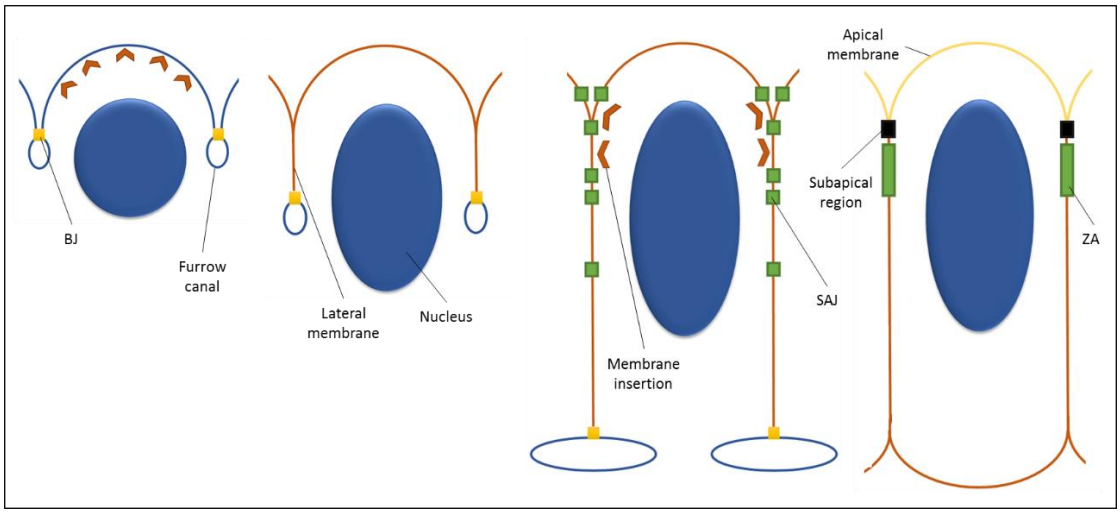

Figure 2 Polarity formation and compartmentalisation in *Drosophila* embryos. At onset of cellularisation, the furrow canals and basal junctions (BJ) are established at membrane domains invaginating between the nuclei. In order for the membrane to invaginate further, membrane material is added apically during early and apico-laterally during late cellularisation stages (Lecuit & Wieschaus 2000). During mid-cellularisation stages, adherens junction precursors in form of spot adherens junctions (SAJ) localise to the lateral membrane and later on mature into zonula adherens (ZA). By the end of cellularisation, the furrow canal compartment resolves into the basal membrane, basal junctions disappear and the subapical region forms composed of many polarity proteins to separate the apical from the baso-lateral compartment. Scheme modified after (Müller 2001)

At the beginning of cellularisation, proteins important to build AJs such as Bazooka (Baz), Arm and E-cadherin localise to apical microvilli at the embryo cortex (Harris & Peifer 2004). Here, Arm and E-cadherin form clusters before SAJs are formed (McGill et al. 2009). Baz is the first protein to mark the sites of apical junction formation and Arm and E-cadherin clusters were shown to be recruited by Baz to these sites (Harris & Peifer 2004; Harris & Peifer 2005; Müller & Wieschaus 1996; McGill et al. 2009). Moreover, Baz localisation itself is dependent on basal-to-apical Dynein transport along microtubules as well as an apical actin scaffold (Harris & Peifer 2005). Thus, the transport and the precise localisation of polarity markers is a very important

process during polarity establishment. However, how this process is exactly regulated is not known in detail.

One model suggests that the establishment of membrane polarity is achieved by the temporally controlled insertion of intracellular vesicles at specific (apical or apico-lateral) sites (Lecuit & Wieschaus 2000; Lecuit et al. 2002). This model predicts that membrane that invaginates first into the embryo derives from vesicle insertions early in cellularisation. It also suggests that protein and membrane sources from the secretory pathway play a major role in not only polarity establishment but also membrane invagination during cellularisation.

1.2.2 Vesicular transport pathways during cellularisation

The formation of around 6000 cells during cellularisation leads to an about 25-fold increase in the embryo surface area (Lecuit & Wieschaus 2000). Thus, membrane synthesis, delivery and redistribution are important processes in cellularisation. Two models have been proposed in the past about where the invaginating membrane comes from. One model suggested that the membrane was mainly newly synthesised inside the cell and transported to the sites of membrane invagination during cellularisation (Lecuit & Wieschaus 2000; Rothwell et al. 1998; Riggs et al. 2003; Burgess et al. 1997). Another model predicted that the membrane for invagination was mainly coming from cortical microvilli that disassembled during cellularisation and, thereby, releasing membrane for immediate distribution into the invagination site (Figard et al. 2013; Figard & Sokac 2014; Fullilove & Jacobson 1971). A recent study connects both models and shows that they might depend on each other (Figard et al. 2016). It suggests that the expansion of the plasma membrane is enabled first through the unfolding of the cortical microvilli which can provide about 42-65% of the membrane required for cell formation. In addition, a burst of exocytosis from internal membrane sources at onset of cellularisation provides the remaining membrane required for membrane invagination. Figard et al

hypothesise that also this exocytosed membrane is stored in form of microvilli until it is released to fuel membrane invagination during fast phase of cellularisation.

Membrane insertion to fuel membrane invagination is now also considered as the main force to lead to invagination (Sisson et al. 2000; Riggs et al. 2003; Riggs et al. 2007; Papoulas et al. 2005; Burgess et al. 1997; Mavor et al. 2016). Inhibition of membrane vesicle transport at different stages was shown to lead to impairment of membrane invagination. Preceding studies assumed that the contractions of an acto-myosin network provide the force for invagination. However, Royou et al found out that invagination of the plasma membrane is nearly unaffected in Myosin II-impaired embryos and, therefore, that the acto-myosin network does not have an important role for vertical membrane invagination during cellularisation (Royou et al. 2004). Albeit, the acto-myosin network is essential for basal closure at the end of cellularisation.

Together with membrane, also proteins are suggested to be transported to the site of membrane invagination (Lecuit & Wieschaus 2000; Rothwell et al. 1999; Riggs et al. 2003). For example, the lateral membrane marker Nrt gets newly synthesised during cellularisation and was shown to be transported from the endoplasmic reticulum (ER) over the Golgi to the recycling endosome. From the recycling endosome, Nrt gets sorted and transported to the plasma membrane. If any of these steps in transport of Nrt is impaired, the protein accumulates in one of the organelles and its delivery to the plasma membrane fails (Lecuit & Wieschaus 2000; Murthy et al. 2010). Additionally, also membrane invagination is abolished in these embryos, presumable due to a lack of membrane exocytosis.

These studies emphasize the importance of membrane delivery for overall cellularisation. Membrane lipids and proteins are both synthesised in the ER and afterwards transported to and partly modified in the Golgi network (Mellman & Nelson 2008; De Matteis & Luini 2008). In contrast to mammals, Golgi in insect cells consists of dispersed vesicles rather than a network of tubules (Ripoche et al. 1994). These Golgi vesicles undergo a dramatic localisation change during cellularisation (Sisson et al. 2000). Whereas they localise to the bases of the nuclei during

the beginning of cellularisation, at the end of cellularisation, Golgi vesicles rapidly localise to the cortex of the newly forming cells (Sisson et al. 2000; Ripoche et al. 1994). These Golgi dynamics were shown to depend on microtubules as well as the motor protein complex Dynein (Lecuit & Wieschaus 2000; Papoulas et al. 2005). Membrane material and proteins from the Golgi are transported to the pericentrosomal recycling endosome and, afterwards, transported to and released into the plasma membrane (Fig.3)(Riggs et al. 2003; Pelissier et al. 2003). The insertion of vesicles into the plasma membrane was shown to be highly polarised (Lecuit & Wieschaus 2000). During slow phase of cellularisation, vesicle insertion was detected solely at the apical membrane, whereas during fast phase, it was detected only at the apico-lateral membrane. This strong spatial restriction of membrane insertion might be a parameter to control cell polarity as presented in the previous section.

Even though the secretory pathway is clearly of high importance for cellularisation, also the endocytic pathway plays a role in membrane invagination (Sokac & Wieschaus 2008a; Fabrowski et al. 2013; Pelissier et al. 2003). Mutants of the small GTPase Rab5 display a reduced membrane growth which suggests that redistribution of membrane material via the endocytic pathway can also affect membrane invagination (Pelissier et al. 2003). Endocytosed vesicles from the plasma membrane are transported in a Rab5-dependent way to the early endosome (Lecuit 2004). From there they can be either transported back to the plasma membrane, sent for degradation to late endosomes and lysosomes or transported to the recycling endosome from which material can also be recycled back to the plasma membrane. The recycling endosome functions therefore as interface between the exocytic and endocytic pathways (Fig.3). In addition to the plasma membrane, endocytosis also takes place at the furrow canal during cellularisation (Sokac & Wieschaus 2008a; Lee & Harris 2013; Lee & Harris 2014). Scission of vesicles from the furrow canal is F-actin-dependent and timely restricted to onset of cellularisation concomitantly to furrow canal formation (Sokac & Wieschaus 2008a). This restriction of endocytosis is important to maintain furrow canal stability by retaining furrow canal components at this site. On the other hand, local endocytosis at the furrow canal seems also to regulate F-actin network formation at

this site as it was shown for the Arf-guanine nucleotide exchange factor (GEF) Steppke that regulates Rho1 levels at the furrow canal via induction of endocytosis (Lee & Harris 2013). Also, the vesicle fusion ability of Syntaxin1 seems to be required for proper F-actin formation at the cellularisation furrows (Burgess et al. 1997). Thus, the F-actin network and the endocytic machinery appear to be closely interlinked and their function mutually controlled during cellularisation.

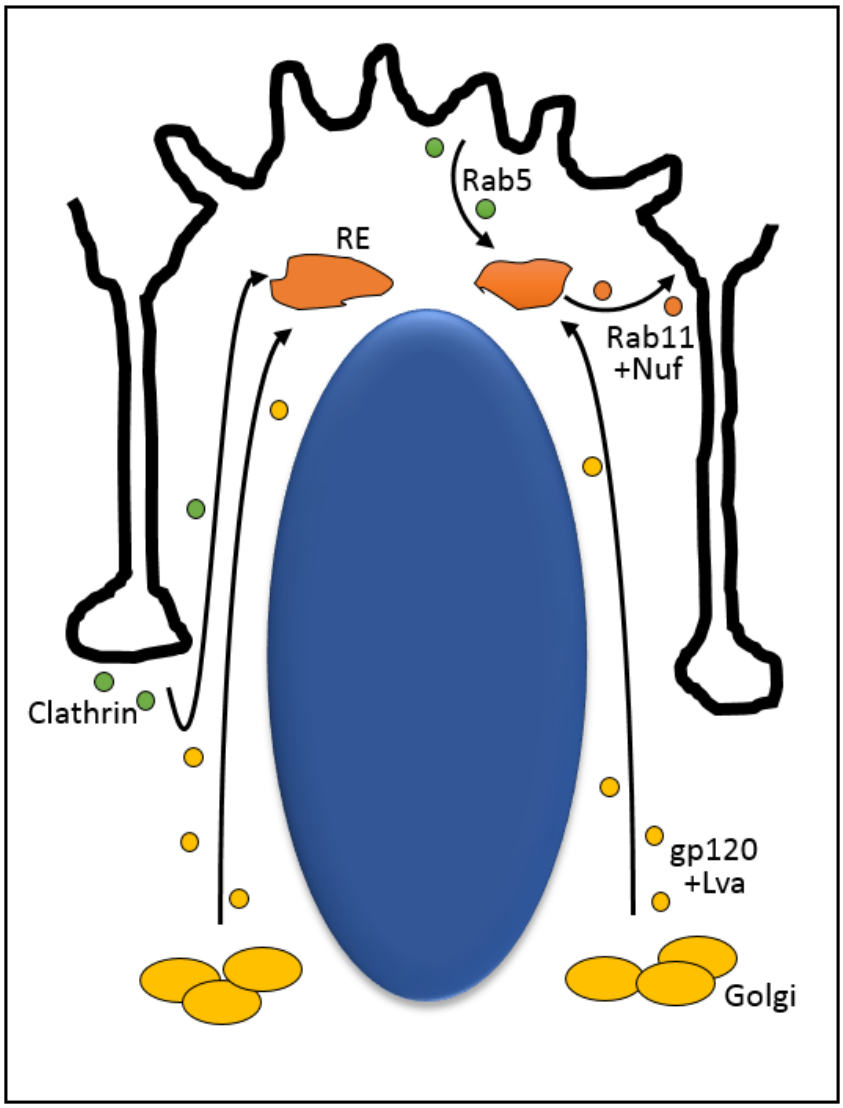

Figure 3 Vesicle transport pathways during cellularisation. Membrane invagination during cellularisation is dependent on the secretory pathway which delivers membrane from the Golgi over the recycling endosome (RE) to the plasma membrane as well as on membrane redistribution from apical microvilli dependent on Rab5. Another pathway involving vesicle transport is Clathrin-mediated endocytosis of material at the furrow canal, a pathway active only during early cellularisation (Sokac & Wieschaus 2008a). Scheme modified after (Lecuit 2004)

1.3 The cytoskeleton network structure during early *Drosophila* embryogenesis

F-actin network dynamics are crucial for regulating vesicular endo- and exocytosis (Eitzen 2003; Lee & Harris 2014; Sokac & Wieschaus 2008a). However, besides the F-actin network, also the microtubule network is an important component of vesicular trafficking as it provides the tracks along which the vesicles get transported. Both cytoskeletal components, F-actin and microtubules, show highly distinct dynamics throughout syncytial divisions and cellularisation in support of the morphological processes that take place during these stages. These dynamics of the microtubule and F-actin networks will be outlined in the following sections.

1.3.1 Cytoskeleton network dynamics during syncytial divisions

Before nuclear migration during syncytial divisions in the earliest stage of *Drosophila* embryogenesis, nuclei divide in the interior of the embryo (Fig.1). Each of these nuclei comprises its own pair of centrosomes and microtubules (Foe et al. 2000). At the same time, F-actin and Myosin II accumulate and overlap at the cortex but do not display any dynamic changes during this stage. After syncytial cycle 9, nuclei migrate from the interior of the embryo to the cortex. Together with the nuclei, also the associated centrosomes migrate to the cortex in a microtubule-dependent manner (Schejter & Wieschaus 1993b). At the cortex, the centrosome pairs get localised between individual nuclei and the cortical membrane and induce restructuring of the overlying F-actin and myosin network (Raff & Glover 1989). In addition, microtubules organised by the centrosome pair surround the nucleus in a highly polarised way with microtubule plus-ends pointing away from the centrosomes and reaching either to the cortex or into the interior of the embryo. The minus-ends of the microtubules stay with the centrosomes and, thereby, enable directed apical and basal transport. As a result, microtubules form a structural compartment with a restricted protein and vesicle intermixing between the different compartments (Frescas et al. 2006).

After nuclei and their associated centrosomes have reached the cortex, division cycle-dependent rearrangements of the cytoskeletal network take place (Foe et al. 2000). Myosin II which showed co-localisation with F-actin before the centrosomes reached the cortex does not show overlapping localisation with F-actin after the arrival of centrosomes and nuclei. During the following syncytial cycles, microtubules organised by the centrosomes cause a separation of F-actin and myosin which prevents contractions of the acto-myosin network and stabilises the cortical area. During interphase, F-actin caps form above each individual nucleus and its apically positioned centrosome pair (Fig.4). These cap structures are suggested to reduce lateral nuclear movement (Schejter & Wieschaus 1993b). Additionally, the microtubules emanating from the centrosomes form an astral array extending apically to the cortex and basally into the interior of the embryo surrounding the nuclei. During pro- and metaphase, the centrosomes migrate along the nucleus to opposite poles and, after nuclear breakdown, spindle arrays emerge from the centrosomes to capture the kinetochores of chromosomes for division. The F-actin network rearranges during this cycle phase to form furrows separating spindles from adjacent nuclear compartments. These metaphase furrows (also called pseudocleavage furrows) are structures made up of plasma membrane invaginating from the cortex. Several proteins are enriched in these furrows, such as F-actin, several F-actin regulator proteins and Anillin (Riggs et al. 2003). The position of the metaphase furrows is thought to be determined by the overlapping region of astral microtubules emerging from neighbouring centrosomes (Riggs et al. 2007; Crest et al. 2012). Metaphase furrows reach a depth of about 8 µm before they retract during the following ana- and telophase (Riggs et al. 2003). The spindle separation by metaphase furrows is important to ensure that spindles do not misalign with neighbouring chromosomes (Postner et al. 1992). Despite the prominent localisation of F-actin to these furrows, it was shown that plasma membrane is the main component to create the barrier between the spindles (Rothwell et al. 1999; Cao et al. 2008). During telophase, new furrows are formed separating the daughter nuclei created in the preceding division and the F-actin network reforms caps above each nucleus (Fig.4).

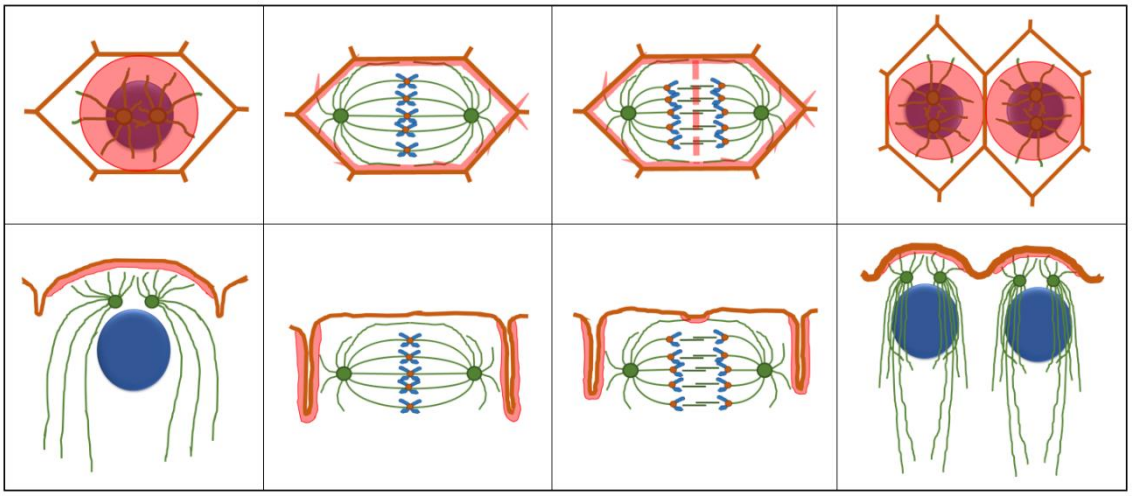

Figure 4 Cytoskeletal organisation during syncytial divisions. F-actin network (red) and microtubule (green) organisation are shown during S-phase, metaphase, anaphase and S-phase of the following cycle. Sagittal views (top panel) as well as cross-sectional views (bottom panel) are depicted. Membrane is shown in brown, nuclei and chromosomes in blue and centrosomes in green with dark green outline.

During syncytial divisions, F-actin and Microtubules were shown to interact (Foe et al. 2000). Experiments using Cytochalasin as F-actin polymerisation inhibitor showed that F-actin is required to link microtubules and the nuclei to the cortex. Additionally, microtubules are likely to be the mediators between centrosomes and F-actin and boost F-actin cap or furrow assembly presumably by Kinesin-dependent transport.

In addition to a requirement of centrosomes and microtubules in correct F-actin localisation during syncytial divisions, also endosomal transport is involved in proper actin dynamics at this stage. The recycling endosomal system was shown to be required for F-actin assembly from caps into metaphase furrows (Rothwell et al. 1998; Riggs et al. 2003; Riggs et al. 2007; Cao et al. 2008). Mutations in genes required for recycling endosomal function (*nuf*, *rab11*) cause defects in F-actin formation at the furrow and ultimately in loss of furrow stability. This F-actin dependence on recycling endosomal transport might be due to transport of actin regulators to the furrows (Cao et al. 2008; Wenzl et al. 2010). Moreover, as previously mentioned, the Arf-GEF Steppke positively regulates Clathrin-dependent endocytosis at metaphase (as well as cellularisation) furrows which reduces Rho1 levels at the furrow (Lee & Harris 2013). This in turn leads to a reduction in actomyosin activity which helps in orchestrating proper membrane growth.

1.3.2 Cytoskeleton network dynamics during cellularisation

After the cortical nuclei completed their 13th division, they enter an elongated interphase. This cycle 14 interphase gives rise to new cells at the cortex and is therefore called cellularisation. Cellularisation is a modified form of cytokinesis and, even though its regulatory system shares a lot of components required also for syncytial division cycles, the regulatory system differs from these cycles in one major aspect: It relies not only on maternally provided genes but also on zygotic gene products (Langley et al. 2014; Tadros et al. 2007). The bulk of zygotic gene transcription starts during cellularisation and cellularisation is the first process requiring zygotic genes. Only a few zygotic genes were found to be specifically expressed during cellularisation. Four of them, called *bottleneck* (*bnk*), *slam*, *nullo* and *serendipity-α* (*sry-α*), are required to regulate F-actin dynamics (He et al. 2016). This underpins the importance of F-actin dynamics during cellularisation.

Cellularisation starts with a visible volume increase and elongation of the cortical nuclei. During the course of cellularisation, the nuclear volume increases by 2.5-fold (Schejter & Wieschaus 1993b). Nuclei are at this stage surrounded by tight microtubule bundles forming an inverted basket structure and these microtubules are required to force nuclei to elongate rather than expand as spheres (Fig.5)(Fullilove & Jacobson 1971; Hampoelz et al. 2011). Similar to syncytial division interphases, microtubules during interphase of cycle 14 emerge from centrosomes apically of the nuclei and stretch their plus-ends either up to the cortex or down into the interior of the embryo with the minus-ends staying connected with the centrosomes. Thereby, microtubules form a scaffold along an apico-basal axis allowing for directed transport of different cargoes along this axis and from the interior of the embryo to the cortex as well as the other way round.

The F-actin network first focusses into interphase caps at the cortex on top of each nucleus but these cap structures expand laterally to form an equally distributed mesh at the cortex (Fig.5)(Schejter & Wieschaus 1993b). Cortical F-actin is important to shape the microvilli which

represent membrane protrusions into the extra-embryo space that serve as membrane reservoir during cellularisation (Fullilove & Jacobson 1971; Figard et al. 2016). In addition, F-actin focusses into a hexagonal array fencing each individual nucleus. This focussing of F-actin into hexagonal arrays is tightly regulated and a prerequisite for furrow canal formation and stability (Mavrakis et al. 2009b; Sokac & Wieschaus 2008b; Sokac & Wieschaus 2008a; Yan et al. 2013; Afshar et al. 2000; Padash Barmchi et al. 2005; Wenzl et al. 2010; Field et al. 2005). By which process the site of furrow canal formation and membrane invagination between the nuclei gets determined is not known. However, the formation of actin structures during the preceding syncytial divisions seems not to be required for cellularisation furrow positioning (Postner et al. 1992). It is speculated that also cellularisation furrow positioning is dependent on the overlap of astral microtubule plus-ends emerging from the centrosomes between nuclei and cortex as it seems to be the case for metaphase furrows (Riggs et al. 2007; Crest et al. 2012). This might be due to transport of specific cargo e.g. recycling endosome-derived vesicles to this particular site (Albertson et al. 2005).

The accumulation of F-actin at the furrow canal is known to be regulated by two different pathways. Accumulation of branched F-actin is encouraged by the Cip4-Scar/WAVE-Arp2/3 pathway (Yan et al. 2013). Branched F-actin is more dynamic than unbranched F-actin and enables vesicle endo- and exocytosis at the associated membrane (Zallen et al. 2002; Yan et al. 2013). It is thought to be prominent only at the very onset of cellularisation when endocytic tubules form at the furrow canal (Sokac & Wieschaus 2008a; Yan et al. 2013). In contrast, linear F-actin formed downstream of the RhoGEF2-Rho1-Dia pathway increases the rigidity of the furrow canal and reduces endocytosis at this site (Webb et al. 2009). It is thought to accumulate at the furrow canal during slow phase of cellularisation, stabilising the furrow canal and enabling its invagination over the course of cellularisation (Sokac & Wieschaus 2008b; Sokac & Wieschaus 2008a; Yan et al. 2013; Lecuit & Wieschaus 2000). Slam and Nullo are both known to regulate the pathway leading to unbranched F-actin and, additionally, have been identified as factors that stabilise the furrow canal (Acharya et al. 2014; Wenzl et al. 2010; Sokac & Wieschaus

2008b). They are assisted by proteins like the septin Peanut and the cortical scaffold protein Anillin (Mavrakis et al. 2014; Field et al. 2005).

The RhoGEF2-Rho1-Dia pathway not only serves to regulate furrow canal stability and membrane invagination but is also required together with Peanut to recruit Myosin II to the furrow after Bnk degradation during fast phase of cellularisation (Mavrakis et al. 2014; Afshar et al. 2000; Padash Barmchi et al. 2005). This enables basal closure of the newly formed cells, a process dependent on actomyosin contractility and the last step during cellularisation. It gives rise to cells of about 5 µm in diameter and 35 µm height that are connected with the yolk plasm by 1 µm wide intercellular bridges (Schejter & Wieschaus 1993b; Warn & Robert-Nicoud 1990).

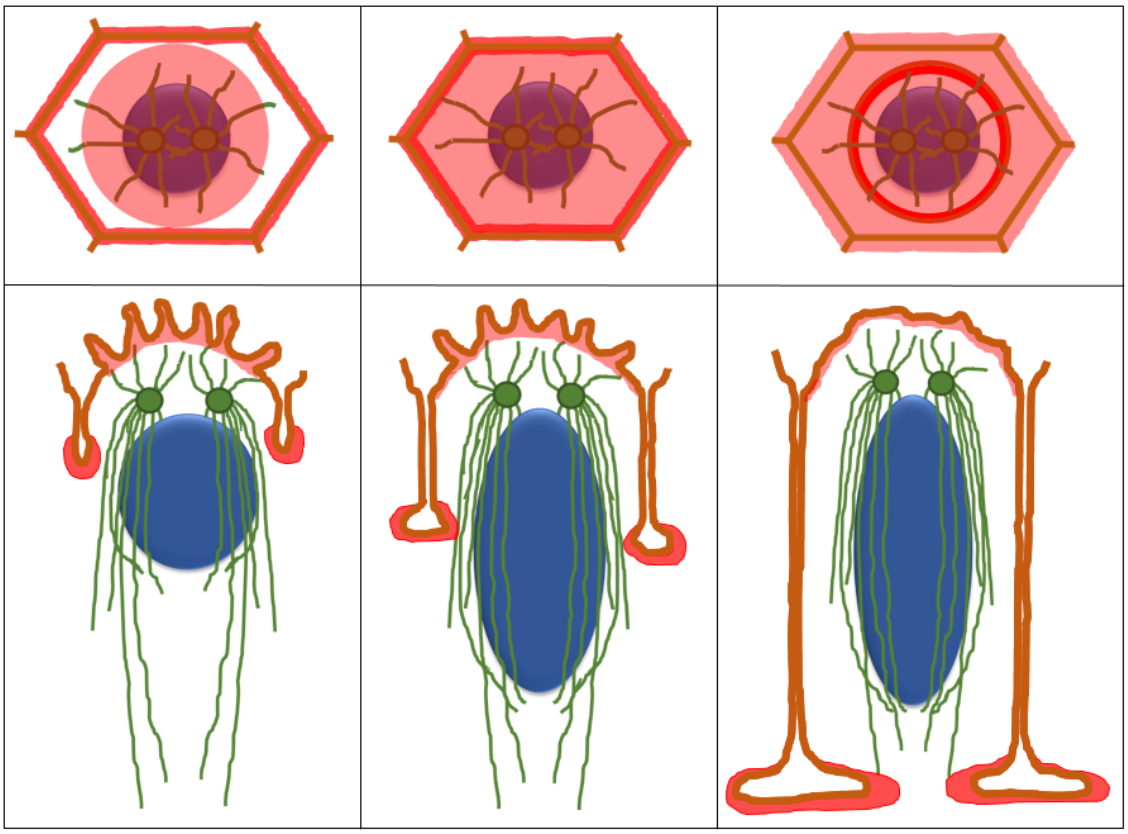

Figure 5 Cytoskeletal organisation during cellularisation. F-actin network (red) and microtubule (green) organisation are shown during early, mid- and late cellularisation. Sagittal views (top panel) as well as cross-sectional views (bottom panel) are depicted. Membrane is shown in brown, nuclei in blue and centrosomes in green with dark green outline.

1.3.3 Microtubule-associated transport during cellularisation

Microtubules form the tracks by which many different cargoes get transported in a polarised manner. An essential requirement for its proper formation not only in mitotic cycles such as syncytial divisions but also during cellularisation has been established in several experiments injecting *Drosophila* embryos with Colchicine to depolymerise microtubules (Crest et al. 2012; Foe & Alberts 1983; Royou et al. 2004; Riggs et al. 2007; Sisson et al. 2000; Schejter & Wieschaus 1993a; Harris & Peifer 2005). During cellularisation, microtubules were shown to be required for membrane invagination, F-actin accumulation at the furrow canal, elongation of the nuclei, transport of Golgi vesicles, and proper localisation of the polarity protein Baz as well as the recycling endosome protein Nuclear fallout (Nuf).

Two motors are known that transport cargoes along microtubule tracks in opposite directions: The Dynein motor protein complex transports its cargo in the direction of the minus-end of microtubules (which is usually attached to the microtubule organising centre/centrosomes); the Kinesin motor protein complex transports its cargo in most cases away from the centrosomes to the microtubule plus-end. Both motors are required for diverse cellular functions, such as transport and positioning of organelles, vesicles and attached proteins, as well as mitotic spindle and chromosome movement (Karki & Holzbaur 1999). Whereas at least 14 different Kinesin classes exist, Dynein only belongs to two different classes: axonemal and cytoplasmic Dynein (Höök & Vallee 2006). Axonemal Dynein is only present in cilia and flagella, regulating their beating activity. Cytoplasmic Dynein is involved in many more cellular functions, it is essential for cell viability and autonomously required in all cells (Höök & Vallee 2006; Gepner et al. 1996). In the following, Dynein is corresponding to cytoplasmic Dynein.

In *Drosophila* embryos, Dynein was shown to be responsible for recycling endosome localisation to the centrosomes influencing metaphase furrow assembly and Dynein is also required for apical Golgi transport during cellularisation affecting furrow invagination (Riggs et al. 2007; Papoulas et al. 2005). Additionally, Dynein is required for Baz basal-to-apical transport early in

cellularisation and apical lipid transport (lipid clouding) during late cellularisation and beginning of gastrulation (Harris & Peifer 2005; Gross et al. 2000; Welte 2015).

Cytoplasmic Dynein consists of a multi-subunit protein complex: Heavy chains, intermediate chains, light chains and light intermediate chains. Each heavy chain includes an about 160 kDa N-terminal domain forming the base of the molecule that is responsible for binding of regulatory co-complexes (Fig.6)(Höök & Vallee 2006). Additionally, the heavy chain contains the about 360 kDa motor domain made up of 6 AAA^+ ATPase units which provide the force through nucleotide hydrolysis for moving the Dynein molecule along microtubules. Moreover, Dynein contains a stalk region made up of antiparallel coiled-coil α-helices attached to a globular structure for microtubule binding and several accessory subunits such as intermediate, light intermediate and light chains (Fig.6). Phosphorylation of these accessory subunits is a common way of regulating Dynein function. Several Dynein subunits were shown to be phosphorylated by different mechanisms in different organisms, leading either to down- (Dell et al. 2000; Addinall et al. 2001; Vaughan et al. 2001; Runnegar et al. 1999) or up-regulation (Whyte et al. 2008; Ikeda et al. 2011; Yang et al. 2005) of Dynein function. Dynein binding to specific cargoes is mainly regulated by different co-complexes, the most important one being the Dynein activating complex Dynactin which mediates most of Dynein functions in eukaryotes (Schroer 2004).

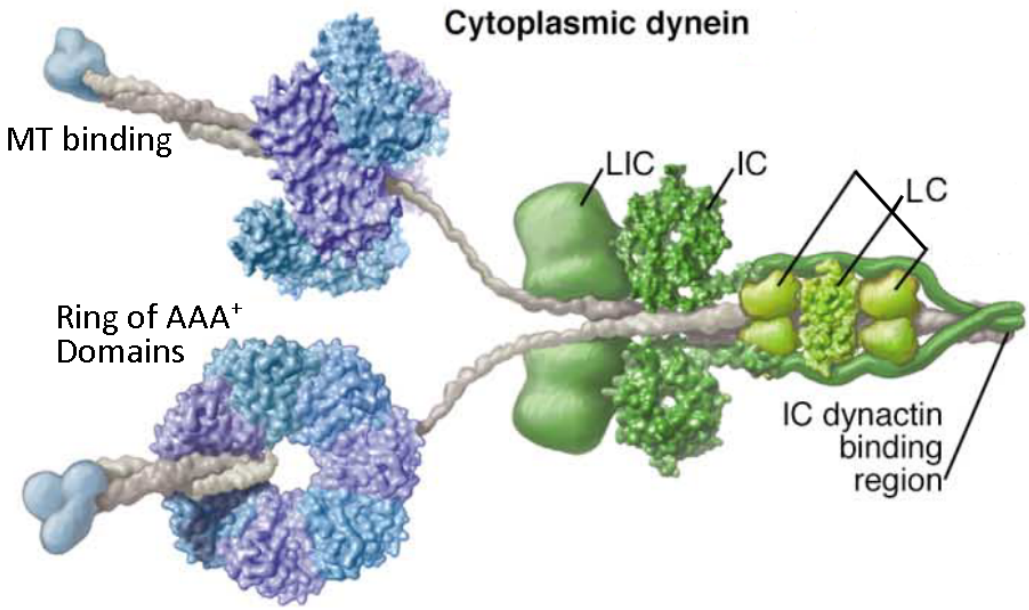

Figure 6 Structure of the Dynein complex. The minus-end directed motor Dynein is a multi-subunit complex made up of two heavy chains (HC) which include the AAA^+ ATPase motor region (blue and purple rings). A coiled-coil domain extending from these rings is connected to a globular head which mediates binding to microtubules (MT). Another coiled-coil domain extends from the motor region that mediates dimerization as well as Dynein light chain (LC), intermediate chain (IC) and light intermediate chain (LIC) binding. The Dynein intermediate chain is required for binding of the Dynactin complex. Figure modified after (Vale 2003)

In comparison to Dynein, Kinesins are much more diverse in their structure and number of subunits with a wide range of tail domains attached to a conserved ATPase core (Vale 2003; Kardon & Vale 2009). This diversity enables Kinesin to recognise and bind multiple cargoes without the mediation of co-complexes. Only three Kinesins are reported so far to affect syncytial divisions and/or cellularisation: the *Drosophila* Kinesin-5 homologue, KLP61F, is required for formation of bipolar spindle arrays in mitosis (Heck et al. 1993; Sharp et al. 2000; Sharp & Rath 2009); Kinesin-1 in *Drosophila* is required to somehow link microtubules (and Dynein) to the actin cortex during interphases of syncytial divisions (Winkler et al. 2015); moreover, antibody injections directed against the *Drosophila* Kinesin-6 homologue, Pav-KLP, showed that this Kinesin is required for proper spindle dynamics in syncytial divisions, furrow ingression during both, syncytial divisions and cellularisation, as well as for F-actin and vesicle distribution and nuclear attachment to the cortex (Sommi et al. 2010).

1.4 Protein kinases

Protein kinases transfer phosphate groups from ATP to target substrate proteins in a reaction called phosphorylation. By addition of a phosphate group to specific sites of a substrate protein, kinases can regulate the enzyme activity of a substrate, mediate its protein-protein interactions, as well as alter its subcellular localisation and stability (Morrison et al. 2000). This can affect nearly all cellular functions including motility, growth, division, metabolism as well as membrane transport and gene expression (Johnson et al. 1998). The human kinome comprises 518 protein kinases and represents one of the largest superfamilies of homologous proteins in eukaryotes (Manning et al. 2002; Hanks & Hunter 1995). The members of this superfamily are defined by a kinase domain including a catalytic core of about 30 kDa (Manning et al. 2002; Hanks et al. 1988). This superfamily can be subdivided into kinases that phosphorylate proteins at serine and threonine residues or at tyrosine residues (Hanks & Hunter 1995). Furthermore, they can be grouped into families by looking for common substrate specificities and modes of regulation.

In comparison to the human kinome, the *Drosophila* kinome comprises around 251 protein kinases, 30 of which are AGC kinases (Morrison et al. 2000). AGC serine/threonine kinases are named after three representative families (cAMP-dependent protein kinase (PKA), cGMP-dependent protein kinase (PKG) and protein kinase C (PKC) family) and a common feature of AGC kinases is a C-terminal hydrophobic motif which helps to keep the catalytic core in an active conformation (Arencibia et al. 2013). AGC kinases are a highly conserved group of kinases and they function in several intracellular signalling pathways. They show a preference to phosphorylate residues that are C-terminal of basic amino acids (Arg and Lys), even though, many substrates of AGC kinases get phosphorylated at non-optimal sequences (Pearce et al. 2010). In most AGC kinases, binding of substrates or membrane is often mediated by domains present in addition to the kinase domain.

1.4.1 MAST kinases

The MAST family of the group of AGC kinases is defined by proteins that contain a C-terminal PDZ domain, an N-terminal DUF1908 domain in addition to the serine/threonine kinase domain (Fig.7)(Pearce et al. 2010). MAST kinases exist in all kingdoms of life, from animals and plants to fungi and bacteria (Arencibia et al. 2013). In mouse, they show a wide-spread expression across various tissues like brain, heart, spleen, lung, liver, skeletal muscle, kidney and testis indicating a broad range of functions (Garland et al. 2008). MAST kinases are also implicated in several human diseases such as breast cancer, inflammatory bowel disease, rabies virulence, cystic fibrosis and secretory diarrhoea (Robinson et al. 2011; Wang et al. 2010; Labbé et al. 2008; Labbé et al. 2012; Terrien et al. 2009; Préhaud et al. 2010; Terrien et al. 2012; Loh et al. 2008; Ren et al. 2013; Wang et al. 2006). The same diversity as seen for the diseases MAST kinases are implicated in can be found among the interaction partners that were shown to bind to or somehow being regulated by the different MAST kinases.

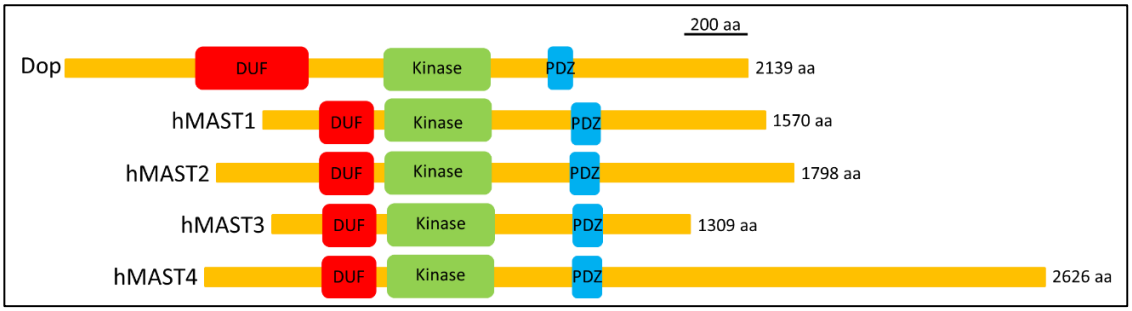

Figure 7 Alignment of the single *Drosophila* MAST kinase Dop with the four MAST kinase homologues in human. MAST kinases are characterised by a serine/threonine kinase domain (green), a PDZ domain (blue) and a domain of unknown function (DUF1908; red). The PDZ domain is known to mediate most of the known protein-protein interaction of these kinases. The sequences of the three known domains are highly conserved between the different members, whereas the sequences surrounding the domains show high variation (Hain 2010).

The first MAST kinase to be identified was MAST2 which was shown to bind indirectly to microtubules at the spermatid manchette in mice via MAPs (microtubule associated proteins) (Walden & Cowan 1993). This association with microtubules gave the family its name: microtubule-associated serine/threonine kinase. Both, MAST1 and MAST2 were shown later to bind to β2-syntrophin in mice (Lumeng et al. 1999). This specific member of the syntrophin

family is only found at neuro-muscular junctions and binds to Utrophin. β2-syntrophin is thought to function as a link between MAST2 and Utrophin at the neuro-muscular junction.

A connection exists between MAST kinase function and breast cancer. Several MAST1 and MAST2 gene fusions were identified in breast cancer cell lines and overexpression of these fused genes lead to enhanced proliferation in benign breast cell lines (Robinson et al. 2011). Moreover, an increased risk for breast cancer was associated with 9 SNPs found in MAST2 (Wang et al. 2010).

MAST1, 2 and 3 were all shown to bind to the tumour suppressor PTEN (phosphatase and tensin homologue) (Adey et al. 2000). Additionally, MAST2 was shown to phosphorylate PTEN (Valiente et al. 2005). The possible impact of this PTEN phosphorylation on PTEN function was not investigated in more detail. However, a possible functional mechanism of PTEN regulation by MAST2 was investigated through another interaction analysed in human neuroblastoma cells. MAST1 and MAST2 were shown to interact with the glycoprotein of the virulent rabies virus in these cells and the binding was shown to inhibit normal MAST2 localisation to apical membranes (Terrien et al. 2009; Préhaud et al. 2010). A follow-up study suggested that binding of the glycoprotein of rabies virus might inhibit binding of PTEN to MAST2 (Terrien et al. 2012). This inhibition seemed to prevent the phosphorylation-dependent nuclear localisation of PTEN and, in turn, inhibited PTEN function in preventing neuronal outgrowth and regeneration. This mechanism might explain the enhanced neuronal survival upon rabies virus infection. Another study which supports this mechanism is based on the result of an RNAi screen to find kinase families that regulate growth cone collapse, neurite retraction and neurite outgrowth (Loh et al. 2008). RNAi directed against MAST2 promotes neurite outgrowth and inhibits (lipopolysaccharide (LPS)-induced) neurite retraction in rat primary midbrain neurons. Therefore, MAST2 function in this system resembles PTEN function which suggests that the functions of both proteins are linked to each other.

Both, MAST2 and MAST3 were shown to be involved in NF-κB activity. MAST3 was found as factor in inflammatory bowel disease (IBD) tissues to increase Toll-like receptor (TLR) 4-dependent NF-κB activity and knock-down of MAST3 resulted in reduced NF-κB activity (Labbé et al. 2008). A follow-up study found that MAST3 acts on the NF-κB pathway by changing gene expression of several genes in the gut of IBD patients and, thereby, triggers immune reactions (Labbé et al. 2012). The direct target of MAST3 in this process remained unknown. These studies highlight a possible involvement of MAST3 in IBD pathogenesis. MAST2 was shown to regulate LPS-induced NF-κB regulation by forming a complex with TRAF6 (TNF receptor-associated factor 6) which resulted in NF-κB inhibition and reducing inflammatory responses (Zhou et al. 2004; Xiong et al. 2004). Thus, MAST2 and MAST3 seem to have opposite functions in NF-κB regulation, MAST2 in inhibiting its function and MAST3 in increasing its function due to different stimuli (TLR4-dependent for MAST3 and LPS-dependent for MAST2).

In addition to IBD and breast cancer, as well as regulation of neuronal survival, MAST kinases are also linked to cystic fibrosis and secretory diarrhoea. MAST2 was shown to form a complex with the cystic fibrosis transmembrane conductance regulator (CFTR), competing with the CFTR-associated ligand (CAL) (Ren et al. 2013). CFTR is an anion channel transporting chloride (Cl^-) and bicarbonate (HCO_3^-) across the membranes of epithelial cells in lung, pancreas, liver, intestine, sweat ducts and the reproductive system and CFTR is implicated in cystic fibrosis and enterotoxin-induced secretory diarrhoea. A specific deletion of CFTR was found in over 90% of cystic fibrosis patients which reduces its functionality. Binding of CAL increases lysosomal degradation of CFTR. The competition with MAST2 for binding to CFTR has potential as a drug target to increase CFTR levels and its functions by overexpressing MAST2. MAST2 also binds to and phosphorylate the Na^+/H^+ exchanger NHE3 (Wang et al. 2006). This phosphorylation by MAST2 was shown to inhibit NHE3 activity. NHE3 is important to maintain normal gastrointestinal physiology and its malfunction leads to impaired absorption and can increase the fluidity of diarrhoea (Ren et al. 2013). The results which show that MAST2 regulates NHE3 as well as CFTR function suggest MAST2 as potential cross-regulator that can possibly assemble

both channels and maybe other proteins into a macromolecular complex, thus, increasing its impact on intestinal physiology.

A yeast 2-hybrid screen identified MAST2 as an interaction partner of Protocadherin LKC (liver, kidney, colon) (Okazaki et al. 2002). Protocadherin LKC induces contact inhibition of cell proliferation and is a potential tumour suppressor. Not much is known about its binding to MAST2. However, Protocadherin LKC might regulate MAST2 subcellular localisation by recruiting it from the cytoplasm to the cortex. MAST1, MAST2 and MAST3 were all found to bind to Adenomatous polyposis coli (APC) (Sotelo et al. 2012). However, no functional impact of this binding has been reported. Additionally, an RNAi screen found Drop out (Dop; CG6498) in *Drosophila* S2 cells as a factor essential for proper chromosome alignment (Bettencourt-Dias et al. 2004).

Thus, MAST kinases seem to be involved in a lot of different processes and have a lot of very distinct binding partners, among those two potential phosphorylation targets (PTEN and NHE3). However, even though elucidating the functions of MAST kinases is of great interest, not much is actually known about the exact mechanism they are involved in and how they are able to influence that many processes. No specific phosphorylation sites have been identified on the potential phosphorylation targets PTEN and NHE3. A functional impact of binding of MAST to many of the different binding partners such as Protocadherin LKC, APC and β2-syntrophin still remains to be investigated. Moreover, specific binding partners or mechanisms are not known for some processes that MAST kinases seem to be involved in, such as hyperproliferation of breast cells induced by MAST1 and MAST2 gene fusions, TLR4-dependent NF-κB activation by MAST3 or chromosome alignment defects in S2 cells due to Dop impairment.

Studies on the single MAST kinase in *Drosophila melanogaster* called *Drop out* might help to model specific MAST kinase functions in a non-redundant background to elucidate a general mechanism of MAST kinase action.

1.5 Drop out function during early embryogenesis

Drop out was first identified in a screen for female sterile mutations on the third chromosome of *Drosophila melanogaster* induced by EMS (Galewsky & Schulz 1992). Embryos with a mutation in one particular gene were shown to undergo abnormal cellularisation. Nuclei in this mutant lose contact to the cortex which led to their exclusion from the forming cells, they did "drop out". Because of this phenotype, the mutant was called *drop out* (*dop*), the specific allele originally analysed was called dop^{1}. In addition to the nuclear phenotype, the cellularisation furrow invaginated to a much lesser extent in the dop^{1} mutant in comparison to the one in *wild type* embryos.

Genetic mapping and DNA sequencing revealed that the gene affected by the mutation is CG6498 encoding for the only MAST kinase homologue represented in *Drosophila melanogaster* (Fig.7) (Hain et al. 2014; Hain 2010)).

In addition to dop^{1}, several other alleles have been previously generated in our lab by EMS mutagenesis and were screened for mutations that failed to complement the maternal lethal phenotype of dop^{1} (Hauer and Müller, unpublished). Some of the identified alleles are shown in Fig.8. They were sequenced by Alistair Langlands and Daniel Hain (Langlands 2012; Hain 2010).

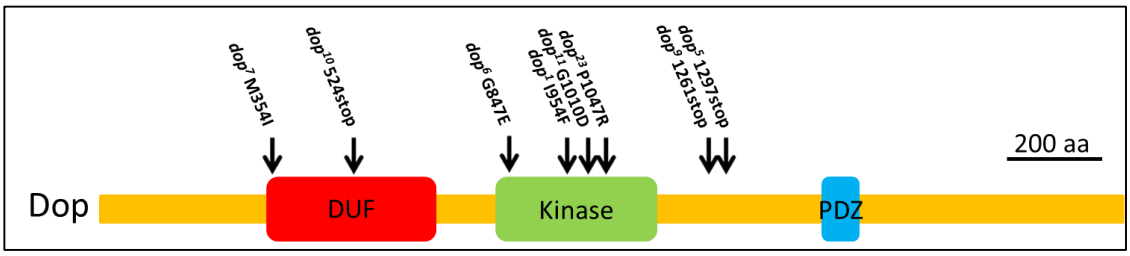

Figure 8 Location and nature of *dop* mutant alleles. The location of the sequenced *dop* mutations are marked by arrows. Modified after (Langlands 2012).

Four of the five missense mutations identified so far are located within the kinase domain of the Dop protein (dop^{1}, dop^{6}, dop^{11} and dop^{23}) indicating the importance of the kinase function for the overall function of the protein. The only identified missense mutation that does not affect the kinase domain is located within the DUF domain of the protein (dop^{7}). This allele suggests that also the DUF domain is important for the function of the Dop protein. Two nonsense

mutations have been identified that introduce a stop codon just amino-terminal of the PDZ domain (*dop*^{5} and *dop*^{9}), Dop protein products would lead to a protein with intact amino-terminus, DUF and kinase domain but deleted PDZ domain and carboxy-terminal sequences. These mutations suggest an important function for the PDZ domain of the protein in addition to the kinase and DUF domain. In addition to the *dop*^{1} allele, an allele that is used in this thesis is the allele *dop*^{10}. This allele introduces a stop codon in the sequence encoding the DUF domain and the translated protein would result in a highly truncated protein, lacking both the kinase and PDZ domain as well as part of the DUF domain. However, a truncated protein could not be detected on western blots using embryo extracts from *dop*^{10} over a chromosomal deficiency (*dop*^{10}/Df(3L)MR15) (Hain 2010). In contrast, a weak protein band was detected using extracts from *dop*^{1} homozygous mutant embryos. These data indicate that *dop*^{1} is a hypomorphic loss-of-function allele, whereas *dop*^{10} represents a protein null and complete loss-of-function allele of *dop*.

Detailed analysis of the *dop*^{1} allele revealed that the mutant embryos have a defect in furrow canal formation (Hain et al. 2014). Furrow canals are normally formed within the first 5 to 8 min of cellularisation (Sokac & Wieschaus 2008b), however, in *dop* mutants no furrow canal was formed 20 min into cellularisation. The protein Slam showed an abnormally broad localisation at the cortex and during membrane invagination in *dop*^{1} mutants (Fig.9) (Meyer et al. 2006).

slam is an early zygotic gene and specifically required for cellularisation in *Drosophila* (Stein et al. 2002). The gene encodes a 135 kDa protein without any identifiable conserved domain apart from a short coiled-coil region and a low similarity to protein phosphatases (Lecuit et al. 2002). No homologous proteins are present for Slam outside of the *Drosophilidae* family. Low levels of Slam are maternally contributed, however, zygotic expression of *slam* after syncytial cycle 10 until late cellularisation was shown as necessary and sufficient for Slam function during *Drosophila* embryogenesis (Stein et al. 2002; Lecuit et al. 2002). Zygotic *slam* mutants display severe defects in membrane invagination during slow and fast phase of cellularisation and

Myosin II as well as RhoGEF2 fail to localise to the furrow canals (Lecuit et al. 2002; Wenzl et al. 2010). Additionally, Slam has a redundant function with Nullo in furrow canal specification and Slam protein localisation to the furrow canal was shown to be dependent on recycling endosome transport (Acharya et al. 2014). Because of the diverse functions of Slam protein during cellularisation, the mislocalisation of Slam that was seen in *dop*^{1} mutants could account for other defects present in these embryos.

In addition to the Slam localisation defect, establishment of different compartments failed during cellularisation in *dop*^{1} embryos. Proteins that usually localise solely to the lateral membrane, such as e.g. Dlg, were also visible at the furrow canal (Fig.9). In addition, RhoA (also called Rho1) which is only found at the furrow canal in *wild type* embryos, displayed extended localisation also at the lateral membrane.

dop^{1} mutant embryos additionally displayed defects in the assembly of epithelial cell junctions. The adherens junction components Arm and E-cadherin failed to focus into BJs as well as AJs during cellularisation and instead remained apical at the cortex (Meyer et al. 2006; Hain et al. 2014). Also the *Drosophila* Par-3 protein Baz, which is required for the establishment of apical AJs, was found to form abnormal aggregates in the cytoplasm and some Baz failed to move apical to the apicolateral membrane where the AJs would form (Fig.9) (Müller & Wieschaus 1996; Harris & Peifer 2004; Hain et al. 2014). All these defects show a specific involvement of Dop in polarity establishment during cellularisation.

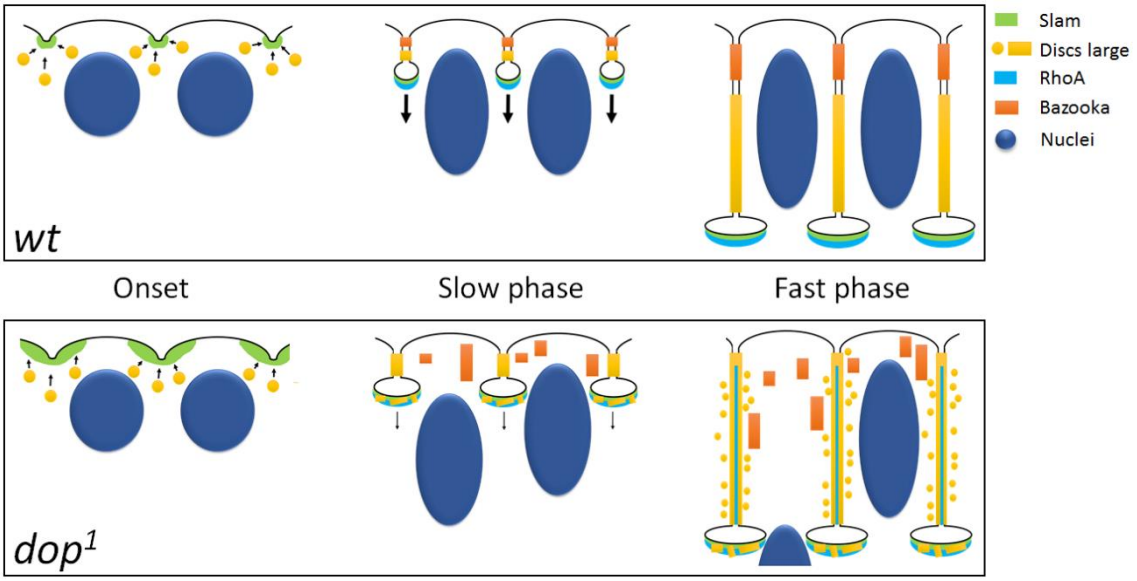

Figure 9 Polarity defects in *dop*^{1} mutant embryos during cellularisation. At onset of cellularisation, Slam protein localises to very distinct internuclear foci to establish the furrow canal in *wild type* embryos. The localisation of Slam is abnormally broadened in *dop*^{1} mutants at this stage and, as a result, the furrow canal is enlarged. During the course of cellularisation, lateral and basal polarity markers localise to distinct membrane regions separated from each other. This separation fails in *dop*^{1} mutants where Dlg spreads into the furrow canal compartment and RhoA localises to the lateral membrane. Also, Baz protein fails to get inserted into the apicolateral membrane region in the mutant but instead accumulates in the apical cytoplasm preventing formation of AJs. Furthermore, lateral membrane proteins show punctate distribution alongside the lateral membrane in *dop*^{1} mutants indicating that they are trapped in vesicles and fail to insert into the membrane. (Hain 2010)

Unfortunately, none of the MAST kinase targets identified in other organisms so far can serve as a good candidate to explain the cellularisation defects seen in *dop* mutants. In the case of the cystic fibrosis factor CFTR, no homologue is known to exist in *Drosophila*. Many of the MAST interaction partners or targets are not expressed during cellularisation as the case for APC, the protocadherin protein Fat and β2-syntrophin (Hayashi et al. 1997; Mahoney et al. 1991; Berkeley Drosophila Genome Project). Other protein targets might be expressed during cellularisation, meaning they are either maternally deposited and/or expressed during early embryogenesis. However, they do not have any reported functions during this stage. Proteins belonging to this category are dTRAF6, the NF-κB homologue Relish and DmNHE3 (Berkeley Drosophila Genome Project). Only the tumour suppressor PTEN (dPTEN in *Drosophila*) was shown to be expressed during cellularisation and to exert a certain function during this process (von Stein et al. 2005). *dPten* mutants showed a delay in posterior membrane formation during cellularisation. However, this defect was likely to be based on an earlier defect in posterior pole cell formation.

Additionally, the PTEN binding site for binding to MAST kinases is not conserved in dPTEN. Thus, it is unlikely that PTEN in flies acts in the same way with Dop as with MAST kinases in humans.

1.5.1 Dependence of Dynein on Dop function

Even though interaction partners of MAST kinases identified in other organisms cannot provide clear candidates for Dop targets during cellularisation, some of the previously identified cellularisation defects point towards an impairment of Dynein-dependent transport.

First, Baz was mislocalised and showed some abnormal basal localisation in *dop*^{1} embryos (Hain et al. 2014). Dynein is required to transport cargoes along microtubules from basal to apical in the early embryo and was shown to be required for Baz transport (Harris & Peifer 2005). An accumulation of Baz at the basal end of microtubules indicate that Dop might affect Dynein transport. Another Dynein-dependent transport process affected in *dop*^{1} mutant embryos is the transport of mRNAs (Bullock et al. 2006; Dix et al. 2013). Specifically, the minus-end directed transport of the apically localising *hairy* mRNA was analysed and found to be significantly impaired in *dop*^{1} mutants during cellularisation (Hain et al. 2014). In addition to impairment of Dynein-dependent transport of Baz protein and mRNA, *dop* mutant embryos fail to undergo Dynein-dependent minus-end transport of lipid droplets during late cellularisation and early gastrulation (Meyer et al. 2006; Gross et al. 2000; Welte 2015). During early cellularisation, Kinesin-1-dependent transport of lipid droplets is up-regulated which results in transport of lipid droplets away from the cortex and the cortical region becomes transparent. This process is called lipid clearing. At the end of cellularisation, Dynein-dependent minus-end transport gets upregulated instead resulting in apical transport of lipid droplets towards the cortex. The caused accumulation of lipid droplets at the cortex leads to a darkening of the cortical area called lipid clouding. This process fails in *dop*^{1} maternally homozygous embryos so that the cortical area stays transparent throughout gastrulation. Even though this defect indicates that Dop affects Dynein-dependent transport, no functional consequences connected to the dynamics of lipid

droplets at this stage are known (Welte 2015). Thus, Dop might affect lipid droplet dynamics at this stage but without any consequences for the following embryo development or viability.

Further support for a function of Dop in Dynein-dependent transport comes from genetic interaction studies and biochemical analysis (Hain et al. 2014; Hain 2010; Langlands 2012). Zygotic double mutants for *dop*^{1} and *short wing*^{1} (*sw*^{1}; mutation allele of the Dynein intermediate chain subunit) as well as *dop*^{1} in combination with *Glued*^{1} (*Gl*^{1}; mutation allele of the Dynactin complex subunit p150/Glued) showed enhanced *sw*^{1} and *dop*^{1} wing phenotypes and *Gl*^{1} eye phenotypes, respectively (Hain et al. 2014). In addition, both mutants enhanced *dop*^{1} membrane invagination defects during cellularisation. These data suggest that Dop might act in the same pathway as Dynein and Dynactin among others involved in membrane invagination.

2D gel electrophoresis using early stage embryo extracts showed a reduction of Dynein intermediate chain (Dic) phosphorylation in *dop*^{1} mutant embryos compared to *wild type*. This suggests that Dop might function in regulating phosphorylation of the Dynein intermediate chain during early embryogenesis. As the intermediate chain has been shown to mediate binding of Dynein to Dynactin, the regulation of this subunit might have important implications for overall Dynein activity (Schroer 2004; Vale 2003).

Another biochemical experiment identified a different Dynein subunit as a potential phosphorylation target of Dop (Langlands 2012). A SILAC screen on embryo extracts from *wild type* and *dop*^{1}/*dop*^{10} mutant embryos undergoing cellularisation was performed. The following mass spectrometry analysis showed a down-regulation of Dynein light intermediate chain (Dlic) phosphorylation in *dop* mutants. Additionally, serine 401 of the Dlic subunit came up as potential phosphorylation site with reduced phosphorylation in *dop* mutants in this experiment. Thus, Dop might affect Dynein function by regulating the phosphorylation state of several of its subunits.

1.6 Aim of the study

The study of Dop function as an *in vivo* model for MAST kinase function might give insights into a mechanism by which MAST kinases act and affect several human diseases. The aim of this PhD study is to analyse the function of Drop out during early cellularisation in *Drosophila* embryos in more detail.

- To understand which is the first requirement of Dop in early embryogenesis, F-actin dynamics are analysed to determine at which stage the first defects occur in *dop* mutants.
- Additionally, defects in maternal complete loss-of-function *dop* mutant embryos are studied to gain insight into the very first process that is affected by the loss of Dop function and to elucidate a possible mechanism by which Dop affects cellularisation.
- Furthermore, Dynein as possible Dop target during early embryogenesis is analysed to test if Dynein can provide a link between Dop impairment and cellularisation defects.

2. Materials and methods

2.1 Materials

2.1.1 Fly strains

Reference strains

Genotype	Description	Donor/origin	Reference
white[1118]	Spontaneous partial deletion of *white*; standard laboratory *wild type* strain	BDSC (BL#3605)	

Table 1 Control line used in this thesis

Mutants

Genotype	Description	Donor/origin	Reference
w[*] ***baz****[815-8] P{w[+mW.hs]=FRT(w[hs])}9-2/****FM7a****; **Sp/CyO***	P-element insertion in the *bazooka* locus on the X-chromosome, balanced over FM7a, second chromosome marked with Sternopleural and balanced with CyO	Hamze Beati	
*w[67c23] P{w[+mC]=lacW}****Dlic[G0065]****/FM7c*	P-element insertion in the *dynein light intermediate chain* locus on the X-chromosome	BDSC (BL# 11696)	(Mische et al. 2008)
y[1] w[*]; ***dop[1]*** *red[1] e[1]/TM6B, Tb[1]*	EMS induced allele of the *drop out* locus on the third chromosome	BDSC (BL# 5242)	(Galewsky & Schulz 1992)
dop[10]*,st,FRT2A/TM3,Sb*	EMS induced allele of the *drop out* locus on the third chromosome	Alistair Langlands	
w; ***ovo[D]FRT2A****/ βTub85[D],ss,e/TM3,Sb*	Dominant female sterile marker allele ovo^D with FRT site or dominant male sterile marker $\beta Tub85^D$ balanced over TM3	BDSC (BL# 2139)	(Chou & Perrimon 1996)

Table 2 Mutant lines used in this thesis

UAS-lines

Genotype	Description	Donor/origin	Reference
*y, w; P{w⁺ p**UASp-wtDlic-linker-GFP**}attP40/CyO*	*wild type* Dlic-GFP under UAS control on the second chromosome	this thesis	
*y, w; P{w⁺ p**UASp-S401DDlic-linker-GFP**}attP40/CyO*	Phospho-mimic S401D mutated Dlic-GFP under UAS control on the second chromosome	this thesis	
*y, w; P{w⁺ p**UASp-S401ADlic-linker-GFP**}attP40/CyO*	Phospho-dead S401A mutated Dlic-GFP under UAS control on the second chromosome	this thesis	
*y, w; P{w⁺ p**UASp-wtDlic-linker-GFP**}attP40/CyO;* ***dop[1], mat-α-Tubulin_VP16[15]Gal4**/TM6B*	*wild type* Dlic-GFP under UAS control on the second chromosome, *drop out [1]* allele on the third chromosome	this thesis	
*y, w; P{w⁺ p**UASp-S401DDlic-linker-GFP**}attP40/CyO;* ***dop[1], mat-α-Tubulin_VP16[15]Gal4**/TM6B*	Phospho-mimic S401D mutated Dlic-GFP under UAS control on the second chromosome, *drop out [1]* allele on the third chromosome	this thesis	
*y, w; P{w⁺ p**UASp-S401ADlic-linker-GFP**}attP40/CyO;* ***dop[1], mat-α-Tubulin_VP16[15]Gal4**/TM6B*	Phospho-dead S401A mutated Dlic-GFP under UAS control on the second chromosome, *drop out [1]* allele on the third chromosome	this thesis	
YFP-ASL; ***UAShDMN**/TSTLR*	Human Dynamitin under UAS control on the third chromosome	Jens Januschke, Dundee, UK	(Januschke et al. 2002)
*w[*]; P{w[+mC]=**UAS-Eb1.GFP**}2/CyO*	EB1-GFP under UAS control on the second chromosome	DGGR (# 109614)	(Rolls et al. 2007)
*w[*]; P{w[+mC]=**UAS-Eb1.GFP**}2/CyO;* ***dop[1]**/TM6B*	EB1-GFP under UAS control on the second chromosome, *drop out [1]* allele on the third chromosome	This thesis	
***UAS:Tubulin-GFP**;;FRTG13 insc^{22}/TSTLR*	Tubulin-GFP under UAS control on the X-chromosome	Jens Januschke, Dundee, UK	

*w[1118];P[w[+], **UAS:Rab11-GFP**]/CyO*	Rab11-GFP under UAS control on the second chromosome	BDSC (BL# 8506)
*w[1118]; P[w[+], **UAS:Rab11-GFP**]/ CyO; **dop[1]**/TM6B*	Rab11-GFP under UAS control on the second chromosome, *drop out [1]* allele on the third chromosome	Daniel Hain

Table 3 UAS effector lines used for protein expression *in situ*

RNAi-lines

Genotype	Description	Donor/origin	Reference
*y[1] sc[*] v[1]; P{y[+t7.7] v[+t1.8]=TRiP.**GL00543**}attP40*	Expression of dsRNA for RNAi of Dhc64C (FBgn0261797) under UAS control, TriP line	BDSC (BL# 36583)	
*y[1] sc[*] v[1]; P{y[+t7.7] v[+t1.8]=TRiP.**HMS01587** } attP2*	Expression of dsRNA for RNAi of Dhc64C (FBgn0261797) under UAS control, TriP line	BDSC (BL# 36698)	

Table 4 RNAi lines used for targeted gene silencing

Gal4 driver lines

Genotype	Description	Donor/origin	Reference
*w; Kr[If]/CyO ; **dop[1], mat-α-Tubulin 15 (rec3)Gal4** / TM6B*	Maternal Gal4 expression under control of the α-Tubulin 15 enhancer and *drop out [1]* allele on the third chromosome	Arno Müller	
*w[1118]; **mat-α-tubulin_VP16[67]Gal4**/CyO*	Maternal Gal4 expression under control of the α-Tubulin 67 enhancer on the second chromosome	Daniel St. Johnston, Cambridge, UK	
*w[1118]; **mat-α-tubulin_VP16[67]Gal4**/CyO; **dop[10]**/TM3, Ser*	Maternal Gal4 expression under control of the α-Tubulin 67 enhancer on the second chromosome, *drop out [10]* allele on the third chromosome	Arno Müller	
*w; **mat-α-tubulin_VP16[67]Gal4**/CyO;*	Maternal Gal4 expression under control of the α-Tubulin 67 and α-Tubulin 67 enhancers on the	Daniel St. Johnston, Cambridge, UK	

mat-α-Tubulin_VP16[15]Gal4*/TM6*	second and third chromosomes	
w[*]; P{w[+m]=**Ubi-GAL4**.U}2/CyO*	Ubiquitous expression of Gal4 under control of the ubiquitin enhancer on the second chromosome	BDSC (BL# 32551)

Table 5 Driver lines used in this thesis

Miscellaneous strains

Genotype	Description	Donor/origin	Reference
y,w, ***hs::FLP****; Sp/CyO;* ***ubi::GFP-FRT2A****/TM6B*	Expression of flippase recombinase under heat shock promoter control on the X-chromosome, construct for ubiquitous expression of GFP coupled to flippase recognition site on the third chromosome	Arno Müller	
*y,w;****sqh::UtrophinGFP****/ CyO*	Recombinant of the actin-binding domain of human Utrophin fused to GFP and expressed under the *spaghetti-squash* promoter	Katja Roeper, Cambridge, UK	(Rauzi et al. 2010)
*y,w;****sqh::UtrophinGFP****/ CyO;* ***dop[1]****/TM6B*	Recombinant of the actin-binding domain of human Utrophin fused to GFP and expressed under the *spaghetti-squash* promoter, *drop out [1]* allele on the third chromosome	this thesis	
w*;****If/CyO****;****MKRS****,Sb/* ***TM6B****,Tb,Hu*	Marker strain with markers and balancers on the first, second and third chromosome	Kevin Johnson, Düsseldorf, Germany	
w[1118]*; In(2LR)****Gla****, wgGla-1 Bc1/****CyO*** *[ftz::lacZ]*	Marker strain with markers and balancers on the first and second chromosome	Tanja Gryzik	
*P{ry[+t7.2]=****hsFLP****}1, y[1] w[1118]; Dr[Mio]/TM3, ry[*] Sb[1]*	Expression of flippase recombinase under heat shock promoter control on the X-chromosome	BDSC (BL# 7)	(Golic et al. 1997)

*P{ry[+t7.2]=**hsFLP**}1, y[1] w[1118]; **dop[10]**,st,FRT2A/TM3,Sb*	Expression of flippase recombinase under heat shock promoter control on the X-chromosome, *drop out [10]* allele on the third chromosome	Arno Müller

Table 6 Lines used for chromosomal balancing, flippase expression and UtrophinGFP expression

2.1.2 Chemicals

Chemical	Donor/distributor
Ciliobrevin D	Jason Swedlow, Dundee, UK (originally Calbiochem, Merck Millipore #250401; concentration of 3000 µM)
Ciliobrevin D	James Chen lab, Stanford, USA (concentration of 7387 µM)
1,4-diazabicyclo[2.2.2]octane (DABCO)	Sigma-Aldrich, St. Louis, USA
Dimethyl sulfoxide (DMSO)	Sigma-Aldrich, St. Louis, USA
6x DNA Gel Loading Dye	Thermo Fisher Scientific, Massachusetts, USA (#R0611)
Fluorescein isothiocyanate-Dextran 500000-Conjugate (FITC-Dextran)	Sigma-Aldrich, St. Louis, USA
Formaldehyde	Sigma-Aldrich, St. Louis, USA
GelRed Nucleic Acid Gel Stain	Biotium (#41003)
GeneRuler 1kb$^+$ DNA Ladder	Thermo Fisher Scientific, Massachusetts, USA (#SM1331)
Glycerol	Sigma-Aldrich, St. Louis, USA
Halocarbon oil 27	Sigma-Aldrich, St. Louis, USA
Heptane	Sigma-Aldrich, St. Louis, USA
Methanol	VWR, Pennsylvania, USA
Mowiol 4-88 (for use 5g dissolved in 20 ml PBS and 10 ml Glycerol)	Sigma-Aldrich, St. Louis, USA
Triton X-100	Sigma-Aldrich, St. Louis, USA

Tween 20	VWR, Pennsylvania, USA

Table 7 Chemicals used in this thesis

2.1.3 Cell lines

Cell line	Antibiotic resistance
E. coli DH5α	no resistance
E. coli XL-1	Tetracycline

Table 8 Cell lines used for cloning

2.1.4 Cloning vectors

Vector	Size	Antibiotic resistance	Purpose	Donor/distributor
pGEX-6P	4984 bp	Ampicillin	original vector with Dlic cloned in	Amersham
pUAST-EBKXN-EGFP	9813 bp	Ampicillin	cloning of Dlic versions to linker-GFP	Tadashi Uemura, Kyoto, Japan (Satoh et al. 2008)
pUASp K10 attb	9537 bp	Ampicillin	somatic and female germline expression *in vivo* under UAS control	Drosophila Gateway collection

Table 9 Cloning vectors used in this thesis

2.1.5 Enzymes

Enzyme	Company	Purpose
Bsu15I (ClaI)	Thermo Fisher Scientific	Test digest
DpnI	Agilent Technologies, QuikChange Lightning Site-Directed Mutagenesis Kit	Template DNA digest after mutagenesis PCR
EcoRI	Thermo Fisher Scientific	Subcloning of Dlic versions into pUAST vector
FastAP	Fermentas	Dephosphorylation of plasmid ends

HpaI (KspAI)	Thermo Fisher Scientific	Test digest
NheI	Thermo Fisher Scientific	Test digest
NotI	Thermo Fisher Scientific	Test digest
Pfu DNA polymerase	Promega	Standard PCR
T4 DNA Ligase	Fermentas, Rapid DNA Ligation Kit	Ligation of PCR products and vector plasmids
XbaI	Thermo Fisher Scientific	Subcloning of Dlic versions into K10 vector

Table 10 Enzymes used for cloning

2.1.6 Oligonucleotides

Name	Sequence (5‘-3‘)	Tm (°C)	Purpose
HS phos-mim for	CAC CAC CGG ACA GAG TGA CCC CAA AAA GAT TGA TCC (36bp)	72.9°C	Mutagenesis of S401 to aspartic acid
HS phos-mim rev	GGA TCA ATC TTT TTG GGG TCA CTC TGT CCG GTG GTG (36bp)	72.9°C	Mutagenesis of S401 to aspartic acid
HS phosdead for	CCA CCG GAC AGA GTG CGC CCA AAA AGA TTG (30bp)	70.9°C	Mutagenesis of S401 to alanine
HS phosdead rev	CAA TCT TTT TGG GCG CAC TCT GTC CGG TGG (30bp)	70.9°C	Mutagenesis of S401 to alanine
Dlic-EcoRI for	GTC TAG AAT TCA TGG CGA TGA ACA GTG GGA C (31bp)	68.2°C	Introduction of EcoRI site to clone Dlic into pUAST vector
new Dlic rev	CAT ATG AAT TCA ACA CTC ACT CTG CGA CAT GTC AAT CTC (39bp)	69.5°C	Introduction of EcoRI site to clone Dlic into pUAST vector
HS XbaI for	CCT CTA GAT TAC TTG TAC AGC TCG TCC (27bp)	65.0°C	Introduction of XbaI site to clone Dlic into K10 vector
HS XbaI rev	CAT CTA GAA TGG CGA TGA ACA GTG GG (26bp)	64.8°C	Introduction of XbaI site to clone Dlic into K10 vector
pUAST reverse new	CTT GCT CAC CAT GCT AGA ACC T (22bp)	60.3°C	test primer for sequencing of Dlic 3‘
Dlic SDM for	GTC GCA GAG TGA GTG TTC AAT TCG TTA ACA GAT C (34bp)	64°C	Mutagenesis of first stop codon

Dlic SDM rev	GAT CTG TTA ACG AAT TGA ACA CTC ACT CTG CGA C (34bp)	64°C	Mutagenesis of first stop codon
Dlic2 SDM for	GTG AGT GTT CAA TTC GTT TAC AGA TCT TGG TAC CAA CTC GAG GCG G (46bp)	70°C	Mutagenesis of second and third stop codon
Dlic2 SDM rev	CCG CCT CGA GTT GGT ACC AAG ATC TGT AAA CGA ATT GAA CAC TCA C (46bp)	70°C	Mutagenesis of second and third stop codon

Table 11 Oligonucleotides used in this thesis

2.1.7 Antibodies

Primary antibodies

Antigen	Host species	Concentration	Donor/distributor	Reference
βTubulin	mouse	1:50	DSHB	E7
Centrosomin (Cnn)	rabbit	1:500	Eric Griffis, Dundee, UK	(Vaizel-Ohayon & Schejter 1999)
Dynein heavy chain (Dhc)	mouse	1:100	DSHB	2C11-2
Epidermal growth factor receptor pathway substrate clone 15 (Eps15)	guinea pig	1:300	Hugo Bellen, Houston, USA	GP59, (Koh et al. 2007)
Green fluorescent protein (GFP)	rabbit	1:250	Invitrogen	
golgi protein 120 (gp120)	mouse	1:500	Calbiochem	no longer available
Kinesin heavy chain (Khc)	rabbit	1:100	Cytoskeleton	
Lava lamp (Lva)	rabbit	1:1000	John Sisson, Texas, USA	(Sisson et al. 2000)
Neurotactin (Nrt)	mouse	1:5	DSHB	BP 106
Nuclear fallout (Nuf)	rabbit	1:250	William Sullivan, Santa Cruz, California, USA	(Rothwell et al. 1998)

Slow-as-molasses (Slam)	rabbit	1:5000	Jörg Großhans, Göttingen, Germany	(Stein et al. 2002)

Table 12 Primary antibodies used in this thesis

Secondary antibodies

Anti-species	Conjugate	Concentration	Distributor
guinea pig	Cy3	1:250	Stratech
guinea pig	Alexa647	1:250	Invitrogen
mouse	Alexa488	1:250	Invitrogen
mouse	Cy3	1:250	Stratech
mouse	Alexa647	1:250	Invitrogen
rabbit	Alexa488	1:250	Invitrogen
rabbit	Cy3	1:250	Stratech
rabbit	Alexa647	1:250	Invitrogen

Table 13 Secondary antibodies used in this thesis

2.1.8 Fluorescent dyes

Dye	Description	Concentration	Distributor
4',6-Diamidino-2-phenylindole dihydrochloride (DAPI)	DNA-binding probe; forms fluorescent complex (excitation at 340 nm; emission at 488 nm)	1:1000 (stock solution: 1 mg/ml in ddH_2O)	Sigma-Aldrich, St. Louis, USA
Phalloidin-Alexa594	fluorophore-coupled phalloidin for detection of filamentous actin (excitation at 581 nm; emission at 609 nm)	1:40 (stock solution: 200 units/ml in methanol)	Invitrogen, Oregon, USA

Table 14 Fluorescent dyes used in this thesis

2.1.9 Commonly used buffers and media

Buffer/media	Composition
PBS	137 mM NaCl 2.7 mM KCl 10 mM Na_2HPO_4 1.76 mM KH_2PO_4 pH 7.4
PBT	PBS 0.1 % Tween 20
PBTx	PBS 0.5 % Triton X-100
TAE	40 mM Tris-Acetate 20 mM NaAcetate 2 mM EDTA pH 8.3
Standard corn meal agar medium	356 g corn grist 47.5 g soy flour 84 g dry yeast 225 g malt extract 75 ml 10 % Nipagin 22.5 ml propionic acid 28 g agar 200 g sugar beet molasses 4.9 l dH_2O
Apple agar plate medium	40 g agar 340 ml apple juice (100 %) 17 g sucrose 30 ml Nipagin (10 %) (100 g Nipagin were dissolved in 1 l 70% Ethanol) in 1 l H_2O
LB medium	1 % Trypton 0.5 % yeast extract 1 % NaCl

Table 15 Buffers and media used in this thesis

2.1.10 Instruments

Instrument	Company	Purpose
Centrifuge 5424	Eppendorf	Different cloning steps

Centrifuge Avanti J-25	Beckman	Midi-scale plasmid preparation
Centrifuge Rotina 380 R	Hettich Zentrifugen	Midi-scale plasmid preparation
Microscope Confocal 710	Zeiss	Microscopy of embryo and ovary stainings
Microscope Confocal SP8	Leica	Fluorescence microscopy of stainings and live-imaging
Microscope BX61 with Orca-ER Digital Camera (Hamamatsu)	Olympus	Bright field live-imaging
Microscope Confocal spinning disk CSU-X1 system	Yokogawa	Fluorescence live-imaging
Microscope Axiovert 135 M	Zeiss	Ciliobrevin injections
Microscope IX70 with CoolSNAP HQ2 CCD Camera (Photometrics)	Olympus	Bright field and fluorescence imaging of injected embryos
BioPhotometer	Eppendorf	DNA concentration measurement
Mastercycler gradient	Eppendorf	Standard and mutagenesis PCR
GenoView and GenoSmart gel documentation system	VWR	Imaging and documentation agarose gels
Visi-Blue Transilluminator	UVP	Excision of DNA from agarose gels
FemtoJet microinjector	Eppendorf	Ciliobrevin injections
InjectMan NI 2 micromanipulator	Eppendorf	Ciliobrevin injections

Table 16 Instruments used in this thesis

2.1.11 Software

Software	Software developer	Purpose
ApE A plasmid editor	M. Wayne Davis, University of Utah	DNA sequence analysis
Illustrator CS5.1	Adobe	Figure labelling
ImageJ/Fiji	Wayne Rasband, National Institutes of Health, Maryland, USA	Image analysis and processing, Plugins: Multiple Kymograph written by J. Rietdorf (FMI Basel) and A. Seitz (EMBL Heidelberg)

Jalview Version 2	(Waterhouse et al. 2009)	Conservation analysis
OMERO	Open Microscopy Environment	Data storage, data visualisation, figure construction
Photoshop CS5.1	Adobe	Figure labelling
SigmaPlot 12.3	Systat Software Inc	Statistical analysis
Volocity	Perkin Elmer	Image acquisition and visualisation

Table 17 Software used in this thesis

2.2 Methods

2.2.1 Fly maintenance and genetics

2.2.1.1 Stock keeping

Fly stocks were kept on standard corn meal agar medium and raised at room temperature (22°C) or at 25°C in small plastic tubes. Selection of specific animals for crossings was accomplished using CO_2 for anaesthetisation.

2.2.1.2 Collection of embryos

To collect embryos for immunostainings, live imaging or hatching rate determination, parental flies were kept in embryo collection cages. The bottom opening was closed by an embryo collection plate with apple juice agar and additional yeast for stimulation.

2.2.1.3 Generation and balancing of transgenic fly strains

The production of transgenic fly lines is based on the introduction of attP sites in the *Drosophila* genome by P-element insertion. The attP site allows the targeted insertion of a plasmid carrying an attB site. By injecting the plasmid into a phiC31 integrase-expressing germ line, the enzyme

recombines both attP and attB sites and integrates the plasmid DNA permanently into the progenies genome (Bischof et al. 2007). In this thesis, *wild type* and phospho-mutant versions of *dynein light intermediate chain* (*dlic*) fused to GFP were cloned into a K10 vector with an Upstream Activating Sequence (UAS) controlling Dlic-GFP expression as well as an attB site for targeted genome insertion (see Fig.10). The injection of the germ line was performed by the Fly Facility, Department of Genetics at the University of Cambridge. Integration was targeted to the second chromosome at position 25C6. After raising the F1 generation, the flies were sent back to our lab. The *white* marker was used to identify successful integrations and flies with reddish eyes were crossed to *w⁻; Gla/CyO* flies to balance the integration with CyO on the second chromosome.

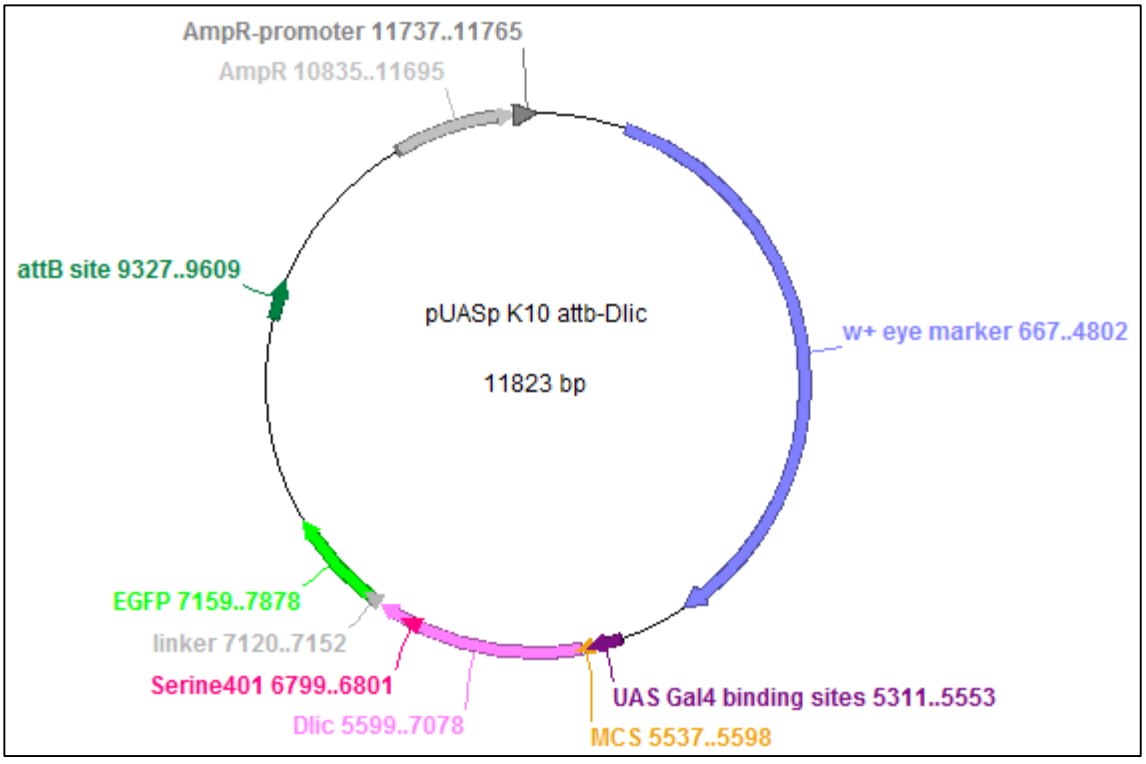

Figure 10 pUASp K10 attb vector with Dlic insert.

2.2.1.4 Creation of germ line clones

Embryos that lack the maternal contribution of a gene that is homozygous lethal can be produced by the induction of germ line clones (or germline mosaics) (Blair 2003). Three

constructs are required in combination. A site-specific recombinase called Flippase (FLP) under control of a heat-shock promoter induces mitotic recombination of two FRT (Flippase recombination target) sites in the genome of proliferating cells (Golic & Lindquist 1989). To create germ cells homozygous for dop^{10}, flies were crossed together to create progeny that carry the dop^{10} allele with FRT site on one chromosome arm of chromosome 3 and an ovo^{D} allele (a dominant female sterile marker which induces lethality of germ cells) with FRT site on the other chromosome arm. By shifting third instar larvae of this progeny to 37°C, FLP expression was activated. FLP creates a break in FRT sites of metaphase chromosomes which may lead to mitotic cross-over between the FRT sites. If such a cross-over occurs in a germ cell during development a possible result is the formation of homozygous mutant ovaries. Third instar larvae have been chosen for mitotic cross-over induction since germ cell precursors do proliferate during this stage. FLP expression was induced on two consecutive days for 2 hours each at 37°C. Eggs produced by females deriving from these larvae are exclusively homozygous for dop^{10} since germ cells either homozygous or heterozygous for ovo^{D} do not produce eggs (Chou & Perrimon 1996). Fig.11 shows the cross performed to produce germ line clone dop^{10} embryos.

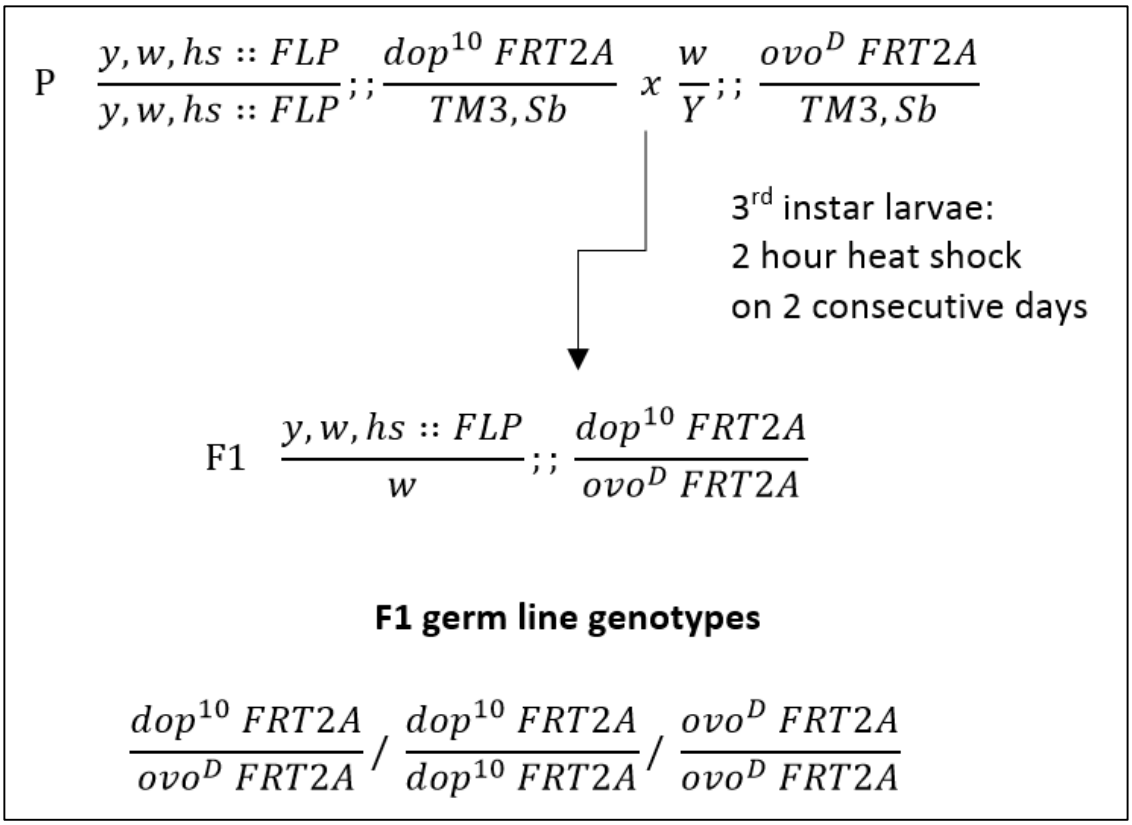

Figure 11 Cross performed to produce germ line clone *dop^{10}* embryos. Females carrying the flippase gene under heat-shock promoter control on the X and the homozygous lethal mutation *dop^{10}* and a FRT site on the third chromosome were crossed to males carrying the *ovo^{D}* female sterile allele and a FRT site on the third chromosome. 3rd instar larvae progeny were heat-shocked to activate FLP expression on 2 consecutive days for 2 hours at 37°C. Females carrying both FRT sites developing from the heat-shocked larvae were separated, crossed to brothers and their progeny further analysed.

2.2.1.5 Generation of follicle clones

Patches of follicle cells homozygous for *dop^{10}* in an egg chamber heterozygous *dop^{10}* can be created similar to creation of germ line clones (Harrison & Perrimon 1993; Horne-Badovinac & Bilder 2005; Blair 2003). Also for follicle clone creation, a *flippase* gene under heat-shock promoter control is required to induce mitotic recombination of two FRT sites (Golic & Lindquist 1989). Flies were crossed together to create progeny that carry the *dop^{10}* allele with FRT site on one chromosome arm of chromosome 3 and, in this experiment, a GFP marker gene under ubiquitin promoter control with FRT site on the other chromosome arm. Adult females were shifted to 37°C to induce mitotic recombination between the FRT sites during egg chamber development. Three types of follicle cells are generated by this method: 1. Follicle cells in which

no mitotic recombination took place (expression of GFP leads to green cells) and follicle cells in which mitotic recombination took place and the progeny did inherit 2. both *dop*^{10} alleles (homozygous for the mutation, no GFP expression) or 3. both *gfp* genes (GFP expression stronger in these cells than in the ones without induced recombination).

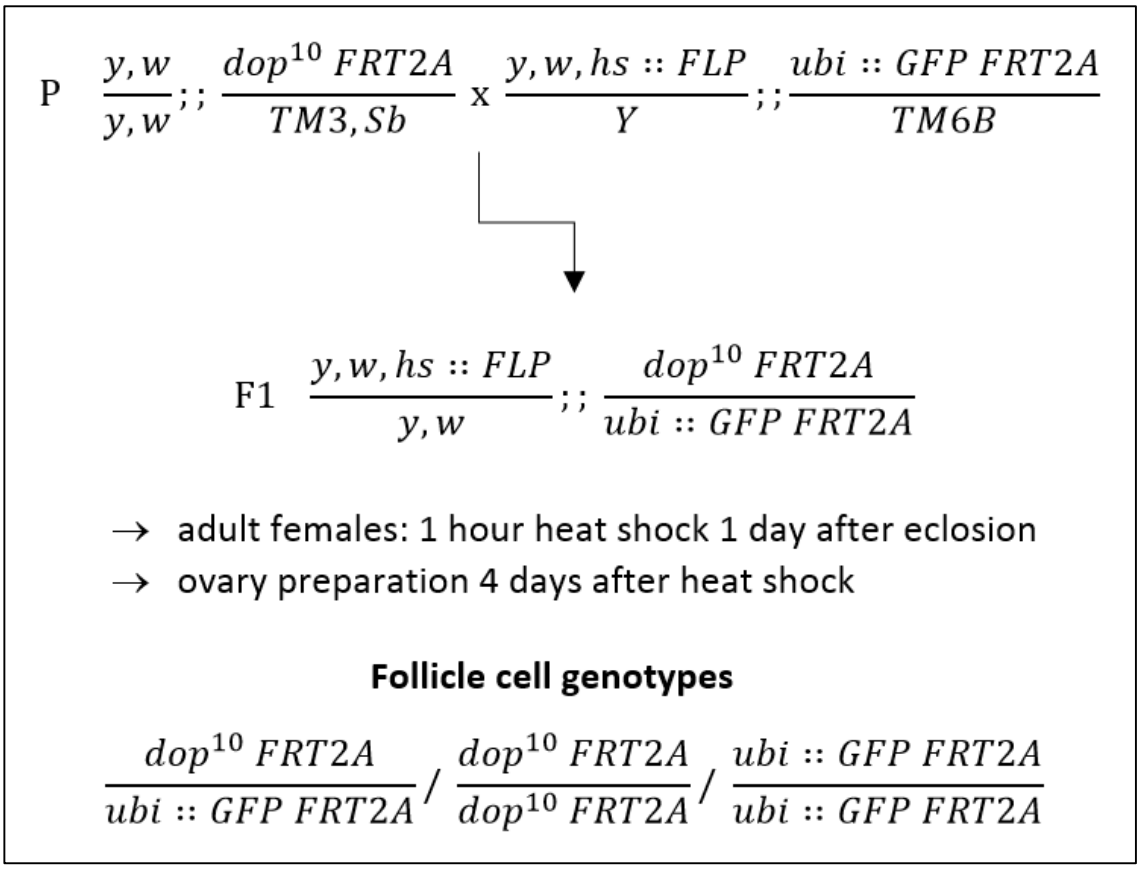

Figure 12 Cross performed to produce follicle cell clones homozygous for *dop*^{10}. Males carrying the flippase gene under heat-shock promoter control on the X and a *gfp* gene under control of an ubiquitin promoter and a FRT site on the third chromosome were crossed to females carrying the homozygous lethal mutation *dop*^{10} and a FRT site on the third chromosome. Adult females carrying the flippase gene, the *dop*^{10} mutation and the *gfp* gene were heat-shocked to activate FLP expression after one day of eclosion for 1 hour at 37°C and crossed to brothers. Ovaries of these females were prepared after 4 days.

2.2.1.6 The UAS/Gal4 system

The Gal4/UAS system enables the targeted temporal and spatial control of gene expression (Brand & Perrimon 1993). In this thesis, the system was used for targeted gene expression of GFP fusion proteins and induction of transcriptional gene silencing using RNA interference

(RNAi). All Gal4 driver, UAS effector and UAS-RNAi lines are listed in the materials section of this thesis.

2.2.1.7 Hatching rate determination

Embryos were collected over night and afterwards transferred and lined up onto fresh apple agar plates. Hatching rates determination was repeated at least three times with maximal 100 embryos of each line. 2 to 3 days after keeping the embryos at the respective temperatures, unhatched and hatched embryos were counted and the percentage calculated as follows: $\frac{hatched\ embryos}{total\ number\ of\ embryos} x100.$

2.2.1.8 Live imaging of protein dynamics and cellularisation processes in embryos

In order to image dynamics of GFP fusion proteins, embryos were dechorionated by bleach and staged in halocarbon oil. Embryos in syncytial cell cycles 10-13 were selected and stuck with heptane glue to a "FluoroDish" (WPI, FD35-100) and covered with halocarbon oil. Different microscopes have been used in this thesis to image GFP fusion proteins (see 2.1.10 Instruments).

For live imaging of membrane growth during cellularisation, embryos in syncytial cell cycles 10-13 were selected in halocarbon oil under a dissection microscope. Afterwards, the embryos were mounted in Halocarbon oil with a cover slip on top and using two cover slips as spacer. A BX61 microscope with Orca-ER Digital Camera was used.

2.2.1.9 Ciliobrevin D injections into embryos

white^{1118} embryos were collected for 10 to 15 min and aged for another hour at 25°C. Afterwards, embryos were dechorionated and aligned on an apple agar plate. Part of the fringe

of a “FluoroDish” (WPI) was removed to create a gap for the injection needle (Femtotips II, Eppendorf #930000043). Embryos were stuck to the dish with heptane glue in such a way that the embryo posterior pole is facing the gap. To prevent embryos from exploding during injection, embryos were dried for 15 to 20 min at room temperature before covering with Halocarbon oil. During the drying time, the needle was prepared. Ciliobrevin D (stock of 7386.65 µM) in a 1:1 mixture with FITC-Dextran was spun down for 1 min to get rid of undissolved particles in the supernatant. Then, microinjection needles were filled with 3 µl of the supernatant. Embryos were injected with differing pressure at a microscope using a FemtoJet microinjector and an InjectMan NI 2 micromanipulator. Afterwards, successfully injected embryos were imaged at an IX70 microscope for 3 hours with a time interval of 20 sec.

2.2.2 Immuno staining techniques

2.2.2.1 Standard fixation of embryos

To collect embryos for fixation at onset of cellularisation, eggs were collected for 1 hour and aged for 1.5 hours at 25°C. The collected embryos were transferred into a collection net, rinsed with water to remove remaining yeast and dechorionated in 100% bleach. To remove the bleach, embryos were washed again and transferred into glass vials with 5 ml 4% formaldehyde in PBS and 5 ml heptane. Embryos were fixed at room temperature for 25 min on a shaker. Afterwards, the bottom formaldehyde phase was removed and replaced by 5 ml methanol. Devitellinisation of the embryos took place by vigorously shaking the vials for 20 sec. Embryos that sunk down into the methanol phase were transferred into a reaction tube and washed three times with methanol before used for immunostaining or stored at -20°C.

2.2.2.2 Methanol-free fixation for phalloidin stainings of embryos

As for the standard fixation, embryos were dechorionised in bleach before the transfer into glass vials. The fixative for phalloidin staining contained 5 ml of 18% formaldehyde final concentration in PBS and 5 ml heptane. Embryos were fixed for 30 min under agitation. Afterwards, the bottom formaldehyde phase was discarded. For manual devitellinisation, embryos were fixed on a microscope slide on a double-faced adhesive tape. A drop of heptane with embryos was pipetted on the tape and the heptane was allowed to dry. To protect the embryos from running dry, they were wetted with PBT. Embryos were liberated from their vitelline membrane by using the tip of a syringe to break up the membrane and pushing the embryos out. The devitellinised embryos were transferred into a reaction tube with PBT, washed and subsequently stained with phalloidin o/N at 4°C.

2.2.2.3 Immunofluorescence staining of embryos

In order to visualise the presence of specific proteins in embryonic tissue, embryos were stained using specific antibodies. Every step was performed on a shaker. Methanol was replaced by PBT and embryos washed three times for 15 min at room temperature. Unspecific binding sites were saturated by incubating the embryos for at least 1 hour in 10% donkey serum in PBT. The epitope specific primary antibody was diluted in 350 µl PBT and 10% donkey serum with the embryos incubated o/N at 4°C. Subsequently, the primary antibody was removed off the embryos, followed by at least four washing steps in PBT and incubated with the fluorophore-coupled secondary antibody at room temperature for 2 hours. In the following, embryos were stained with DAPI for 10 min, washed at least four times for 15 min and embedded on a microscope slide with Mowiol and DABCO.

2.2.2.4 Preparation, fixation and staining of ovaries

Females of the respective fly lines were anaesthetised and killed by removing their heads. The abdomen was opened by tweezers and the ovaries isolated and spread. Afterwards, ovaries were fixed in pre-cooled 4% formaldehyde in PBS on ice for 15 min. After the fixation, formaldehyde was replaced by PBT and ovaries washed three times for 10 min. For phalloidin staining, ovaries were immediately mixed with phalloidin in PBT and 10% donkey serum and incubated o/N at 4°C. To stain with antibodies, ovaries were blocked after the washing steps with PBTx and 10% donkey serum for at least 3 hours before primary antibody was applied. Further staining followed the same protocol as embryo stainings (see section 1.1.2.3.).

2.2.3 Molecular biology

2.2.3.1 Site-directed mutagenesis PCR

To perform site-directed mutagenesis on *dynein light intermediate chain* Serine 401, the QuikChange Lightning Site-Directed Mutagenesis Kit (Agilent Technologies, #210519) was used. Reactions containing 12.5 pmol mutagenesis-oligonucleotides and 116.5 ng template DNA (Dlic in pGEX-6P) were performed according to the protocol of the manufacturer. The final volume was set to 50 µl in all reactions. Table 18 shows the PCR parameters used for the site-directed mutagenesis PCR for phospho-mimic (S401D) and non-phosphorylatable (S401A) versions of Serine401 in Dlic.

Lid temperature: 112°C			
	Cycles	Temperature	Time
Initial denaturation		95°C	2 min
Denaturation	18	95°C	30 sec
Annealing		60°C	30 sec
Elongation		68°C	4 min 20 sec
Final elongation		68°C	5 min
	storage at	10°C	

Table 18 PCR parameters used for site-directed mutagenesis PCR

After each PCR reaction, 2 µl of DpnI enzyme provided by the kit were added to the reaction and incubated for 1 hour at 37°C to digest methylated template DNA.

2.2.3.2 PCR

Polymerase chain reactions (PCR) were performed to create specific enzyme restriction sites to the *dynein light intermediate chain* constructs for subcloning into another vector. The reactions were performed in a final volume of 40-50 µl containing 50-100 pmol oligonucleotides and 80-240 ng template DNA. Table 19 shows the standard PCR parameters used for the PCR reactions.

Lid temperature: 105°C			
	Cycles	Temperature	Time
Initial denaturation		95°C	2 min
Denaturation	34	95°C	30 sec
Annealing		58-65°C	1 min
Elongation		72°C	1 min/kb
Final elongation		72°C	5 min
	storage at	4°C	

Table 19 Parameters used for PCR reactions in this thesis

2.2.3.3 Restriction of plasmid DNA and PCR fragments

For analytical restriction reactions, 0.5 µg of DNA was digested by 5 U of enzyme in a volume of 20 µl for 2 hours at 37°C. For cloning purposes, the restriction reactions were scaled up to 5 µg plasmid DNA and 10 µg insert DNA. After the restrictions, enzymes were heat inactivated at enzyme-specific temperatures for 30 min.

2.2.3.4 Agarose gel electrophoresis

DNA PCR products or restriction products were separated according to their length by conventional agarose gel electrophoresis. 1% horizontal agarose gels in TAE buffer were used to separate DNA fragments mixed with 6x DNA Gel Loading Dye. Gels were run at 100 V for 30-40 min. DNA bands were visualised by 3 µl GelRed mixed to the gel and on a GenoView and GenoSmart gel documentation system using UV light. The length of each DNA fragment was estimated by comparison to a GeneRuler 1kb^{+} DNA Ladder.

2.2.3.5 Isolation of DNA fragments from agarose gels

To isolate DNA fragments of a certain size or to clean-up PCR reactions, DNA fragments were separated on an agarose gel. The DNA bands of interest were excised from the gel using an UV transilluminator and a scalpel and placed into a reaction tube. The DNA fragments were eluted and separated from the gel using the Wizard SV Gel and PCR Clean-Up System (Promega; #A9281) following the manufacturer's protocol.

2.2.3.6 Ligation of PCR fragments into plasmid vectors

For ligation of linearised and dephosphorylated plasmids with PCR fragments, the Rapid DNA Ligation Kit (Fermentas #K1422) was used. 100 ng of vector DNA was set into the ligation

reaction together with Insert DNA in either 1:3 or 1:6 molar excess over vector. 5 U of T4 DNA Ligase were added to the reaction with a total volume of 20 µl. The ligation mixture was incubated for 2 hours at 37°C.

2.2.3.7 Heat shock transformation of DNA into *E. coli* cells

Chemical competent cells were taken out of a -80°C freezer and thawed on ice. 45 µl for each sample were aliquoted into pre-chilled 14-ml BD Falcon polypropylene round-bottom tubes. 2-3 µl of DNA were gently mixed with the cells and the reaction incubated for 30 min on ice. 0.5 ml LB medium per reaction were pre-heated in a water bath to 42°C. After the 30 min incubation time, the reaction mix was heat-pulsed in the water bath at 42°C for 30 seconds and subsequently chilled on ice for 2 min. Pre-heated 0.5 ml LB medium was added to each reaction and the tubes incubated at 37°C for 1 hour shaking at 225-250 rpm. Afterwards, different volumes of cells in solution were plated on LB Ampicillin selective medium plates and grown o/N at 37°C.

2.2.3.8 Cultivation of *E. coli*

Liquid cultures of *E. coli* strains were grown in Luria-Bertani (LB) medium at 37°C. For bacteria selection, ampicillin was added to the medium to a final concentration of 100 µg/ml. Bacteria colonies were grown on LB agar plates containing 2% agar.

2.2.3.9 Plasmid preparation (mini scale)

To isolate plasmid DNA from cells, single colonies from over-night plates were picked and transferred into 3 ml of LB selection medium (Ampicillin 1:500 concentration). The culture was grown over night at 37°C on a shaker. Plasmid mini preparation from this culture was performed using the QIAprep Spin Miniprep Kit (QIAGEN #27106) following the manufacturer's instructions.

2.2.3.10Plasmid preparation (midi scale)

To perform a plasmid midi-preparation, 3 ml of LB selection medium (Ampicillin 1:500 concentration) were inoculated with single colonies and grown over night at 37°C on a shaker. 150 µl of this pre-culture was transferred into 75 ml of LB selection medium and again grown over night at 37°C on a shaker. Plasmid midi preparation from this culture was performed using the QIAGEN Plasmid Midiprep Kit (QIAGEN #12143) following the manufacturer's instructions.

2.2.3.11Spectrophotometer-measurement of DNA concentration

DNA concentrations were measured using a spectrophotometer at the wavelength of λ=260nm (light absorbance of nucleic acid). 1 µl of DNA sample was diluted in 99 µl dH_20 and measurements were taken against a blank (100 µl dH_20). Values were given in ng/µl.

3. Results

3.1 Part 1: Identification of the requirement of maternal *drop out* function

Introduction

The maternal effect mutation *drop out* (*dop*) was first identified for its effects on cellularisation of *Drosophila* embryos, leading to embryonic lethality (Galewsky & Schulz 1992). Previous work showed that hypomorphic alleles of *dop* disturb cortical membrane compartmentalisation by affecting the localisation of specific polarity proteins (Hain et al. 2014). Furthermore, *dop* affects normal furrow canal formation and focussed localisation of furrow canal proteins and F-actin at internuclear sites. The gene *dop* has been mapped to the *CG6498* locus and encodes the single *Drosophila* homolog of microtubule-associated serine/threonine (MAST) kinase family. Even though MAST kinases are implicated in several human diseases, MAST kinase function is poorly understood on the cellular and molecular level (Labbé et al. 2008; Loh et al. 2008; Robinson et al. 2011). Previous studies suggest that Dop function is implicated in Dynein-dependent transport and in phosphorylation control of two Dynein subunits, Dynein light chain and Dynein light intermediate chain (Hain et al. 2014; Langlands 2012). However, all the phenotypes observed with direct implication on Dynein function (lipid droplet transport, mRNA transport, Bazooka localisation, genetic interactions with *short wing* and *Glued*) taken together cannot explain the comprehensive defects seen during cellularisation in *dop* mutants. Either Dynein regulates more processes than the previously shown ones to affect cellularisation or other cellular events are affected by Dop leading to cellularisation phenotypes in *dop* mutants.

One cellular process that could lead to the observed cellularisation defects in *dop* mutants could affect the regulation of F-actin dynamics. As outlined in the introduction, F-actin fulfils many different tasks during cellularisation and is essential for membrane invagination. It is involved in stabilising the cortex and specific cortical structures like the furrow canal (Sokac & Wieschaus 2008b; Foe & Alberts 1983; Edgar et al. 1987), it is required for endosomal trafficking (Lee &

Harris 2014; Lee & Harris 2013; Sokac & Wieschaus 2008a) and it was shown to interact with microtubules, possibly anchoring them to the cortex (Foe et al. 2000).

F-actin localisation was previously examined in fixed embryos obtained from *dop*^{1} homozygous mutant mothers (Hain et al. 2014). In these mutant embryos, a high amount of F-actin stays at the cortex and the lateral membranes throughout cellularisation. Additionally, F-actin does not focus into distinct internuclear foci where the furrow canal should form but stays broad at the tip of the invaginating membrane, leaving no distinct space for the nuclei. These data clearly show that F-actin is not localising properly to the furrow canal compartment during cellularisation. However, the cause of this defect is not known, in part, because no information about the dynamics and the timing of F-actin mislocalisation has been available. Imaging F-actin dynamics in a living embryo during syncytial divisions and cellularisation could provide the information about when F-actin starts to mislocalise in *dop* mutants and how the defect is emerging, which then in turn could give a hint on the molecular function of Dop.

3.1.1 Embryos derived from *dop* mutant mothers fail to establish actin rich furrow canals in cellularisation

The F-actin network is a central component of cellularisation and its malformation could lead to the mislocalisation of other proteins similar to what was shown for *dop*^{1} mutants. In order to investigate whether F-actin is defective and to visualise F-actin dynamics in *dop* mutants, an Utrophin-GFP construct driven by the *spaghetti squash* (*sqh*) promoter was used for live-imaging. The *sqh* promoter drives expression maternally as well as zygotically and ubiquitously throughout embryogenesis (Karess et al. 1991). Utrophin is an actin binding protein required to link the intracellular actin cytoskeleton to the extracellular matrix (Tinsley et al. 1994; Zuellig et al. 2011). In this construct, the actin-binding domain (~30 kDa) of the large Utrophin protein (395 kDa) has been fused to eGFP (Moores et al. 2000; Rauzi et al. 2010). It has been demonstrated that the actin-binding domain binds to F-actin without stabilising it and without

interfering with F-actin-dependent processes (Burkel et al. 2007). Live imaging of this construct in embryos during cellularisation was used to test whether actin network formation is affected in *dop* mutants (Fig.13).

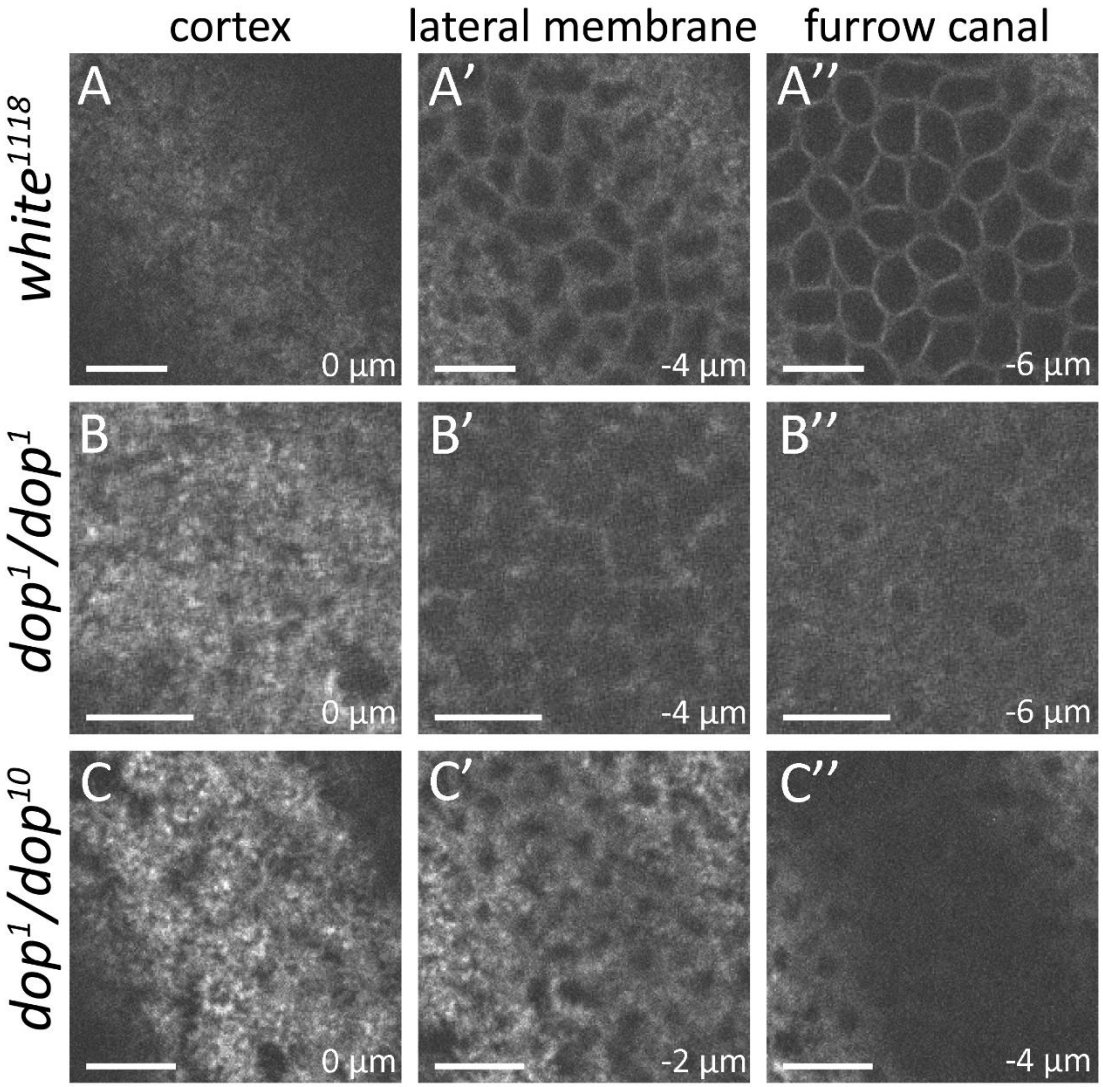

Figure 13 F-actin fails to localise to furrow canals and lateral membrane in hypomorphic *dop* mutants. Images taken from time lapse videos on embryos with a *sqh-Utrophin-GFP* construct 50 min after onset of cellularisation and 75 min after S-phase of cell cycle 13. Cell cycle 13 S-phase was determined by the last cap structure formation prior to cellularisation. Three different z-levels for *wild type* (A-A''), homozygous dop^1 (B-B'') and dop^1/dop^{10} (C-C'') embryos are depicted showing the cortex (A, B, C), the lateral membrane (A', B', C') and the level of the furrow canal (A'', B'', C''). The depth of the z-plane in respect to the cortex is indicated. (Penetrance of phenotype in both *dop* mutants: 100%; $white^{1118}$ n = 16, dop^1/dop^1 n = 6, dop^1/dop^{10} n = 8) Scale bars represent 10 µm.

During late stages of cellularisation, the F-actin network is spread over the cortex of *wild type* and dop^1 homozygous and dop^1/dop^{10} hemizygous embryos (Fig.13 A, B, C). This F-actin structure emerged from broadening actin caps at onset of cellularisation and is present throughout the

cellularisation process not only in *wild type* but also in mutant embryos. During membrane invagination, F-actin accumulates in a distinct honeycomb-like pattern at the furrow canal (Fig.13 A'') as well as at the lateral membrane (Fig.13 A') in *wild type* embryos. However, in both mutants the F-actin network is highly broadened at the furrow canal (Fig.13 B'', C'') and also along the forming lateral membrane (Fig.13 B', C'). This demonstrates a strong defect in focussing of the F-actin network during furrow canal invagination in *dop* mutants. Moreover, in homozygous dop^{1} mutants and dop^{1}/dop^{10} mutants differences in Utrophin-GFP signal depth can be seen. 50 minutes after cellularisation onset, the Utrophin-GFP signal in dop^{1} mutants reached a depth of 6 µm similar to *wild type* (Fig.13 A'', B''). However, in dop^{1}/dop^{10} mutants the signal stays right below the cortex at a depth of 2 µm and no lateral membrane formation occurs at all (Fig.13 C', C''). This indicates a difference in membrane growth between the dop^{1} homozygous and the stronger dop^{1}/dop^{10} transheterozygous mutants.

3.1.2 Embryos derived from *dop* mutant mothers exhibit defects in F-actin network formation during syncytial divisions

Homozygous dop^{1} mutants and hemizygous dop^{1}/dop^{10} mutants both show severe defects in F-actin localisation during cellularisation. However, Dop protein is already present during syncytial division stages during which F-actin also plays a fundamental role (Hain 2010; Foe et al. 2000). Earlier studies suggested that syncytial divisions were overall normal in embryos maternally homozygous for dop^{1} (Galewsky & Schulz 1992). However, nothing is known about F-actin network formation during these stages in *dop* mutant embryos. In order to address whether Dop affects F-actin localisation in syncytial divisions as well as during cellularisation, Utrophin-GFP localisation during the last syncytial divisions in *wild type*, dop^{1} homozygous and dop^{1}/dop^{10} hemizygous embryos was analysed (Fig.14).

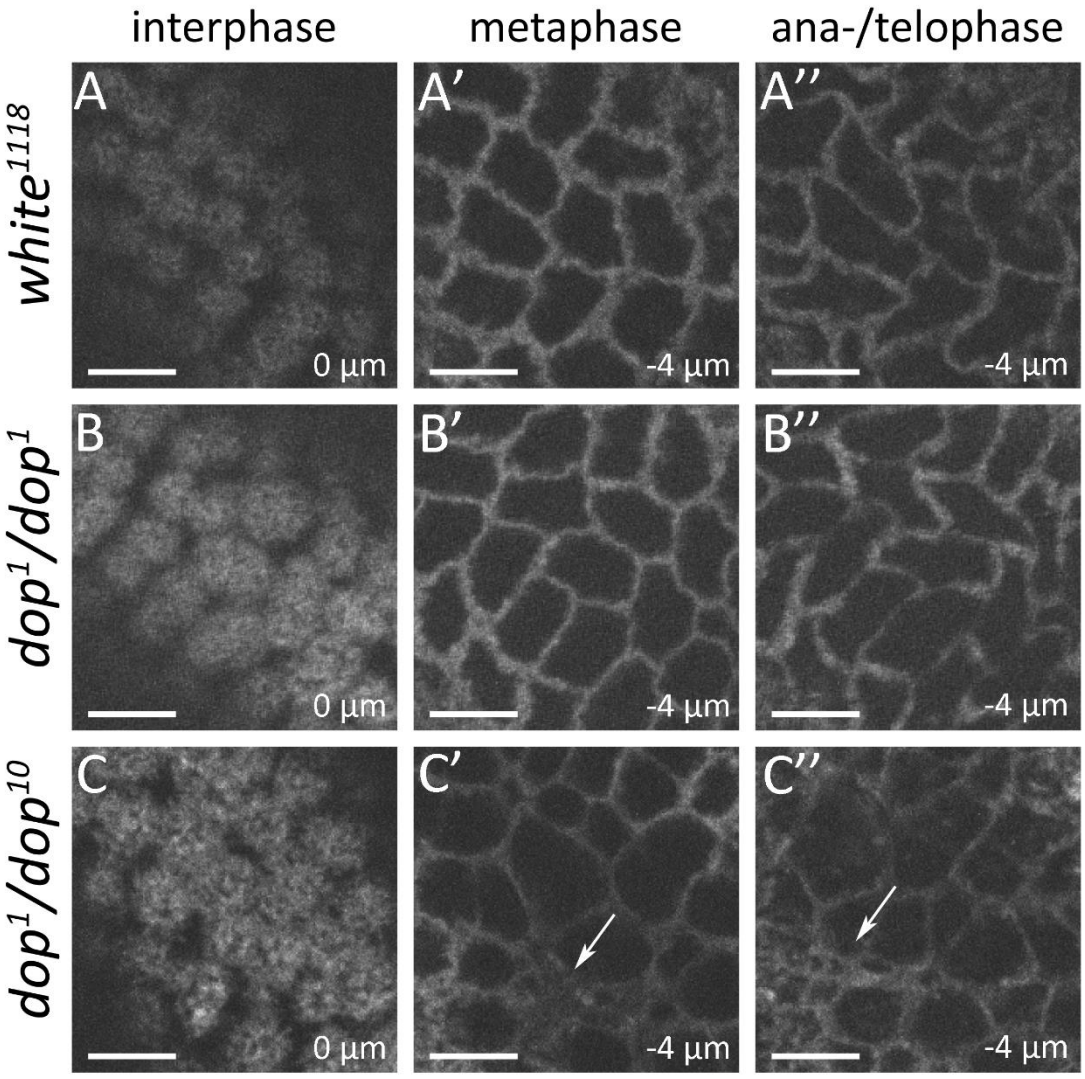

Figure 14 Actin network structures during syncytial divisions in *wild type* and *dop* mutant embryos. Images from *sqh-Utrophin-GFP* time lapse videos of *wild type*, homozygous dop^1 and dop^1/dop^{10} embryos showing the three main structures that form during the 13th syncytial division. Actin caps during interphase (A, B, C), pseudocleavage furrows during metaphase (A', B', C') and dispersing furrows during ana- and telophase (A'', B'', C'') are visible in *wild type* (A-A'') and embryos of both *dop* mutants (B-B'', C-C''). Note that the space between the furrows varies in dop^1/dop^{10} embryos (arrows in C', C''). (Penetrance of phenotype in dop^1/dop^{10}: 50%; $white^{1118}$ n = 11, dop^1/dop^1 n = 3, dop^1/dop^{10} n = 8) The depth in respect to the cortex is indicated in µm. Scale bars represent 10 µm.

As revealed by the Utrophin-GFP construct, *wild type* and both *dop* mutant embryos form actin structures during the last 3 syncytial divisions resembling F-actin structures in published studies (Foe et al. 2000; Schejter & Wieschaus 1993b). Throughout the syncytial cell cycles 11 to 13, F-actin caps are formed (Fig.14 A, B, C), disperse and refocus into furrows (Fig.14 A', B', C'). In the following, these furrows reshape and form new furrows between daughter nuclei (Fig.14 A'', B'', C''). Finally, the furrows disperse and give rise to smaller F-actin caps above each nucleus again. All these structures are formed in *wild type* and *dop* mutant embryos. However, in contrast to

wild type and homozygous *dop*^{1} mutants, *dop*^{1}/*dop*^{10} mutants display a partially irregular shape of the F-actin furrow network. In *dop*^{1}/*dop*^{10} mutant embryos, spaces between the furrows are variable in extent and locally seem to form an actin patch with nearly no space in between (arrows Fig.14 C', C''). Thus, *dop* mutants seem to display an F-actin defect already during syncytial divisions which is only visible in strong heteroallelic combination of *dop*^{1}/*dop*^{10} mutants (with a penetrance of 50%).

3.1.3 The F-actin network shows mild defects in *dop*^{1}/*dop*^{10} mutants at onset of cellularisation

The previous results indicate that the actin network in *dop* mutants is not properly focussed into furrow canals during furrow invagination. During syncytial divisions, *dop* seems to exhibit an additional doses effect since *dop*^{1}/*dop*^{10} mutants display a defect in F-actin localisation which is not present in weaker homozygous *dop*^{1} mutants. However, compared to the severe defect in actin localisation during cellularisation, the defect visible in *dop*^{1}/*dop*^{10} mutants during syncytial divisions is mild and the penetrance was not 100% as during cellularisation. Therefore, it is interesting to see how the F-actin network is formed in *dop* mutants during the transition of the last syncytial division to cellularisation which seems to represent a transition of low to high dependency on Dop function. Onset of cellularisation was defined as timepoint 25 min after F-actin cap formation during the last syncytial division.

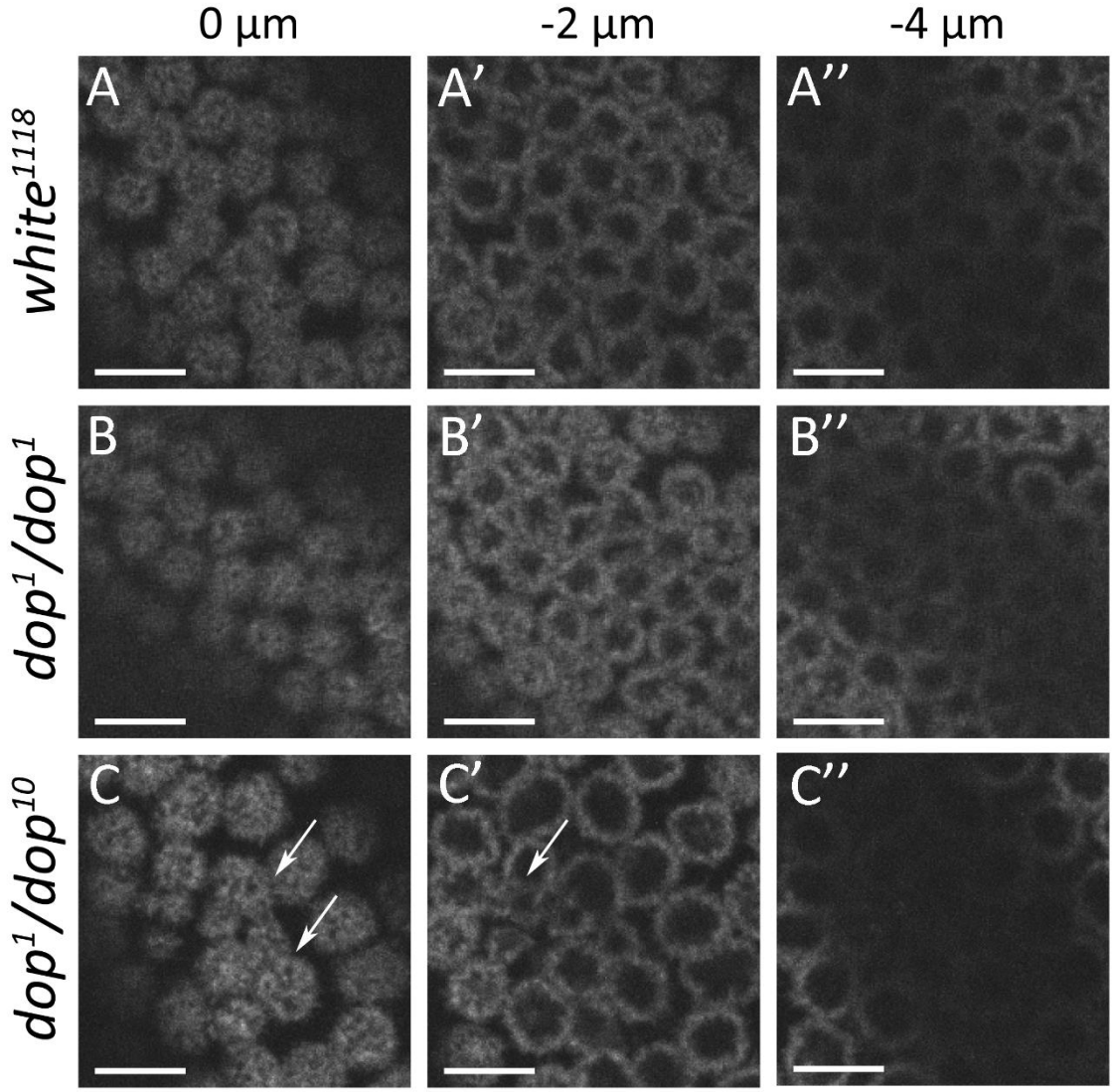

Figure 15 Actin network formation at cellularisation onset in *wild type* and *dop* mutant embryos. Images from *sqh-Utrophin-GFP* time lapse videos of *wild type*, homozygous dop^1 and dop^1/dop^{10} embryos showing F-actin cap structures that form at onset of cellularisation. Images show different z-levels starting from the embryo cortex (0 µm; A, B, C) and going down to 2 µm (A', B', C') and 4 µm (A'', B'', C'') below the cortex. Note that dop^1/dop^{10} mutants display actin caps that are unequally spaced and smaller in size (arrows in C, C'). (Penetrance of phenotype in dop^1/dop^{10}: 50%; $white^{1118}$ n = 14, dop^1/dop^1 n = 3, dop^1/dop^{10} n = 8) Scale bars represent 10 µm.

At onset of cellularisation, not only *wild type* embryos but also both the dop^1 and the dop^1/dop^{10} mutants form actin caps at the surface of the embryo (Fig.15 A, B, C). A mild abnormality in actin cap formation is visible in embryos derived from dop^1/dop^{10} mutant mothers (Fig.15 C, C'): the cap structures have distinct sizes and are not separated locally from each other as it is visible in *wild type* and dop^1 homozygous mutants (Fig.15 C in comparison with A and B). The caps reach a similar depth of about 4 µm in both *wild type* and *dop* mutant embryos (Fig.15 A'', B'', C''). Caps are still separated at their base and furrows are not yet formed. The caps later on spread

out laterally to form the more uniformly distributed cap structure visible in Fig.13 and which is similarly formed in *wild type* and both *dop* mutants. In summary, a defect of F-actin distribution similar to the syncytial division defect is visible in stronger dop^1/dop^{10} mutants during onset of cellularisation which does not account for the stronger defect visible at the furrow canal during later cellularisation stages.

3.1.4 The F-actin network defect during cellularisation of embryos derived from *dop* mutant mothers develops over 30 min from onset of cellularisation

The previous results show that the severe defect of F-actin network formation visible in *dop* mutant embryos after 50 min of cellularisation is not yet visible right at onset of cellularisation. To further define the timing of the F-actin defect and get more detail about its development over time, Utrophin-GFP localisation in *wild type*, dop^1 homozygous and dop^1/dop^{10} hemizygous embryos was determined over a time course of 50 min from onset to late cellularisation (Fig.16).

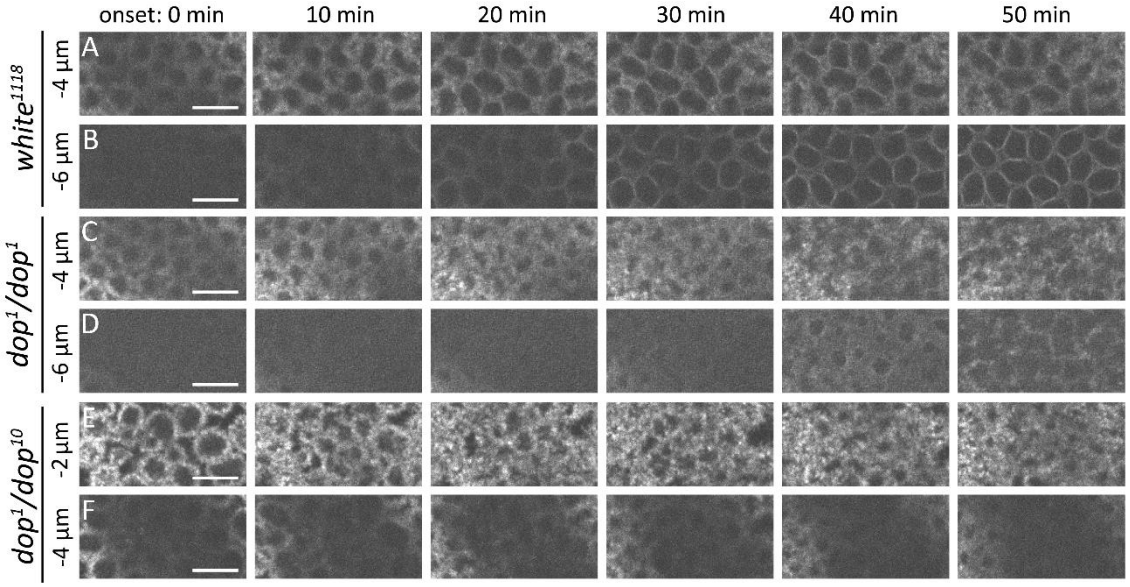

Figure 16 F-actin broadens instead of focusses its localisation during cellularisation in *dop* mutants. Images from *sqh-Utrophin-GFP* time lapse videos of *wild type*, homozygous dop^1 and dop^1/dop^{10} embryos. Depicted are images of six different time-points showing progress of furrow formation during cellularisation (0 to 50 min from onset of cellularisation) and of two different z-levels: A, C and E show the bases of actin caps at onset of cellularisation (-4 µm below the cortex: A, C; -2 µm below the cortex: E) and B, D and F show the invaginating actin-rich furrow (-6 µm below the cortex: B, D; -4 µm below the cortex: F). Scale bars represent 10 µm.

Visualising Utrophin-GFP localisation during cellularisation over time (Fig.16) shows that F-actin starts to focus into an internuclear structure at the bases of the F-actin caps during the first 10 min of cellularisation in *wild type* embryos (-4 µm; Fig.16 A). This focussing is intensified during the following 20 min. About 30 min after onset of cellularisation, a fully-formed honeycomb-like F-actin network invaginated -6 µm below the cortex (Fig.16 B). In *dop* mutant embryos, F-actin becomes more dispersed instead of focussed into internuclear spaces in the first 30 min of cellularisation (Fig.16 C, E). A broadened F-actin structure invaginates in homozygous dop^{1} mutants about 10 min later compared to *wild type*, whereas F-actin stays within the apical 2 µm in dop^{1}/dop^{10} embryos. These data implicate Dop function in the process that leads to the invagination of the F-actin network. Timing and location of F-actin focussing at the bases of the F-actin caps coincides with the formation of the furrow canal after about 5 to 8 min after onset of cellularisation at a depth of 5 µm (Sokac & Wieschaus 2008b). During that period, the first severe F-actin localisation defect becomes visible.

Analysis of Utrophin-GFP localisation during early *Drosophila* embryogenesis revealed two different F-actin phenotypes in *dop* mutants: one displays an F-actin localisation defect during syncytial divisions in only 50% of strong hypomorphic *dop* mutant embryos. This defect affects only patches of the embryo cortex, where specific actin structures like the metaphase furrows either fail to leave space for microtubules and DNA or the spaces are enlarged. The other defect displays an F-actin defect in all embryos of both dop^{1} homozygous and dop^{1}/dop^{10} hemizygous mutants. This defect is highly uniform compared to the defect during syncytial divisions. The F-actin network at the furrow canal level is highly broadened and this phenotype is visible at the whole embryo cortex. It is not known whether both defects are caused by the same Dop-dependent mechanism or by different Dop-dependent mechanisms. Both possibilities will be discussed later.

3.1.5 Clonal analysis reveals a specific function for *dop* in cellularisation

During *Drosophila* oogenesis, the developing oocyte is surrounded by somatic follicle cells. These cells have a high impact on shaping and patterning of the oocyte and the embryo (Horne-Badovinac & Bilder 2005). If the mother is mutant for a gene which affects the follicle cells, this mutation can influence embryonic development. It is therefore possible that a putative defect in the follicle cells contributes to the defects during syncytial divisions and cellularisation in embryos derived from *dop* homozygous or hemizygous females.

Thus, maternal *dop* mutant embryos were analysed which derive from ovaries with normal follicle cells. Since *dop* is a maternal gene, germ line clone-derived embryos in females heterozygous for the dop^{10} mutation were generated (see Methods section for further details). This enables us to separate somatic follicle cell effects from mutant germ line effects. Moreover, this method allows to generate embryos homozygous mutant for maternal contributions even if the mutation is homozygous lethal in the mother (Blair 2003). This aspect is important because females zygotically mutant for the so far strongest and only protein null allele dop^{10} showed very low viability and, in case of eclosion, low fertility (Hain 2010). The heterozygosity of the mother for the dop^{10} allele secures her viability and fertility.

3.1.5.1 Germ line clones for dop^{10} show no defects during syncytial divisions

All the studies addressing the requirement of Dop function during cellularisation have studied effects of hypomorphic alleles or null alleles hemizygous over a chromosomal deficiency (dop^{10}/Df(3L)MR15). The hypomorphic alleles pose a problem because of residual function of Dop and maybe masking some of the functions Dop has during early embryogenesis. The use of the deletion creates the problem that Df(3L) MR15 deletes or partially deletes three genes which could contribute to the phenotypes observed. Additionally, phenotypes in those embryos could be due to *dop* mutations in the maternal somatic follicle cells. To address specifically *dop* mutant

null phenotypes due to Dop loss-of-function in the germ line, germ line clone-derived embryos homozygous for the *dop* null allele dop^{10} were generated. Following up on the previous results, indicating that Dop may have dose-dependent functions during syncytial divisions and cellularisation, F-actin localisation was first examined in fixed germ line clone dop^{10} embryos during these stages (Fig.17).

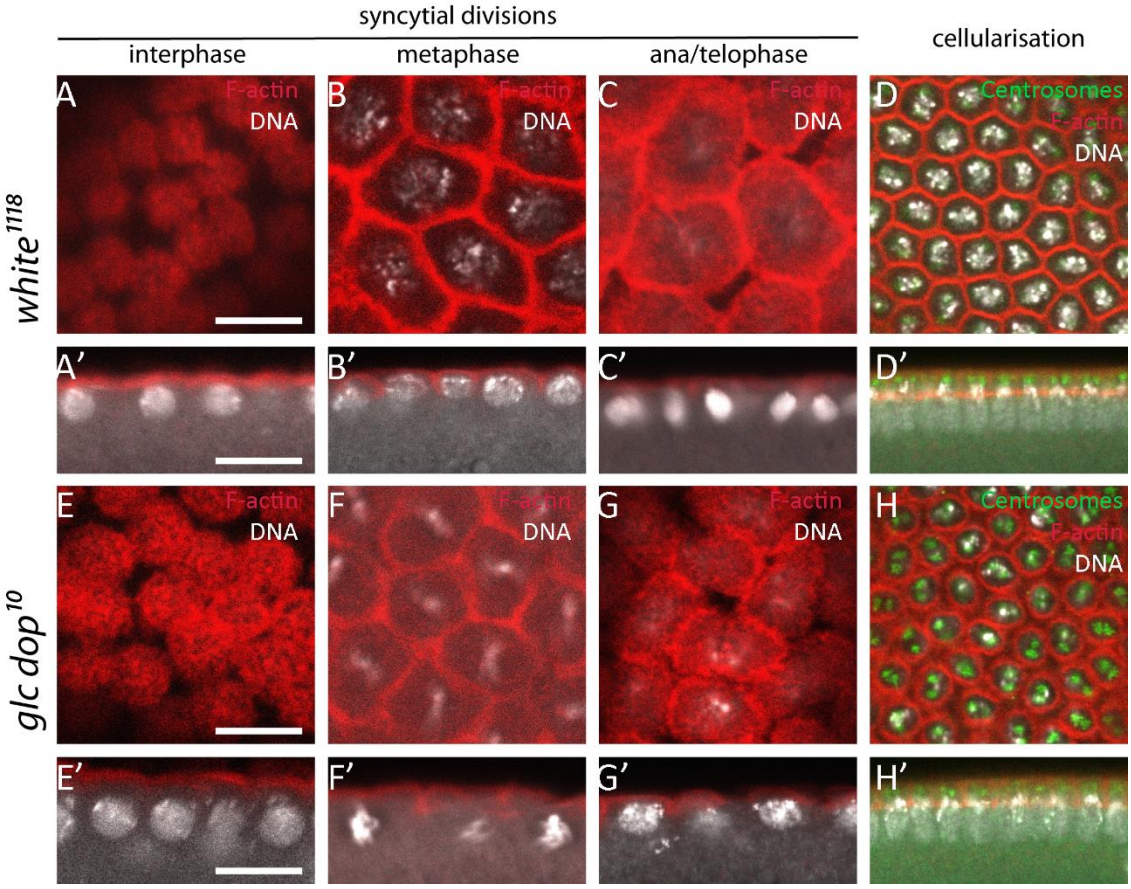

Figure 17 F-actin structures in *wild type* and germ line clone dop^{10} mutant embryos during syncytial divisions and cellularisation. Formaldehyde-fixed *wild type* and germ line clone dop^{10} mutant embryos stained with phalloidin (F-actin; red) and DAPI (DNA; white) and in cellularisation with antibodies against Centrosomin (centrosomes; green). Shown are sagittal-sections (A-H) and cross-sections (A'-H') of each embryo. *wild type* as well as dop^{10} germ line clone (glc) embryos show F-actin cap structures (A, A', E, E'), pseudocleavage furrows (B, B', F, F') and dispersing furrows (C, C', G, G') during syncytial divisions. Note that during cellularisation, F-actin focusses into a distinct honeycomb-like structure in *wild type* embryos but is broadened in *dop* mutant embryos (D, D', H, H'). Scale bars represent 10 µm.

Both *wild type* and mutant embryos display the F-actin structures characteristic for syncytial divisions in early *Drosophila* development. The structures correspond to the Utrophin-GFP structures in time lapse movies of *wild type* embryos (Fig.17 A-C, E-G in comparison with Fig.14 A-A''). Syncytial divisions seem to proceed properly in germ line clone mutants since all

metaphase furrows surround only one nucleus (Fig.17 F, F'). However, during cellularisation F-actin fails to focus into a honeycomb-like structure in germ line clone-derived embryos and F-actin remains at a centrosomal level (Fig.17 H, H'). This mislocalisation phenotype during cellularisation is very similar to Utrophin-GFP localisation in hypomorphic *dop* mutants and contains both, F-actin broadened localisation during cellularisation and the absence of invagination. In contrast, no F-actin defect is visible during syncytial divisions in germ line clone derived dop^{10} embryos. The absence of a syncytial F-actin defect in germ line clone derived dop^{10} embryos excludes that the defect seen in hypomorphic dop^{1}/dop^{10} hemizygous embryos during syncytial divisions is a pure dose-dependent defect because Dop function is even more impaired in germ line clone derived dop^{10} embryos. Thus, the syncytial division defect would have been expected to be even stronger in germ line clone derived dop^{10} embryos. A possible involvement of follicle cell function defects in creating the dop^{1}/dop^{10} hemizygous mutant phenotype during syncytial divisions will be investigated in section 3.1.5.3.

3.1.5.2 The slow and fast phases of cellularisation require Dop function

Several studies demonstrated that homozygous dop^{1} embryos show a strong delay in membrane growth during the slow phase but normal membrane growth during fast phase of cellularisation (Hain et al. 2014; Hain al et. 2010; Meyer et al. 2006). In contrast, hemizygous dop^{10} mutants in trans to a chromosomal deficiency for the *dop* locus display only weak membrane growth during both phases (Hain 2010). A complete *dop* loss-of-function is expected to resemble the dop^{10}/deficiency membrane growth phenotype if mutated follicle cells have no impact on membrane growth during cellularisation. Phalloidin stainings on fixed germ line clone dop^{10} embryos suggested already that not only F-actin localisation but also membrane invagination is impaired in these complete loss-of-function mutants. To see to what extent membrane invagination is affected and to compare this with the data for hypomorphic *dop* mutants,

kymographs of bright field movies on *wild type* and germ line clone *dop*^{10} embryos were created to image membrane growth over time (Fig.18).

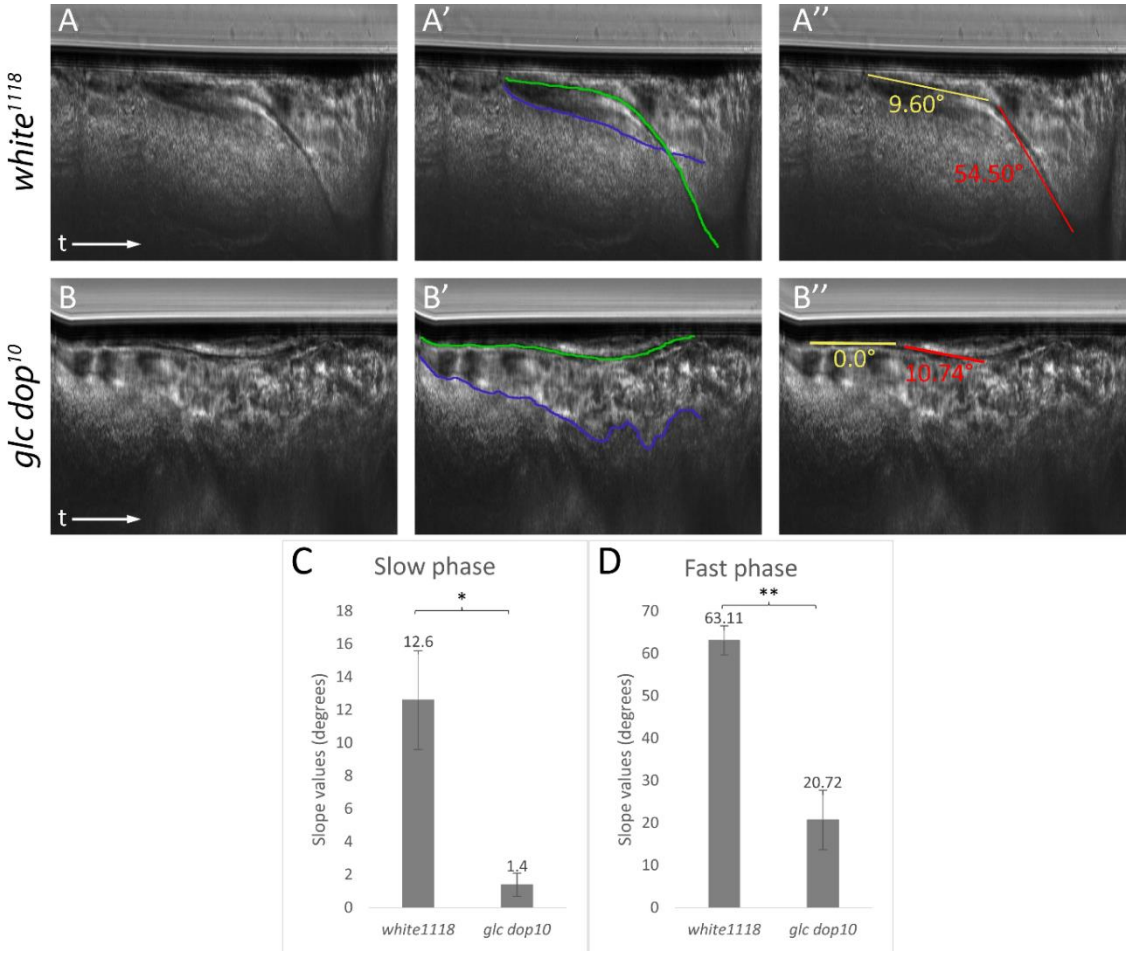

Figure 18 Germ line clone-derived embryos maternally homozygous for *dop*^{10} show significant decrease in membrane growth during slow phase and fast phase of cellularisation. Membrane growth was measured using kymographs generated from bright field movies using ImageJ. An area of interest of 1 by 400 pixels at the same position in every movie frame was selected. Assembly of the selected regions created an image showing the progression of the membrane in time. The kymographs (A, B) were analysed by marking the membrane furrow (green) and the basal ends of the nuclei (blue) (A', B'). In addition, the progression of membrane growth in degrees was determined (ImageJ) for slow phase (yellow) and fast phase (red) by measuring the angle between the invaginating membrane front and the outer membrane of the embryo (A'', B''). The time progression is indicated by t (A, B). Comparison of membrane invagination slopes between *wild type* and germ line clone *dop*^{10} embryos shows a significant reduction in membrane growth during slow (C) and fast phase (D) of cellularisation in the mutant. (Two tailed *t*-test, *p<0.05, **p<0.01; +/- SEM; slow phase: *white*^{1118} n = 2, glc *dop*^{10} n = 3; fast phase: *white*^{1118} n = 4, glc *dop*^{10} n = 3)

Wild type embryos display membrane growth that can be clearly divided into slow phase (membrane invagination slope of 9.60°) and fast phase (invagination slope of 54.50°) (Fig.18 A-A''). In contrast, in germ line clone *dop*^{10} embryos membrane invagination is strongly impaired (Fig.18 B-B''). There is very little membrane invagination visible during the first 40 min of

cellularisation (slow phase; Fig.18 B'', C) and a minor increase in membrane growth compared to *wild type* during fast phase (Fig.18 B'', D). Even though the elongation of the nuclei is not affected in germ line clone dop^{10} mutants (Fig.18 B'), the basal ends of the nuclei leave their normal strung orientation and start to fluctuate from onset of fast phase on.

These kymographs show that maternal homozygous dop^{10} mutants have a much more severe membrane invagination defect than the ones seen in dop^{1} homozygous embryos (slow phase: 7.46°; fast phase: 43.15°) (Hain et al. 2014). In the complete loss-of-function mutant embryos, neither membrane invagination during slow phase nor during fast phase is similar to *wild type*. Additionally, germ line clone homozygous dop^{10} mutants resemble membrane invagination rates similar to what has been shown for dop^{10}/deficiency embryos (Hain 2010). This result was expected if Dop function during cellularisation is based on Dop function in the germ line and not in maternal somatic cells (like follicle cells). Therefore, these data indicate that Dop function is required in the germ line to ensure membrane invagination during slow phase as well as fast phase of cellularisation.

3.1.5.3 Dop loss-of-function has no effect on follicle cell morphogenesis

Live-imaging of Utrophin-GFP expressing dop^{1}/dop^{10} hemizygous mutant embryos and stainings on germ line clone dop^{10} mutant embryos showed a discrepancy in syncytial division phenotypes. Whereas embryos derived from dop^{1}/dop^{10} hemizygous mothers exhibited defects, embryos derived from dop^{10} germ line clones showed normal F-actin localisation in syncytial divisions and exhibited defects exclusively during cellularisation. These data suggest that there might be an additional requirement for Dop in somatic follicle cells which are mutant in embryos derived from dop^{1}/dop^{10} hemizygous mothers but not in embryos derived from dop^{10} germ line clones. Follicle cells are somatic maternal tissue and emerge from dividing somatic stem cells to surround the 16 germ cell cysts that give rise to the oocyte (Horne-Badovinac & Bilder 2005). Molecular signalling between follicle cells and the oocyte is essential to establish the future

embryonic body axes. Additionally, both the egg yolk as well as the eggshell are produced by the follicle cell epithelium and secreted from the apical site facing the oocyte during late stages of oogenesis. Thereby, follicle cells have a huge impact on embryonic development. Moreover, the monolayered follicle cell epithelium is a well-established system to study epithelial morphogenesis and polarity (Müller 2000; Horne-Badovinac & Bilder 2005). To investigate the possibility that follicle cells mutant for *dop* are causing syncytial defects in embryos derived from dop^{1}/dop^{10} hemizygous females, mosaic follicle epithelia homozygous for dop^{10} were generated in dop^{10} heterozygous females (see Methods section for details). The overall structure of these follicle cells was examined by phalloidin and anti-tubulin stainings (Fig.19).

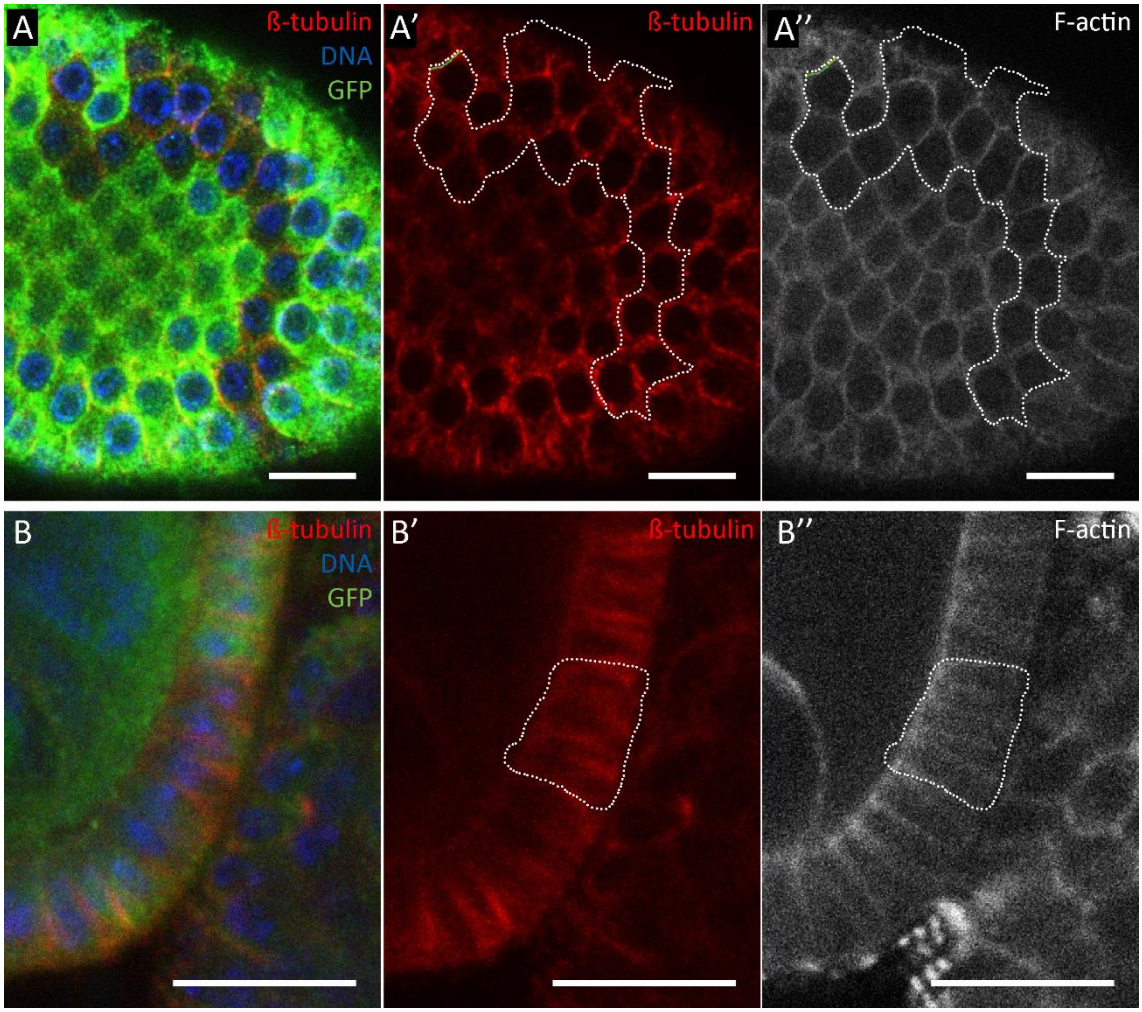

Figure 19 The morphology of follicle cells homozygous for dop^{10} is unaffected. Top view (A-A'') and cross section (B-B'') of follicle clones homozygous for dop^{10}. Egg chambers were fixed and stained with DAPI (DNA; blue), phalloidin (F-actin; white) and antibodies against GFP (green) and β-tubulin (red). Homozygous dop^{10} follicle cells (cells without GFP expression, dashed lines) show cell morphologies comparable to *wild type* (cells with GFP expression). Microtubule (A', B') and

F-actin (A'', B'') network formation are indistinguishable from *wild type* cells. Egg chamber A-A'': stage 9; egg chamber B-B'': stage 7. Scale bars represent 10 µm.

Follicle cells in *wild type* egg chambers accumulate actin at their apical site (facing the oocyte and the nurse cells) and the microtubules form arrays along the apicobasal axis orienting their minus-ends apically and their plus-ends basally (Baum et al. 2000; Clark et al. 1997; Doerflinger et al. 2003). Somatic follicle cells homozygous for dop^{10} did not show a morphological difference compared to surrounding follicle cells heterozygous for dop^{10}. Follicle cells lacking Dop function are indistinguishable from *wild type* cells in size and shape, as well as F-actin and β-tubulin distribution (Fig.19). Also the specific polarity of both microtubule network and F-actin network in follicle epithelia is maintained in dop^{10} homozygous cells (Fig.19 B', B''). This result indicates that while function in the germ line is essential, *dop* appears not to be required for overall follicle cell morphology and polarity. Thus, *dop* mutations might affect follicle cells in more subtle ways or *dop* is dispensable for normal follicle cell function. Moreover, this result shows that a function for Dop in follicle cells is unlikely to account for F-actin defects seen in dop^{1}/dop^{10} hemizygous mutant embryos during syncytial divisions. The cause for this phenotype is still unknown and will be discussed later.

3.1.6 Conclusion of Results Part 1

In this chapter, the requirement of Dop for early embryogenesis has been explored to determine the time and the specific location of its requirement. The results show that Dop is crucial for F-actin localisation during cellularisation. In *dop* mutants, F-actin formed a broadened structure where the furrow canals should form and did not focus into a distinct honeycomb-like structure. This defect develops during the first 30 min of cellularisation and concomitantly with furrow canal assembly. Another process during cellularisation requiring Dop function is membrane invagination. This process showed a clear dose-dependency of Dop function: the partial loss of function allele dop^{1} affected membrane invagination only during slow phase, whereas complete loss-of function mutants created by the germ line mosaic technique severely affected both slow

and fast phase. This result demonstrates that Dop function for cellularisation is required in the germ cells. Moreover, it shows that it is important to study *dop* null mutants to reveal Dop requirement in all Dop-dependent processes (e.g. membrane invagination). Another F-actin defect was visible only in strong hypomorphic dop^{1}/dop^{10} mutant embryos during syncytial divisions but not in the germ line clone-derived *dop* null mutants. This defect could not be explained by a loss-of-function of Dop in follicle cells, which do not seem to depend on Dop function, and its cause remains to be investigated.

3.2 Part 2: Exploring the mechanism of Dop function during cellularisation

Introduction

Drop out has been studied intensively in our lab and a lot of phenotypes caused by *dop* mutations have been discovered (Meyer et al. 2006; Hain et al. 2010; Hain et al. 2014; Hain 2010; Langlands 2012). Many of these phenotypes affect processes based on Dynein transport function, such as Dynein-dependent transport of Bazooka, lipid droplets and mRNA (Hain et al. 2014; Meyer et al. 2006; Harris & Peifer 2005; Gross et al. 2000; Bullock et al. 2006; Wilkie & Davis 2001). Additionally, genetic interaction studies with dop^1 and $short\ wing^1$ (allele of the *dynein intermediate chain* gene) as well as dop^1 and $Glued^1$ (allele of the Dynactin subunit required for Dynein and Dynactin interaction) double mutants show enhanced phenotypes in adult wing and eye as well as membrane growth during embryo cellularisation compared to the respective single mutants (Hain et al. 2014). In addition to these genetic studies, also two biochemical studies support a function of Dop in the control of Dynein. Dynein intermediate chain protein displays a reduced phosphorylation in dop^1 mutant embryo extracts compared to *wild type* despite equal overall levels of protein (Hain et al. 2014). Moreover, a SILAC screen identified Dynein light intermediate chain protein as a possible phosphorylation target of Dop (Langlands 2012). Dop-dependent phosphorylation of Dynein could have major impact on Dynein function as it has been shown for Dynein subunit phosphorylations in several other studies (Vaughan et al. 2001; Runnegar et al. 1999; Whyte et al. 2008; Yang et al. 2005; Mische et al. 2008).

Dynein is involved in many different cellular processes and its function is essential for cellular and organismic viability (Gepner et al. 1996; Karki & Holzbaur 1999). Thus, a malfunction of Dynein in *dop* mutants could account for many, if not all, defects seen in these mutants. Also defects seen in the F-actin network localisation presented in Results Part 1 could be due to malfunctioning of Dynein-dependent transport since Dynein is required for transport of actin regulators and possibly F-actin itself (Cao et al. 2008; Acharya et al. 2014; Rothwell et al. 1999;

Albertson et al. 2008). Additionally, Dynein regulates transport and localisation of proteins required for polarity establishment, such as Bazooka and Slam (Slow-as-molasses) (Harris & Peifer 2005; Acharya et al. 2014). Another Dynein-dependent transport process important for cellularisation is membrane addition from intra-cellular and recycled sources via transport of Golgi-derived and endosomal vesicles (Lecuit & Wieschaus 2000; Papoulas et al. 2005; Riggs et al. 2007; Sisson et al. 2000; Pelissier et al. 2003; Figard et al. 2016). Testing whether the transport of any of these Dynein cargoes is affected in *dop* mutants could provide a direct link between Dop function, Dynein and cellularisation.

3.2.1 Overall microtubule organisation and polarity is not affected in *dop* mutants during cellularisation

An experiment on mRNA particle transport showed that Dop is required for minus-end directed microtubule transport (Hain et al. 2014). The net apical, i.e. minus-end directed movement of mRNA particles was significantly reduced in *dop* mutant embryos. One reason for this phenotype could be that dynamics or overall length of microtubules is altered. To investigate this, a transgenic EB1-GFP construct expressed under control of a maternal α-tubulin Gal4 driver was imaged in *dop* mutant embryos and compared to *wild type*. EB1 is a microtubule plus end-binding protein and as such marks the growing plus-ends of microtubules, thereby indicating direction and speed of microtubule growth (Tirnauer et al. 1999; Berrueta et al. 1998). In *wild type* embryos, EB1 comets are expected to emerge from the centrosomes between the nuclei and the embryo cortex. As the microtubules elongate and form a basket-like structure surrounding the nuclei, EB1 is expected to move in direction of the embryo interior. Additionally, EB1 comets should be visible moving from the centrosomes to the cortex as astral microtubules emerge.

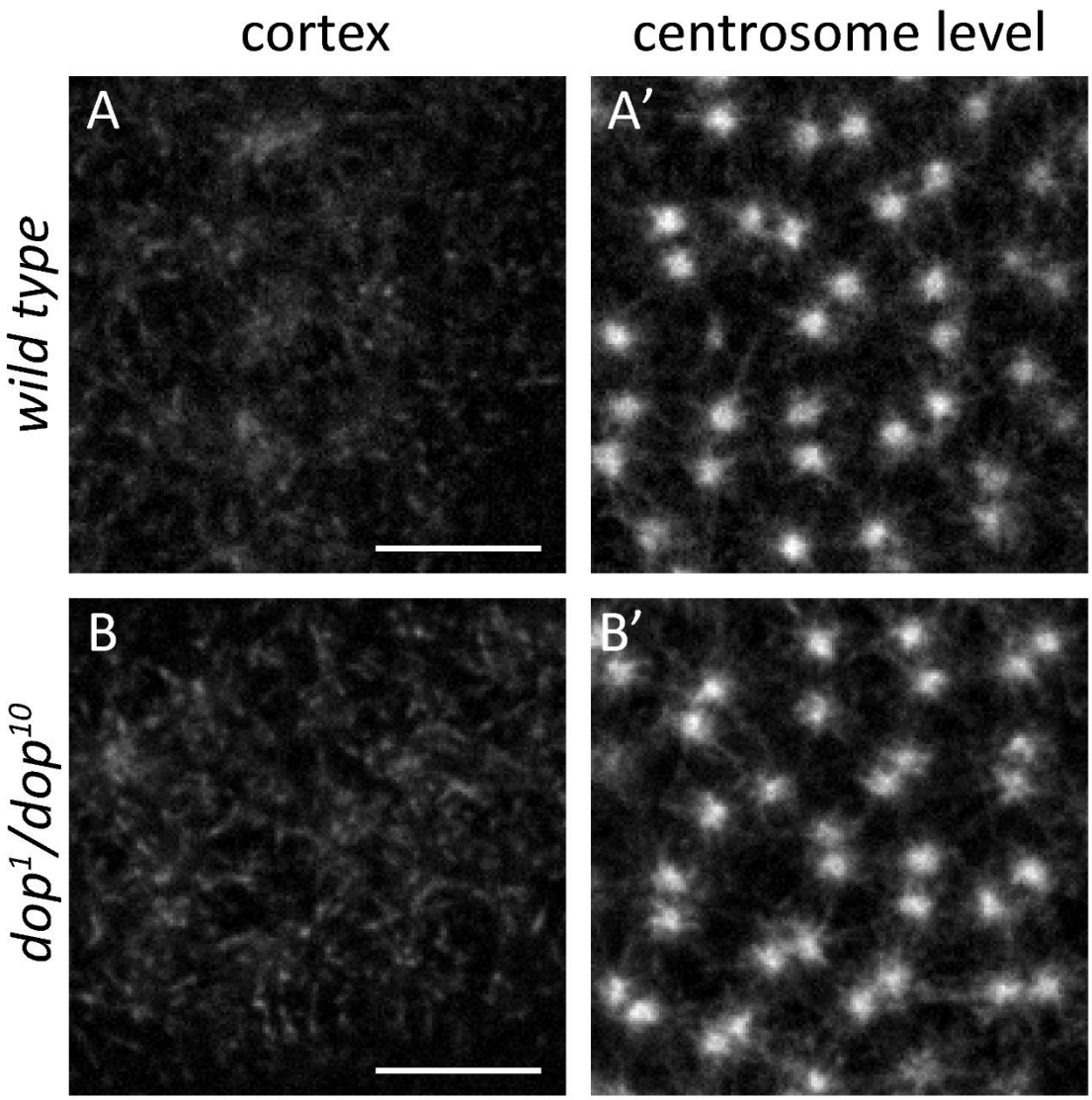

Figure 20 Microtubule distribution is not altered during cellularisation in *dop* mutants. Images taken from time-lapse recordings of EB1-GFP expressing embryos under control of the maternal α-tubulin Gal4 driver during cellularisation. Images show EB1-GFP localisation at the cortex (A, B) and on the centrosome level (A', B') of the embryo in *wild type* and dop^{1}/dop^{10} mutants, respectively. Note that microtubule distribution and polarity is similar in the mutant (B, B') compared to *wild type* (A, A') embryos. Scale bars represent 10 µm.

Imaging of the EB1-GFP construct revealed a similar microtubule distribution in *wild type* and *dop* mutant embryos (Fig.20). Comets of EB1-GFP emerge from the centrosomes and move into the interior of the embryo to a similar extent in *wild type* and dop^{1}/dop^{10} transheterozygous embryos (Fig.20 A', B' and movies provided). Also astral microtubules (indicated by EB1-GFP comets emerging from centrosomes and moving to the embryo surface) are formed to a similar extent in *wild type* and dop^{1}/dop^{10} mutant embryos (Fig.20 A, B). This result indicates that the dynamics of microtubule formation are similar in *wild type* and *dop* mutants. Thus, Dop function seems not to have a major impact on general microtubule dynamics as judged by EB1-GFP

binding. This result supports previous data on fixed embryos stained for β-tubulin which show that microtubule organisation per se is not affected in *dop* mutants (Hain et al. 2014).

3.2.2 Embryos from *dop* mutant mothers show defects in Golgi and endosomal vesicle localisation during cellularisation

3.2.2.1 Apical Golgi particle localisation is impaired in *dop* mutants

During cellularisation, Golgi-derived vesicles move along microtubules in a Dynein-dependent manner to the apical cortex of the newly forming cells where they accumulate during late cellularisation stages (Papoulas et al. 2005; Sisson et al. 2000; Ripoche et al. 1994). This movement is required for furrow ingression during cellularisation (Sisson et al. 2000; Papoulas et al. 2005). Therefore, Dynein-dependent Golgi transport could provide a link between membrane invagination defects seen in *dop* mutants and Dynein dependency on Dop function. In order to localise Golgi-derived vesicles in *dop* mutant embryos, fixed embryos were stained using an antibody against the Golgi-resident protein 120 (gp120), a 120 kDa protein localising to the Golgi membrane (Stanley et al. 1997) (Fig.21). The staining and quantification were performed by Dr. Arno Müller.

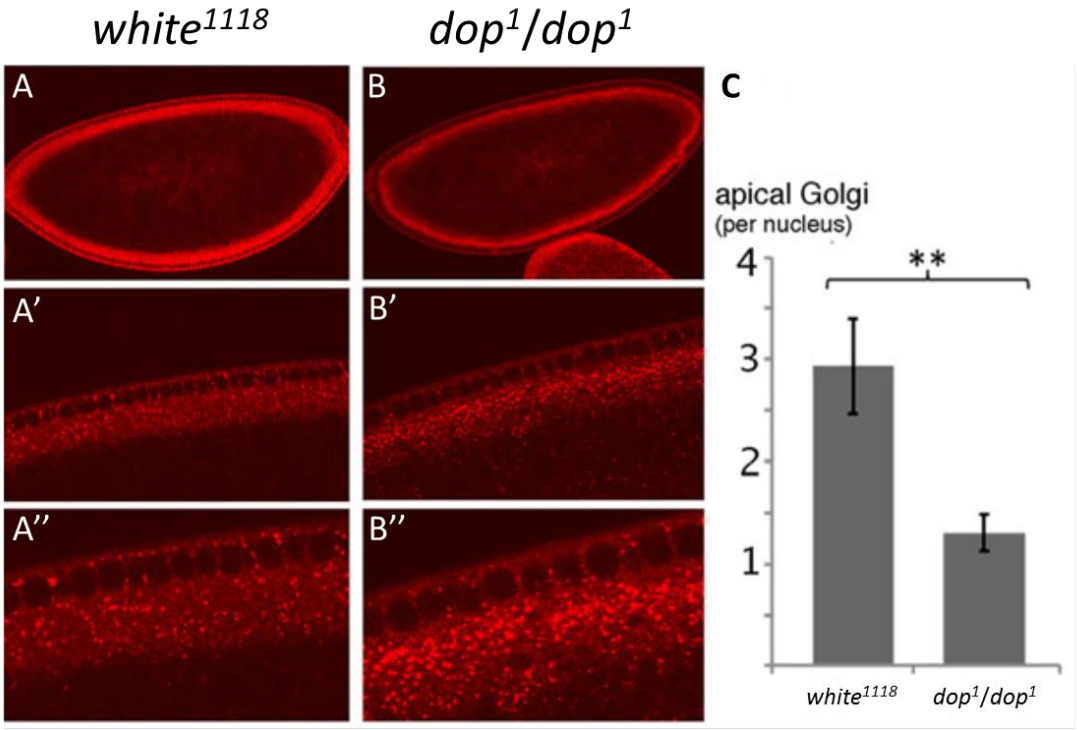

Figure 21 Apical Golgi particle localisation is impaired in *dop* mutants. Anti-gp120 Golgi antibody staining of fixed *white*^{1118} and *dop*^{1}/*dop*^{1} embryos during early cellularisation (A, B). Detail views of the cortical embryo area (A', A'', B', B''). Quantification of apical Golgi particles reveals a significant reduction in apical Golgi particles in *dop* mutant embryos (C). (*t*-test, **p<0.01; +/- SEM; *white*^{1118} n=7; *dop*^{1}/*dop*^{1} n=9). Images and quantification by Dr. Arno Müller.

Stainings against gp120 revealed that Golgi-derived vesicles are abundant in both *wild type* and *dop* mutant embryos during cellularisation (Fig.21 A-A'', B-B''). Quantification of Golgi particles localising apically of the nuclei revealed that the number is significantly reduced in *dop* mutants compared to *wild type* (Fig.21 C). These data indicate that not Golgi number but Golgi transport via Dynein is impaired in *dop* mutants.

3.2.2.2 Rab11 endosomal vesicles display a more compact localisation at the centrosomes in *dop* mutants compared to *wild type*

In addition to Golgi transport, also recycling endosomal trafficking and exocytosis are required for cellularisation to enable furrow ingression specifically during slow phase (Figard et al. 2016; Riggs et al. 2003; Rothwell et al. 1998; Pelissier et al. 2003). Impairment of Rab11 (a small GTPase required for recycling endosome targeting) function exhibits similar defects compared to *dop* mutants (Pelissier et al. 2003). These defects include membrane invagination impairment, a

nuclear drop out phenotype, as well as Slam and F-actin broadening at the furrow canal (Pelissier et al. 2003; Riggs et al. 2003; Riggs et al. 2007). In accordance with a specific requirement during slow phase, Rab11 shows a specific pericentrosomal localisation only during this stage of cellularisation (Pelissier et al. 2003). After slow phase, Rab11 disperses into small vesicular structures. To see if recycling endosome localisation is affected in *dop* mutants, *wild type* (heterozygous for the dop^{1} mutation) and dop^{1}/dop^{10} transheterozygous mutant embryos expressing Rab11-GFP were analysed during slow phase of cellularisation (Fig.22).

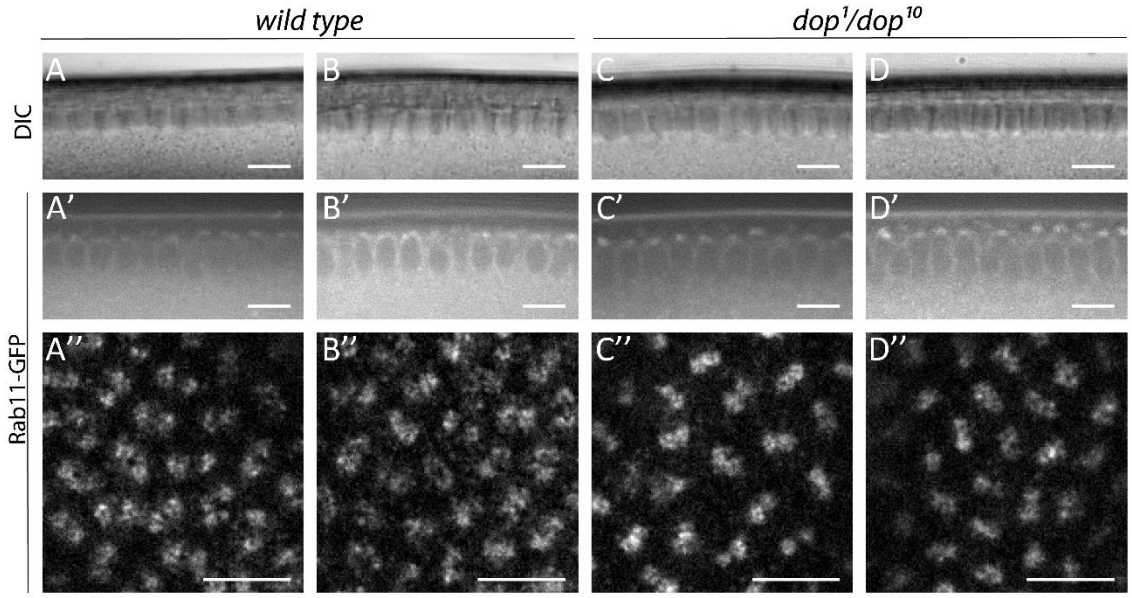

Figure 22 Rab11 endosomal vesicles display a more compact localisation at the centrosomes in *dop* mutants compared to *wild type*. Images taken from time-lapse recordings of Rab11-GFP expressing embryos under control of the maternal α-tubulin Gal4 driver during cellularisation. Images show Rab11-GFP localisation at the embryo cortex (A'', B'', C'', D'') and in cross-sections (A', B', C', D') in *wild type* (A, B) and dop^{1}/dop^{10} mutants (C, D), respectively. Differential interference contrast (DIC) images show the nuclei elongation status as reference for cellularisation timing (A, B, C, D). Rab11-GFP signal localisation is more compact in mutants (C'', D'') compared to *wild type* embryos (A'', B''). Scale bars represent 10 µm.

During slow phase of cellularisation (Fig.22 and movies provided), Rab11 endosomal vesicles show dynamic localisation to, and in the vicinity of, the centrosomes apical to each nucleus both in *wild type* embryos and embryos derived from dop^{1}/dop^{10} transheterozygous mothers. This localisation is consistent with what has been reported for Rab11 localisation during early cellularisation in other studies (Pelissier et al. 2003). However, compared to *wild type* in *dop* mutants Rab11-GFP was more concentrated to the centrosomal area (Fig.22 A'', B'', C'', D''). Together with the previous finding showing that apical Golgi localisation is impaired in *dop*

mutants, these data indicate that Dop is required for proper distribution of the endomembrane system which could provide a link to membrane growth defects seen in *dop* mutants. It also indicates that Dop regulates organelle transport in the *Drosophila* embryo. However, the available data point to an involvement in different transport processes: Apical localisation of Golgi particles is clearly a Dynein-dependent, microtubule minus-end-directed transport process which seems to be affected by Dop function impairment. In contrast, the tight localisation of Rab11 endosomes in *dop* mutants points to an involvement of Dop function in Kinesin-dependent, microtubule plus-end-directed transport. Both these possibilities will be discussed later.

3.2.3 Golgi as well as endosomal vesicle localisation show impairment in complete loss-of-function *dop* mutants

3.2.3.1 Apical Golgi particle localisation requires Dop function

Apical Golgi particle localisation in dop^{1}/dop^{10} hypomorphic mutants was significantly reduced in cross-sections of mutant embryos compared to *wild type* (Hain et al. 2014). In order to see if there is a difference in complete loss-of-function *dop* mutants compared to the hypomorphic condition, transversal sections of *wild type* and complete loss-of-function *dop* mutant embryos stained against Lava lamp (Lva), a Golgi-associated protein involved in Dynein-dependent movement of Golgi particles, were imaged and projections of the first apical 5 µm in embryos at onset of cellularisation were analysed (Fig.23) (Papoulas et al. 2005; Sisson et al. 2000).

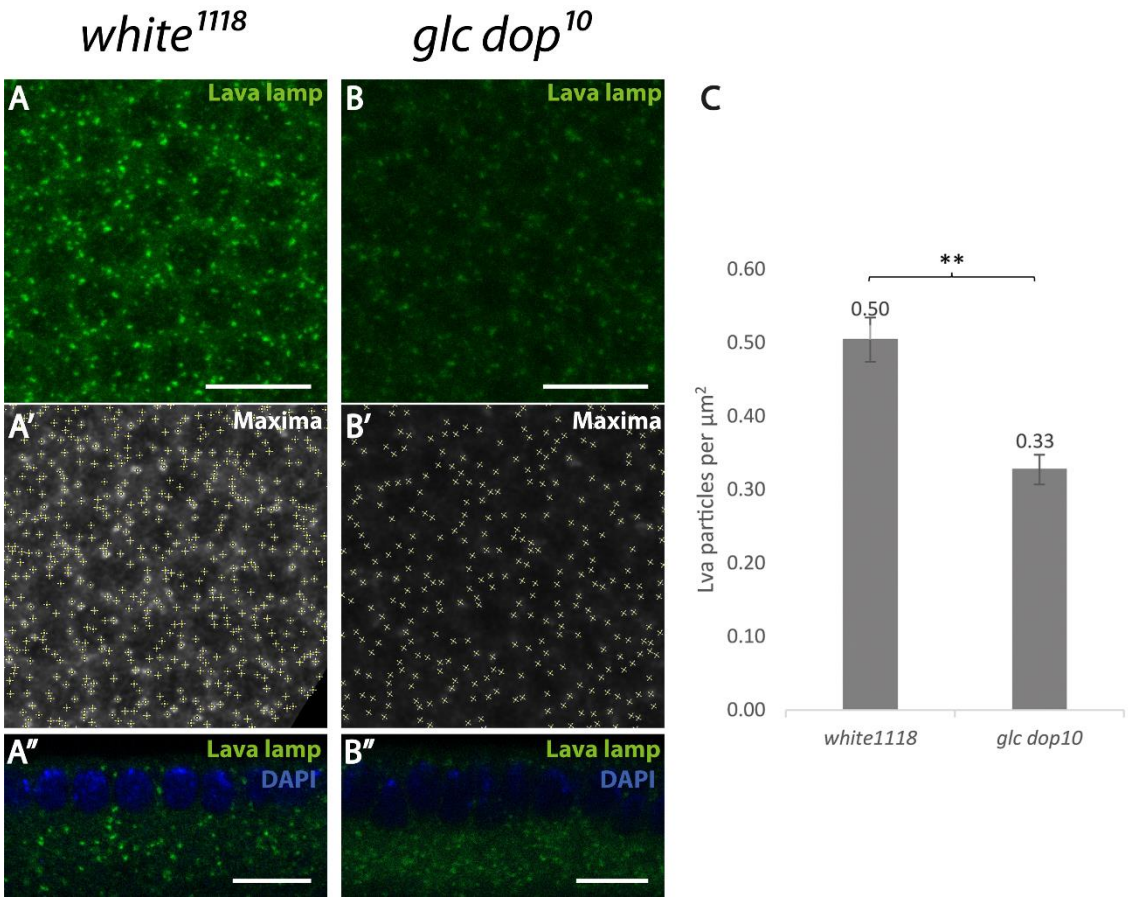

Figure 23 Lava lamp-positive Golgi particles display a reduced number in the apical 5 µm in complete loss-of-function *dop* mutants. Images show a projection of the first apical 5 µm from the cortex (A, A', B, B') and cross-sections (A'', B'') of the same *wild type* (A, A', A'') and germ line clone *dop*^{10} mutant embryos (B, B', B''). Embryos were fixed and stained for the Golgi protein Lava lamp (Lva, green) as well as DAPI (only shown in A'', B''). ImageJ was used to determine signal maxima for calculating the number of apical Golgi particles in both lines per µm^2 (A', B'). Quantification of Golgi particles reveals a significant reduction of apical Golgi particles in *dop* mutant embryos compared to *wild type* (C). (Two tailed *t*-test, **p<0.01; +/- SEM; *white*^{1118} n = 4, glc *dop10* n = 3). Scale bars represent 10 µm.

Analysis of Lava lamp punctae in *wild type* and germ line clone *dop*^{10} mutant embryos in the first apical 5 µm of embryo transversal views showed a significant reduction of Lva-positive particles in the mutant (Fig. 23). This result shows that apical Golgi localisation is affected in both hypomorphic *dop*^{1}/*dop*^{10} mutants as well as complete loss-of-function germ line clone *dop*^{10} mutants, and is likely caused by a defect in its transport by Dynein to the apical domain (Papoulas et al. 2005).

3.2.3.2 Dop affects endosomal transport during cellularisation

Rab11-positive endosomal vesicles are mislocalised in dop^{1}/dop^{10} transheterozygous embryos and focus more around the centrosomes than in *wild type* (Hain et al. 2014). To look for endosomal distribution in germ line clone dop^{10} mutants, two different markers of the endosomal pathway were analysed. Nuclear fallout (Nuf) is a Rab11 effector, co-localises with Rab11 at the recycling endosome during cellularisation and is required for membrane addition and actin organisation at the elongating furrow during this stage (Cao et al. 2008; Riggs et al. 2003; Riggs et al. 2007). Both, Rab11 and Nuf function in an exocytic step of endosomal trafficking, delivering membrane and membrane-associated proteins from the recycling endosome to the plasma membrane (Ullrich et al. 1996; Lecuit & Wieschaus 2000; Riggs et al. 2003; Rothwell et al. 1999). In contrast, Eps15 (Epidermal growth factor receptor Pathway Substrate clone 15) is a member of the Clathrin coated vesicle transport and functions in endocytosis, endosomal protein sorting and cytoskeletal organization (Koh et al. 2007; Roxrud et al. 2008). Its function in *Drosophila* is well studied in the nervous system during larval stages where Eps15 has an essential role in synaptic vesicle recycling (Koh et al. 2007; Majumdar et al. 2006). Localisation of Eps15 and Nuf in respect to each other and in respect to β-tubulin was analysed by immunostaining of fixed *wild type* and germ line clone dop^{10} mutant embryos (Fig.24).

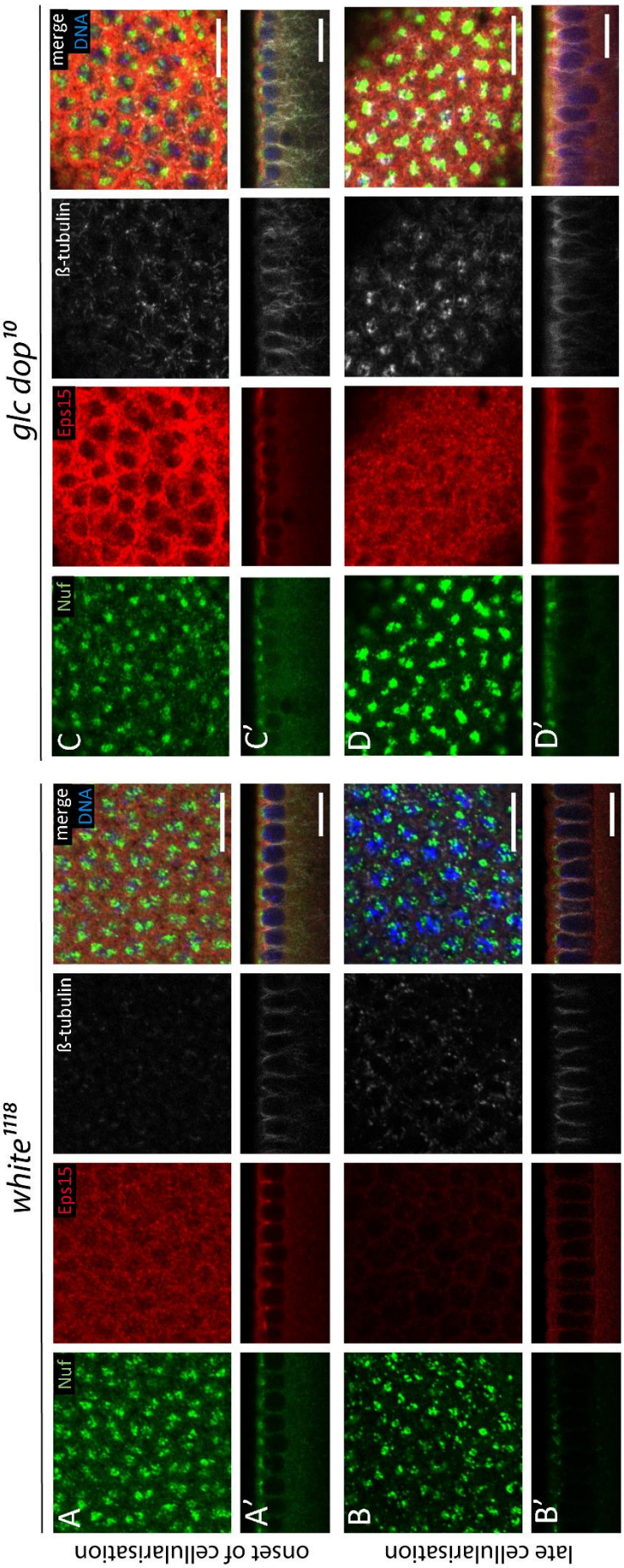

Figure 24 Endosomal transport marker Nuclear fallout shows a localisation distinct from Eps15 and has a phenotype in *dop* mutants reminiscent of Rab11 localisation. Formaldehyde-fixed *wild type* and germ line clone *dop*^{10} mutant embryos stained for Nuclear fallout (Nuf, green), Eps15 (red), β-tubulin (white) and with DAPI (DNA; blue). Shown are cross-sections (A'-D') and sagittal-sections (A-D) of each embryo during onset (A, A', C, C') and late cellularisation (B, B', D, D'). Nuf is localised to the centrosomes apical of the nuclei in both *wild type* and mutant embryos (A', C', B' D'). Note that its localisation during late cellularisation is more compact in *dop* mutants (D) compared to *wild type* (B). Scale bars represent 10 µm.

During cellularisation, Nuclear fallout (Nuf) is mostly localised at the centrosomes apical to the nuclei in both *wild type* and complete loss-of-function *dop* mutants (Fig.24 green channel). This localisation differs from Eps15 localisation which in contrast localises to the furrow canal and the lateral membrane (Fig.24 red channel). The localisation at the furrow canal supports the role of Eps15 in Clathrin coated vesicle transport since Clathrin components localise to the furrow canal which is the major site of endocytosis during early cellularisation (Albertson et al. 2005; Sokac & Wieschaus 2008a). Microtubule bundles do not co-localise with either the centrosomes or the furrow canal but are localised tightly around the nuclei and, thereby, in proximity to the emerging lateral membranes (Fig.24 white channel). Basally of the nuclei, Nuf and Eps15-positive punctae can be seen which are possibly co-localised with microtubules. However, the resolution is not high enough to substantiate this possibility. The stainings show that Nuf and Eps15 are localising to different components of the endosomal pathway which is consistent with their different functions during endosomal trafficking. β-tubulin localisation is not disturbed in complete loss-of-function *dop* mutants, however, during late cellularisation the microtubule baskets surrounding the nuclei stay with the nuclei when they get pushed away from the cortex whereas the centrosomes stay at the cortex (Fig.24 D‘) which is consistent with previous stainings done on dop^{1} hypomorphic mutants (Hain 2010). In complete loss-of-function *dop* mutants, Nuf seems to localise in a more compact way around the centrosomes during late cellularisation compared to *wild type* (Fig.24 B, B‘, D, D‘). This phenotype is reminiscent of the phenotype seen for Rab11-GFP localisation in dop^{1}/dop^{10} mutant embryos (Hain et al. 2014). This similarity is expected because Nuf and Rab11 have been shown to co-localise at recycling endosomes in a mutually dependent way (Riggs et al. 2003). This result shows that the Nuf- and Rab11-dependent transport of vesicles from the recycling endosome to the plasma membrane is also impaired in complete loss-of-function *dop* mutant embryos. In addition, also Eps15 shows an altered localisation in germ line clone dop^{10} mutant embryos (Fig.24 C, C’, D, D’). Whereas Eps15 localises mainly to internuclear foci and the furrow canal during cellularisation in *wild type* embryos (Fig.24 A, A’, B, B’), in *dop* mutants, Eps15 localisation is broadened and resembles the

localisation of F-actin in hypomorphic and complete loss-of-function mutants as shown earlier in this thesis. This mislocalisation of an endocytic factor at the furrow canal could have implications for other furrow canal proteins. This possibility will be investigated in the following experiments.

3.2.4 Exploring a possible mechanism of Dop function during cellularisation

3.2.4.1 Furrow canal initiator protein Slam is mislocalised in *dop* mutants

Analysis of proteins specifically localising to the furrow canal during cellularisation point to broadening of this structure in *dop* mutants (Hain et al. 2014; Hain 2010 and this thesis). Furrow canal specification is dependent on the redundant function of the two early zygotic genes *slam* (*slow-as-molasses*) and *nullo* (Acharya et al. 2014). Additionally, *slam* is required for furrow invagination in a non-redundant manner, a process that is also impaired in *dop* mutants as shown above. Slam has been shown to mislocalise in dop^{1} homozygous embryos (Hain et al. 2014). Thus, Slam could provide a link between Dop function during cellularisation and two major phenotypes in *dop* mutants (i.e. furrow canal formation and membrane invagination defects). To see if Slam also mislocalises in the complete loss-of-function mutant for dop^{10}, immunostainings against this protein have been performed (Fig.25).

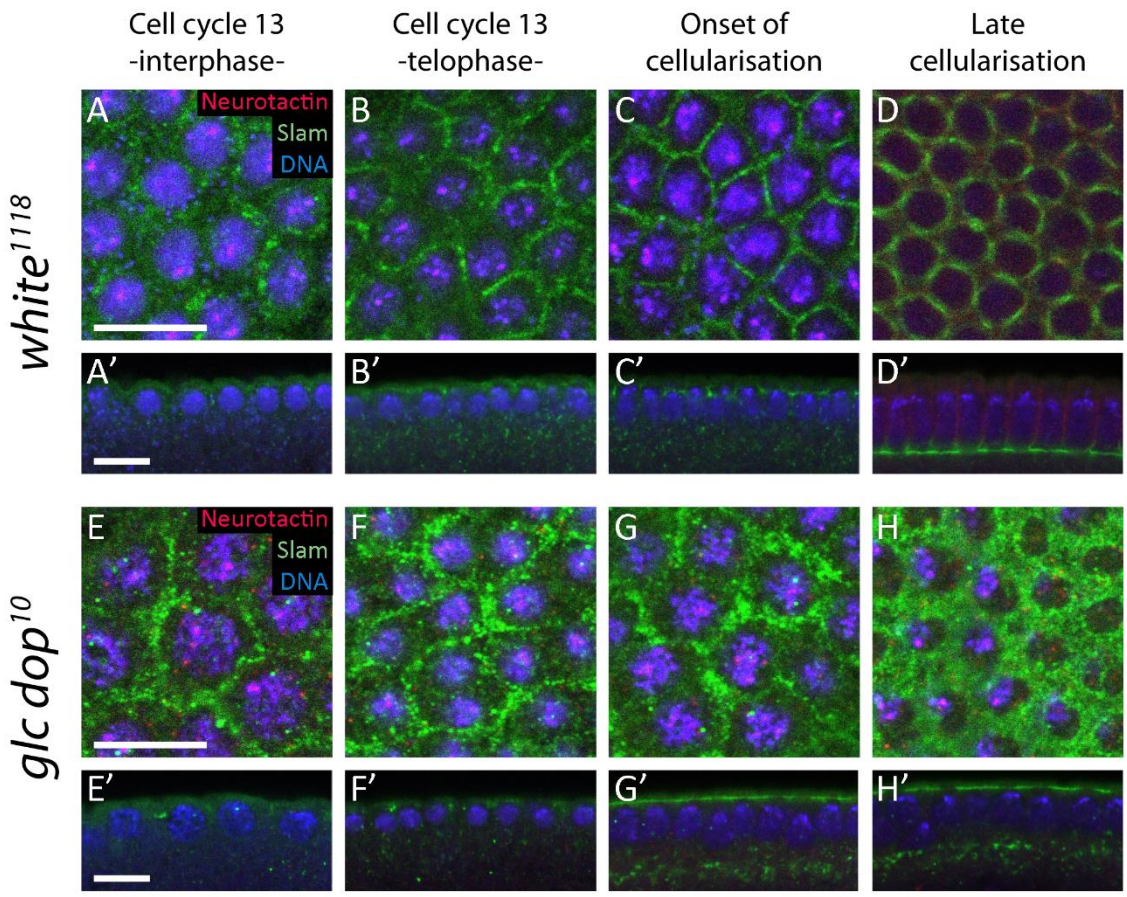

Figure 25 Slam mislocalises already during the last syncytial division in complete *dop*^{10} loss-of-function mutants. Formaldehyde-fixed *wild type* and germ line clone *dop*^{10} mutant embryos stained for Slam (green), Neurotactin (red, membrane marker) and DNA (blue). Shown are cross-sections (A-H) and sagittal-sections (A'-H') of each embryo. During telophase of cell cycle 13, Slam starts to focus into later furrows in *wild type* embryos (B), whereas in germ line clone *dop*^{10} mutants, Slam remains broadened and punctate throughout cellularisation (F, G, H). Scale bars represent 10 µm.

In *wild type* embryos, Slam displays a punctate and uneven distribution in the internuclear space during interphase of syncytial cell cycle 13 (Fig.25 A, A'). However, already during telophase of cell cycle 13, Slam punctae connect to focus at the site of the later furrows (Fig.25 B, B'). This focussing is not visible in germ line clone *dop*^{10} mutants (Fig.25 F, F'). Instead, the punctate localisation of Slam persists during cellularisation (Fig.25 G, G', H, H'). During cellularisation, Slam overall localisation is broadened at the internuclear space resembling a phenotype also characteristic for F-actin distribution. The similarity of F-actin and Slam phenotypes in germ line clone *dop*^{10} mutants could be due to an involvement of Slam in F-actin localisation. Slam has been shown to recruit the F-actin regulator RhoGEF2 and non-muscle Myosin II to the sites of membrane invagination (Wenzl et al. 2010; Lecuit et al. 2002). Furthermore, RhoGEF2 is required for F-actin accumulation at the furrow canal and embryos mutant for RhoGEF2 display

enlarged furrow canals (Padash Barmchi et al. 2005; Grosshans et al. 2005). Therefore, this result could provide a link between Slam in F-actin mislocalisation and furrow canal malformation in *dop* mutants.

3.2.4.2 Eps15 co-localises with Slam at the furrow canal and gets mislocalised in *dop* mutants

It is published that Slam localisation to the furrow is controlled by the Nuf/Rab11-dependent recycling endosome (Acharya et al. 2014). Slam localisation in turn enables RhoGEF2 recruitment to the furrow canal and thereby maintains F-actin stability at the invaginating furrows (Cao et al. 2008; Wenzl et al. 2010). However, Slam is not directly transported by Nuf/Rab11-positive recycling endosomes because Slam did not co-localise with Rab11 proteins (Acharya et al. 2014). Instead, it was proposed that Nuf/Rab11-positive vesicles transport a receptor to the furrow canal that binds Slam and restrict it to the furrow canal. Slam protein localisation is dynamic only during onset of cellularisation (Acharya et al. 2014). Thus, Dop function in affecting Slam localisation must be required at this stage. During this period also the endocytic endosomal protein Eps15 is mislocalised as shown earlier (Fig.24). In order to see if not only exocytosis but also endocytosis could play a role in Slam dynamics during onset of cellularisation, co-staining of Eps15 with Slam has been performed (Fig.26).

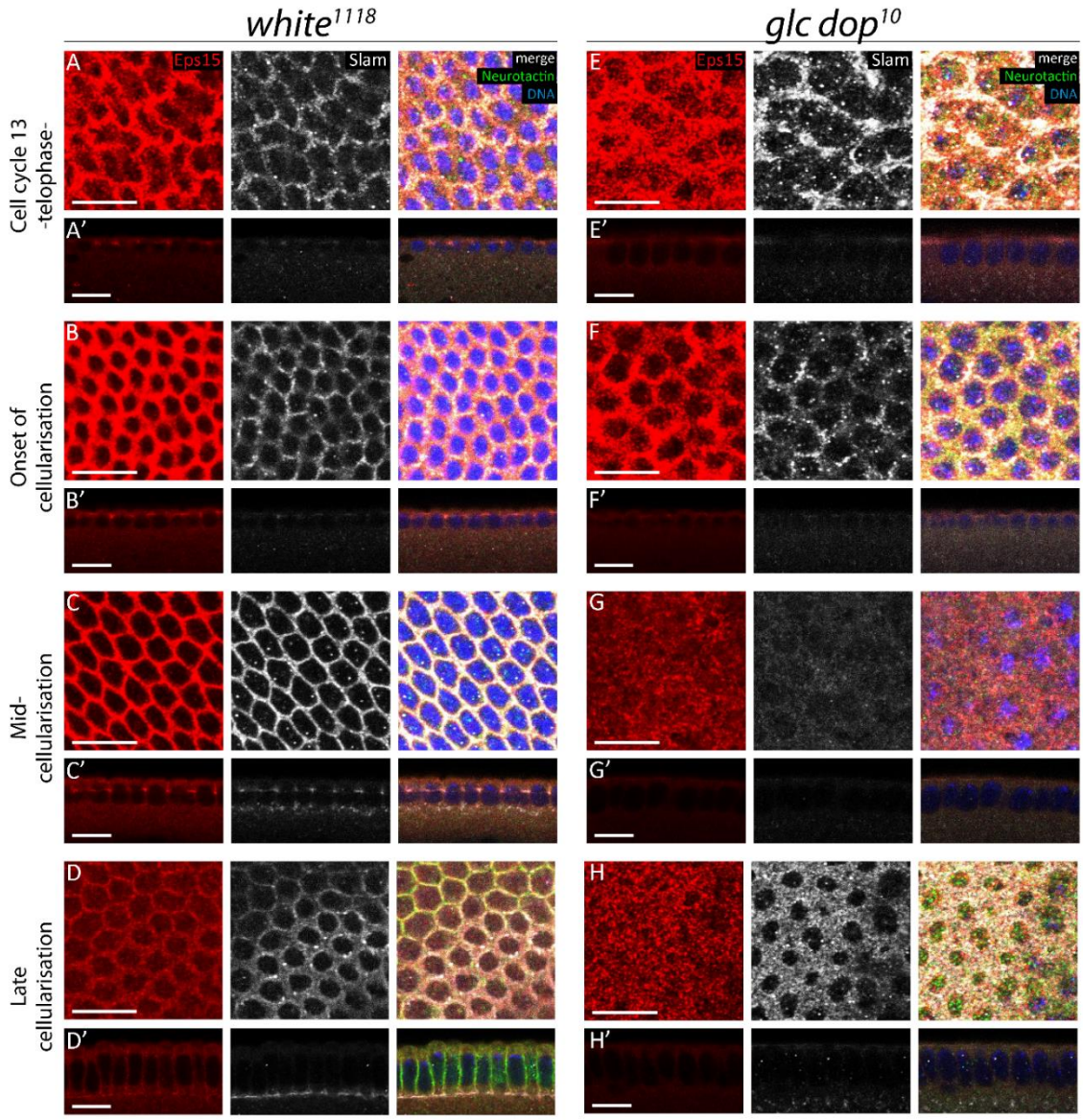

Figure 26 Eps15 co-localises with Slam and is mislocalised in complete *dop*^{10} loss-of-function mutants. Formaldehyde-fixed *wild type* and germ line clone *dop*^{10} mutant embryos stained for Eps15 (red), Slam (white), Neurotactin (green, membrane marker) and DNA (blue). Shown are sagittal-sections (A-H) and cross-sections (A'-H') of each embryo. In *wild type* (A-D') as well as in *dop* mutants, Slam co-localises with Eps15. Both proteins are mislocalised during cellularisation in *dop* mutants (E-H'). Scale bars represent 10 µm.

During telophase of cell cycle 13, Eps15 begins to accumulate into a pseudo-hexagonal pattern (Fig.26 A, A'). At onset of cellularisation, it accumulates to the future furrow canal region apical to the nuclei in a broad distribution in *wild type* (Fig.26 B, B'). During mid-cellularisation, this distribution sharpens to internuclear foci when the furrow canal invaginates into the embryo (Fig.26 C, C'). Eps15 is mainly localised to the furrow canal but is also visible at the forming lateral membrane. At late cellularisation, Eps15 is not as focussed to the furrow canal as in mid-cellularisation but is localising to the furrow canal and the lateral membrane to a similar extent

(Fig.26 D, D‘). The focus into a furrow canal structure and internuclear foci is not visible at any stage in germ line clone *dop*^{10} mutants (Fig.26 E-H). Eps15 localisation is punctate with an accumulation apical to the nuclei throughout cellularisation. Eps15 protein is co-localising with Slam protein during cellularisation in *wild type* as well as germ line clone *dop*^{10} mutants. However, Slam is not localising to the lateral membrane like Eps15 but solely to the furrow canal (Fig.26 C‘, D‘). This indicates that Eps15-positive vesicles could be responsible for Slam exchange and endocytosis at the furrows. Additionally, Eps15 may also initiate endocytosis of other cargo that is possibly localised to the furrow canal as well as the lateral membrane. Furthermore, FRAP experiments propose that Slam protein is transported to the furrow canal just at onset of cellularisation but the exchange rate of Slam at the furrow canal in later cellularisation is very low (Acharya et al. 2014). Other proteins localising to the furrow canal in a more dynamic manner throughout cellularisation like e.g. RhoGEF2 are therefore also possible cargoes of Eps15-positive vesicles. Riggs et al report that Nuf-recycling endosomal transport is Dynein-dependent (Riggs et al. 2007). It would be interesting to investigate if also the endocytic trafficking is Dynein-dependent. This could provide an interesting link between an endosomal recycling phenotype, Dynein and Drop out function.

3.2.4.3 Analysis of Kinesin heavy chain and Dynein heavy chain protein localisations during cellularisation

In addition to previous studies, many of the phenotypes described in this thesis suggest a defect in Dynein and/or Kinesin function in *dop* mutants (Hain et al. 2014; Hain 2010; Langlands 2012; Meyer et al. 2006). Additionally, a study in Daniel Hains thesis on germ line clone–derived embryos mutant for the *kinesin light chain* shows cellularisation defects similar to *dop* mutants (i.e. embryo lethality during cellularisation, severe nuclear drop out and impairment of membrane invagination) (Hain 2010). However, no reliable data are available that show Dynein or Kinesin localisation in *dop* mutant embryos which could possibly give further insights into

Dynein or Kinesin malfunction. To test for the localisation of both transporter proteins, fixed embryos were immunostained against Dynein heavy chain and Kinesin heavy chain, in addition to Eps15 to elucidate potential co-localisations (Fig.27).

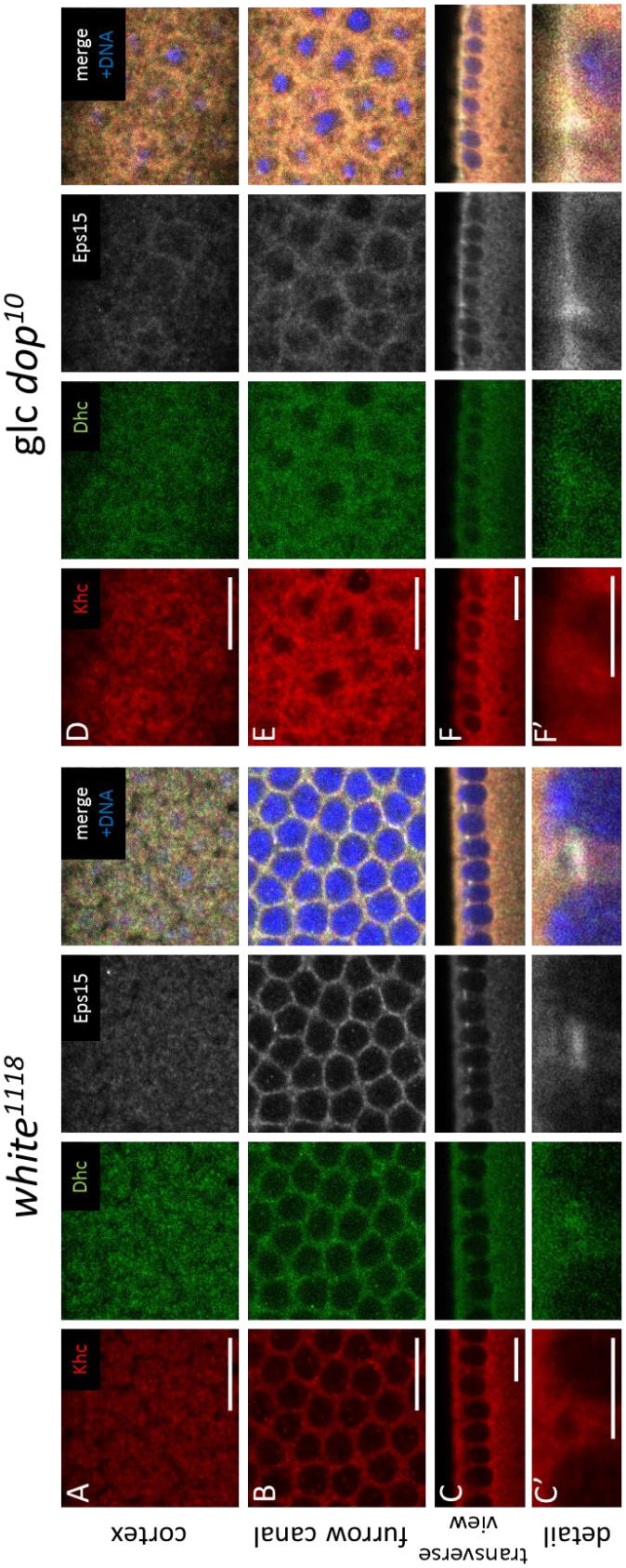

Figure 27 Dynein heavy chain shows co-localisation with Eps15 at the furrow canal. Formaldehyde-fixed *wild type* and germ line clone *dop*^{10} mutant embryos stained for Kinesin heavy chain (Khc, red), Dynein heavy chain (Dhc, green), Eps15 (white) and DNA (blue). Shown are sagittal-sections (A, B, D, E), cross-sections (C-F) and furrow canal details of the cross-sections (C', F') of each embryo. Scale bars represent 10 µm (in A-F) and 5 µm (in C', F').

At onset of cellularisation, both Dynein heavy chain (Dhc; Fig.27 green channel) and Kinesin heavy chain (Khc; Fig.27 red channel) localise all around the nuclei in a punctate fashion both in *wild type* and complete loss-of-function *dop* mutants (Fig.27 A-C, D-F). In *wild type*, Khc and Dhc seem to localise strongly apically and basally to the nuclei. Lateral of the nuclei there is a weak accumulation of Dhc visible at the furrow canal, co-localising with Eps15 (Fig.27 C, C'). In complete loss-of-function dop^{10} mutants, no furrow canal is visible and Eps15 stays broadly along the cortex with some accumulations at internuclear foci (Fig.27 D, E, F). It seems that Dhc shows some accumulation at the same sites as Eps15 in contrast to Khc. However, it cannot be determined if this localisation is specific (Fig.27 F'). All three stainings against Khc, Dhc and Eps15 seem to be stronger in complete loss-of-function *dop* mutants compared to *wild type* (Fig.27 A-C, D-F). This could be due to an artefact because *wild type* and complete loss-of-function *dop* mutant embryos were stained in separate tubes and a lower number of complete loss-of-function *dop* mutant embryos were stained compared to *wild type*. Therefore, the antibodies might have had a higher dilution in the *wild type* embryo tube compared to the *dop* mutant embryo tube.

The co-localisation of Dynein heavy chain and Eps15 at the furrow canal in *wild type* embryos suggests the possibility of a Dynein-dependence of Eps15 localisation at this site. However, it could not be determined if this relation is disturbed in complete loss-of-function *dop* mutants. Further stainings using more specific antibodies or different fixation methods are needed to determine if Kinesin and/or Dynein are mislocalised in germ line clone dop^{10} mutant embryos.

3.2.5 Conclusion of Results Part 2

In this Results part, localisations of different proteins representative for major cellular processes have been analysed in *dop* mutants to determine by which mechanism Dop affects cellularisation. The focus was set on processes that are dependent on Dynein function and that have been shown previously to have an impact on *Drosophila* cellularisation. It was shown that

Golgi as well as endosomal trafficking was impaired in *dop* mutants. These defects were visible in hypomorphic dop^{1}/dop^{10} mutant embryos as well as complete loss-of-function germ line clone embryos homozygous for dop^{10} mutants. As revealed by live-imaging of microtubule formation by tracking EB1-GFP and in accordance with previous stainings against β-tubulin (Hain et al. 2014), the microtubule network seemed to be unaltered in *dop* mutants and is therefore unlikely as a cause for the defects in microtubule-dependent transport. Two different stages of endosomal transport have been analysed, one stage by analysing Rab11 and Nuf localisation which mark vesicles on the way from the recycling endosome to the plasma membrane for exocytosis, and another stage where Eps15 marks membrane sites targeted for endocytosis. Both stages showed altered protein localisations in *dop* mutants compared to *wild type*. Whereas Rab11 and Nuf display a more restricted localisation to the centrosomes and microtubule minus-ends which is more suggestive for a malfunction of Kinesin than of Dynein, Eps15 showed a broadened localisation at the furrow canal in *dop* mutants, similar to what has been seen for F-actin localisation and other furrow canal proteins (Hain et al. 2014). This shows that both exo- and endocytosis of endosomal trafficking seem to be affected in *dop* mutants. In addition, Slam, a protein required during cellularisation for furrow canal formation and membrane invagination, showed the same broadened appearance at the furrow canal as Eps15 and co-localised with this endocytic marker. This raises the possibility that impaired endocytosis could account for protein mislocalisation at the furrow canal and furrow canal broadening. This hypothesis will be discussed later together with the suggestion of further experiments to test this hypothesis. Moreover, it would be interesting to test if this Eps15 mislocalisation could be caused by Dynein malfunction in *dop* mutants. As a starting point in addressing this possibility, stainings against both microtubule motors Dynein and Kinesin as well as Eps15 were performed to test for co-localisations. The stainings showed a weak accumulation of Dynein and a strong accumulation of Eps15 at the furrow canal of *wild type* embryos in early cellularisation. However, the background signal was too strong in both Kinesin and Dynein stainings to determine any further localisation and to make a definitive statement about the localisation in *dop* mutants.

Further experiments will be needed to determine Dynein and Kinesin localisation in *dop* mutants and their impact on cellularisation processes.

3.3 Part 3: Studying Dynein as potential *drop out* target

Introduction

Cytoplasmic Dynein is a multiprotein complex essential for cell viability in *Drosophila* (Gepner et al. 1996; McGrail & Hays 1997). It is involved in many cellular processes such as minus-end directed transport of organelles and vesicles, mitotic spindle morphogenesis and chromosome movements as well as nuclear positioning (see Karki & Holzbaur 1999 for review). The phosphorylation of several of its subunits was shown as being important for Dynein regulation (Addinall et al. 2001; Dell et al. 2000; Ikeda et al. 2011; Runnegar et al. 1999; Vaughan et al. 2001; Whyte et al. 2008; Yang et al. 2005). Previously, it was found that phosphorylation of Dynein intermediate chain (Dic) as well as phosphorylation of Dynein light intermediate chain (Dlic) was reduced in *dop* mutant embryos (Hain et al. 2014; Langlands 2012). This suggested that Dop is required for regulating phosphorylation of these Dynein subunits. Additionally, the mutant allele dop^{1} showed genetic interaction with $short\ wing^{1}$ (a loss-of-function allele of *dic*) and $Glued^{1}$ (a dominant-negative mutation affecting the Dynactin complex subunit p150/Glued (*p150/Gl*)). An impairment of Dynein function by *dop* mutations was also implied by phenotypes seen in *dop* mutant embryos affecting Dynein-dependent transport processes, such as Bazooka protein, pair rule gene products and lipid droplet transport (Gross et al. 2000; Meyer et al. 2006; Hain et al. 2014). Apart from these Dynein-dependent processes which provided a link between Dop and cellularisation, Dynein was shown to be directly involved in proper furrow invagination by transport of Golgi vesicles, two processes also affected in *dop* mutants (Papoulas et al. 2005; this thesis). Thus, Dynein regulation by Dop could provide a mechanistic basis between Dop function and cellularisation.

3.3.1 Attempts to inhibit Dynein function specifically during cellularisation

Studies done by Daniel Hain indicated a link between Dop function and Dynein transport during cellularisation (Hain 2010; Hain et al. 2014). The function of Dynein-dependent microtubule transport in cellularisation is not known in detail because Dynein is required for many processes occurring prior to this developmental stage and, therefore, Dynein mutants do not develop normally up to this stage. To get around this problem, Papoulas et al., 2005 looked at Dynein function during cellularisation by injecting a Dynein heavy chain antibody. They found that cell membrane invagination was disturbed during fast phase in injected embryos but focussed more on the impact of Dynein impairment on Golgi vesicle movements than on further defects occurring by Dynein inhibition (Papoulas et al. 2005). However, Dynein could provide a strong link between Dop function and cellularisation defects like furrow formation impairment, membrane invagination defect and F-actin mislocalisation. Thus, it would be interesting to look at embryos with impaired Dynein function in more detail.

3.3.1.1 Dynamitin zygotic overexpression

One way to inhibit Dynein function is the expression of a subunit of the Dynactin complex called Dynamitin. Dynamitin overexpression was shown to lead to dissociation of Dynactin from Dynein and therefore an inhibition of Dynein function (Echeverri et al. 1996; LaMonte et al. 2002; Januschke et al. 2002). In *Drosophila*, maternal overexpression of Dynamitin leads to eggs with abnormal dorsoventral polarity (Januschke et al. 2002).

To investigate an effect of Dynein impairment on cellularisation, Dynamitin was overexpressed zygotically by crossing females carrying a maternal α-tubulin Gal4 driver to males carrying the UAS:(human)Dynamitin effector. Gal4 is expressed throughout early embryogenesis, however, in this cross Dynamitin should be expressed at the maternal to zygotic transition, so just prior to cellularisation. This should provide a tool to inhibit Dynein specifically from cellularisation

onwards. The purity of the fly stock carrying the UAS::Dynamitin effector was verified by the presence of the published phenotypes in embryos maternally expressing the human Dynamitin construct (Januschke et al. 2002; see Appendix Fig.S1). To test if Dynamitin overexpression can alter cellularisation, time-lapse movies of cellularisation were produced and membrane invagination measured by generating kymographs (Fig.28).

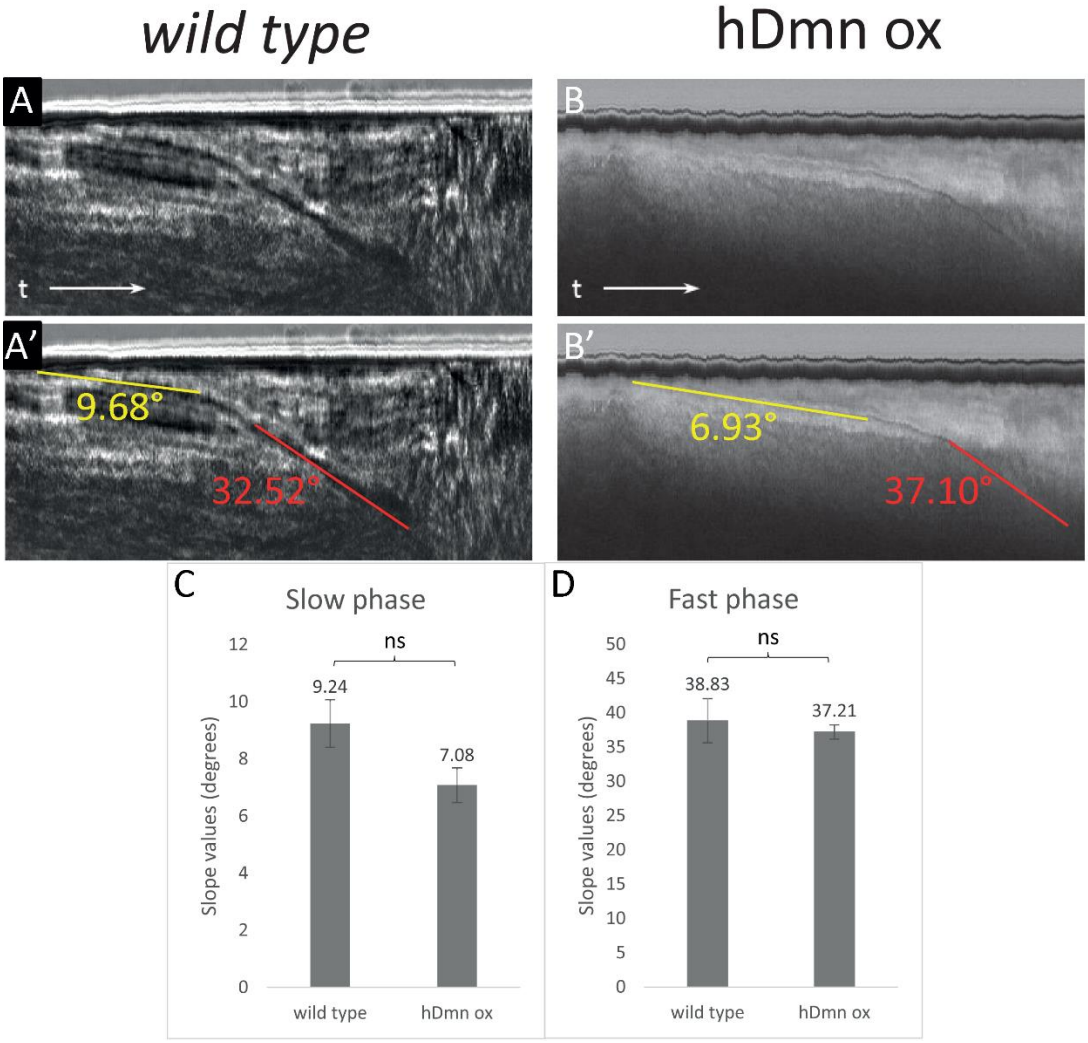

Figure 28 Zygotic Dynamitin overexpression with a single maternal driver does not impair cellularisation in *Drosophila* embryos. Membrane growth in *wild type* embryos (A, A') or embryos expressing human Dynamitin under control of a single maternal α-tubulin Gal4 driver (hDmn ox; B, B') was measured in kymographs generated from bright field movies using ImageJ. An area of interest of 1 by 180 pixels at the same position in every movie frame was selected. Assembly of the selected regions created an image showing the progression of the membrane in time (A, B). The progression of membrane growth was analysed for slow phase (yellow) and fast phase (red) by measuring the angle between the invaginating membrane front and the outer membrane of the embryo (A', B'). The time progression is indicated by t (A, B). Comparison of membrane invagination slopes shows no significant difference during slow or fast phase of

cellularisation in Dynamitin overexpressing compared to *wild type* embryos (C, D). (Two tailed *t*-test, ns = not significant; +/- SEM; *wild type* n = 3, hDmn ox n = 3)

Analysis of membrane invagination during cellularisation in embryos overexpressing Dynamitin in comparison to *wild type* embryos does not show an overall defect (Fig.28). Membrane invagination can be separated into slow phase (yellow line) and fast phase (red line) both in *wild type* and Dynamitin overexpressing embryos. Membrane invagination rates were not significantly different between both conditions, even though a tendency is visible showing that slow phase in Dynamitin overexpressing embryos might be impaired (Fig.28 C, D). The sample sizes for both conditions were not high enough, thus, the power of the performed *t*-test was below the desired power of 0.800 (at only 0.363 for slow phase). To verify an impairment of slow phase, more embryos have to be analysed. Even if slow phase of cellularisation is impaired in embryos overexpressing Dynamitin, this seems not to have a strong impact on further development because embryos developed normally throughout embryogenesis up to hatching (no data obtained).

Dynamitin overexpressed with a single maternal α-tubulin Gal4 driver did not show a strong effect on membrane invagination during cellularisation and later embryogenesis (Fig.28). To aim for the highest zygotic expression possible, Dynamitin expression was promoted using a strong double-driver (maternal α-tubulin driver on the second and third chromosome) at 18°C (optimal temperature for strongest maternal Gal4 expression). Expression was induced by crossing females carrying the maternal α-tubulin Gal4-double driver to males carrying the UAS::(human)Dynamitin effector. As in the previous experiment, Dynamitin in this experiment set-up should get expressed just prior to cellularisation. To test its possible effects on embryo development by Dynein impairment, embryo hatching rates were determined (Fig.29).

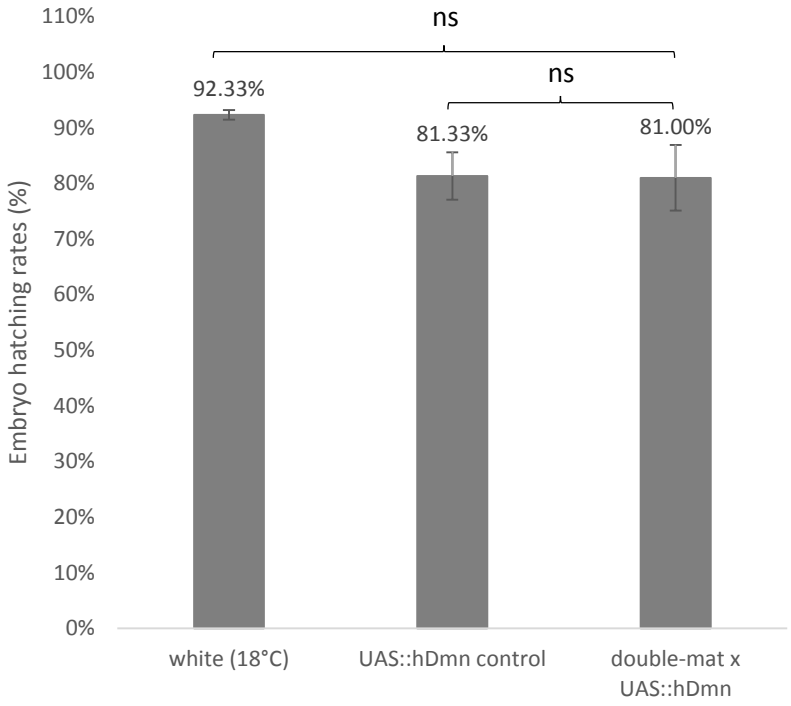

Figure 29 Zygotic Dynamitin overexpression with a double maternal driver does not have an effect on embryo hatching rates. Survival rates of *wild type* embryos (white (18°C)), embryos without driver construct (UAS::hDmn control) and embryos expressing human Dynamitin under control of a maternal α-tubulin Gal4 driver on the second and third chromosome (double-mat x UAS::hDmn) are shown. Hatching rates have been determined at 18°C. No significant difference in hatching rates can be detected between embryos expressing Dynamitin and the control lines. (Two tailed *t*-test, ns = not significant; +/- SEM; at least 3 independent tests have been performed; Number of eggs (total): *white* (18°C) = 300, UAS::hDmn control = 300, double-mat x UAS::hDmn = 379)

The determined hatching rate of zygotic Dynamitin overexpression was slightly reduced compared to *wild type* flies at 18°C (Fig.29). However, it was comparable to the survival rates of embryos carrying the UAS effector construct alone and the difference was not significant. Thus, the reduced survival rate was unlikely to be caused by a strong inhibition of Dynein function. Strong Dynein inhibition was the aim of this experiment, thus, this experiment has not been followed up and different tools were tested as an alternative.

3.3.1.2 Ciliobrevin injections

Injecting embryos at onset of cellularisation with Ciliobrevin D (a small molecule that inhibits Dynein by blocking its ATP binding site in a reversible manner) could provide another tool to inhibit Dynein specifically during cellularisation (Firestone et al. 2012). Ciliobrevin D was shown

to inhibit Dynein in various cell types (murine NIH-3T3, *Xenopus* melanophores, *Drosophila* S2 cells, murine IMCD3 cells) as well as in mouse oocytes and *Drosophila* embryos during late embryogenesis (Hyman et al. 2009; Ye et al. 2013; Łuksza et al. 2013; Le Droguen et al. 2015). Ciliobrevin D from two different sources and different concentrations were used (see Materials section). Only data from embryos injected with Ciliobrevin D donated by the James Chen lab are shown (concentration injected: 7387 µM). Injections were verified by co-injection of Dextran-FITC (see Appendix Fig.S2). To test if Ciliobrevin D injection has an effect on cellularisation, development of injected and uninjected control embryos (*wild type* condition) was recorded over the course of cellularisation using bright field imaging and membrane invagination was analysed on kymographs (Fig.30).

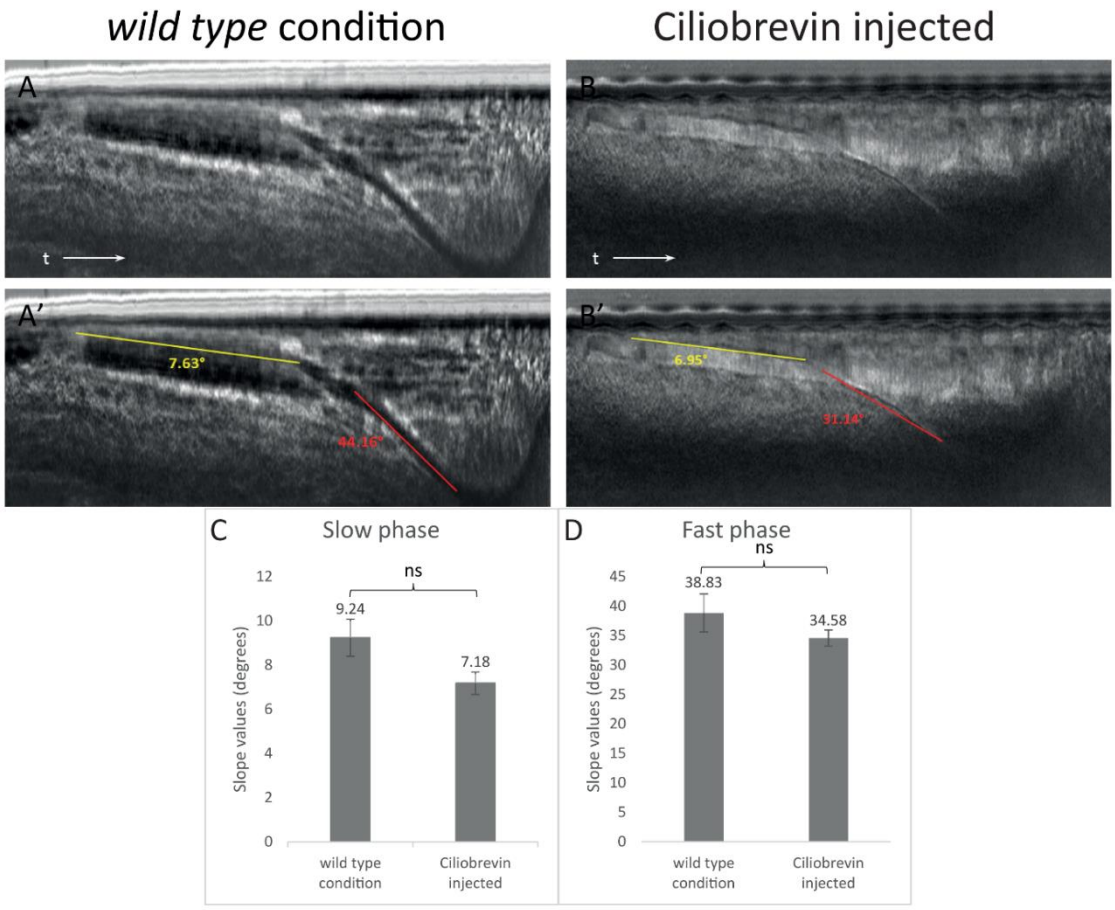

Figure 30 Analysis of membrane invagination during cellularisation reveals no significant difference in Ciliobrevin injected embryos compared to uninjected embryos. Membrane growth in uninjected embryos (*wild type* condition) or embryos injected with Ciliobrevin D was measured using kymographs generated from bright field movies using ImageJ. An area of interest of 1 by 180 pixels at the same position in every movie frame was selected. Assembly of the selected regions created an image showing the progression of the membrane in time (A, B). The progression of membrane growth was analysed for slow phase (yellow) and fast phase (red)

by measuring the angle between the invaginating membrane front and the outer membrane of the embryo (A', B'). The time progression is indicated by t (A, B). No significant difference in membrane growth between uninjected and Ciliobrevin D injected embryos could be detected during slow or fast phase of cellularisation (C, D). Imaging at 18°C. (Two tailed *t*-test, ns = not significant; +/- SEM; slow phase: uninjected n = 3 (controls in this experiment are the same as in the Dynamitin overexpression experiment), Ciliobrevin D-injected n = 11; fast phase: uninjected n = 3, Ciliobrevin D-injected n = 10)

Embryos injected with Ciliobrevin D underwent cellularisation clearly dividable into slow phase (yellow line) and fast phase (red line) (Fig.30 B'). At 18°C, the change of slow phase to fast phase occurred ~50 min after onset of cellularisation in embryos with and without Ciliobrevin injection. Membrane invagination rates were not significantly different in Ciliobrevin D-injected embryos compared to uninjected embryos (Fig.30 C, D). Additionally, embryos developed normally throughout embryogenesis (no data obtained). If Ciliobrevin D is inhibiting Dynein in this system, these data indicate that Dynein has no or just a minor effect on cellularisation. However, the data presented here comprise certain weaknesses: First, the sample sizes for the uninjected condition are very low and the power of the performed *t*-test for both slow phase (= 0.417) and fast phase (= 0.257) of cellularisation was below the desired power of 0.800. Thus, more embryos have to be imaged to get a convincing result and to see a possible effect on the timing of membrane invagination. Second, it is not clear if Ciliobrevin D used in this experiment is inhibiting Dynein. A clear effect at least on fast phase during cellularisation would be expected upon Dynein inhibition according to published results (Papoulas et al. 2005). Therefore, a new experiment had to be set up to verify Dynein impairment upon Ciliobrevin D injections in early embryos.

3.3.1.2.1 Test for specific effects of Ciliobrevin D on Dynein function during syncytial divisions

No significant difference in membrane invagination rates and timings could be detected due to Ciliobrevin D injections and embryos developed through whole embryogenesis. This result would indicate that Dynein does not have an essential function during cellularisation and embryogenesis. However, it had not been verified that Ciliobrevin D inhibits Dynein in early embryos in the used assay. Robinson et al. reported free centrosomes and multipolar spindle

arrays during syncytial divisions in embryos mutant for *dynein heavy chain* (Robinson et al. 1999). To test for Dynein inhibition by Ciliobrevin D, embryos expressing Tubulin-GFP were injected during syncytial divisions either with DMSO/Dextran-FITC or with Ciliobrevin D/ Dextran-FITC and analysed for spindle defects reported in Robinson et al. (Fig.31).

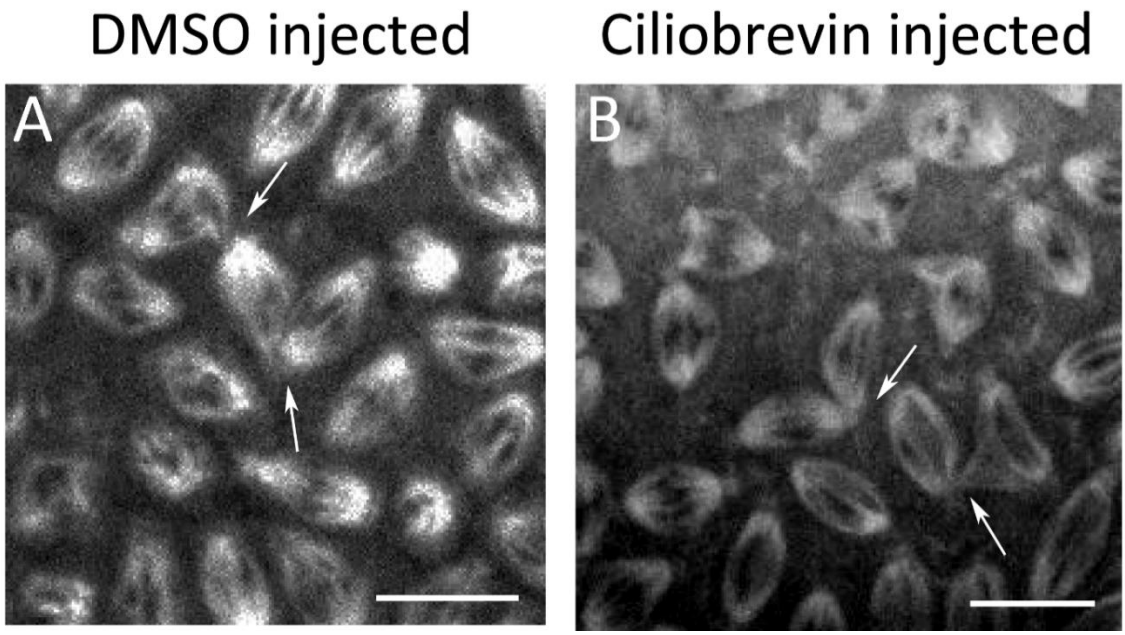

Figure 31 Spindle array formation during syncytial divisions. Images taken from time-lapse recordings of Tubulin-GFP expressing embryos under control of a maternal α-tubulin Gal4 driver during syncytial divisions. Embryos were either injected with DMSO and Dextran-FITC (A) or Ciliobrevin D and Dextran-FITC (B). Arrows point to multipolar spindle arrays in DMSO and Ciliobrevin D injected embryos. (DMSO-injected n = 3, Ciliobrevin D-injected n = 5) Scale bars represent 10 µm.

Embryos injected with either DMSO or Ciliobrevin D show multipolar spindle arrays (Fig.31 A, B; see arrows). The penetrance of the phenotype has not been determined. However, these data show that even by injecting DMSO phenotypes similar to *dhc* mutants can be created. This made it impossible to determine Ciliobrevin D effects on Dynein function using this assay. Due to a lack of available assays to determine Ciliobrevin D effects on Dynein function in early embryos, no further experiments using Ciliobrevin D have been performed.

3.3.1.3 Dhc64C-RNAi maternal overexpression

Another attempt to interfere with Dynein function was performed using overexpression of RNAi against *Dynein heavy chain 64C* (*Dhc64C*)-encoded transcripts. The *Dhc64C* was shown to be essential for oogenesis and overall cell survival in *Drosophila* (McGrail & Hays 1997; Rasmusson et al. 1994; Gepner et al. 1996). An assay had to be developed that reduced Dynein function but enabled oogenesis and development of embryos up to cellularisation to look for Dynein impairment effects during this particular stage. The dosage of Dhc64C-RNAi supply was crucial in this experiment. The UAS/Gal4 system is temperature sensitive, usually driving more expression at high temperatures up to 30°C than at lower temperatures (Brand & Perrimon 1993). In contrast, the driver-construct used in this assay (maternal α-tubulin Gal4 driver) shows a reverse temperature-dependence with driving higher expression at low temperatures and lower expression at high temperatures (Jörg Großhans, personal communication). Consistent with this, females driving an RNAi construct against Dynein heavy chain 64C on the second chromosome ($Dhc64C^{GL00543}$) with a single maternal α-tubulin Gal4 driver did not lay any eggs at 18°C or 25°C but layed fertilised eggs at 29°C. To test if Dhc64C-RNAi significantly inhibits Dynein function under this condition, hatching rates of layed eggs with normal overall appearance have been determined at 29°C (Fig.32). Two different RNAi constructs against Dynein heavy chain 64C were analysed.

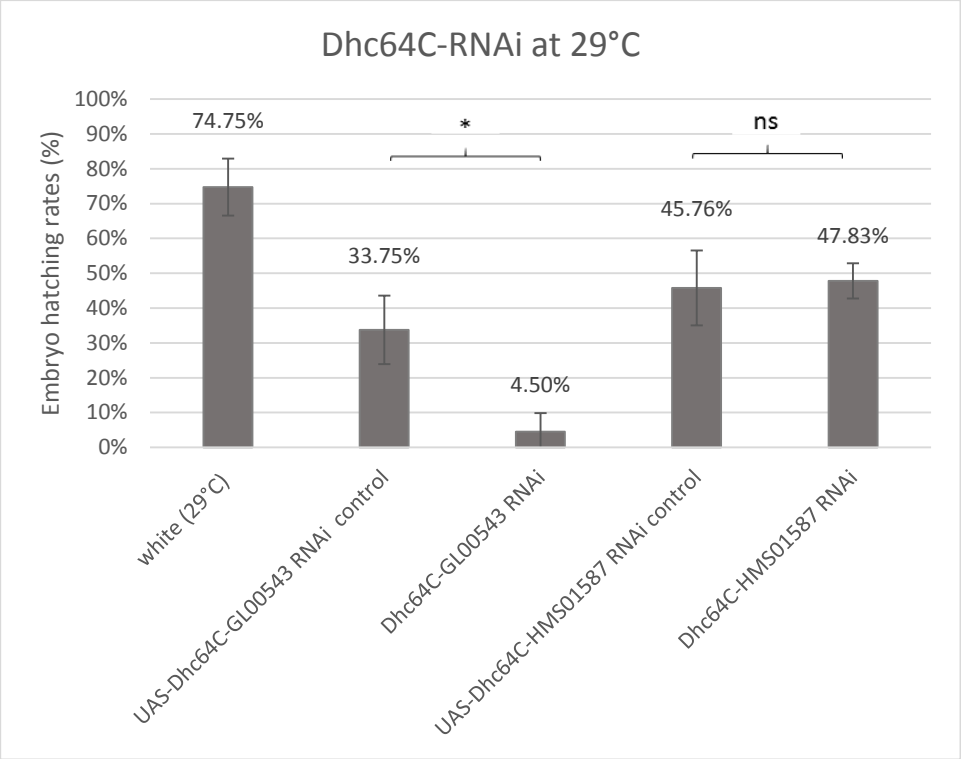

Figure 32 Dynein heavy chain 64C^{GL00543}-RNAi expression at 29°C shows highly reduced embryonic survival. Survival rates of embryos expressing one of two different RNAi constructs against Dynein heavy chain 64C under control of a single maternal α-tubulin Gal4 driver are shown. Hatching rates of *wild type* embryos (white (29°C)) and embryos carrying just the effector construct and not the driver (UAS-Dhc64C^{GL00543} RNAi control, UAS-Dhc64C^{HMS01587} RNAi control) were used as controls. Embryos carrying either of two Dhc64C-RNAi constructs were analysed (construct either on the second chromosome (Dhc64C^{GL00543} RNAi) or on the third chromosome (Dhc64C^{HMS01587} RNAi)). Hatching rates have been determined at 29°C. (Mann-Whitney Rank Sum Test, *p<0.05; ns = not significant; +/- SEM; at least 3 independent tests have been performed for each condition; Number of eggs (total): white (29°C) = 297, UAS-Dhc64C^{GL00543} RNAi control = 323, Dhc64C^{GL00543} RNAi = 265, UAS-Dhc64C^{HMS01587} RNAi control = 295, Dhc64C^{HMS01587} RNAi = 207)

Embryos driving either of the two Dhc64C-RNAi constructs (Dhc64C^{GL00543} RNAi or Dhc64C^{HMS01587} RNAi) show a reduction in embryonic survival compared to *wild type* control embryos (white (29°C)) (Fig.32). However, only the construct on the second chromosome shows a significantly reduced hatching rate compared to its effector-only control (UAS-Dhc64C^{GL00543} RNAi control), whereas the construct on the third chromosome shows a similar hatching rate compared to its effector-only control (UAS-Dhc64C^{HMS01587} RNAi control). Both constructs target different sites of the Dhc64C transcripts which is likely to cause the differences in the efficiency of the knock-down (Fig.33) (Ni et al. 2011).

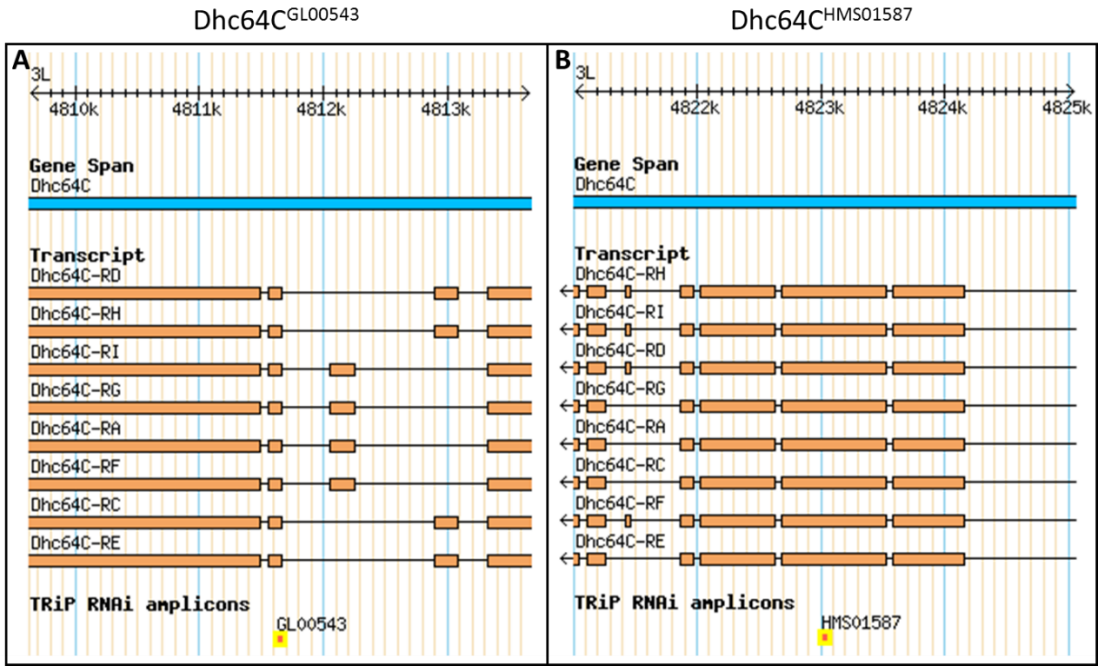

Figure 33 RNAi constructs used to target Dhc64C transcripts. Shown are the Dhc64C-RNAi target sites of both tested Dhc64C-RNAi constructs (Dhc64C^{GL00543} and Dhc64C^{HMS01587}) which target different exons present in all eight Dhc64C transcripts. (A) The construct on the second chromosome (Dhc64C^{GL00543}) targets the transcript sequence from 3L between 4,811,640 and 4,811,660. (B) The construct on the third chromosome (Dhc64C^{HMS01587}) targets the transcript sequence from 3L between 4,823,022 and 4,823,042. Figure modified after FlyBase.

The Dhc64C-RNAi construct on the second chromosome shows an about 16-fold reduction in the hatching rate compared to *wild type* embryos (Fig.32). Therefore, it is a promising tool to inhibit Dynein during embryogenesis and to look for defects during cellularisation.

3.3.2 DlicGFP localisation is not affected in hypomorphic *dop* mutants during either syncytial divisions or cellularisation

Dynein is an important candidate as potential Drop out target (Hain et al. 2014). However, not much is known about its localisation in *dop* mutants. Antibody stainings have not been successful (using an antibody against Dynein heavy chain protein from DSHB, this thesis) or not reproducible (using an antibody against Dynein heavy chain protein from Thomas Hays lab (Hays et al. 1994), done by Daniel Hain, unpublished). One subunit of cytoplasmic Dynein is the Dynein light intermediate chain (Dlic) (Mische et al. 2008). This subunit is essential for oocyte development, zygotic development and required for mitosis in *Drosophila*. Whereas two genes

encode for many isoforms of the Dlic in vertebrates, *Drosophila* only contains one gene encoding for two isoforms of which many differentially-phosphorylated forms exist. The Dynein subunit Dlic is an interesting protein for analysis because it was shown as a possible target for Dop function (Langlands 2012). In order to test if Dynein localisation is impaired in *dop* mutants, a DlicGFP construct was imaged in *dop* mutant embryos in comparison to *wild type* during syncytial divisions (Fig.34) and cellularisation (Fig.35).

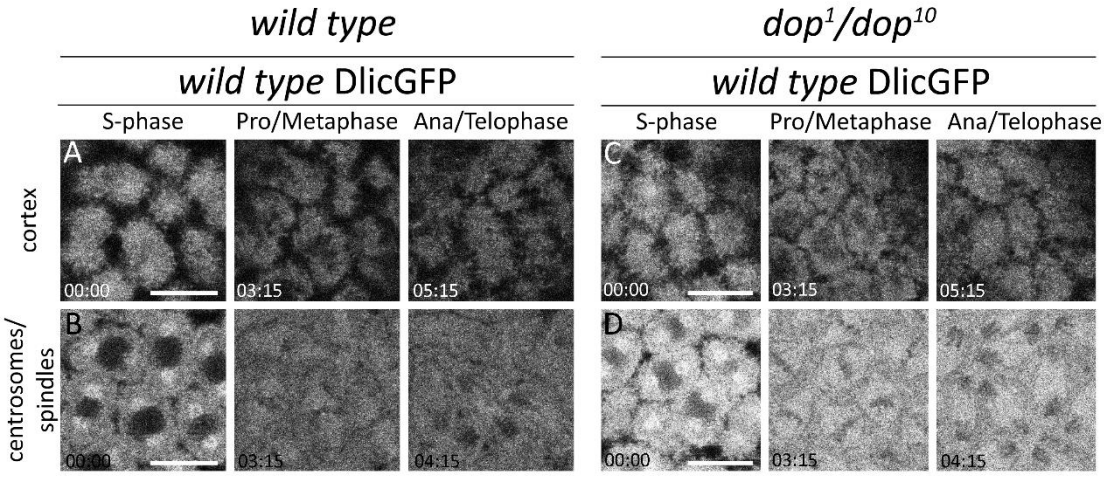

Figure 34 During syncytial cycle 13, *wild type* DlicGFP shows similar localisation in *wild type* and *dop* mutant embryos. Images taken from time-lapse recordings of *wild type* embryos (A, B) and *dop*^{1}*/dop*^{10} mutant embryos (C, D) expressing *wild type* DlicGFP under control of a double maternal α-tubulin Gal4 driver. Shown is DlicGFP signal at the cortex (A, C) as well as at the centrosomes/spindles of the embryos (B, D) during 3 different stages of syncytial cell cycle 13 (S-phase, Pro/Metaphase, Ana/Telophase). Images of different structures in one construct do not always show the same embryo. Time after cycle 13 S-phase indicated in min. Scale bars represent 10 µm.

DlicGFP in *wild type* as well as *dop*^{1}*/dop*^{10} mutant embryos localise to distinct structures during syncytial divisions (Fig.34). In S-phase, DlicGFP accumulates mainly at the centrosomes at either side of the nucleus (Fig.34 first frames B, D). DlicGFP does not localise to the nucleus. Another signal is visible apical of the centrosomes (Fig.34 first frames A, C). This signal is filamentous and may be due to DlicGFP binding to astral microtubules. It is visible in a cap-like structure reminiscent of F-actin caps. Otherwise, DlicGFP imaging displays a diffuse signal all over the first apical 5 µm which is maybe due to a pool of unbound Dlic. However, it could also be caused by an excess of DlicGFP due to its overexpression in addition to endogenously-derived Dlic in the embryo. During prophase and after nuclear breakdown, DlicGFP signal invades the area that was

occupied before by the nuclei (Fig.34 second frames B, D). The signal at the cap structures weakens and spreads out laterally (Fig.34 second frames A, C). DlicGFP still localises to centrosomes but is weaker than during S-phase. During metaphase, DlicGFP marks the spindle arrays appearing between the centrosomes. The signal at the centrosomes and the spindles is similarly strong. The metaphase plate is visible between the spindle arrays as area without any DlicGFP signal. During ana- and telophase, DlicGFP stays with elongating spindles and localises as well with central spindles (Fig.34 third frames B, D). The caps start to re-form as the nuclei reassemble (Fig.34 third frames A, C).

All these above described localisations of DlicGFP are visible in both *wild type* and dop^{1}/dop^{10} mutant embryos to a similar extent. This indicates that Dlic is not mislocalised during syncytial divisions in dop^{1}/dop^{10} mutant embryos.

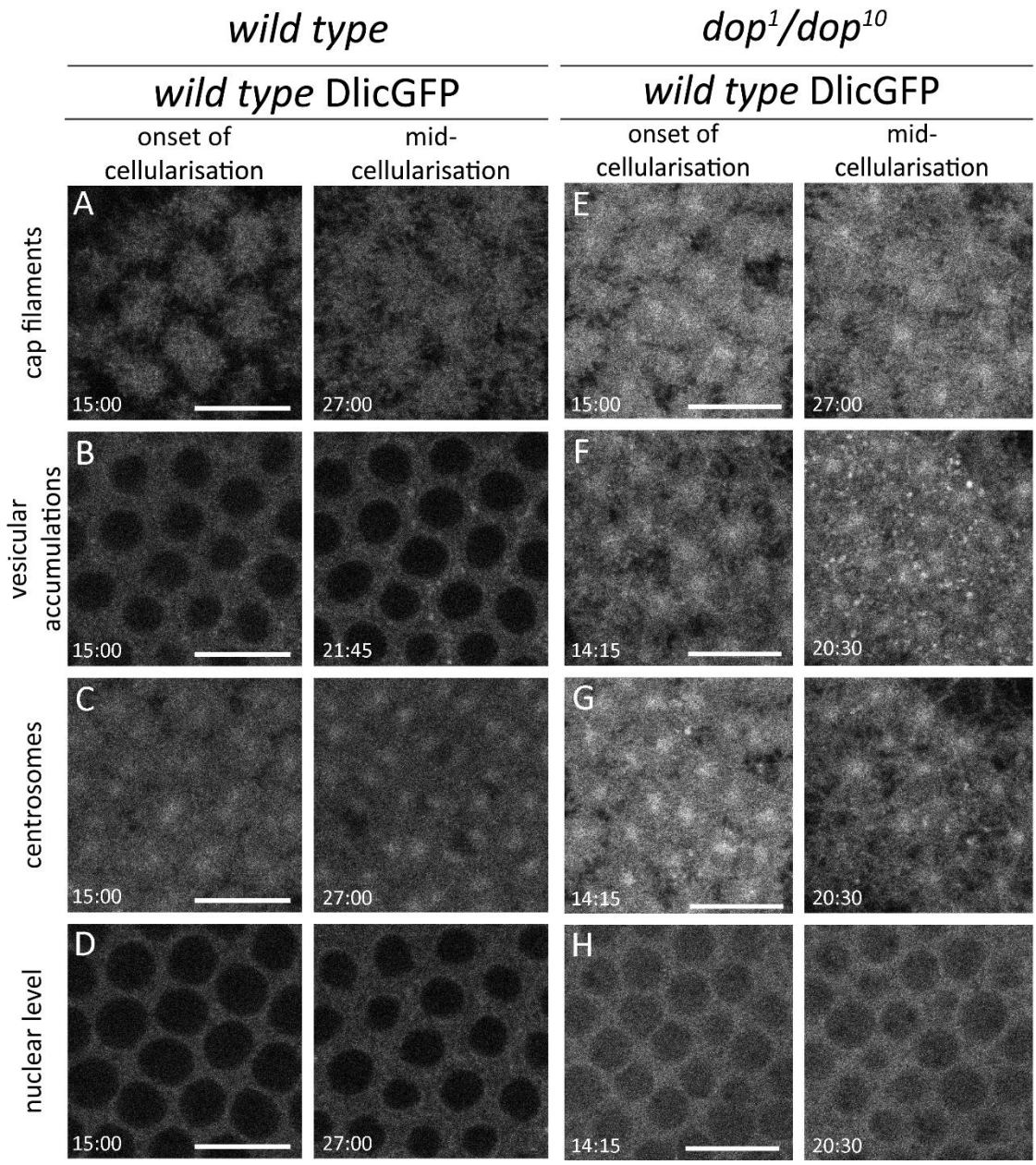

Figure 35 During cellularisation, *wild type* DlicGFP localises similarly in *dop* mutants compared to *wild type* embryos but shows a higher number and stronger accumulation to punctate structures. Images taken from time-lapse recordings of *wild type* embryos (A-D) and dop^{1}/dop^{10} mutant embryos (E-H) expressing *wild type* DlicGFP under control of a double maternal α-tubulin Gal4 driver. Note the prominent structures visible due to DlicGFP signal localisation during onset and mid-cellularisation: cap filaments (A, E), vesicular accumulations (B, F), centrosomes (C, G) and at nuclear level (D, H). Time after cycle 13 S-phase indicated in min. Scale bars represent 10 µm.

DlicGFP localisation in dop^{1}/dop^{10} mutant embryos is similar to *wild type* during cellularisation (Fig.35). DlicGFP localises to filamentous structures, presumably astral microtubules, at the cortex in a dynamic manner (Fig.35 first frames A, E). Similar to F-actin caps, the filamentous structure spreads out to build a layer of dynamic filaments on the surface during the course of cellularisation (Fig.35 second frames A, E). DlicGFP accumulates at the centrosomes throughout

cellularisation (Fig.35 C, G). The nuclei display a shape change during cellularisation going from a round shape to a “bumpy” shape likely to be due to squeezing of the nuclei by microtubules (Fig.35 D, H) which is reported to affect nuclear elongation during cellularisation (Brandt et al. 2006). *dop*^{1}*/dop*^{10} mutant embryos do not undergo this shape change comparable to *wild type* embryos. However, nuclei in many cases lose their cortical contact and migrate basally.

One difference between DlicGFP localisation in *wild type* and *dop*^{1}*/dop*^{10} mutant embryos is detectable. In *wild type*, punctate accumulations of DlicGFP are apparent throughout cellularisation but migrate basally during the course of cellularisation (Fig.35 B). Maybe these punctate structures are localising to and move inwards together with the invaginating furrow canal. In *dop*^{1}*/dop*^{10} mutant embryos, more punctae are detectable and they display a stronger DlicGFP signal than *wild type* embryos (Fig.35 F). Additionally, they do not move basally during cellularisation but stay in the first apical 5 µm.

What nature these punctate structures are could not be determined. It would be interesting to know if they belong to a specific trafficking route or if they are accumulating degradation products that may arise because the embryo is beginning to die at this stage. However, whatever nature the accumulations are, they seem not to influence the wild typic DlicGFP localisation which is still present in *dop*^{1}*/dop*^{10} mutant embryos.

3.3.3 Studying effects of Dop target Dynein light intermediate chain Serine 401 phospho-mutants

dop mutations affect different Dynein transport-dependent processes during or prior to cellularisation like lipid droplet clouding, Bazooka transport or mRNA transport (Meyer et al. 2006; Hain et al. 2014). Alistair Langlands found evidence through SILAC proteomic analyses that Dynein light intermediate chain (Dlic) phosphorylation is reduced in *dop* mutants (Langlands 2012). Specifically, the phosphorylation at Serine 401 showed a reduced phosphorylation in *dop*

mutant embryos compared to *wild type*. Serine 401 of Dlic is a highly-conserved amino acid present in at least one Dynein light intermediate chain homologue of *Drosophila*, mouse (*Mus musculus*), chicken (*Gallus gallus*) and human (*Homo sapiens*) (Fig.36).

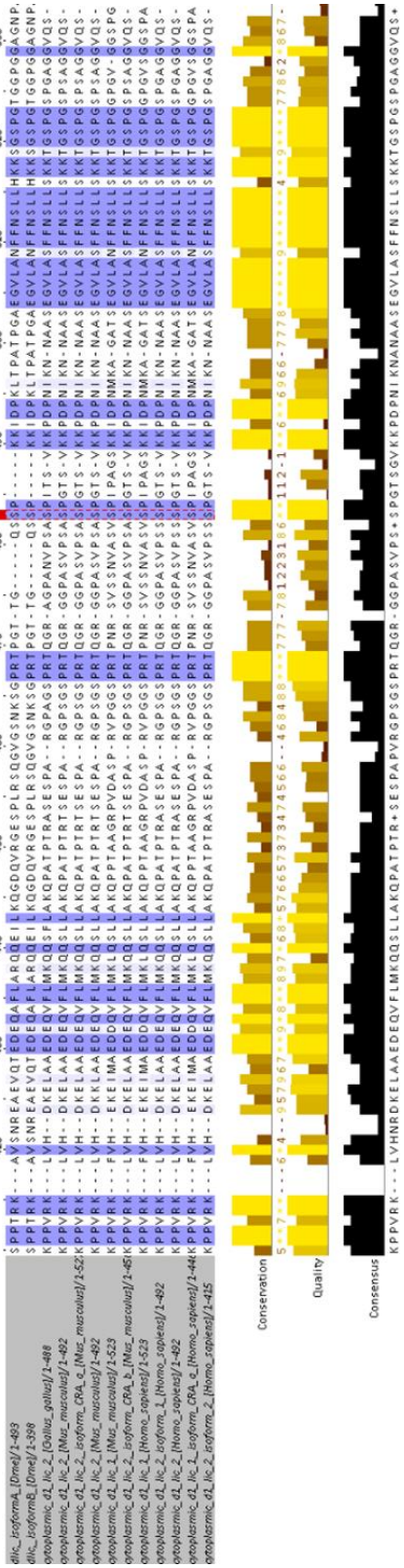

Figure 36 Analysis of Dlic S401 conservation. Conservation compared between Dynein light intermediate chain forms of *Drosophila melanogaster*, *Gallus gallus*, *Mus musculus* and *Homo sapiens*. A detail view displays the sequence around Serine 401 (red box) in several Dynein light intermediate chain forms in the chosen organisms. Colour-coding indicates the conservation of each individual amino acid in the Dlic sequence (dark-blue= highly conserved, light-blue= conservation, no blue= no conservation). Serine 401 in Dlic is a highly conserved amino acid and present in at least one Dlic isoform in each organism analysed. Jalview used for analysis.

No function has been reported so far for the phosphorylation of this particular serine in the above mentioned organisms. To investigate the developmental impact of this Serine 401 and its phosphorylation status, a non-phosphorylatable Dlic (Serine 401 mutated to an Alanine) and a Dlic which mimics phosphorylation (Serine 401 mutated to Aspartic acid) were created and cloned into a vector under UAS control and with GFP tag. The analysis was focussed on syncytial divisions and cellularisation in *wild type* and *dop* mutant embryos.

3.3.3.1 Phospho-mimic and non-phosphorylatable forms of Dlic S401 do not have an effect on DlicGFP localisation in *wild type* embryos

A SILAC screen performed by Alistair Langlands indicated Dlic as a potential substrate of Dop (Langlands 2012). Additionally, Serine 401 came out as a phosphorylation site whose phosphorylation was potentially dependent on Dop function. To see if the regulation of this specific Serine has an impact on cellularisation in *Drosophila* embryos or at overall embryogenesis, *wild type*, phospho-mimic (S401D DlicGFP) and non-phosphorylatable (S401A DlicGFP) forms of Dlic Serine 401 were expressed in *wild type* embryos. Maternal expression of the DlicGFP constructs was controlled by a maternal α-tubulin Gal4 driver. The localisation of both DlicGFP mutant versions during syncytial divisions (Fig.37) and cellularisation (Fig.38) was analysed and compared to the localisation of *wild type* Dlic.

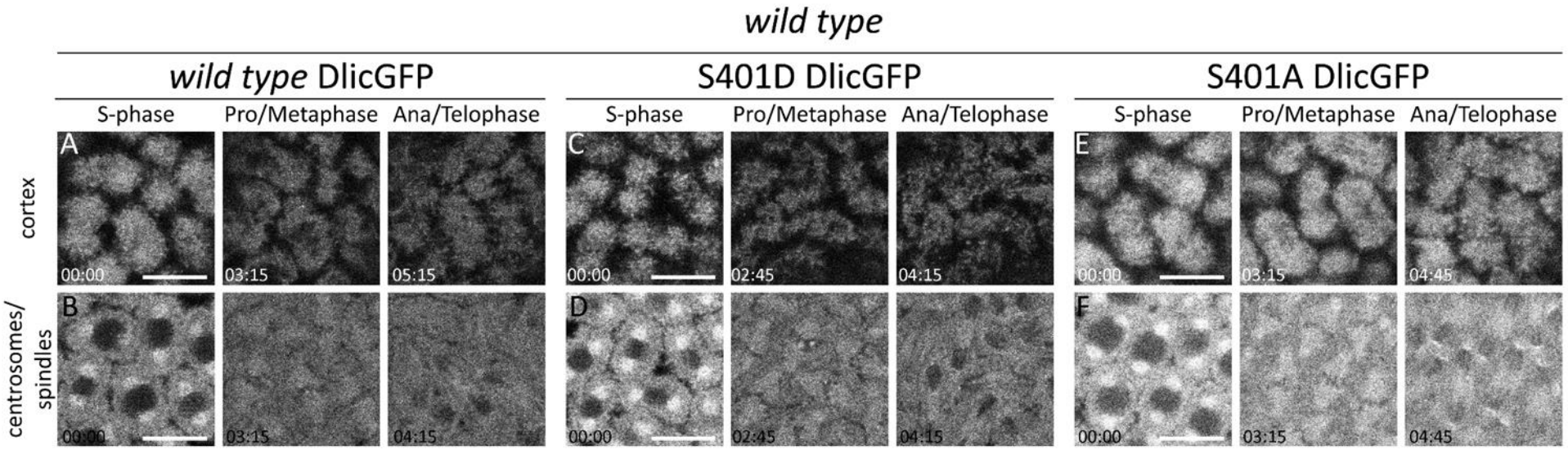

Figure 37 During syncytial cycle 13, *wild type*, S401D mutant and S401A mutant DlicGFP show similar localisation to prominent structures in *wild type* embryos. Images taken from time-lapse recordings of *wild type* embryos expressing DlicGFP with either a *wild type* form of Dlic (A, B) or Dlic Serine401 mutated to aspartic acid (S401D; C,D) or mutated to Alanine (S401A; E,F) under control of a double maternal α-tubulin Gal4 driver. Shown is DlicGFP signal at the cortex (A, C, E) as well as at the centrosomes/spindles of the embryos (B, D, F) during 3 different stages of syncytial cell cycle 13 (S-phase, Pro/Metaphase, Ana/Telophase). Note that the localisation of DlicGFP is not altered in either of the two phospho-mutants for Serine 401 (C, D, E, F) compared to the *wild type* version (A, B). Images of the different structures in one construct do not always show the same embryo. Time after cycle 13 S-phase indicated in min. Scale bars represent 10 µm.

A strong difference of the overall signal intensity is visible in the shown embryos expressing the different DlicGFP constructs in *wild type* background (Fig.37). The expression strength varied a lot between the embryos of each DlicGFP construct and there is no overall difference detectable between embryos expressing different constructs. A few more examples are shown in the appendix to show the variations of signal intensities (Appendix Fig.S3).

Phospho-mimic or non-phosphorylatable versions of DlicGFP expressed in a *wild type* background (endogenous *wild type* Dlic expressed) do not have an effect on DlicGFP construct localisation during syncytial divisions. As in *wild type* DlicGFP (Fig.37 A, B), phospho-mimic (Fig.37 C, D) and non-phosphorylatable (Fig.37 E, F) versions of DlicGFP localise mainly to the centrosomes as well as spindles during syncytial divisions. They also form cap structures during S-phase reminiscent of F-actin caps which spread out during the division.

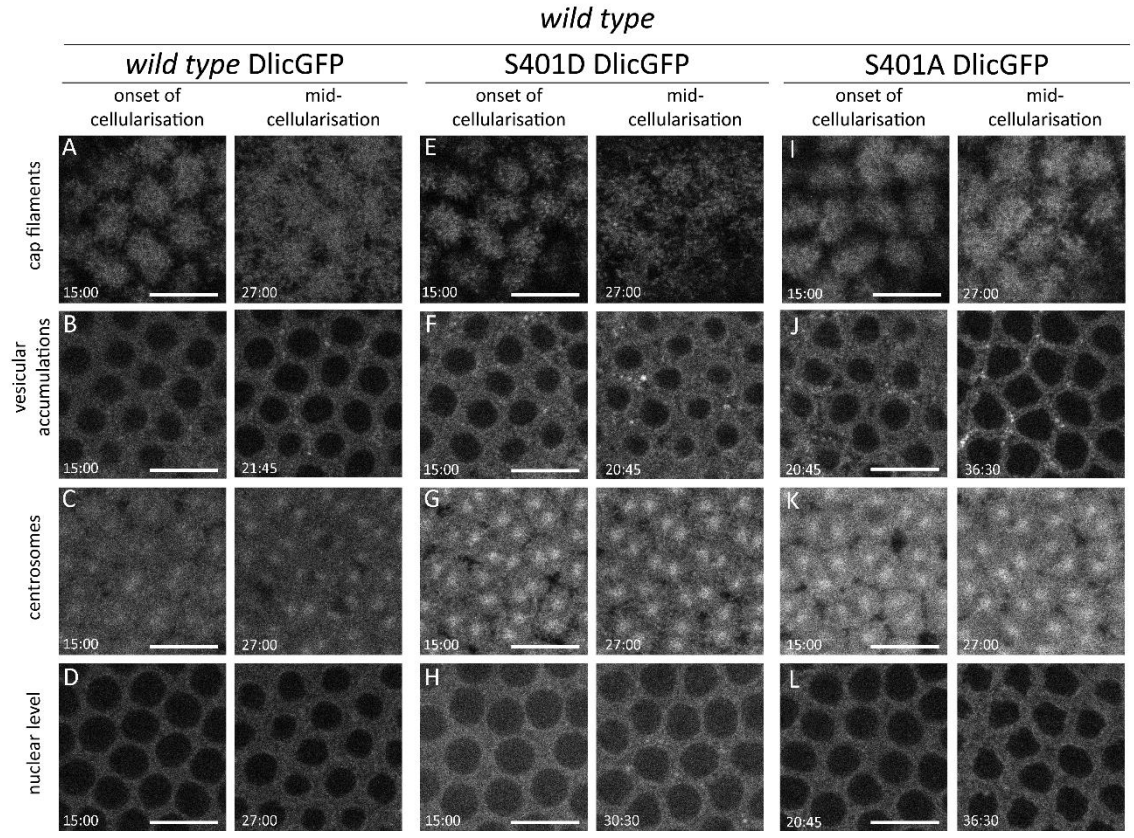

Figure 38 During cellularisation, *wild type*, S401D mutant and S401A mutant DlicGFP show similar localisation to prominent structures in *wild type* embryos. Images taken from time-lapse recordings of *wild type* embryos expressing either *wild type* (A-D), S401D (E-H) or S401A (I-L) versions of Serine 401 in DlicGFP under control of a double maternal α-tubulin Gal4 driver. Shown are the prominent structures visible due to DlicGFP signal localisation during onset and mid-cellularisation: cap filaments (A, E, I), vesicular accumulations (B, F, J), centrosomes (C, G,

K) and at nuclear level (D, H, L). Note that all three DlicGFP Serine 401 versions localise to the same structures. Images of the different structures in one construct do not always show the same embryo. Time after cycle 13 S-phase indicated in min. Scale bars represent 10 µm.

During cellularisation, phospho-mimic and non-phosphorylatable DlicGFP localise similar to different structures in *wild type* embryos as seen for *wild type* DlicGFP fusion protein localisation (Fig.38). All three DlicGFP versions form filamentous cap structures that spread out during the course of cellularisation (Fig.38 A, E, I). During cellularisation, few small DlicGFP-positive punctate accumulations form that migrate into the interior of the embryo (Fig.38 B, F, J). These punctae are very small and visible usually only in one 0.5 µm z-section. Slight differences of their signal strength or size might be based on how they got captured by the microscope. Some more examples of these punctate structures can be found in the appendix (Appendix Fig.S4). These DlicGFP accumulations might get pushed into the embryo by the invaginating membrane. However, how they migrate into the embryo and what these punctate structures are is not known. Throughout cellularisation, all DlicGFP versions localise to the centrosomes (Fig.38 C, G, K). In embryos expressing either of the three DlicGFP versions, nuclei undergo a conformational change from a rounded to a „bumpy“ shape. This shape change of nuclei is not specific to any of the DlicGFP versions.

The previously mentioned SILAC screen indicated that Serine401 in Dynein light intermediate chain is less phosphorylated in *drop out* mutants than in *wild type*. The hypothesis is that this reduced phosphorylation could account for phenotypes seen in *dop* mutants. The non-phosphorylatable form of S401 in Dlic should lead to an artificially reduced phosphorylation and could possibly mimic some *dop* mutant phenotypes. However, neither phospho-mutant version of S401 in DlicGFP showed an obvious effect on DlicGFP localisation in *wild type* embryos in neither syncytial divisions nor cellularisation. On the other hand, these data do not indicate if the phospho-mutants have an effect which is independent of protein localisation. On overall observations, cellularisation was not affected to an extent as in *dop* mutants (no data obtained). Further studies are needed to look in more detail for *dop* phenotypes.

3.3.3.2 Phospho-mimic and non-phosphorylatable forms of Dlic S401 do not have an effect on embryo survival in *wild type* background

To test if phospho-mutants of Dlic have an effect on overall embryonic survival in a competition background with endogenous *wild type* Dlic, hatching rates were determined of *wild type* embryos expressing either *wild type* (wt), phospho-mimic (S401D) or non-phosphorylatable (S401A) versions of DlicGFP (Fig.39).

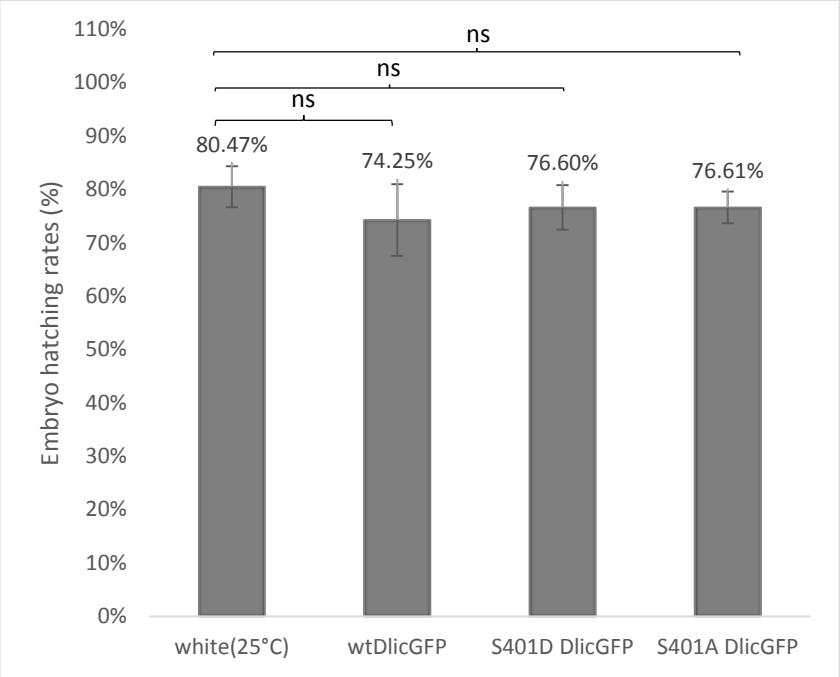

Figure 39 Dlic S401 phospho-mutant expression in *wild type* embryos does not affect embryonic survival rates. Survival rates of *wild type* embryos expressing either a *wild type* form of Dlic (wtDlicGFP), Dlic S401D or Dlic S401A. Expression under control of a double maternal α-tubulin Gal4 driver. *wild type* (white (25°)) hatching rates were used as a control. Hatching rates have been determined at 25°C. None of the DlicGFP protein versions expressed in a *wild type* background impair embryo survival rates significantly compared to *wild type* embryos. (Two tailed *t*-test, ns = not significant; +/- SEM; at least 3 independent tests have been performed for each condition; Number of eggs (total): white(25°C) = 297, wtDlicGFP = 365, S401D DlicGFP = 355, S401A DlicGFP = 329)

The expression of all three DlicGFP versions resulted in embryo hatching rates similar to the *wild type* control (white (25°), Fig.39). This result shows that at least in a *wild type* background the overexpression of phospho-mutant forms of Serine 401 in Dynein light intermediate chain does not affect embryo survival. Thus, this result does not mimic the embryonic lethality seen in *drop out* mutants. However, it is possible that effects are masked by the endogenous *wild type* Dlic in the system.

3.3.3.3 Phospho-mimic and non-phosphorylatable forms of Dlic S401 do not have an effect on DlicGFP localisation in *dop* mutant embryos

Serine 401 of Dlic showed reduced phosphorylation in dop^{1}/dop^{10} transheterozygous mutants as revealed by a SILAC screen. Dlic S401 mutants that are not phosphorylatable at this particular site should possibly be able to mimic this situation in *wild type* embryos. However, non-phosphorylatable mutant versions of S401 in DlicGFP seem not to affect embryo development similar to *dop* mutants when expressed in *wild type* embryos. In *dop* mutants that were shown to have reduced phosphorylation of Dlic S401, maybe a Dlic S401 mutant mimicking phosphorylation could substitute for reduced endogenous Dlic S401 phosphorylation. To see if phospho-mimic mutant versions of Serine 401 in DlicGFP could rescue phenotypes in *dop* mutants, *wild type* and phospho-mutant versions of DlicGFP were expressed in dop^{1}/dop^{10} transheterozygous mutant embryos and analysed for DlicGFP protein localisations during syncytial divisions (Fig.40) and cellularisation (Fig.41).

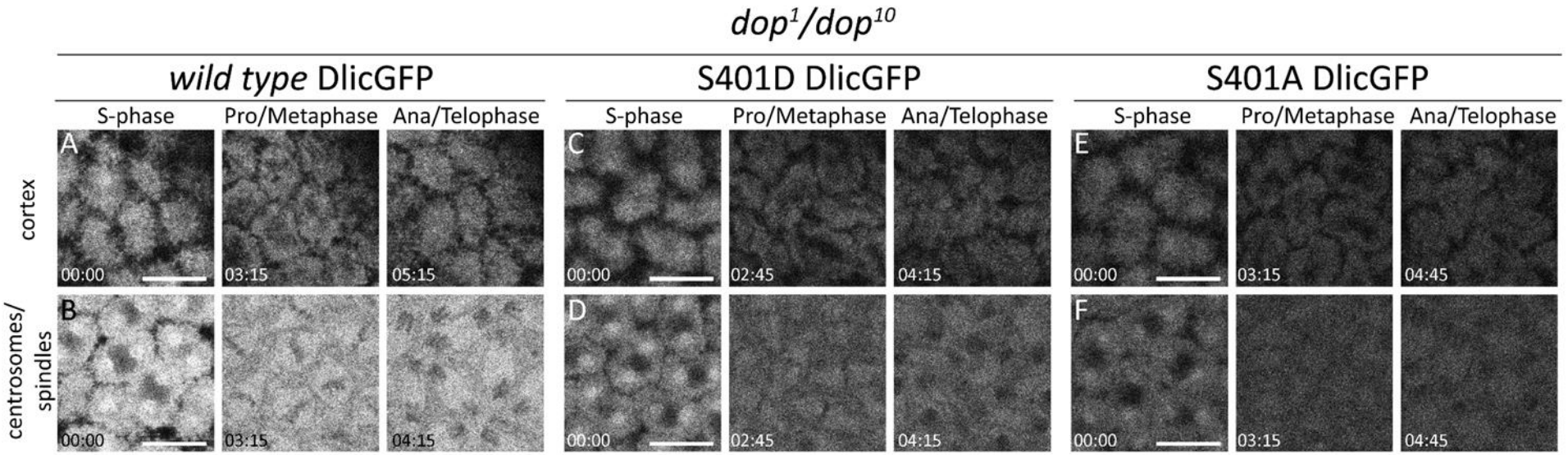

Figure 40 During syncytial cycle 13, neither *wild type* nor S401D mutant or S401A mutant DlicGFP-expressing *dop* mutant embryos display localisation defects of Dlic. Images taken from time-lapse recordings of *dop*^{1}/*dop*^{10} mutant embryos expressing either *wild type* (A, B), S401D (C, D) or S401A (E, F) versions of Serine 401 in DlicGFP under control of a double maternal α-tubulin Gal4 driver. Shown is DlicGFP signal at the cortex (A, C, E) as well as at the centrosomes/spindles of the embryos (B, D, F) during 3 different stages of syncytial cell cycle 13 (S-phase, Pro/Metaphase, Ana/Telophase). Note that no localisation difference is visible between the different Dlic versions. Images of the different structures in one construct do not always show the same embryo. Time after cycle 13 S-phase indicated in min. Scale bars represent 10 µm.

Phospho-mimic or non-phosphorylatable versions of DlicGFP expressed in a *dop*^{1}/*dop*^{10} mutant background do not change DlicGFP localisations in comparison to *wild type* DlicGFP (Fig.40). As seen previously in *wild type* embryos expressing phospho-mimic and non-phosphorylatable versions of DlicGFP, all DlicGFP versions expressed in *dop* mutant background localise to centrosomes, spindles (Fig.40 B, D, F) and filamentous caps (Fig.40 A, C, E) during syncytial divisions.

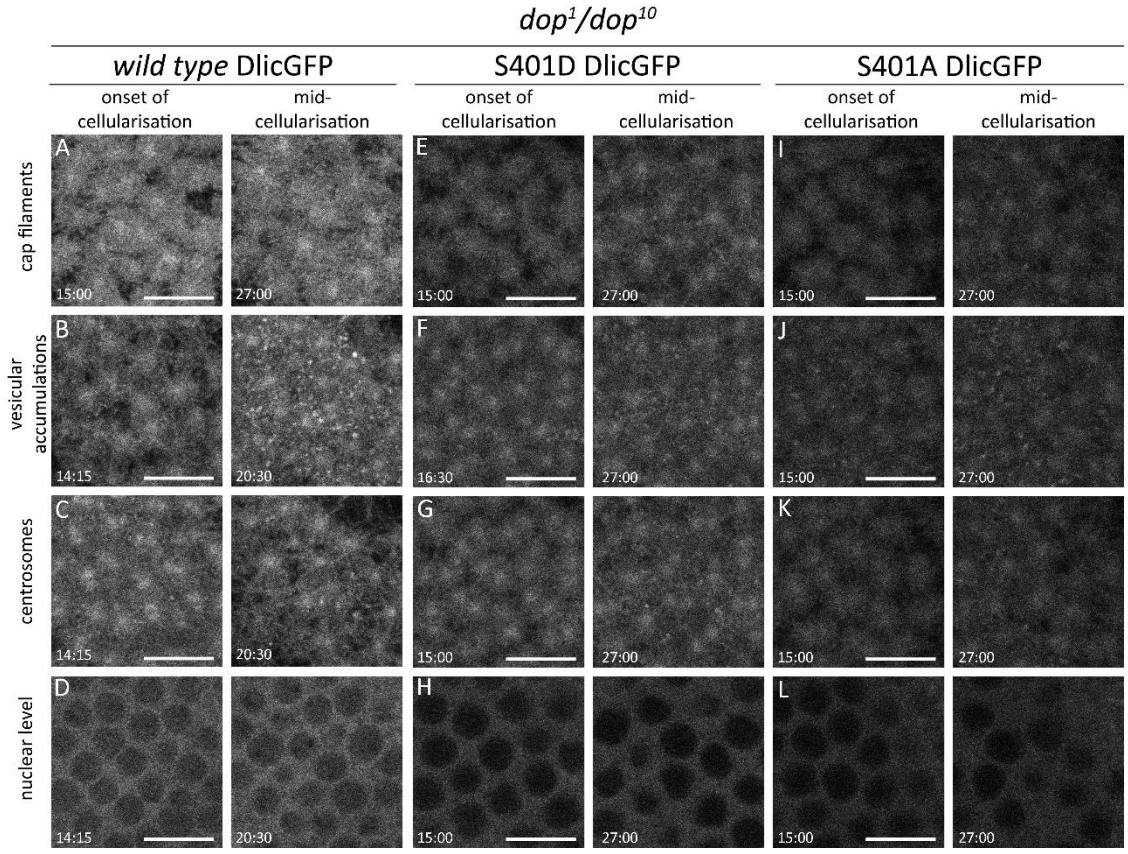

Figure 41 During cellularisation, *dop* mutant embryos expressing *wild type*, S401D mutant and S401A mutant DlicGFP show similar localisation defects of Dlic. Images taken from time-lapse recordings of *dop*^{1}/*dop*^{10} mutant embryos expressing either *wild type* (A-D), S401D (E-H) or S401A (I-L) versions of S401 in DlicGFP under control of a double maternal α-tubulin Gal4 driver. Shown are the prominent structures visible due to DlicGFP signal localisation during onset and mid-cellularisation: cap filaments (A, E, I), vesicular accumulations (B, F, J), centrosomes (C, G, K) and at nuclear level (D, H, L). Images of the different structures in one construct do not always show the same embryo. Time after cycle 13 S-phase indicated in min. Scale bars represent 10 µm.

Also during cellularisation, no specific localisation differences are detectable between the three S401 DlicGFP constructs (Fig.41). DlicGFP localises to the filamentous cap structures (Fig.41 A, E, I) and centrosomes (Fig.41 C, G, K) throughout cellularisation. Additionally, the nuclear drop out phenotype is present in embryos expressing either of the three DlicGFP versions (more examples

can be found in the appendix Fig.S5). However, more vesicular accumulations are visible in *dop* mutant embryos expressing either of the three DlicGFP constructs compared to *wild type* embryos expressing these constructs. The vesicular accumulations are visible in mutant embryos expressing either construct to a similar extent (Fig.41 B, F, J). This means that neither of the mutants was able to rescue the only clear DlicGFP localisation phenotype visible in dop^{1}/dop^{10} mutants in comparison to *wild type* embryos.

3.3.3.4 The phospho-mimic form of Dlic S401 can rescue lethality of *dop* hypomorphic mutations

To test if mutant forms of Dlic can rescue *drop out*-induced lethality, hatching rates of dop^{1}/dop^{10} transheterozygous embryos expressing either *wild type* (wt), phospho-mimic (S401D) or non-phosphorylatable (S401A) versions of DlicGFP were determined (Fig.42).

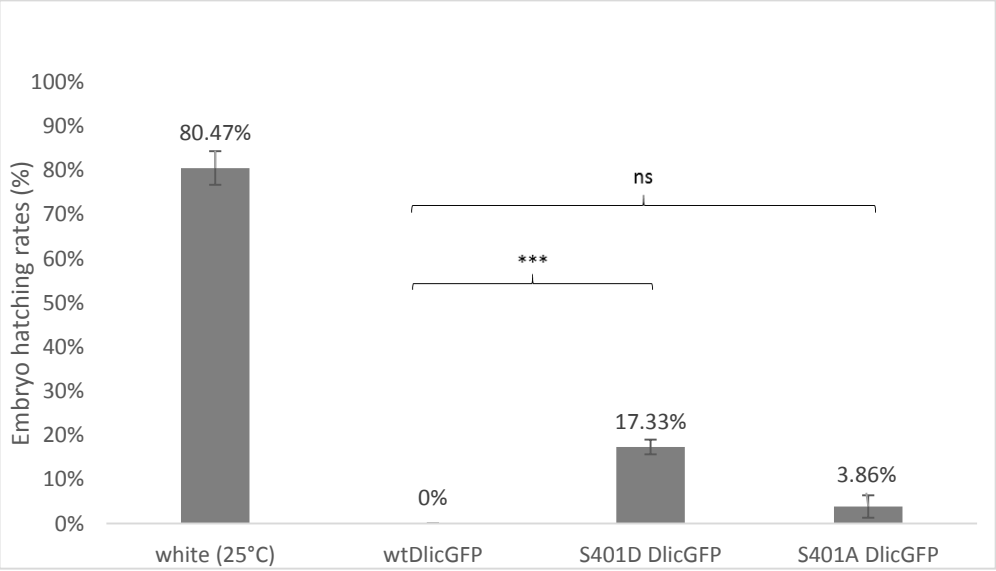

Figure 42 S401D expression in dop^{1}/dop^{10} mutant embryos is able to rescue *dop* embryonic lethality. Survival rates of dop^{1}/dop^{10} mutant embryos expressing either a *wild type* form of Dlic (wtDlicGFP) or Dlic Serine401 mutated to aspartic acid (S401D) or mutated to Alanine (S401A) are shown. Expression under control of a double maternal α-tubulin Gal4 driver. *wild type* (white (25°C)) hatching rates were used as a control. Hatching rates have been determined at 25°C. Embryos expressing S401D mutant versions of DlicGFP hatch in a highly significant number compared to *wild type* DlicGFP in dop^{1}/dop^{10} embryos. Even though some embryos expressing S401A mutant versions of DlicGFP also hatch, the percentage is not significant compared to *wild type* DlicGFP. (Two tailed *t*-test, ***p<0.001; ns = not significant; +/- SEM; at least 3 independent tests have been performed for each condition; Number of eggs (total): white(25°C) = 297, wtDlicGFP = 300, S401D DlicGFP = 300, S401A DlicGFP = 700)

Maternally mutant dop^{1}/dop^{10} embryos are 100% lethal. By bringing in *wild type* DlicGFP, the lethality rate did not change and all the tested embryos died (Fig.42). In contrast, dop^{1}/dop^{10} mutant embryos expressing phospho-mimic versions of DlicGFP survived at a rate of 17.33%. This suggests that the artificial form of Dlic which mimics a phosphorylation at position 401 partially reverses a defect caused by reduced Dlic phosphorylation in *dop* mutants. Furthermore, this result supports a role of Dop in regulating the phosphorylation state of Serine 401 in Dlic and thereby affecting embryo viability. However, also 3.86% of the non-phosphorylatable mutants of Dlic survived (rate was not significant). These mutants mimic a non-phosphorylation state of Serine 401 like it was seen in *dop* mutants. They would therefore not be expected to rescue a *dop* phenotype. It might be that the expression of a non-phosphorylatable S401 Dlic version somehow affects phosphorylation levels of the endogenous non-mutant Dlic in the system. Further experiments should be performed to validate the rescue and to look in detail into effects on cellularisation due to the different phosphorylation states of Dlic Serine 401 in *dop* mutant embryos.

3.3.3.5 Can artificial DlicGFP expression rescue lethality of a *dlic* mutation during larval stages?

To verify that the artificially created DlicGFP versions function like the endogenous *wild type* version of Dlic and can substitute for its function in a mutant background, crosses were set-up that create flies with the $Dlic^{G0065}$ mutation on the X-chromosome and express one of the three synthesised and characterised versions of DlicGFP under control of an *ubiquitin*-Gal4 driver (Fig.43).

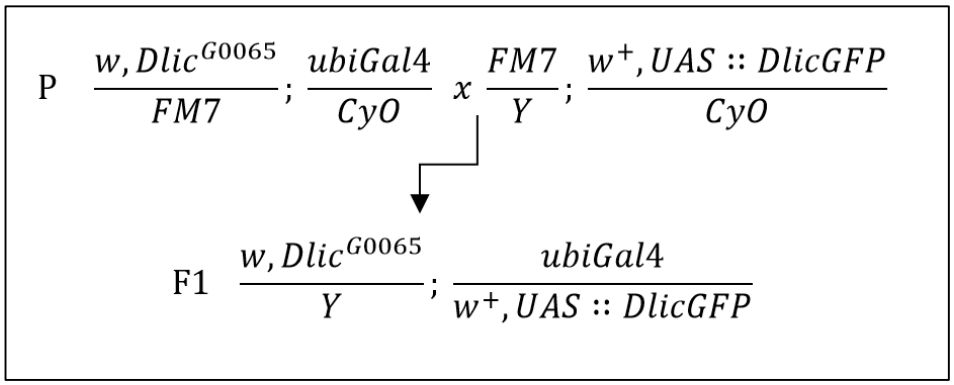

Figure 43 Cross performed to test rescue in males carrying the *Dlic^{G0065}* mutation and expressing *ubiquitin*-Gal4 (*ubi*Gal4) driven DlicGFP. Note that DlicGFP is representative for all three Dlic Serine401 versions (*wild type*, phospho-mimic, non-phosphorylatable). Crosses were all performed at 25°C.

ubiquitin-Gal4 drives expression throughout *Drosophila* development and in all cells (Bloomington Stock Report). The Dlic gene is essential for *Drosophila* viability and the allele *Dlic^{G0065}* is recessive lethal during the first and second larval instars (Mische et al. 2008; Peter et al. 2002). Due to this allele being recessive, either both X chromosomes in females have to carry this allele to create the desired background phenotype (larval lethality) or the only X chromosome of male flies has to be mutant. Fathers of progeny to create *Dlic^{G0065}* mutant flies cannot carry this allele on their X chromosome because they would die during larval stages not creating any progeny. Thus, due to the nature of the cross, only male progeny could be generated that were hemizygous for *Dlic^{G0065}* on the X-chromosome. These males could be identified by the lack of the dominant eye marker Bar which is connected to the X chromosomal FM7 balancer. Therefore, adult flies were counted that hatched from their pupal cases and it was analysed if males underwent eclosion that were hemizygous for *Dlic^{G0065}* (not displaying the Bar eye phenotype).

	Adult flies (total)	hatched males (total)	males with GFP expression	males hemizygous for *Dlic*^{G0065} (without Bar phenotype)
wild type DlicGFP	149	56 all FM7	20 all FM7	none
phospho-mimic DlicGFP	304	94 all FM7	26 all FM7	none
non-phosphorylatable DlicGFP	176	77 all FM7	18 all FM7	none

Table 20 Analysis of the *Dlic*^{G0065} ubi::Gal4>>UAS::DlicGFP rescue crosses.

According to Mendelian inheritance, the probability to get males hemizygous for *Dlic*^{G0065} expressing DlicGFP was 1:6. However, none of the hatching adult males were hemizygous for the *Dlic*^{G0065} mutation (Table 20). This result indicates that either none of the DlicGFP versions created in this thesis is functional and can therefore not rescue lethality of the *Dlic*^{G0065} mutation during larval stages or that the expression with *ubiquitin*-Gal4 used as driver for Dlic expression was not high enough or did not resemble the endogenous Dlic expression patterns well enough to substitute for Dlic function in *Dlic*^{G0065} mutants. Further experiments have to be performed to distinguish between these possibilities.

3.3.4 Conclusion of Results Part 3

In this Results part, different tools have been developed and used to establish a method to specifically impair Dynein function during cellularisation to investigate its impact on different cellularisation processes and to study Dynein as a potential link between Dop function and cellularisation (Hain et al. 2014; Langlands 2012). Neither Dynamitin zygotic overexpression nor Ciliobrevin D injections at onset of cellularisation showed a strong expected and desired effect on Dynein function. However, maternal Dynein heavy chain-RNAi expression of one construct directed against the essential Dhc64C gene showed significant embryo survival defects

compared to the effector-only control. In the future, embryos expressing this Dhc64C^{GL00543} RNAi construct and surviving up to cellularisation should be analysed to test for defects during cellularisation caused by Dynein impairment. This analysis could provide important insights into how Dop could impair cellularisation through a direct or indirect link provided by Dynein.

Another focus of this part was the study of the potential Dop target Dynein light intermediate chain (Langlands 2012). The phosphorylation of this Dynein subunit was shown to be dependent on Dop function. Therefore, it was tested if Dop also affects its localisation by imaging a DlicGFP construct in *dop* mutant embryos in comparison to *wild type*. The localisation of Dlic seemed not to be overall affected in *dop* mutants, apart from some vesicular accumulations that were more numerous and showed stronger DlicGFP signal in the mutant during cellularisation. A SILAC screen that was previously done identified Serine 401 of Dlic as a specific site affected by Dop function. Therefore, non-phosphorylatable and phospho-mimic forms of this Dlic site were generated and, fused to GFP, expressed in *wild type* and *dop* mutant embryos to analyse any possible impact this particular phosphorylation site might have on DlicGFP localisation and embryo survival. In *wild type* embryos (expressing also the endogenous *wild type* version of Dlic), neither mutant form of S401 showed an effect neither on DlicGFP localisation nor on embryo survival in comparison to *wild type* DlicGFP. Also in *dop* mutant background, neither DlicGFP mutant version changed the localisation seen for *wild type* DlicGFP in the mutant. However, the phospho-mimic version of DlicGFP S401 showed a significant rescue of embryo viability in *dop* mutants which raises the possibility that a reduction in phosphorylation of Dlic S401 as identified in *dop* mutants causes embryo lethality in *dop* mutants. Further experiments need to be done to support this indication. With the previous experiments, the question if different phosphorylation states of Dlic S401 are able to rescue phenotypes seen in *dop* mutants by presumably substituting for a malfunction of endogenous *wild type* Dlic has been addressed. Important to know in this context is if the different versions of Dlic S401 fused to GFP are able to take over the function of endogenous Dlic. Therefore, an experiment was set-up to test if the artificially created DlicGFP versions can rescue the larval lethality of the *Dlic^{G0065}* allele. No rescue

of lethality could be identified by expression of the different DlicGFP versions, neither *wild type* nor phospho-mutant. However, also this experiment needs further verification by using a different (stronger) driver and a *wild type* DlicGFP version as control created by Satoh et al. which was shown to rescue Dlic function in arborisation of neurons (Satoh et al. 2008).

4. Discussion

This thesis describes an approach to identify the specific function(s) of the Drop out (Dop) kinase during cellularisation. *drop out* was first discovered by Galewsky and Schulz as a locus on the third chromosome important for proper cellularisation during *Drosophila melanogaster* embryogenesis (Galewsky & Schulz 1992). Previously, *drop out* was identified in our lab as a mutation in a hitherto uncharacterised gene named *CG6498* and further analysis showed that this gene encodes for the single member of the MAST kinase family in *Drosophila melanogaster* (Hain et al. 2014). The MAST kinases are a poorly characterised family belonging to the AGC kinase subfamily of protein kinases (Pearce et al. 2010; Arencibia et al. 2013). MAST kinases have a domain of unknown function (DUF), an AGC kinase domain and a PDZ domain in common. Even though members of the MAST kinase family are implicated in several human diseases, not much is known about their function and about the mechanism by which they affect cells and tissues. The ongoing study on Drop out in *Drosophila* embryos is aimed to find the general mechanism by which this single homologue of the MAST kinases in the fly ensures proper cell behaviour and affects cell viability. Many defects were found until now that are caused by mutations in *drop out* (Hain et al. 2014; Hain 2010; Langlands 2012; Meyer et al. 2006). However, most of the studies are based on hypomorphic alleles of *dop* and few on null alleles hemizygous over a chromosomal deficiency (dop^{10}/Df(3L)MR15). In this study, phenotypes of a complete null allele of Dop were described for the first time using embryos derived from dop^{10} germ line clones.

4.1 Furrow canal formation and specification is the first morphological event that requires Dop function

Analysis of the complete loss-of-function mutant embryos revealed that Drop out is required for cellularisation but not for syncytial divisions of *Drosophila* embryogenesis. The first morphological defects in *dop* mutants were seen at onset of cellularisation and comprised a

failure in specification and proper formation of the furrow canal. This defect was apparent via imaging of the F-actin network in hypomorphic *dop* embryos. The observation that F-actin in *dop* mutants gets more dispersed over time but initially localises correctly to internuclear spaces suggests that the initial accumulation of F-actin at destined furrow sites is not impaired in the mutants. However, the restriction to the furrows seems to be defective. What processes and proteins could be important to restrict F-actin to distinct furrow sites?

The protein Discontinuous actin hexagon (Dah) is a good candidate to link F-actin to the furrow canal membrane: a) Dah associates indirectly with membranes as well as F-actin, b) it is localised at the furrow canal during cellularisation, c) it was shown to be required for furrow formation during cellularisation and d) Dah localises to vesicles that are often associated with actin (Rothwell et al. 1999; Zhang et al. 1996; Zhang et al. 2000). Additionally, Dah could provide a link between the *dop* mutant F-actin phenotype and endosomal transport phenotype because Dah localisation to the furrow is Nuf- and Rab11-dependent (Zhang et al. 2000; Riggs et al. 2003). Dah protein might be trapped in recycling endosomal vesicles as they fail to move along microtubules to the furrow sites and instead remain pericentrosomal as seen in *dop* mutants. Therefore, it would be interesting to see if Dah shows any localisation defects in *dop* mutants.

Another protein that could be responsible to restrict F-actin to the furrows is Slow-as-molasses (Slam). Slam is required for recruiting RhoGEF2 to the furrow (Wenzl et al. 2010). In turn, RhoGEF2 is required for Rho1 activation and, thus, F-actin polymerisation (Padash Barmchi et al. 2005; Crawford et al. 1998). Therefore, Slam could account for localised polymerisation and accumulation of F-actin. Data presented in this thesis and in Hain et al., 2014 show that Slam is similarly mislocalised as F-actin during cellularisation which would further support an involvement of Slam in the F-actin phenotype (Hain et al. 2014). Moreover, Slam localisation is like Dah localisation dependent on recycling endosome function. Thus, if the broadened Slam localisation that was seen in *dop* mutants is caused by endosomal transport this could also be responsible for the broadened F-actin polymerisation in *dop* mutants (Acharya et al. 2014).

Thus, it is likely that *dop* mutants indirectly affect F-actin restriction to the furrow by inhibiting recycling endosomal transport.

4.2 Slam and Eps15 protein localisation just prior to cellularisation are the first processes requiring Dop function

The first protein localisation defects could be detected for Slam and Eps15 (Epidermal growth factor receptor pathway substrate clone 15) proteins during telophase of cell cycle 13 just prior to cellularisation and, therefore, slightly earlier than any morphological defect in *dop* mutants. Syncytial division 13 up to telophase, did not show any defects in protein localisation. Slam protein localisation was shown to depend on the recycling endosome (Acharya et al. 2014). It was proposed that the localisation of Slam by the recycling endosome takes place through an indirect mechanism because no co-localisation between recycling endosome and Slam could be detected. It was suggested that localisation of Slam to the furrow canal is restricted by the transport of an anchor that Slam binds to. The localisation phenotype of Slam in *dop* complete loss-of-function mutants could as well be based on an indirect mechanism. Slam protein localises to internuclear regions throughout cellularisation even though these regions are broadened in *dop* mutants. Thus, the initial localisation of Slam protein seems not to be affected in *dop* embryos, in contrast to the restriction of Slam protein to specific and narrow internuclear spaces. This restriction could be mediated by the particular anchor that might be transported by the recycling endosome to the furrow canal region at telophase of cycle 13 and onset of cellularisation. In *dop* mutants, the Slam broadening might be due to this anchor missing from this particular site and, thus, could be explained by impaired recycling endosome transport.

Instead of anchoring proteins to the furrow, targeted localisation of furrow canal proteins could also be achieved by a constant clearing of the cortex removing furrow-specific proteins that become localised too close to the centrosomes. A process like this could avoid furrow canal formation apically of the nuclei and would be dependent on astral microtubules and supposedly

on Dynein-dependent transport from the plus-ends at the cortex to the minus-ends at the centrosomes. *dop* mutants might affect furrow-restriction of proteins by impairment of this Dynein-dependent cortical clearing. This hypothesis includes a model which proposes that centrosomes define the position of the furrows through overlapping arrays of astral microtubules and interaction of the microtubule plus-ends with the cortex (Riggs et al. 2007; Glotzer 2004; Crest et al. 2012). It has been proposed for metaphase furrows and cytokinetic furrows but could equally be important for cellularisation furrows.

Not only Slam but also Eps15 displayed a defect just prior to onset of cellularisation in *dop* mutants. The Slam and Eps15 defects were very similar in that both proteins failed to focus into narrow internuclear furrows and remained punctate and broadened throughout cellularisation. The nature of these punctate structures was not determined but both Slam and Eps15 seemed to co-localise to these structures. In mammalian cells, Eps15 is a protein involved in Clathrin-dependent and –independent endocytosis (Benmerah et al. 1998; Benmerah et al. 1999; Salcini et al. 1999; Savio et al. 2016; Sigismund et al. 2005; Carbone et al. 1997). Eps15 was also shown to localise to early endosomes and to interact with Hrs (Hepatocyte growth factor-regulated tyrosine kinase substrate) in endosomal sorting of internalised receptors (Bean et al. 2000; Bache et al. 2003; Roxrud et al. 2008). In *Drosophila*, the function of Eps15 has been studied at the neuromuscular junction where it is required for synaptic vesicle endocytosis and recycling by maintaining high concentrations of endocytic proteins at synaptic membranes (Majumdar et al. 2006; Koh et al. 2007). To our knowledge, Eps15 has not been studied during early embryogenesis. However, its accumulation at the furrow canal in *wild type* embryos during cellularisation indicates that Eps15 fulfils a role in endocytosis also in this system because other endocytic proteins were shown to localise to the furrow canal as well (Lee & Harris 2014; Sokac & Wieschaus 2008a). As a protein involved in endocytosis, Eps15 could be important for recycling of various proteins. Its co-localisation with Slam at the furrow canal and in vesicular structures indicates a possible role for Eps15 in Slam recycling. As revealed by FRAP experiments, Slam localisation to the furrow canal is highly stable apart from onset of cellularisation (Acharya

et al. 2014). In contrast, the PDZ domain of RhoGEF2 and Amphiphysin were highly dynamic throughout cellularisation. The specific dynamics of these proteins must be controlled by a mechanism that recycles them away and back to the furrow canal. Clathrin-dependent endocytosis and, therefore, the endocytic protein Eps15 are possibly involved in the recycling away part of this mechanism. How the endocytic machinery is able to ensure the specific dynamics of each protein at the furrow canal remains to be investigated. However, the endocytic machinery was shown to be highly selective for transmembrane proteins with certain motifs (Whitney et al. 1995). Therefore, it could provide a suitable mechanism for the timely and spatially restricted transport of specific proteins away from the furrow canal during cellularisation. However, Eps15 is not restricted to the furrow canal but also localises to lateral membranes during late stages of cellularisation. This might indicate that endocytosis also takes place at lateral membranes which would suggest a different set of targets for the endocytic machinery. In the context of cellularisation phenotypes in *dop* mutant embryos, impaired endocytosis at the furrow canal could lead to broadening of the furrow canal due to withholding of membrane material and connected proteins. However, Eps15 localisation is also broadened at the furrow canal and not absent from this structure as revealed in this thesis, thus, there is no direct evidence so far that endocytosis is impaired. To test whether there is a defect in endocytosis, localisation of other endocytic proteins should be analysed in *wild type* and *dop* mutants.

4.2.1 Experiments to test furrow canal formation

Furrow canal formation was discovered as the first morphological phenotype in *dop* mutants. Additionally, Slam and Eps15, two proteins that localise to this structure, were shown to be the first proteins that mislocalise in *dop* mutants. It is not known in detail how the membrane is affected by the *dop* mutation. Most furrow canal markers are mislocalised in *dop* mutants in the same way, showing a broadened localisation and failing to focus into a narrow furrow structure.

The question to address is what the protein mislocalisations are based on. It might be that a normal furrow canal structure is built in *dop* mutants which does not resemble the broadened phenotype of most of its marker proteins. However, it is more likely that also the membrane shows a broadened phenotype. Several proteins that localise to the furrow canal are known to interact with membranes such as Slam and Dah (Wenzl et al. 2010; Zhang et al. 2000). Therefore, they should either be influenced by the membrane shape or themselves influencing the shape of the membrane. It would be interesting to know at what point the membrane gets misshaped and which proteins mislocalise before this event. These proteins are most likely influencing membrane invagination during furrow formation. A tool to label membranes is the phosphatidylinositol-3,4,5-P_3 (PI(3,4,5)P_3)-binding domain (PH domain) of the General receptor for phosphoinositides-1 (GRP1) which could be particularly useful because it can be used for live-imaging (Dasgupta et al. 2009). This domain of the GRP1 protein is available fused to GFP and under control of the UAS promoter.

The questions to address in this experiment are the following: Does Dop possibly affect a protein that links membrane and other furrow canal proteins? Or does Dop affect the localisation of a protein that would be important for furrow canal membrane invagination and shaping?

In case that the membrane at the furrow canal does not resemble the broadened shape of its markers during cellularisation, all the proteins that could be important for linking membrane and other furrow canal proteins should be looked at in detail. The protein Dah is a good candidate in this case because of its proposed function as actin-membrane linker (as discussed above).

In case that the membrane is broadened, it needs to be investigated what proteins could be responsible. Different proteins were shown to cause a furrow canal broadening when their function is impaired.

For example, *steppke* mutants and mutants affecting the Steppke interactor Stepping stone show broadened furrows during cellularisation (Lee & Harris 2013; Liu et al. 2014). Steppke is important to increase endocytosis by controlling F-actin networks at the plasma membrane. It does so by reducing Rho1 protein levels. Thus, looking at localisation of Steppke in *dop* mutants and also looking in detail at Rho1 levels could give a hint on a mechanism by which the shape of the furrow canal is altered in *dop* mutants.

A broadened phenotype of the furrow canal in mutants of the endocytic regulator Steppke indicated that a reduction in endocytosis can indeed lead to furrow canal broadening. This possibility was discussed also in the context of Eps15 mislocalisation/broadening at the furrow canal. Besides Steppke and Eps15, also many other factors could lead to an impaired endocytosis.

One of these factors is Amphiphysin (Amph), a BAR domain-containing protein found to act in endocytosis during cellularisation by forming tubules at the furrow canal that can be pinched-off by dynamin (Su et al. 2013; Takei et al. 1999). These furrow tip tubules are indicators for the efficiency of endocytosis at the furrow canal and can be marked by antibodies directed against Amph (Sokac & Wieschaus 2008a). Thus, it would be interesting to test if any difference can be detected in their appearance in *dop* mutants and *wild type* embryos. High resolution microscopy is required for this experiment because the tip tubules are very thin.

Additionally, also impairment of Kinesin- or Dynein-dependent transport along microtubules could result in a defect of endocytosis by a failure to transport the vesicles away from the furrow canal, suggesting yet another link between Dop function and function of microtubule motor proteins.

Also a mutation in *bottleneck* (*bnk*), one of the early zygotic genes, causes a broadened furrow canal phenotype by premature basal closure due to untimely recruitment of Myosin II to the furrow canal (Schejter & Wieschaus 1993a; Theurkauf 1994). This basal closure is brought about

by actin and myosin contractions and causes furrow canal broadening resembling the furrow canal phenotype in *dop* mutants (Reversi et al. 2014). It might be that Dop affects Bnk function and, thereby, the shape of the furrow canal. In the same context, it would be possible that Dop affects the levels of PI(3,4,5)P_3 at the furrow membrane which were shown to stabilise Bnk at the furrows and counteract actomyosin contractility (Reversi et al. 2014).

The lipid composition of the plasma membrane is of great importance for different processes in the cell, for example cell migration, proliferation, differentiation and intracellular trafficking (Xi et al. 2014). The formation of cortical domains with distinct lipid compositions was shown to be critical for cytokinesis in different organisms (Albertson et al. 2005; Logan & Mandato 2006; Wong et al. 2007). Especially the control of two phosphoinositides, PI(4,5)P_2 and PI(3,4,5)P_3, as well as the control of proteins important for their generation were shown to be essential for actin network organisation and furrow stability as well as furrow ingression during cytokinesis (Logan & Mandato 2006; Wong et al. 2007; Xi et al. 2014; Reversi et al. 2014; Wong et al. 2005). In *Drosophila*, PI(4,5)P_2 impairment and mutants for PI4K, important for PI(4,5)P_2 generation, led to furrow regression and defective cytokinesis in male germ cells (Wong et al. 2005; Brill et al. 2000). In contrast, PI(3,4,5)P_3 and PI3K were shown to counteract PI(4,5)P_2 function at the furrow and seem to be down-regulated during furrow ingression in cytokinesis (Logan & Mandato 2006). Defects in PI(4,5)P_2 generation in *Drosophila* embryos mutant for *pten* resulted in actin organisation defects, defects in nuclear migration and divisions during syncytial cycles, and defects in pole cell formation (von Stein et al. 2005). One study analyses PI(4,5)P_2 and PI(3,4,5)P_3 functions during *Drosophila* cellularisation (Reversi et al. 2014). This study suggests that high levels of PI(4,5)P_2 are required for actomyosin assembly and contractility during basal closure. During slow phase of cellularisation, PI(4,5)P_2 function is counteracted by PI(3,4,5)P_3 and Bnk that are both required to maintain the actin hexagonal arrays, to restrict actomyosin constriction and to prevent plasma membrane lateral expansion. If the balance of both phosphoinositides would be disturbed by *dop* mutations, this could possibly lead to the broadening of the furrow canal and associated proteins during cellularisation. Since the lipid

composition is also important for intracellular transport processes, an overall change of this lipid composition could also affect vesicle distribution which was defective as well in *dop* mutants.

Earlier studies in our lab show that the apical microvilli pool at the cortical plasma membrane does not diminish during the course of cellularisation in *dop* mutant embryos the way it does in *wild type* embryos (Hain et al. 2014). This microvilli pool serves as membrane reservoir for furrow invagination (Figard et al. 2013; Figard et al. 2016), its persistence in *dop* mutants suggests that a mechanism is defective that would redistribute the microvilli membrane into the furrow. It could also suggest that the lipid composition might be affected in *dop* mutants due to a failure in a mechanism that regulates lipid transport and, thereby, lipid distribution along the different plasma membrane compartments. To test this possibility, high resolution analysis of differential lipid distribution would need to be performed to see a possible difference in specific lipid distributions between *wild type* and *dop* mutant embryos.

4.3 Overall follicle cell morphogenesis is not dependent on Dop function

Previously, it was discussed that the first F-actin defect in complete loss of function dop^{10} mutant embryos appeared in cellularisation. However, Utrophin-GFP live-imaging revealed that in 50% of dop^{1}/dop^{10} transheterozygous mutant embryos defects were visible already during syncytial divisions. These defects were not visible in complete loss-of-function dop^{10} mutants. One difference between hypomorphic dop^{1}/dop^{10} transheterozygous mutant and dop^{10} germ line clone-derived mutant embryos that could explain an earlier defect in the hypomorphic mutant would be a somatic follicle cell defect caused by the *dop* mutation in the mother. Follicle cells are somatic maternal tissue that surround the germ cells in the egg chambers. They are responsible for the production and secretion of yolk proteins and egg shell components such as the vitelline membrane and the chorion (Pascucci et al. 1996). The chorion includes specific structures such as the dorsal appendages, which are important for gas exchange between embryo and environment, the operculum, which represents a weakened region at the anterior

of the eggshell through which the larvae can hatch, and the anterior micropyle, which functions as a sperm entry point during fertilisation (Horne-Badovinac & Bilder 2005). Apart from their importance to produce and secrete these important extra-embryonic layers, follicle cells are also required to mediate signalling from the oocyte in order to determine the embryonic body axes. Therefore, a mutation in the follicle cells impairing their function could affect later on the development of the germ line-derived embryo and, maybe, specifically affect cortical structures in the embryo that are immediately underlying the vitelline membrane and chorion. Hypothetically, a malformation of these extra-embryonic layers due to follicle cell defects could possibly affect the F-actin cytoskeleton at the cortex of the embryos in a way seen in hypomorphic dop^{1}/dop^{10} transheterozygous mutant embryos. If the syncytial defect seen in these dop^{1}/dop^{10} mutants is based on a defect in follicle cells, these cells must have a requirement of Dop function for their own function. However, induced follicle cell clones homozygous for dop^{10} did not show an overall difference in neither morphology nor microtubule nor F-actin network abundance or polarity compared to neighbouring *wild type* follicle cells. Thus, follicle cell formation and presumably function did not seem to depend on Dop function. However, a possible protein or mRNA perdurance in the mutant cells cannot be ruled out. Follicle clones that did not express GFP were analysed which should be homozygous for the dop^{10} allele and, therefore, unable to express a functional Dop protein themselves. However, it is not known how stable the Dop protein is. The cell the mutant cell derives from was heterozygous for *dop* and might have expressed the protein or *dop* mRNA in high abundance. Thereby, the mutant cell might have inherited a lot of functional Dop protein or mRNA. Depending on how stable the protein/mRNA is, this inherited Dop protein/mRNA might mask defects that could be detected in follicle cells derived from ovaries of *dop* mutant mothers. Two ways exist to test for a possible masking defect in this experiment. One would use a functional Drop out antibody to test for the abundance of Dop protein in the mutant follicle cells. Unfortunately, the antibodies against Dop generated in the past showed low specificity for the Dop protein and cannot be used. Another way of validating that Dop protein is not required for

follicle cell formation is to look at follicle cells in ovaries derived from *dop*^{1}/*dop*^{10} mutant mothers. Here, all cells are mutant for *dop*. However, a problem with this experiment might be that there is no internal *wild type* control available in these ovaries and mutant follicle cells have to be compared with follicle cells of ovaries derived from *wild type* females.

4.4 Dop is required for membrane invagination during slow as well as fast phase of cellularisation

dop complete loss-of-function mutant embryos derived from germ line clones showed F-actin defects only during cellularisation but not during syncytial divisions and the first protein localisation defects were seen with anti-Slam and anti-Eps15 stainings on embryos just prior to cellularisation. However, the most striking result obtained by the germ line clone analysis was the effect on membrane invagination. Previous results on *dop* hypomorphic mutants showed a defect on membrane invagination that was visible only during slow phase of cellularisation resulting in membrane invagination of between 20 and 25 µm by the end of cellularisation (Meyer et al. 2006; Hain et al. 2014). In contrast, complete loss-of-function *dop*^{10} mutants derived from germ line clones displayed strong defects with membrane growth of just a few µm by the end of the whole cellularisation process. This result clearly shows that Dop function directly or indirectly affects the membrane invagination process during slow as well as fast phase of cellularisation. However, it might be as proposed for hypomorphic mutants of *dop* that also the complete loss-of-function *dop* mutant only affects the slow phase of membrane invagination. In this case, a much stronger inhibition of slow phase might be delaying fast phase to an extent that gastrulation movements start before fast phase can occur.

How Dop affects membrane invagination during cellularisation is not known. As previously discussed, Dop seems to be required for formation and specification of the furrow canal which is a prerequisite for furrow invagination (Crawford et al. 1998; Grosshans et al. 2005; Acharya et al. 2014). Thus, Dop could affect membrane invagination indirectly by affecting the furrow canal.

Additionally, data presented in this thesis obtained from hypomorphic as well as complete loss-of-function *dop* mutants show a requirement for Dop function in localisation and distribution of Golgi and recycling endosomal vesicles. Both Golgi and recycling endosomal pathways were shown to be required as membrane supply and, as a result, for membrane invagination during cellularisation (Lecuit & Wieschaus 2000; Papoulas et al. 2005; Riggs et al. 2007; Sisson et al. 2000; Pelissier et al. 2003; Figard et al. 2016). Thus, the impairment of both pathways could be the cause for the membrane invagination defect seen in *dop* mutants.

Moreover, the apical membrane reservoir stored as microvilli at the beginning of cellularisation persists throughout cellularisation in *dop* mutants, which indicates that *dop* mutants are defective in a mechanism that redistributes membrane from the apical reservoir to the invaginating furrows (Hain et al. 2014; Figard et al. 2016; Fabrowski et al. 2013). These data also indicate that vesicle trafficking might be impaired in *dop* mutants.

4.5 Dop function is required for vesicle transport along microtubules

Both hypomorphic and complete loss-of-function mutants for *dop* displayed defects in Golgi as well as recycling endosome localisation and distribution. However, the defects observed for either of these organelles were very different. Nuf (Nuclear fallout) and Rab11, two components of the recycling endosomal pathway, showed a tight localisation at the centrosomes and, therefore, the microtubule minus-ends in *dop* mutant embryos rather than a more dispersed localisation around the centrosomes and supposedly along microtubules. In contrast, Lava lamp (Lva) and Golgi protein 120 kDa (gp120), two markers of Golgi vesicle membranes, showed reduced apical and, thus, less microtubule minus-end localisation during cellularisation in *dop* mutant embryos compared to *wild type*. As a result, the defect observed for endosomal transport looks like a defect in Kinesin-dependent transport away from the centrosomes whereas the defect in Golgi localisation looks like a defect in Dynein-dependent transport.

A general defect affecting microtubules is unlikely to cause these phenotypes because overall microtubule formation, length and polarity seemed not to be affected in *dop* mutants as revealed by live-imaging using the plus-end binding protein EB1 fused to GFP (this thesis) and previous stainings against β-tubulin (Hain et al. 2014).

4.5.1 Proteins that could be responsible for recycling endosome localisation defects in *dop* mutants

The Nuf and Rab11 localisation in *dop* mutants is more focussed to the centrosomal area and, therefore, the microtubule minus-ends. This might be due to a defect in transporting recycling endosome vesicles away from the centrosomes and to the plasma membrane for exocytosis which is presumably dependent on Kinesin function (Riggs et al. 2003; Riggs et al. 2007). Many different Kinesins fulfil distinct functions (Höök & Vallee 2006). Maybe Dop affects only a subset of Kinesins during cellularisation and, thereby, only a subset of Kinesin overall function. The mitotic Kinesin-6 (called Pav-KLP in *Drosophila*) is the most promising candidate of the Kinesins to be affected by Dop function: mutants of Pav-KLP show highly reduced membrane invagination, reduced F-actin at the furrow canal, misaligned and falling out nuclei as well as an effect on the microtubule basket structure surrounding the nuclei during cellularisation, some of these phenotypes resembling phenotypes in *dop* mutants (Sommi et al. 2010; Hain et al. 2014). Additionally, Pav-KLP inhibition impairs Nuf distribution during syncytial divisions similar to how *dop* mutants impair Nuf and Rab11 distribution during cellularisation. The Nuf phenotype in Pav-KLP impaired embryos is caused by an inhibition of the microtubule plus-end transport of endosomal vesicles for exocytosis and possibly actin or actin regulators along astral microtubules to the plasma membrane. In contrast, the minus-end directed transport by Dynein motor proteins seems to be unimpaired in Pav-KLP impaired embryos. Antibodies against Pav-KLP could be used to look if the localisation or maybe the concentration of this particular Kinesin is affected in *dop* mutant embryos. It might be that Dynein is required to transport different

cargoes to microtubule minus-ends at the centrosomes and from there Kinesin could be responsible to transport the cargoes to the cortex through astral microtubules. However, in this model the question remains why only the recycling endosomes so far showed a tight localisation around the centrosomes, thus, the microtubule minus-ends and other possible cargoes like e.g. F-actin and other furrow markers like Slam, Patj and Eps15 localise to the cortex away from centrosomes at the microtubule plus-ends. Their plus-end localisation speaks against a Pav-KLP involvement in the localisation phenotypes in *dop* mutants. However, possibly, different Kinesins are responsible for endosomal vesicle transport and the localisation of the furrow markers and only the Kinesin required for endosomal vesicle transport is affected by Dop.

Apart from Kinesin, also Rab11 malfunction could lead to the observed Nuf/Rab11 phenotype. In contrast to the Arfophilin Nuf, Rab11 is not required for vesicle biogenesis but for targeting of recycling endosomal vesicles (Hickson et al. 2003; Riggs et al. 2007). Thus, it might be that Rab11 malfunction could lead to a recycling endosome localisation defect as seen in *dop* mutants. In case that Dop function affects Rab11 function, in *dop* mutants Rab11 might fail to target the recycling endosomal vesicles to the plasma membrane. In favour of a link between Dop and Rab11 function is the observation that Slam protein shows the same broadening at the furrow canal in *rab11* mutants as observed in *dop* mutants (Pelissier et al. 2003; Hain et al. 2014). Additionally, Rab11 is required for membrane growth during cellularisation, another function it has in common with Dop. Maybe Rab11 function is required for a Kinesin-dependent transport away from the centrosomes which is counteracted by the Nuf-mediated Dynein-dependent transport to the centrosomes (Riggs et al. 2007).

In addition, the Nuf and Rab11 phenotypes in *dop* mutants look similar to *shibire*/*dynamin* mutants with slightly bigger but less dispersed recycling endosomes around the centrosomes (Pelissier et al. 2003). Furthermore, the transmembrane protein Neurotactin (Nrt) is not inserted into the plasma membrane in either *shibire* or *dop* mutants. During cellularisation, Nrt is newly synthesised in the endoplasmic reticulum (Lecuit & Wieschaus 2000; Pelissier et al. 2003;

Hortsch et al. 1990). From there it is transported over the Golgi to the early endosome and over the recycling endosome to the plasma membrane. Afterwards, it accumulates by a yet unknown mechanism at the newly forming lateral membrane. In *dop* mutants, Nrt shows abnormal apical aggregations similar to *shibire* mutants, which could well be co-localising with Rab11/Nuf-positive endosomes indicating that Nrt gets trapped in the recycling endosome (Pelissier et al. 2003; Hain et al. 2014). Thus, Dynamin is another important factor to look at in *dop* mutants. However, it must be taken into account that Dynamin functions in several different vesicle formation processes in the cell. Dynamin is also required for pinching off vesicles at the trans-Golgi network in mammalian cells, in vesicle formation at the plasma membrane and at the endoplasmic reticulum (van Dam & Stoorvogel 2002; McNiven 1998; Yoon et al. 1998). It needs to be determined whether Dop affects dynamin function at either or all of these sites of vesicle formation.

To test which function of the Golgi and/or recycling endosomal pathway is impaired in *dop* mutants, it would be interesting to go back to Nrt localisation analysis. By looking in detail at the localisation of Nrt in *dop* mutant embryos and maybe by performing co-labelling with endoplasmic reticulum-, Golgi- and recycling endosome-markers, this could provide a hint on the stage of the Nrt transport process in which a defect occurs in *dop* mutants. If Dynamin function is affected at any stage of this process, an accumulation of Nrt would be expected in either of the subcellular organelles endoplasmic reticulum, Golgi or recycling endosome. In case that Rab11 function is affected, Nrt would be expected to either accumulate in a subcellular recycling endosome or to disperse and not being targeted to the plasma membrane. If either Dynein or Kinesin transport is affected, an accumulation of Nrt should be visible at either plus- or minus-ends of microtubules. Analysing the specific localisations of either of these proteins in *wild type* and *dop* mutants could provide further hints on whether their function is disturbed.

4.5.2 Dynein as possible link between Dop and cellularisation

Dynein-dependent transport is required for lipid clouding, Bazooka (Baz) transport and mRNA transport, processes which are defective in *dop* mutant embryos (Hain et al. 2014; Meyer et al. 2006; Harris & Peifer 2005). In addition, Dynein impairment could also be responsible for *dop* mutant F-actin localisation defects since Dynein is required for transport of actin regulators and possibly F-actin itself (Cao et al. 2008; Acharya et al. 2014; Rothwell et al. 1999; Albertson et al. 2008). Also, the defect seen in *dop* mutant embryos showing a reduction in the apical localisation of Golgi vesicles during cellularisation could be based on an impairment of Dynein-dependent transport from the basal microtubule plus-ends in the interior of the embryo to the apical microtubule minus-ends near the embryo cortex. Supporting this hypothesis, previous evidence suggests that Golgi vesicle transport is Dynein-dependent during cellularisation (Papoulas et al. 2005). Moreover, Papoulas et al., 2005 observed that not only Golgi transport but also furrow formation are dependent on Dynein, another clear phenotype visible in *dop* mutant embryos. Thus, it is likely that Dynein transport is dependent on Dop function and that several phenotypes visible in *dop* mutants are based on a malfunction of Dynein-dependent transport, including the microtubule minus-end directed transport of Golgi vesicles seen in this thesis.

4.5.3 Dynein and Kinesin localisation in *dop* mutants

A first attempt has been performed in this thesis to elucidate the question how Dynein and Kinesin are localised in *dop* mutants in comparison to *wild type* embryos. However, this experiment could not answer this question because the antibody staining only showed punctate localisations of Dynein and Kinesin heavy chains in both *wild type* and *dop* mutant embryos. No clear accumulations of either protein could be identified in *dop* mutants due to high background signal and maybe low protein specificity of either antibody. A weak accumulation of Dynein was detected in *wild type* embryos, co-localising with Eps15 at the furrow canal. This could indicate

a possible dependence of Eps15 transport on Dynein function. However, further experiments have to be performed using other tools to image Dynein and Kinesin in *wild type* and *dop* mutant embryos to determine if the localisation of either protein complex is disturbed in *dop* mutants.

4.5.4 Dynein inhibition attempts to test for Dynein requirements during cellularisation

All *dop* mutant phenotypes with a clear link to Dynein function such as lipid droplet clouding as well as Baz and mRNA transport do not have a known direct implication for early cellularisation morphological processes which are also affected in *dop* mutants such as furrow canal formation and membrane invagination. Other phenotypes with link to cellularisation like recycling endosome localisation are unlikely to be caused by Dynein impairment in *dop* mutants because of their observed microtubule minus-end localisation. The only phenotype with clear link between Dynein and an important cellular process during cellularisation in *dop* mutants is Golgi transport which was shown to be required for membrane invagination (Lecuit & Wieschaus 2000; Papoulas et al. 2005; Sisson et al. 2000). The Dynein complex function is essential for cell viability and it is thought to act in more transport processes than the previously described Golgi, Baz, mRNA and lipid droplet transport and comprises a much more global role during cellularisation (Gepner et al. 1996). However, not much is known about its actual function during the cellularisation process.

Apart from the described phenotypic links connecting *dop* mutations and Dynein malfunctions, also biochemical analysis suggested an effect of Dop function on Dynein-dependent transport (Hain et al. 2014; Langlands 2012). 2D gel electrophoresis showed that Dynein intermediate chain phosphorylation is dependent on Dop function (Hain et al. 2014). Moreover, a SILAC screen identified Dynein light intermediate chain as possible (direct or indirect) phosphorylation target of Dop (Langlands 2012). As a further support for Dynein as functional target of Dop, genetic interaction studies with Dynein (*short wing*^{1}) and Dynactin (*Glued*^{1}) subunits showed enhanced *dop*^{1} phenotypes when combined with this *dop* mutant allele (Hain et al. 2014).

To elucidate the requirement for Dynein in cellularisation, the establishment of an assay to inhibit Dynein function specifically during cellularisation was attempted. As previously mentioned, Dynein is needed for cell viability and as well for proper oocyte and embryo development (Gepner et al. 1996; Mische et al. 2008; Januschke et al. 2002; Robinson et al. 1999). Thus, mutants for important Dynein subunits would impair its function too much to ensure embryo development up to cellularisation. Other strategies were used to find conditions to analyse Dynein impairment consequences specifically during cellularisation.

4.5.4.1 Dynamitin overexpression as attempt to inhibit Dynein function

The first attempt used Dynamitin overexpression to inhibit Dynein. Dynamitin is a subunit of the Dynactin complex which is important for Dynein overall functions in the cell (Schroer 2004). Overexpression of Dynamitin was shown to result in Dynactin complex disassembly and, thereby, an inhibition of Dynein function (LaMonte et al. 2002; Echeverri et al. 1996; Januschke et al. 2002). The experiment was set up with the UAS::(human)Dynamitin construct carried by the father and a single or double maternal α-tubulin Gal4 driver carried by the mother. This experiment set-up should make use of the Gal4 protein that is provided by the mother in the oocyte and early embryo and which should be able to activate Dynamitin expression with the construct provided by the father just at the maternal-to-zygotic transition.

The maternal-to-zygotic transition is the first phase where a bulk of zygotic genes get expressed which are important for further embryo development after maternally provided components get degraded (Tadros et al. 2007; Langley et al. 2014). It takes place just before cellularisation which is also the first developmental stage that relies upon zygotic gene expression (Tadros et al. 2007). The set-up of the cross was chosen to make sure that Dynamitin gets expressed and inhibits Dynein specifically during cellularisation. The aim was to avoid an expression of Dynamitin and inhibition of Dynein during earlier stages to not interfere with the essential

function of Dynein for oocyte specification and syncytial divisions (Januschke et al. 2002; Robinson et al. 1999).

Unfortunately, neither expression with a single α-tubulin Gal4 driver nor expression with a double α-tubulin Gal4 driver showed strong defects during cellularisation or reduced overall embryo viability. Two possible explanations for this result are that either Dynamitin was not expressed using the maternal α-tubulin Gal4 driver or it did not inhibit Dynein function in the system. The latter explanation is unlikely due to the many studies using Dynamitin as Dynein inhibitor, especially, one study which uses Dynamitin as Dynein inhibitor in the *Drosophila* oocyte and, therefore, a system closely related to *Drosophila* embryos (Echeverri et al. 1996; Burkhardt et al. 1997; LaMonte et al. 2002; Januschke et al. 2002). It is more likely that Dynamitin was not expressed in the system or not to a sufficient level. It might be that the UAS construct was not accessible for the Gal4 protein at the maternal-to-zygotic transition maybe due to its DNA packing status. Even if the DNA was accessible during later stages of embryogenesis, the Gal4 protein might have been degraded by that point which would explain the overall embryo viability throughout embryogenesis. Even though Dynamitin in the construct was fused to a myc-tag, the expression has not been verified. Using an antibody specific for this myc tag would answer if Dynamitin gets expressed in the chosen experiment set-up.

4.5.4.2 Ciliobrevin D injections as attempt to inhibit Dynein function

A different approach to inhibit Dynein specifically during cellularisation used the Dynein inhibitor molecule Ciliobrevin D. Ciliobrevin D inhibits Dynein by blocking its ATP binding site (Firestone et al. 2012). It was used to inhibit Dynein in different cell types (murine NIH-3T3, *Xenopus* melanophores, *Drosophila* S2 cells, murine IMCD3 cells) as well as in mouse oocytes and *Drosophila* embryos during late embryogenesis (Hyman et al. 2009; Ye et al. 2013; Łuksza et al. 2013; Le Droguen et al. 2015).

In this experiment, Ciliobrevin D from two different sources were used. Injection of Ciliobrevin D donated by Jason Swedlow's lab (Centre for Gene Regulation and Expression, Dundee) showed overall embryo viability and no effects on cellularisation (data not shown). Personal communication (Katharina Schleicher, Jason Swedlow lab) further elucidated that HeLa cells incubated with this specific Ciliobrevin D did also not show a Dynein inhibition effect. Thus, it was assumed that the Ciliobrevin from this particular source is defective. Ciliobrevin D from the James Chen lab was further tested. Also injection of this Ciliobrevin D did not show a significant defect during cellularisation and embryos were seen to develop until late embryogenesis. This could be due to Ciliobrevin D not being functional in early embryos. During late embryogenesis (stages 14 and 16), Ciliobrevin D was shown to inhibit Dynein-dependent localisation of recycling endosomes, as well as Baz and E-cadherin in tracheal cells (Le Droguen et al. 2015). In this paper, embryos were incubated for 3 hours with Ciliobrevin D before fixation. This protocol could not be applied to inhibit Dynein during cellularisation because the incubation time alone exceeded the time between egg laying and cellularisation. However, the question remains why injection of Ciliobrevin D could not affect Dynein function in the early embryo. Injection of a substance into an embryo guarantees the uptake and is an even more powerful method than incubation with this particular substance. Maybe the injected Ciliobrevin D was not functional in embryos at onset of cellularisation because it got stored away and degraded in the many yolk bodies in the centre of the embryo. These yolk bodies are easily accessible and plentiful at this stage of embryogenesis but diminish during the course of embryogenesis (Callaini et al. 1990).

Both Ciliobrevin D- and DMSO-injected embryos displayed multipolar spindle arrays, a defect reported for Dynein mutant embryos (Robinson et al. 1999). This made it impossible to test for Ciliobrevin D effects in early embryos. Dimethyl sulfoxide (DMSO), which is widely used in cell biological applications, was used in this case as a solvent which is in general well-tolerated by cells even if it has many characteristics that can affect cells and tissues (Yu & Quinn 1994). It is not possible to identify if the injection of DMSO into embryos during syncytial divisions caused

the spindle array defects that were observed or if the injections themselves caused these defects.

4.5.4.3 Dynein heavy chain RNAi expression as attempt to inhibit Dynein function

A third attempt to impair Dynein function in early embryos used RNAi (RNA interference) directed against Dynein heavy chain 64C transcripts. The gene encoding for Dhc64C was shown to be essential for *Drosophila* development starting from oogenesis and it gets maternally provided and expressed throughout embryogenesis (Gepner et al. 1996; Rasmusson et al. 1994; McGrail & Hays 1997). The aim of this experiment was to express RNAi against Dhc64C transcripts maternally, thereby inhibiting Dynein function from oogenesis onwards but finding a condition by which development during oogenesis and embryogenesis up to cellularisation is overall unimpaired, followed by looking for possible defects that occur during cellularisation due to Dynein impairment.

Embryos expressing the Dhc64C^{GL00543} RNAi construct on the second chromosome showed an about 16-fold reduction in the hatching rate compared to *wild type* embryos This suggests that Dynein is impaired in these embryos to some extent and the 4.5% of embryos that hatched reflect a low escaper rate. As a next step it would be interesting to look for embryos that show an overall normal development up to cellularisation and to see if they display any defects during cellularisation that could be based on Dynein malfunction. Expression of Dhc64C^{GL00543} RNAi could provide an important tool to investigate Dynein-dependent processes essential for cellularisation.

4.5.5 Studies on Dlic as possible Dop target

As previously mentioned, a SILAC screen identified Dynein light intermediate chain (Dlic), a subunit of the Dynein complex, as possible phosphorylation target of Dop (Langlands 2012). In

more detail, phosphorylation of Serine 401 (S401) in Dlic seemed to depend on Dop function. Therefore, it was interesting to see on one hand how Dlic functions and is localised in *dop* mutant embryos in comparison to *wild type* and on the other hand if impairment of the phosphorylation state of this particular Serine 401 could change its function and/or localisation.

dlic is the only gene encoding a Light intermediate chain Dynein-subunit in *Drosophila* (Mische et al. 2008). Thus, this subunit can be easily modified using genetic techniques. Three different forms of Dlic were created and cloned to test for its overall function and the function of the phosphorylation state of its Serine 401. A *wild type* Dlic with no amino acid changes, a non-phosphorylatable form of Dlic S401 (S401A) and a phospho-mimic form of Dlic S401 (S401D) were each fused to GFP and maternally expressed in *wild type* and *dop* mutant embryos.

The localisation of the *wild type* DlicGFP version was highly similar in *wild type* and *dop* mutants both during syncytial divisions and during cellularisation. The only detectable difference concerned an increase in DlicGFP punctae numbers in *dop* mutants compared to *wild type* during cellularisation. It could not be determined what these punctate structures are. They might be accumulations of excessive DlicGFP protein. However, this would not explain why more of these structures are present in *dop* mutant embryos. One hypothesis is that these punctae are part of a Dynein-dependent transport pathway which either terminates or commences from the furrow canal. This hypothesis would explain why the punctae move into the interior in *wild type* embryos presumably together with the furrow canal. The presumed localisation to the furrow canal would suggest that the punctate structures are part of the endocytic machinery which localises to this structure (Lee & Harris 2014; Sokac & Wieschaus 2008a). It might be that the number in DlicGFP-positive punctae is increased in *dop* mutant embryos due to a failure of them to fuse with their target structure or to get transported away from the furrow canal. A more thorough understanding of Golgi and endosomal pathway defects in *dop* mutants as discussed earlier might help to explain the vesicular accumulation phenotype seen in this experiment.

Comparison of the localisation of both phospho-mutant and *wild type* versions of DlicGFP could not show any differences. Neither in *wild type* nor in *dop* mutant embryos did any of the three DlicGFP versions display a localisation distinct from the other versions. This suggests that the phosphorylation state of Serine 401 has no major impact on Dlic localisation. It also suggests that if any of the phenotypes visible in *dop* mutants are caused by a reduction in Serine 401 phosphorylation, these phenotypes are not caused by a mislocalisation of Dlic. Still, phosphorylation of Serine 401 could be important for the overall function of Dlic without affecting its localisation.

To test the possibility that S401 phosphorylation affects overall Dynein function, embryo hatching rates were determined for each DlicGFP version expressed in *wild type* and *dop* mutant embryos. In *wild type* background, the hatching rates were not significantly altered in the embryos expressing either of the three DlicGFP versions. However, in this context it cannot be excluded that effects of the DlicGFP phospho-mutant versions are masked by the functional *wild type* endogenous version being present as well.

The dop^{1}/dop^{10} mutation leads to lethality in all embryos, and the lethality was not rescued by expressing the *wild type* version of DlicGFP under maternal α-tubulin driver control. In contrast, expression of the phospho-mimic version of DlicGFP showed a hatching rate of embryos with a dop^{1}/dop^{10} background that was highly significant compared to the *wild type* version suggesting that the phosphorylation of S401 is indeed important for embryo survival and that *dop* lethality is based on impaired phosphorylation of Dlic S401. The result involves as well that cellularisation can be rescued (at least to a certain extent) in *dop* mutant embryos by the phospho-mimic version of Dlic S401, otherwise no embryo would survive. Detailed analysis should follow now to elucidate which of the many different *dop* phenotypes during cellularisation are rescued by the expression of the phospho-mimic S401D Dlic version.

Surprisingly, also expression of the non-phosphorylatable version of DlicGFP was able to rescue embryo lethality to a low and not statistical significant percentage. This result suggests that also

the non-phosphorylatable form of Dlic S401 might have a hitherto inexplicable rescue function in *dop* mutants which needs to be further investigated.

4.5.6 Further analysis of the rescue potential of the different Dlic S401 versions

To rescue phenotypes of *dop* mutants as suggested for hatching rates in the last experiment, the cloned DlicGFP versions must be able to take over endogenous Dlic function in a background where this Dlic function is disturbed. The ability of each DlicGFP version created in this thesis to take over endogenous Dlic function in *dlic* mutants was therefore tested. However, no rescue could be detected with either phospho-mutant Dlic or *wild type* Dlic fused to GFP and expressed with an *ubiquitin*-Gal4 driver. This driver was chosen because it drives expression throughout *Drosophila* development and in all cells (Bloomington Stock Report). However, it might be that the rate of expression was too low to substitute for Dlic function. It could also be that the fusion of the GFP molecule interferes with the Dlic function. To overcome this problem a GGGGSGGGGSGGGGS-linker between Dlic and GFP was used to separate both proteins from each other. This linker was used in a previous transgenic construct fusing Dlic and GFP by Tadashi Uemura's lab and the different versions of Dlic were fused to GFP by using the vector provided by his lab (Satoh et al. 2008). The DlicGFP construct created in Tadashi Uemura's lab was shown to rescue arborisation phenotypes in neurons which were based on Dynein functional impairment caused by a mutation in *dlic*. The rescue experiment needs to be repeated using a different driver and using the DlicGFP construct from Tadashi Uemura's lab as positive control.

4.6 Dop effects in view of MAST kinase functions

Drop out is the single homologue in *Drosophila* of the four MAST (Microtubule-associated serine/threonine) kinases in human. The human MAST kinases were associated with many different diseases such as breast cancer, inflammatory bowel disease, rabies virulence,

neurodegenerative disorder, cystic fibrosis and enterotoxin-induced secretory diarrhoea (Robinson et al. 2011; Wang et al. 2010; Labbé et al. 2008; Labbé et al. 2012; Terrien et al. 2009; Terrien et al. 2012; Préhaud et al. 2010; Loh et al. 2008; Ren et al. 2013; Wang et al. 2006). The mentioned implications were mainly raised by proteins that were somehow involved in these diseases and shown to interact with either one or more of these MAST kinases. However, as outlined in the introduction, none of the MAST kinase interaction partners are promising candidates to explain the cellularisation defects visible in *Drosophila dop* mutants, either their *Drosophila* homologues are not expressed during cellularisation or their functions suggest different phenotypes.

Previous PhD theses focussed mainly on the establishment of cell polarity during cellularisation that is highly affected in *dop* mutants. However, this study reveals that the first morphological defect in *dop* mutants occurs prior to epithelial polarity establishment already during onset of cellularisation and affects furrow canal formation. Proteins that are connected to this defect are all somehow involved in and regulated by vesicle transport (both Dynein- and Kinesin-dependent). Vesicle transport is a fundamental process in eukaryotic cells, involving a network of different but connected mechanisms, and is required for different aspects of signalling pathways (Stenmark 2009; Seaman et al. 1996). Thus, the vesicle transport processes that are affected by Dop function could provide an indication on a connecting process that human MAST kinases may collectively regulate. This, however, assumes that Dop and human MAST kinases have not only related protein structures and sequences but also related functions.

Until now, only one of the MAST kinase targets has reported direct implications in vesicular transport. This target is the Cystic fibrosis transmembrane conductance regulator (CFTR), a cAMP-activated anion channel in the plasma membranes of lung, pancreas, liver, intestine, sweat ducts and the reproductive system (Ren et al. 2013). A genetic screen identified MAST2 as CFTR interaction partner and further experiments elucidated MAST2 as positive regulator for CFTR expression and function. These positive effects are presumably caused by a competitive

binding to the C-terminus of CFTR between MAST2 and the CFTR-associated ligand (CAL). The expression of MAST2 inhibits CAL-binding to CFTR in a dose-dependent manner and, therefore, prevents CAL-induced CFTR lysosomal degradation. CAL itself is a Golgi-associated protein and localises mainly to the trans-Golgi network and to a lower extent to lysosome membranes. An inhibition of Golgi transport to the plasma membrane would possibly also prevent binding of CAL to CFTR and have the same effects as MAST2 overexpression. However, this seems not the mechanism MAST2 is involved in. Instead, MAST2 binds CFTR directly and prevents CAL-binding this way.

Many studies discovered effects of MAST kinase function in neuronal cells (Lumeng et al. 1999; Loh et al. 2008; Terrien et al. 2009; Préhaud et al. 2010; Terrien et al. 2012; Garland et al. 2008; Yano et al. 2003). For example, the function of MAST3 restricts neurite outgrowth and favours neurite retraction, possibly via an interaction with PTEN (Loh et al. 2008; Terrien et al. 2012). Also vesicle trafficking is important for neuronal development and function (Cameron et al. 1993; Villarroel-Campos et al. 2016). Impaired vesicle trafficking can lead to neurodegenerative diseases (Schreij et al. 2016; Jain & Ganesh 2016). It might be that MAST kinase function somehow regulates vesicle trafficking in neurons like it is seen for Dop in *Drosophila* cellularisation. However, also in neuronal function none of the identified MAST kinase interaction partners give a direct hint on vesicle trafficking. It still needs to be determined if Dop in *Drosophila* cellularisation has similar functions to MAST kinases in mammals.

4.7 Cellularisation and cytokinesis

Cellularisation is often referred to as a specialised form of cytokinesis and it can be used as model to elucidate new mechanisms important for conventional cytokinesis (Beronja & Tepass 2002; Albertson et al. 2005). Cytokinesis is the process in which one cell gets divided into two daughter cells.

The clear difference between cellularisation and cytokinesis is that during *Drosophila* cellularisation a single cell gets divided into around 6000 cells and this process takes place just below the cortex of the cell. Moreover, the formation of cells during cellularisation does not involve a central constriction of the parental cell as in cytokinesis of most animal cells (Glotzer 1997) but the invagination of cortical membrane at many thousand sites all around the cortex. The central constriction during cytokinesis is directed by the central spindle that occurs during anaphase of the cell cycle and both, F-actin and myosin are required for furrow formation (Giansanti et al. 2001; D'Avino et al. 2005; Cheffings et al. 2016). In contrast, during cellularisation division takes place in an elongated interphase and the site of furrow formation is thought to be determined by overlapping astral microtubules but not the central spindle (Crest et al. 2012). As in cytokinesis, the formation of cellularisation furrows is dependent on F-actin localisation, however, myosin seems not to be important for this process (Royou et al. 2004).

Cellularisation is specifically controlled by early zygotic genes that are solely expressed during this particular stage and do not play a role during conventional cytokinesis. These genes provide one of the main factors that sets apart the process of cellularisation and conventional cytokinesis. Four of these early zygotic genes regulate F-actin network dynamics (He et al. 2016). Moreover, a switch in the activity after cellularisation from the F-actin regulator RhoGEF2 to another F-actin regulator, called RhoGEF Pebble, was proposed as a key mechanism inducing furrow formation at the central spindle during the first conventional cytokinesis (Crest et al. 2012). Thus, the differential regulation of the F-actin network seems to be the main distinction between both processes.

Despite the clear differences, both conventional cytokinesis and cellularisation share the same distinct stages: (i) cleavage plane or furrow ingression site specification, respectively; (ii) furrow assembly and furrow ingression; (iii) as well as cell separation or basal closure, respectively (Glotzer 1997). Additionally, both processes rely on distinct dynamic regulation of the microtubule and F-actin cytoskeleton, and on vesicle transport and fusion. The secretory vesicle

pathway as well as the endocytic pathway are required for both cellularisation and cytokinesis (Albertson et al. 2005; Swanson & Poodry 1981). The endocytic machinery in both processes is localised at the furrow tips. However, its function in these processes is not completely understood. Further investigation of its role during cellularisation might also give important insight into its function during cytokinesis.

Plant cell cytokinesis is another specialised form of cytokinesis and involves the formation of a so-called phragmoplast emanating from the cell centre and extending to the cortex by vesicle fusion in the cytoplasm (Bednarek & Falbel 2002). Such a mechanism of furrow formation has not been observed during cellularisation. Vesicle exocytosis at this stage of *Drosophila* embryogenesis occurs at very restricted places along the plasma membrane, first apical during slow phase and apico-lateral during fast phase (Lecuit & Wieschaus 2000). However, a mechanism involving a phragmoplast-like membrane structure might be important for the final step of cell separation and furrow membrane fusion during conventional cytokinesis (Albertson et al. 2005).

The function of maternally provided Dop on conventional cytokinesis has not been tested because *dop* mutants are lethal prior to the first conventional cytokinesis in Drosophila embryos. However, elucidating its function during cellularisation could also identify its possible function during cytokinesis.

4.8 Conclusion

The aim of this PhD thesis was to analyse the function of Drop out during early cellularisation in *Drosophila* embryos and to elucidate a possible mechanism by which Dop could possibly affect cellularisation.

Live-imaging of the F-actin network using a Utrophin-GFP construct revealed that the first morphological defect occurring in *dop* mutants was the malformation of the furrow canal about

5 to 8 minutes after onset of cellularisation. In comparison with analysis of the F-actin network in complete loss-of-function mutants, it was shown that syncytial divisions seem to be unaffected by *dop* mutants. However, the first phenotype that was visible occurred just prior to cellularisation during the last telophase of syncytial cell cycle 13 and before establishment of the furrow canal. The phenotype showed that the localisations of both Slam protein and Eps15 protein were affected at first in the old furrows between the nuclei at the cortex and later on in the new furrows. Both proteins showed broadened and punctate distribution. Figure 44 B illustrates this defect. F-actin in contrast localised similar to *wild type* at this early stage. It could not be determined what causes the phenotype of the broadened distribution of furrow markers. Further studies are needed to elucidate this question. However, it is likely that also the furrow canal membrane resembles a broadened shape after onset of cellularisation (Fig.44 D).

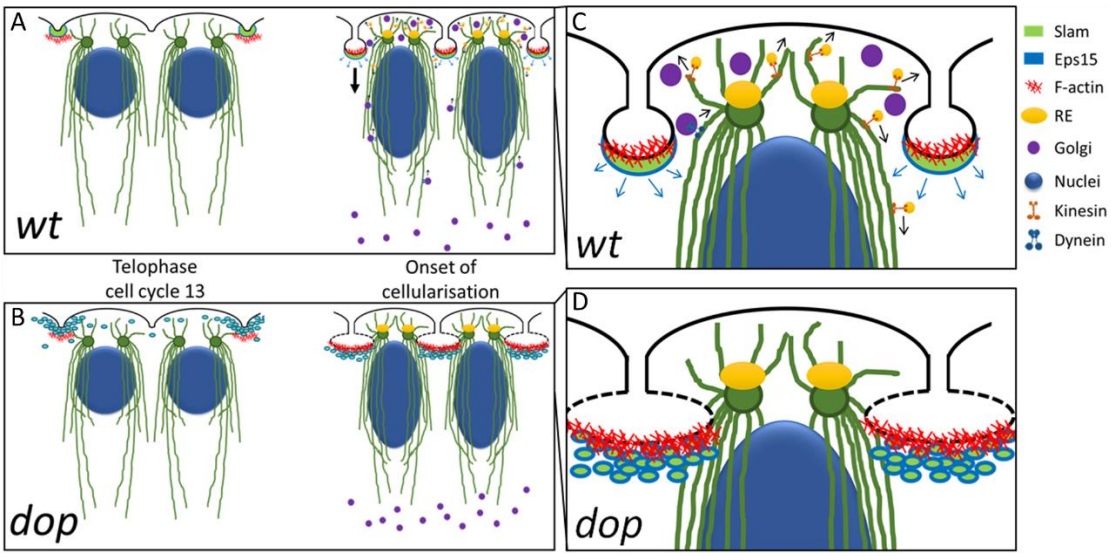

Figure 44 Model for consequences of *dop* complete loss-of-function on vesicle trafficking, protein localisation and furrow formation. The earliest phenotype visible in complete loss-of-function mutants for *dop* is visible during telophase of the last syncytial division in cell cycle 13. At this stage, Slam- and Eps15-containing vesicles fail to focus into narrow furrows surrounding newly established daughter nuclei (B). F-actin focussing to these furrows in the mutants is similar to *wild type* at this stage (A, B). Later during onset of cellularisation, F-actin is highly broadened as well as other furrow canal markers like Eps15 and Slam. The furrow canal membrane might be broadened as well (dashed line B, D). Dynein-dependent transport of Golgi vesicles as well as Kinesin-dependent transport of recycling endosomes (RE) is impaired at this stage (D in comparison to C). As a consequence, no membrane material is added to enable membrane invagination in the mutant. Broadening of the furrow canal and broadened localisation of furrow canal markers might be due to an impairment of endocytic transport.

Immediately after the furrow canal was established in *wild type* embryos, the membrane started to invaginate and to enclose the nuclei. In contrast, membrane invagination barely occurred in *dop* complete loss-of-function mutants and both slow phase as well as fast phase were shown to be strongly affected.

A mechanism that could affect both protein localisation as well as membrane invagination is vesicle trafficking. Both Golgi as well as recycling endosomal transport were affected in hypomorphic as well as complete loss-of-function *dop* mutants as shown by Rab11-GFP live-imaging and stainings against Nuf, gp120 and Lva. Another question remains about the mechanism by which these trafficking pathways are affected. The localisation of the recycling endosomal markers Rab11 and Nuf pointed to a functional impairment of Kinesin, whereas both Golgi markers Lva and gp120 pointed to a functional impairment of Dynein. Protein localisation studies of proteins transported by both pathways such as Neurotactin could possibly elucidate at which stage this transport mechanism is impaired.

Because of previous studies that showed a possible link between Dop function and Dynein phosphorylation, the question arose which phenotypes of *dop* mutants could be explained by a misregulation of Dynein function during cellularisation. The detailed functions of Dynein in cellularisation are not well known. Therefore, different tools were tested for their ability to inhibit Dynein function in *wild type* embryos specifically during cellularisation. Only overexpression of RNAi directed against *dynein heavy chain 64C* transcripts showed a promising effect on embryo viability suggesting that Dynein function is indeed inhibited. Now, embryos need to be analysed in detail to elucidate phenotypes that Dynein impairment creates during cellularisation.

Furthermore, DlicGFP constructs were created that either carried a *wild type* version of Dlic or a phospho-mutant (non-phosphorylatable or phospho-mimic) version of Dlic Serine 401, a proposed target of Dop. All these constructs were expressed in *wild type* and *dop* mutant embryos to see possible effects on protein localisation and embryo survival. It was shown that

neither of the constructs displayed a difference in the DlicGFP localisation during syncytial divisions or cellularisation, neither in *wild type* nor in *dop* mutant embryos. Only one difference could be detected by expressing DlicGFP (either version) in *wild type* and *dop* mutant embryos. During cellularisation, vesicular accumulations of unknown nature appeared in higher numbers in the mutant. What these accumulations are or what they are caused by could not be identified in the time course of this thesis.

Hatching rate analysis revealed that the phospho-mimic version of DlicGFP was able to rescue the lethality of dop^{1}/dop^{10} transheterozygous mutant embryos. This study suggests that phosphorylation of Serine 401 might have a role in passing on Dop function in this system. However, neither the *wild type* nor any of the phospho-mutant versions of DlicGFP were able to rescue the lethality of the larval lethal $Dlic^{G0065}$ allele in an experiment using *ubiquitin*-Gal4 as driver, indicating that the constructs might be unable to substitute entirely for the function of endogenous Dlic in *dlic* mutants. Further experiments have to be performed to see if this failure of rescue is based on low expression of the construct by a driver line that is not suitable to drive Dlic expression to an efficient extent.

Detailed analysis of cellularisation in *dop* mutant embryos expressing phospho-mimic Dlic S401 are a very exciting future direction in this project provided that the created DlicGFP versions can be proven as taking over endogenous Dlic function. Additionally, further analysis of vesicle trafficking pathways during cellularisation in *dop* mutants and description of cellularisation phenotypes caused by Dynein impairment using $Dhc64C^{GL00543}$ RNAi as a tool provide an exciting base for future experiments to further elucidate Dop function during early embryogenesis.

4.9 Directions for future research

Part of the future work will be aimed at addressing further questions that emerged while gaining the results of this thesis.

In this and previous theses, it was shown that several proteins which specifically localise to the furrow canal, such as Slam, Rho1, F-actin and Eps15, display a broadened localisation at this structure in *dop* mutants. This suggests that the furrow canal membrane is broadened as well. However, electron microscopic images suggest that no furrow canal structure is formed at all in *dop* mutant embryos (Hain et al. 2014). To finally elucidate how the furrow canal membrane is shaped in *dop* mutants, membrane markers such as the PI(3,4,5)P_3-binding construct Grp1-PH-GFP should be used to directly image the furrow canal membrane in *dop* mutants and to perform co-stainings with other furrow canal markers. This experiment might help to understand if at the furrow canal in *dop* mutants a protein is affected that links proteins to membrane (such as for example the protein Dah) or that restricts furrow membrane broadening (such as for example Bnk).

Eps15, a Clathrin-dependent endocytosis regulator protein, showed a broadened localisation at the furrow canal in *dop* mutant embryos. This Eps15 mislocalisation is assumed to be a secondary defect based on broadening of a structure Eps15 is localising to. However, in this context the question arose if the endocytic trafficking pathway is impaired in addition to the exocytic Golgi and recycling endosome pathway in *dop* mutants. To test this possibility, other proteins important for the endocytic pathway such as Rab5, Amph, Dynamin or Clathrin should be looked at in *dop* mutant embryos in comparison to *wild type* to see if they display any localisation differences between both genetic conditions.

In this thesis, *dop* mutants were shown to display localisation differences in comparison to *wild type* concerning their Golgi and recycling endosomal vesicles. Whereas the Golgi localisation defect pointed towards a defect in dynein-dependent transport, the recycling endosome localisation defect suggested an impairment of Kinesin-dependent transport. An attempt to determine Dynein and Kinesin localisation in *dop* mutants in comparison to *wild type* embryos was performed in this thesis using antibodies directed against the Dynein and the Kinesin heavy chain subunit, respectively. However, the antibody stainings were not specific enough to draw

any conclusions. Thus, other tools should be tested to verify Dynein and Kinesin localisations in *dop* mutant and *wild type* embryos.

One other tool to test the localisation of Dynein was used in this thesis, imaging a Dynein light intermediate chain-GFP fusion construct in *dop* mutants as well as *wild type* background. The only detectable DlicGFP localisation difference between both genetic conditions was a higher number of punctate accumulations present in *dop* mutant embryos. The nature of these punctate structures is unknown. However, they might belong to one of the vesicular transport pathways and, because the punctae are more numerous in *dop* mutants, they could give a further indication for a defect in one of these pathways in *dop* mutants. To test this possibility, co-immunostainings of DlicGFP expressing embryos should be performed using antibodies raised against markers for the different vesicular transport pathways, such as Lva (Golgi), Nuf (recycling endosome), Rab5 (early endosome) and Clathrin (Clathrin-dependent endocytosis).

Rab11-GFP imaging and Nuf stainings suggested that a Kinesin-dependent transport process of recycling endosome vesicles might be affected in *dop* mutants. One Kinesin that shows similar mutant phenotypes in comparison to *dop* mutants during cellularisation is the Kinesin Pav-KLP. Therefore, it would be interesting to see how this particular Kinesin is localised in *dop* mutant embryos in comparison to *wild type* to test if also Pav-KLP-dependent transport processes are affected in *dop* mutants.

Additionally, to determine at which stage of the exocytic transport pathway a defect occurs in *dop* mutant embryos, a detailed analysis of Nrt protein localisation should be performed. This protein was shown to be transported through both, Golgi and endosomal vesicles. Thus, testing its localisation or possibly accumulation in a specific organelle in *dop* mutants could indicate a specific transport step that is defective in these mutants and suggest proteins important for this particular transport step that could be affected.

One of the questions tried to be addressed in this thesis was whether Dop function is required for somatic follicle cell morphogenesis. In the performed experiment, follicle cell clones homozygous mutant for *dop*^{10} were analysed in egg chambers otherwise heterozygous for the *dop* mutation. The result suggested that Dop function is not required for follicle cell morphogenesis. However, a Dop protein or mRNA perdurance in the cytoplasm of the analysed follicle clones could not be excluded. Therefore, this experiment should be repeated on egg chambers derived from *dop*^{1}/*dop*^{10} transheterozygous mutant mothers instead of using the follicle cell clone technique on egg chambers derived from heterozygous *dop* mutant females. In case that Dop function turns out to be required for follicle cell morphogenesis, this result could explain the F-actin syncytial division defect seen in embryos derived from *dop*^{1}/*dop*^{10} mutant females that was not present in germ line clone-derived *dop*^{10} homozygous mutant embryos.

In addition to future work that should be performed to answer questions which emerged in the course of this thesis, also pending questions should be addressed by experiments using tools developed or tested in this thesis.

One of these experiments tries to determine the requirement of Dynein during cellularisation. In this thesis, the expression of an RNAi construct directed against the heavy chain subunit of Dynein was found as possible tool to address this Dynein requirement. The future work will focus on the detailed analysis of cellularisation in embryos expressing the Dhc64C^{GL00543} RNAi construct and that develop normally up to cellularisation. Embryos should be fixed and stained for markers important for cellularisation like Slam and F-actin, as well as vesicle trafficking markers such as Lva (Golgi) and Nuf (recycling endosome). Additionally, membrane growth should be monitored in these embryos by bright field imaging on living embryos. Thus, these experiments will cover processes that are known to be affected in *dop* mutants and elucidate which of the *dop* defects could be based on dynein impairment.

In this thesis, it was shown that the expression of the phospho-mimic S401D Dlic version can rescue lethality of *dop* mutant embryos. Detailed analysis of these embryos should follow now to elucidate which of the many different *dop* phenotypes during cellularisation are rescued by the expression of the phospho-mimic S401D Dlic version. Embryos should be fixed and stained for markers of processes important for cellularisation, first of all Slam protein which shows a clear and distinct localisation defect from the beginning of cellularisation in *dop* mutants.

In connection to further phospho-mimic S401D Dlic rescue analysis in *dop* mutants, the rescue experiment addressing the capabilities of the phospho-mutant versions of Dlic to substitute for endogenous Dlic function has to be repeated using a different driver and using the DlicGFP construct from Tadashi Uemura's lab as positive control. This experiment should verify that the synthesised versions of Dlic fused to GFP are able to take over endogenous Dlic function during cellularisation in a background where this Dlic function might be impaired, as proposed for *dop* mutants.

5. References

Acharya, S. et al., 2014. Function and dynamics of slam in furrow formation in early Drosophila embryo. *Developmental biology*, 386(2), pp.371–84.

Addinall, S.G. et al., 2001. Phosphorylation by cdc2-CyclinB1 kinase releases cytoplasmic dynein from membranes. *The Journal of biological chemistry*, 276(19), pp.15939–44.

Adey, N.B. et al., 2000. Threonine Phosphorylation of the MMAC1 / PTEN PDZ Binding Domain Both Inhibits and Stimulates PDZ Binding Advances in Brief Inhibits and Stimulates PDZ Binding. *Cancer Research*, 60(1), pp.35–37.

Afshar, K., Stuart, B. & Wasserman, S.A., 2000. Functional analysis of the Drosophila Diaphanous FH protein in early embryonic development. *Development*, 127(9), pp.1887–1897.

Albertson, R. et al., 2008. Vesicles and actin are targeted to the cleavage furrow via furrow microtubules and the central spindle. *The Journal of cell biology*, 181(5), pp.777–90.

Albertson, R., Riggs, B. & Sullivan, W., 2005. Membrane traffic: a driving force in cytokinesis. *Trends in cell biology*, 15(2), pp.92–101.

Arencibia, J.M. et al., 2013. AGC protein kinases: from structural mechanism of regulation to allosteric drug development for the treatment of human diseases. *Biochimica et biophysica acta*, 1834(7), pp.1302–21.

Baum, B., Li, W. & Perrimon, N., 2000. A cyclase-associated protein regulates actin and cell polarity during Drosophila oogenesis and in yeast. *Current Biology*, 10(16), pp.964–973.

Bednarek, S.Y. & Falbel, T.G., 2002. Membrane trafficking during plant cytokinesis. *Traffic (Copenhagen, Denmark)*, 3(9), pp.621–629.

Benmerah, A. et al., 1998. Ap-2/Eps15 interaction is required for receptor-mediated endocytosis. *Journal of Cell Biology*, 140(5), pp.1055–1062.

Benmerah, A. et al., 1999. Inhibition of clathrin-coated pit assembly by an Eps15 mutant. *Journal of cell science*, 112(9), pp.1303–1311.

Beronja, S. & Tepass, U., 2002. Cellular Morphogenesis : slow-as-molasses Accelerates Polarized Membrane Growth. *Developmental Cell*, 2(4), pp.382–384.

Berrueta, L. et al., 1998. The adenomatous polyposis coli-binding protein EB1 is associated with cytoplasmic and spindle microtubules. *Proceedings of the National Academy of Sciences of the United States of America*, 95(18), pp.10596–10601.

Bettencourt-Dias, M. et al., 2004. Genome-wide survey of protein kinases required for cell cycle progression. *Nature*, 432(7020), pp.980–7.

Bischof, J. et al., 2007. An optimized transgenesis system for Drosophila using germ-line-specific phiC31 integrases. *Proceedings of the National Academy of Sciences of the United States of America*, 104(9), pp.3312–7.

Blair, S.S., 2003. Genetic mosaic techniques for studying Drosophila development. *Development (Cambridge, England)*, 130(21), pp.5065–72.

Brand, A.H. & Perrimon, N., 1993. Targeted gene expression as a means of altering cell fates and generating dominant phenotypes. *Development*, 118(2), pp.401–415.

Brandt, A. et al., 2006. Developmental control of nuclear size and shape by Kugelkern and Kurzkern. *Current biology : CB*, 16(6), pp.543–52.

Brill, J.A. et al., 2000. A phospholipid kinase regulates actin organization and intercellular bridge formation during germline cytokinesis. *Development*, 127(17), pp.3855–3864.

Bullock, S.L. et al., 2006. Guidance of Bidirectional Motor Complexes by mRNA Cargoes through Control of Dynein Number and Activity. *Current Biology*, 16(14), pp.1447–1452.

Burgess, R.W., Deitcher, D.L. & Schwarz, T.L., 1997. The synaptic protein syntaxin1 is required for cellularization of Drosophila embryos. *Journal of Cell Biology*, 138(4), pp.861–875.

Burkel, B.M., von Dassow, G. & Bement, W.M., 2007. Versatile fluorescent probes for actin filaments based on the actin-binding domain of utrophin. *Cell motility and the cytoskeleton*, 64(11), pp.822–32.

Burkhardt, J.K. et al., 1997. Overexpression of the dynamitin (p50) subunit of the dynactin complex disrupts dynein-dependent maintenance of membrane organelle distribution. *The Journal of cell biology*, 139(2), pp.469–84.

Callaini, G., Dallai, R. & Riparbelli, M.G., 1990. Behaviour of yolk nuclei during early embryogenesis in Drosophila melanogaster. *Bolletino di zoologia*, 57(3), pp.215–220.

Cameron, P., Mundigl, O. & De Camilli, P., 1993. Traffic of synaptic vesicle proteins in polarized and nonpolarized cells. *Journal of cell science*, 17, pp.93–100.

Cao, J. et al., 2008. Nuf, a Rab11 effector, maintains cytokinetic furrow integrity by promoting local actin polymerization. *The Journal of cell biology*, 182(2), pp.301–13.

Carbone, R. et al., 1997. eps15 and eps15R Are Essential Components of the Endocytic Pathway. *Cancer research*, 57, pp.5498–5504.

Cheffings, T.H., Burroughs, N.J. & Balasubramanian, M.K., 2016. Actomyosin Ring Formation and Tension Generation in Eukaryotic Cytokinesis. *Current Biology*, 26(15), pp.R719–R737.

Chou, T. & Perrimon, N., 1996. The Autosomal FLP-DFS Technique for Generating Germline Mosaics. *Genetics*, 144, pp.1673–1679.

Clark, I.E., Jan, L.Y. & Jan, Y.N., 1997. Reciprocal localization of Nod and kinesin fusion proteins indicates microtubule polarity in the Drosophila oocyte, epithelium, neuron and muscle. *Development (Cambridge, England)*, 124(2), pp.461–70.

Crawford, J.M. et al., 1998. Cellularization in Drosophila melanogaster is disrupted by the inhibition of rho activity and the activation of Cdc42 function. *Developmental biology*, 204(1), pp.151–164.

Crest, J., Concha-Moore, K. & Sullivan, W., 2012. RhoGEF and Positioning of Rappaport-like Furrows in the Early Drosophila Embryo. *Current Biology*, 22(21), pp.2037–2041.

D'Avino, P.P., Savoian, M.S. & Glover, D.M., 2005. Cleavage furrow formation and ingression during animal cytokinesis: a microtubule legacy. *Journal of cell science*, 118(8), pp.1549–58.

van Dam, E.M. & Stoorvogel, W., 2002. Dynamin-dependent Transferrin Receptor Recycling by Endosome-derived Clathrin-coated Vesicles. *Molecular biology of the cell*, 13(6), pp.169–182.

Dasgupta, U. et al., 2009. Ceramide kinase regulates phospholipase C and phosphatidylinositol

4, 5, bisphosphate in phototransduction. *Proceedings of the National Academy of Sciences of the United States of America*, 106(47), pp.20063–20068.

Dell, K.R., Turck, C.W. & Vale, R.D., 2000. Mitotic phosphorylation of the dynein light intermediate chain is mediated by cdc2 kinase. *Traffic (Copenhagen, Denmark)*, 1(1), pp.38–44.

Dix, C.I. et al., 2013. Lissencephaly-1 promotes the recruitment of dynein and dynactin to transported mRNAs. *The Journal of cell biology*, 202(3), pp.479–94.

Doerflinger, H. et al., 2003. The role of PAR-1 in regulating the polarised microtubule cytoskeleton in the Drosophila follicular epithelium. *Development (Cambridge, England)*, 130(17), pp.3965–3975.

Le Droguen, P.-M. et al., 2015. Microtubule-dependent apical restriction of recycling endosomes sustains adherens junctions during morphogenesis of the Drosophila tracheal system. *Development*, 142(2), pp.363–374.

Echeverri, C.J. et al., 1996. Molecular characterization of the 50-kD subunit of dynactin reveals function for the complex in chromosome alignment and spindle organization during mitosis. *Journal of Cell Biology*, 132(4), pp.617–633.

Edgar, B.A., O'Dell, G.M. & Schubiger, G., 1987. Cytoarchitecture and the patterning of fushi-tarazu expression in the Drosophila blastoderm. *Genes and Development*, 1, pp.1226–1237.

Eitzen, G., 2003. Actin remodeling to facilitate membrane fusion. *Biochimica et Biophysica Acta*, 1641(2-3), pp.175–181.

Fabrowski, P. et al., 2013. Tubular endocytosis drives remodelling of the apical surface during epithelial morphogenesis in Drosophila. *Nature communications*, 4(2244).

Field, C.M. et al., 2005. Characterization of anillin mutants reveals essential roles in septin localization and plasma membrane integrity. *Development (Cambridge, England)*, 132(12), pp.2849–2860.

Figard, L. et al., 2016. Membrane Supply and Demand Regulates F-Actin in a Cell Surface Reservoir. *Developmental Cell*, 37(3), pp.267–278.

Figard, L. et al., 2013. The Plasma Membrane Flattens Out to Fuel Cell-Surface Growth during Drosophila Cellularization. *Developmental cell*, 27(6), pp.1–8.

Figard, L. & Sokac, A.M., 2014. A membrane reservoir at the cell surface: unfolding the plasma membrane to fuel cell shape change. *Bioarchitecture*, 4(2), pp.39–46.

Firestone, A.J. et al., 2012. Small-molecule inhibitors of the AAA+ ATPase motor cytoplasmic dynein. *Nature*, 484(7392), pp.125–9.

Foe, V.E. & Alberts, B.M., 1983. Studies of nuclear and cytoplasmic behaviour during the five mitotic cycles that precede gastrulation in Drosophila embryogenesis. *Journal of cell science*, 61, pp.31–70.

Foe, V.E., Field, C.M. & Odell, G.M., 2000. Microtubules and mitotic cycle phase modulate spatiotemporal distributions of F-actin and myosin II in Drosophila syncytial blastoderm embryos. *Development (Cambridge, England)*, 127(9), pp.1767–87.

Frescas, D. et al., 2006. The secretory membrane system in the Drosophila syncytial blastoderm

embryo exists as functionally compartmentalized units around individual nuclei. *Journal of Cell Biology*, 173(2), pp.219–230.

Fullilove, S.L. & Jacobson, A.G., 1971. Nuclear elongation and cytokinesis in Drosophila montana. *Developmental Biology*, 26(4), pp.560–577.

Galewsky, S. & Schulz, R.A., 1992. Drop out: a third chromosome maternal-effect locus required for formation of the Drosophila cellular blastoderm. *Molecular reproduction and development*, 32(4), pp.331–8.

Garland, P. et al., 2008. Expression of the MAST family of serine/threonine kinases. *Brain research*, 1195, pp.12–9.

Gepner, J. et al., 1996. Cytoplasmic Dynein Function Is Essential in Drosophila melanogaster. *Genetics*, 142(3), pp.865–878.

Giansanti, M.G. et al., 2001. Drosophila male meiosis as a model system for the study of cytokinesis in animal cells. *Cell structure and function*, 26(6), pp.609–17.

Glotzer, M., 2004. Cleavage furrow positioning. *Journal of Cell Biology*, 164(3), pp.347–351.

Glotzer, M., 1997. Cytokinesis. *Current Biology*, 7(5), pp.274–276.

Golic, K.G. & Lindquist, S., 1989. The FLP recombinase of yeast catalyzes site-specific recombination in the Drosophila genome. *Cell*, 59(3), pp.499–509.

Golic, M.M. et al., 1997. FLP-mediated DNA mobilization to specific target sites in Drosophila chromosomes. *Nucleic acids research*, 25(18), pp.3665–71.

Gross, S.P. et al., 2000. Dynein-mediated cargo transport in vivo: A switch controls travel distance. *Journal of Cell Biology*, 148(5), pp.945–955.

Grosshans, J. et al., 2005. RhoGEF2 and the formin Dia control the formation of the furrow canal by directed actin assembly during Drosophila cellularisation. *Development (Cambridge, England)*, 132(5), pp.1009–20.

Hain, D., 2010. *Genetic and molecular analysis of drop out, the single homolog of the vertebrate MAST kinases in Drosophila melanogaster*. University of Dundee.

Hain, D. et al., 2010. Natural variation of the amino-terminal glutamine-rich domain in Drosophila argonaute2 is not associated with developmental defects. *PloS one*, 5(12), pp.1–14.

Hain, D. et al., 2014. The Drosophila MAST kinase Drop out is required to initiate membrane compartmentalisation during cellularisation and regulates dynein-based transport. *Development*, 141(10), pp.2119–2130.

Hampoelz, B. et al., 2011. Microtubule-induced nuclear envelope fluctuations control chromatin dynamics in Drosophila embryos. *Development*, 138(16), pp.3377–3386.

Hanks, S.K. & Hunter, T., 1995. The eukaryotic protein kinase superfamily : kinase (catalytic) domain structure and classification. *The FASEB Journal*, 9, pp.576–596.

Hanks, S.K., Quinn, A.M. & Hunter, T., 1988. The protein kinase family: conserved features and deduced phylogeny of the catalytic domains. *Science Translational Medicine*, 241(4861), pp.42–52.

Harris, T.J.C. & Peifer, M., 2004. Adherens junction-dependent and -independent steps in the

establishment of epithelial cell polarity in Drosophila. *The Journal of cell biology*, 167(1), pp.135–47.

Harris, T.J.C. & Peifer, M., 2005. The positioning and segregation of apical cues during epithelial polarity establishment in Drosophila. *The Journal of cell biology*, 170(5), pp.813–23.

Harrison, D.A. & Perrimon, N., 1993. Simple and efficient generation of marked clones in Drosophila. *Current Biology*, 3(7), pp.424–433.

Hayashi, S. et al., 1997. A Drosophila homolog of the tumor suppressor gene adenomatous polyposis coli down-regulates -catenin but its zygotic expression is not essential for the regulation of Armadillo. *Proceedings of the National Academy of Sciences of the United States of America*, 94(1), pp.242–247.

Hays, T.S. et al., 1994. A cytoplasmic dynein motor in Drosophila: identification and localization during embryogenesis. *Journal of cell science*, 107(6), pp.1557–69.

He, B., Martin, A. & Wieschaus, E., 2016. Flow-dependent myosin recruitment during Drosophila cellularization requires zygotic dunk activity. *Development*, 143(13), pp.2417–2430.

Heck, M.M.S. et al., 1993. The Kinesin-like Protein KLP6IF Is Essential for Mitosis in Drosophila Margarete. *Journal of Cell Biology*, 123(3), pp.665–679.

Hickson, G.R.X. et al., 2003. Arfophilins Are Dual Arf/Rab 11 Binding Proteins That Regulate Recycling Endosome Distribution and Are Related to Drosophila Nuclear Fallout. *Molecular biology of the cell*, 14(July), pp.2908–2920.

Höök, P. & Vallee, R.B., 2006. The dynein family at a glance. *Journal of cell science*, 119(21), pp.4369–71.

Horne-Badovinac, S. & Bilder, D., 2005. Mass transit: Epithelial morphogenesis in the Drosophila egg chamber. *Developmental Dynamics*, 232(3), pp.559–574.

Hortsch, M. et al., 1990. Drosophila neurotactin , a surface glycoprotein with homology to serine esterases, is dynamically expressed during embryogenesis. *Development*, 110(4), pp.1327–1340.

Hunter, C. & Wieschaus, E., 2000. Regulated expression of nullo is required for the formation of distinct apical and basal adherens junctions in the Drosophila blastoderm. *Journal of Cell Biology*, 150(2), pp.391–401.

Hyman, J.M. et al., 2009. Small-molecule inhibitors reveal multiple strategies for Hedgehog pathway blockade. *Proceedings of the National Academy of Sciences of the United States of America*, 106(33), pp.14132–7.

Ikeda, K. et al., 2011. CK1 activates minus-end-directed transport of membrane organelles along microtubules. *Molecular biology of the cell*, 22(8), pp.1321–9.

Jain, N. & Ganesh, S., 2016. Emerging nexus between RAB GTPases, autophagy and neurodegeneration. *Autophagy*, 12(5), pp.900–904.

Januschke, J. et al., 2002. Polar transport in the Drosophila oocyte requires Dynein and Kinesin I cooperation. *Current biology*, 12(23), pp.1971–81.

Johnson, L.N. et al., 1998. The structural basis for substrate recognition and control by protein kinases. *FEBS Letters*, 430(1-2), pp.1–11.

Kardon, J.R. & Vale, R.D., 2009. Regulators of the cytoplasmic dynein motor. *Nature reviews.*

Molecular cell biology, 10(12), pp.854–865.

Karess, R.E. et al., 1991. The Regulatory Light Chain of Nonmuscle Myosin Is Encoded by spaghetti-squash, a Gene Required for Cytokinesis in Drosophila. *Cell*, 65, pp.1177–1189.

Karki, S. & Holzbaur, E.L.F., 1999. Cytoplasmic dynein and dynactin in cell division and intracellular transport. *Current Opinion in Cell Biology*, 11, pp.45–53.

Koh, T.-W. et al., 2007. Eps15 and Dap160 control synaptic vesicle membrane retrieval and synapse development. *The Journal of cell biology*, 178(2), pp.309–22.

Labbé, C. et al., 2012. Genome-wide Expression Profiling Implicates a MAST3-Regulated Gene Set in Colonic Mucosal Inflammation of Ulcerative Colitis Patients. *Inflamm Bowel Dis.*, 18(6), pp.1072–1080.

Labbé, C. et al., 2008. MAST3: a novel IBD risk factor that modulates TLR4 signaling. *Genes and immunity*, 9(7), pp.602–12.

LaMonte, B.H. et al., 2002. Disruption of dynein/dynactin inhibits axonal transport in motor neurons causing late-onset progressive degeneration. *Neuron*, 34(5), pp.715–27.

Langlands, A., 2012. *Identifying targets of the MAST kinase Drop out through genetic and proteomic analysis in Drosophila melanogaster*. University of Dundee.

Langley, A.R. et al., 2014. New insights into the maternal to zygotic transition. *Development*, 141(20), pp.3834–3841.

Lecuit, T., 2004. Junctions and vesicular trafficking during Drosophila cellularization. *Journal of cell science*, 117(16), pp.3427–33.

Lecuit, T., Samanta, R. & Wieschaus, E., 2002. slam encodes a developmental regulator of polarized membrane growth during cleavage of the Drosophila embryo. *Developmental cell*, 2(4), pp.425–36.

Lecuit, T. & Wieschaus, E., 2000. Polarized Insertion of New Membrane from a Cytoplasmic Reservoir during Cleavage of the Drosophila Embryo. *The Journal of cell biology*, 150(4), pp.849–860.

Lee, D.M. & Harris, T.J.C., 2013. An Arf-GEF regulates antagonism between endocytosis and the cytoskeleton for Drosophila blastoderm development. *Current Biology*, 23(21), pp.2110–20.

Lee, D.M. & Harris, T.J.C., 2014. Coordinating the cytoskeleton and endocytosis for regulated plasma membrane growth in the early Drosophila embryo. *Bioarchitecture*, 4(2), pp.68–74.

Liu, J. et al., 2014. Stepping stone: a cytohesin adaptor for membrane cytoskeleton restraint in the syncytial Drosophila embryo. *Molecular Biology of the Cell*, 26(4), pp.711–725.

Lo, P., Hawrot, H. & Georgiou, M., 2012. Apicobasal polarity and its role in cancer progression. *BioMolecular Concepts*, 3(6), pp.505–521.

Logan, M.R. & Mandato, C.A., 2006. Regulation of the actin cytoskeleton by PIP2 in cytokinesis. *Biology of the cell / under the auspices of the European Cell Biology Organization*, 98(6), pp.377–388.

Loh, S.H.Y. et al., 2008. Identification of new kinase clusters required for neurite outgrowth and retraction by a loss-of-function RNA interference screen. *Cell death and differentiation*, 15(2), pp.283–98.

Łuksza, M. et al., 2013. Rebuilding MTOCs upon centriole loss during mouse oogenesis. *Developmental Biology*, 382(1), pp.48–56.

Lumeng, C. et al., 1999. Interactions between beta 2-syntrophin and a family of microtubule-associated serine/threonine kinases. *Nature neuroscience*, 2(7), pp.611–7.

Mahoney, P.A. et al., 1991. The fat tumor suppressor gene in Drosophila encodes a novel member of the cadherin gene superfamily. *Cell*, 67(5), pp.853–868.

Majumdar, A., Ramagiri, S. & Rikhy, R., 2006. Drosophila homologue of Eps15 is essential for synaptic vesicle recycling. *Experimental Cell Research*, 312, pp.2288–2298.

Manning, G. et al., 2002. The Protein Kinase Complement of the Human Genome. *Science Translational Medicine*, 298(5600), pp.1912–1934.

De Matteis, M.A. & Luini, A., 2008. Exiting the Golgi complex. *Nature reviews. Molecular cell biology*, 9(4), pp.273–284.

Mavor, L.M. et al., 2016. Rab8 directs furrow ingression and membrane addition during epithelial formation in Drosophila melanogaster. *Development*, 143(5), pp.892–903.

Mavrakis, M. et al., 2014. Septins promote F-actin ring formation by crosslinking actin filaments into curved bundles. *Nature cell biology*, 16, pp.322–334.

Mavrakis, M., Rikhy, R. & Lippincott-Schwartz, J., 2009a. Cells within a cell: Insights into cellular architecture and polarization from the organization of the early fly embryo. *Communicative & Integrative Biology*, 2(4), pp.313–314.

Mavrakis, M., Rikhy, R. & Lippincott-Schwartz, J., 2009b. Plasma Membrane Polarity and Compartmentalization are Established Before Cellularization in the Fly Embryo. *Dev Cell*, 16(1), pp.93–104.

Mazumdar, A. & Mazumdar, M., 2002. How one becomes many: blastoderm cellularization in Drosophila melanogaster. *Bioessays*, 24, pp.1012–1022.

McGill, M.A., Mckinley, R.F.A. & Harris, T.J.C., 2009. Independent cadherin–catenin and Bazooka clusters interact to assemble adherens junctions. *Journal of Cell Biology*, 185(5), pp.787–796.

McGrail, M. & Hays, T.S., 1997. The microtubule motor cytoplasmic dynein is required for spindle orientation during germline cell divisions and oocyte differentiation in Drosophila. *Development*, 124(12), pp.2409–19.

McNiven, M.A., 1998. Dynamin: A molecular motor with pinchase action. *Cell*, 94(2), pp.151–154.

Mellman, I. & Nelson, W.J., 2008. Coordinated protein sorting, targeting and distribution in polarized cells. *Nat Rev Mol Cell Biol*, 9(11), pp.833–845.

Meyer, W.J. et al., 2006. Overlapping functions of Argonaute proteins in patterning and morphogenesis of Drosophila embryos. *PLoS genetics*, 2(8), pp.1224–39.

Mische, S. et al., 2008. Dynein Light Intermediate Chain : An Essential Subunit That Contributes to Spindle Checkpoint Inactivation. *Molecular biology of the cell*, 19, pp.4918–4929.

Moores, C.A., Keep, N.H. & Kendrick-Jones, J., 2000. Structure of the utrophin actin-binding domain bound to F-actin reveals binding by an induced fit mechanism. *Journal of molecular biology*, 297(2), pp.465–80.

Morrison, D.K., Murakami, M.S. & Cleghon, V., 2000. Protein kinases and phosphatases in the drosophila genome [In Process Citation]. *J Cell Biol*, 150(2), pp.F57–62.

Müller, H.-A.J., 2003. Epithelial Polarity in Flies: More Than Just Crumbs. *Developmental cell*, 4, pp.1–3.

Müller, H.-A.J., 2000. Genetic Control of Epithelial Cell Polarity: Lessons From Drosophila. *Developmental Dynamics*, 218, pp.52–67.

Müller, H.-A.J., 2001. Of mice, frogs and flies: generation of membrane asymmetries in early development. *Development, growth & differentiation*, 43(4), pp.327–42.

Müller, H.-A.J. & Wieschaus, E., 1996. armadillo, bazooka, and stardust are critical for early stages in formation of the zonula adherens and maintenance of the polarized blastoderm epithelium in Drosophila. *The Journal of cell biology*, 134(1), pp.149–63.

Murthy, M. et al., 2010. Sec5, a member of the exocyst complex, mediates Drosophila embryo cellularization. *Development*, 137(16), pp.2773–2783.

Ni, J.-Q. et al., 2011. A genome-scale shRNA resource for transgenic RNAi in Drosophila. *Nature methods*, 8(5), pp.405–7.

Okazaki, N. et al., 2002. Protocadherin LKC, a new candidate for a tumor suppressor of colon and liver cancers, its association with contact inhibition of cell proliferation. *Carcinogenesis*, 23(7), pp.1139–1148.

Padash Barmchi, M., Rogers, S. & Häcker, U., 2005. DRhoGEF2 regulates actin organization and contractility in the Drosophila blastoderm embryo. *jcb*, 168(4), pp.575–585.

Papoulas, O., Hays, T.S. & Sisson, J.C., 2005. The golgin Lava lamp mediates dynein-based Golgi movements during Drosophila cellularization. *Nature cell biology*, 7(6), pp.612–8.

Pascucci, T. et al., 1996. Eggshell Assembly in Drosophila: Processing and Localization of Vitelline Membrane and Chorion Proteins. *Developmental Biology*, 177(2), pp.590–598.

Pearce, L.R., Komander, D. & Alessi, D.R., 2010. The nuts and bolts of AGC protein kinases. *Nature reviews. Molecular cell biology*, 11(1), pp.9–22.

Pelissier, A., Chauvin, J.-P. & Lecuit, T., 2003. Trafficking through Rab11 Endosomes Is Required for Cellularization during Drosophila Embryogenesis. *Current Biology*, 13(21), pp.1848–1857.

Peter, A. et al., 2002. Mapping and identification of essential gene functions on the X chromosome of Drosophila. *EMBO Rep*, 3(1), pp.34–38.

Postner, M.A., Miller, K.G. & Wieschaus, E.F., 1992. Maternal Effect Mutations of the sponge Locus Affect Actin Cytoskeletal Rearrangements in Drosophila melanogaster Embryos. *The Journal of cell biology*, 119(5), pp.1205–1218.

Préhaud, C. et al., 2010. Attenuation of rabies virulence: takeover by the cytoplasmic domain of its envelope protein. *Science signaling*, 3(105), pp.1–10.

Raff, J.W. & Glover, D.M., 1989. Centrosomes, and not nuclei, initiate pole cell formation in Drosophila embryos. *Cell*, 57(4), pp.611–9.

Rasmusson, K. et al., 1994. A family of dynein genes in Drosophila melanogaster. *Molecular biology of the cell*, 5(1), pp.45–55.

Rauzi, M., Lenne, P.-F. & Lecuit, T., 2010. Planar polarized actomyosin contractile flows control epithelial junction remodelling. *Nature*, 468(7327), pp.1110–4.

Ren, A. et al., 2013. MAST205 competes with cystic fibrosis transmembrane conductance regulator (CFTR)-associated ligand for binding to CFTR to regulate CFTR-mediated fluid transport. *The Journal of biological chemistry*, 288(17), pp.12325–34.

Reversi, A. et al., 2014. Plasma membrane phosphoinositide balance regulates cell shape during Drosophila embryo morphogenesis. *The Journal of cell biology*, 205(3), pp.395–408.

Riggs, B. et al., 2003. Actin cytoskeleton remodeling during early Drosophila furrow formation requires recycling endosomal components Nuclear-fallout and Rab11. *The Journal of cell biology*, 163(1), pp.143–154.

Riggs, B. et al., 2007. The Concentration of Nuf, a Rab11 Effector, at the Microtubule-organizing Center Is Cell Cycle–regulated, Dynein-dependent, and Coincides with Furrow Formation. *Molecular biology of the cell*, 18, pp.3313–3322.

Ripoche, J. et al., 1994. Location of Golgi membranes with reference to dividing nuclei in syncytial Drosophila embryos. *Proceedings of the National Academy of Sciences of the United States of America*, 91, pp.1878–1882.

Robinson, D.R. et al., 2011. Functionally recurrent rearrangements of the MAST kinase and Notch gene families in breast cancer. *Nature medicine*, 17(12), pp.1646–51.

Robinson, J.T. et al., 1999. Cytoplasmic Dynein Is Required for the Nuclear Attachment and Migration of Centrosomes during Mitosis in Drosophila. *jcb*, 146(3), pp.597–608.

Rolls, M.M. et al., 2007. Polarity and intracellular compartmentalization of Drosophila neurons. *Neural development*, 2(7).

Rothwell, W.F. et al., 1998. Nuclear-fallout, a Drosophila protein that cycles from the cytoplasm to the centrosomes, regulates cortical microfilament organization. *Development*, 125, pp.1295–1303.

Rothwell, W.F. et al., 1999. The Drosophila centrosomal protein Nuf is required for recruiting Dah, a membrane associated protein, to furrows in the early embryo. *Journal of cell science*, 112, pp.2885–2893.

Roxrud, I. et al., 2008. An endosomally localized isoform of Eps15 interacts with Hrs to mediate degradation of epidermal growth factor receptor. *Journal of Cell Biology*, 180(6), pp.1205–1218.

Royou, A. et al., 2004. Reassessing the Role and Dynamics of Nonmuscle Myosin II during Furrow Formation in Early Drosophila Embryos. *Molecular biology of the cell*, 15, pp.838–850.

Runnegar, M.T., Wei, X. & Hamm-alvarez, S.F., 1999. Increased protein phosphorylation of cytoplasmic dynein results in impaired motor function. *Biochemical Journal*, 342, pp.1–6.

Salcini, A.E. et al., 1999. Epidermal growth factor receptor pathway substrate 15, Eps15. *International Journal of Biochemistry and Cell Biology*, 31(3), pp.805–809.

Satoh, D. et al., 2008. Spatial control of branching within dendritic arbors by dynein-dependent transport of Rab5-endosomes. *Nature cell biology*, 10(10), pp.1164–1171.

Savio, M.G. et al., 2016. USP9X Controls EGFR Fate by Deubiquitinating the Endocytic Adaptor Eps15. *Current Biology*, 26, pp.1–11.

Schejter, E.D. & Wieschaus, E., 1993a. bottleneck acts as a regulator of the microfilament network governing cellularization of the Drosophila embryo. *Cell*, 75(2), pp.373–85.

Schejter, E.D. & Wieschaus, E., 1993b. FUNCTIONAL ELEMENTS OF THE CYTOSKELETON IN THE EARLY DROSOPHILA EMBRYO. *Annu. Rev. Cell Biol.*, 9, pp.67–99.

Schreij, A.M.A., Fon, E.A. & McPherson, P.S., 2016. Endocytic membrane trafficking and neurodegenerative disease. *Cellular and Molecular Life Sciences*, 73(8), pp.1529–1545.

Schroer, T.A., 2004. Dynactin. *Annual Review of Cell and Developmental Biology*, 20(1), pp.759–779.

Seaman, M.N.J., Burd, C.G. & Emr, S.D., 1996. Receptor signaling and the regulation of endocytic membrane transport. *Current Opinion In Cell Biology*, 8(4), pp.549–556.

Sharp, D.J. et al., 2000. Functional coordination of three mitotic motors in Drosophila embryos. *Molecular biology of the cell*, 11, pp.241–253.

Sharp, D.J. & Rath, U., 2009. Mitosis: KLP61F Goes Wee! *Current Biology*, 19(19), pp.R899–R901.

Sigismund, S. et al., 2005. Clathrin-independent endocytosis of ubiquitinated cargos. *Proceedings of the National Academy of Sciences of the United States of America*, 102(8), pp.2760–2765.

Sisson, J.C. et al., 2000. Lava Lamp, a Novel Peripheral Golgi Protein, Is Required for Drosophila melanogaster Cellularization. *The Journal of cell biology*, 151(4), pp.905–917.

Sokac, A.M. & Wieschaus, E., 2008a. Local Actin-Dependent Endocytosis Is Zygotically Controlled to Initiate Drosophila Cellularization. *Developmental Cell*, 14(5), pp.775–786.

Sokac, A.M. & Wieschaus, E., 2008b. Zygotically controlled F-actin establishes cortical compartments to stabilize furrows during Drosophila cellularization. *Journal of cell science*, 121(11), pp.1815–24.

Sommi, P. et al., 2010. A mitotic kinesin-6, Pav-KLP, mediates interdependent cortical reorganization and spindle dynamics in Drosophila embryos. *Journal of Cell Science*, 123(11), pp.1862–1872.

Sotelo, N.S. et al., 2012. A functional network of the tumor suppressors APC, hDlg, and PTEN, that relies on recognition of specific PDZ-domains. *Journal of Cellular Biochemistry*, 113(8), pp.2661–2670.

Stanley, H., Botas, J. & Malhotra, V., 1997. The mechanism of Golgi segregation during mitosis is cell type-specific. *Proceedings of the National Academy of Sciences of the United States of America*, 94(26), pp.14467–70.

Stein, J.A. et al., 2002. Slow as molasses is required for polarized membrane growth and germ cell migration in Drosophila. *Development*, 129(16), pp.3925–34.

von Stein, W. et al., 2005. Direct association of Bazooka/PAR-3 with the lipid phosphatase PTEN reveals a link between the PAR/aPKC complex and phosphoinositide signaling. *Development (Cambridge, England)*, 132(7), pp.1675–86.

Stenmark, H., 2009. Rab GTPases as coordinators of vesicle traffic. *Nature reviews. Molecular cell biology*, 10(8), pp.513–525.

Su, J. et al., 2013. The BAR domain of amphiphysin is required for cleavage furrow tip–tubule formation during cellularization in Drosophila embryos. *Molecular biology of the cell*, 24,

pp.1444–1453.

Swanson, M.M. & Poodry, C. a, 1981. The shibire mutant of Drosophila: A probe for the study of embryonic development. *Dev. Biol.*, 84, pp.465–470.

Tadros, W., Westwood, J.T. & Lipshitz, H.D., 2007. The Mother-to-Child Transition. *Developmental Cell*, 12(6), pp.847–849.

Takei, K. et al., 1999. Functional partnership between amphiphysin and dynamin in clathrin-mediated endocytosis. *Nature cell biology*, 1(1), pp.33–39.

Terrien, E. et al., 2009. 1H, 13C and 15N resonance assignments of the PDZ of microtubule-associated serine/threonine kinase 205 (MAST205) in complex with the C-terminal motif from the rabies virus glycoprotein. *Biomolecular NMR Assignments*, 3(1), pp.45–48.

Terrien, E. et al., 2012. Interference with the PTEN-MAST2 Interaction by a Viral Protein Leads to Cellular Relocalization of PTEN. *Science signaling*, 5(237), pp.1–12.

Theurkauf, W.E., 1994. Through the bottleneck. *Current Biology*, 4(1), pp.76–78.

Tinsley, J.M. et al., 1994. Increasing complexity of the dystrophin-associated protein complex. *Proceedings of the National Academy of Sciences of the United States of America*, 91(18), pp.8307–13.

Tirnauer, J.S. et al., 1999. Yeast Bim1p promotes the G1-specific dynamics of microtubules. *Journal of Cell Biology*, 145(5), pp.993–1007.

Tram, U., Riggs, B. & Sullivan, W., 2002. Cleavage and Gastrulation in Drosophila Embryos. *Encyclopedia of life science*, 10, pp.1–7.

Ullrich, O. et al., 1996. Rab11 Regulates Recycling through the Pericentriolar Recycling Endosome. *The Journal of cell biology*, 135(4), pp.913–924.

Vaizel-Ohayon, D. & Schejter, E.D., 1999. Mutations in centrosomin reveal requirements for centrosomal function during early Drosophila embryogenesis. *Current Biology*, 9(16), pp.889–898.

Vale, R.D., 2003. The Molecular Motor Toolbox for Intracellular Transport. *Cell*, 112(4), pp.467–480.

Valiente, M. et al., 2005. Binding of PTEN to specific PDZ domains contributes to PTEN protein stability and phosphorylation by microtubule-associated serine/threonine kinases. *The Journal of biological chemistry*, 280(32), pp.28936–43.

Vaughan, P.S., Leszyk, J.D. & Vaughan, K.T., 2001. Cytoplasmic dynein intermediate chain phosphorylation regulates binding to dynactin. *The Journal of biological chemistry*, 276(28), pp.26171–9.

Villarroel-Campos, D., Bronfman, F.C. & Gonzalez-Billault, C., 2016. Rab GTPase signaling in neurite outgrowth and axon specification. *Cytoskeleton (Hoboken, N.J.)*, 00(Stage 5), pp.1–10.

Walden, P.D. & Cowan, N.J., 1993. A Novel 205-Kilodalton Testis-Specific Serine/Threonine Protein Kinase Associated with Microtubules of the Spermatid Manchette. *Mol. Cell. Biol.*, 13(12), pp.7625–7635.

Wang, D. et al., 2006. Coexpression of MAST205 inhibits the activity of Na+/H+ exchanger NHE3. *American journal of physiology. Renal physiology*, 290(2), pp.F428–37.

Wang, X. et al., 2010. Association of Genetic Variation in Mitotic Kinases with Breast Cancer Risk. *Breast cancer research and treatment*, 119(2), pp.453–462.

Warn, R.M. & Robert-Nicoud, M., 1990. F-actin organization during the cellularization of the Drosophila embryo as revealed with a confocal laser scanning microscope. *Journal of cell science*, 96(1), pp.35–42.

Waterhouse, A.M. et al., 2009. Jalview Version 2-A multiple sequence alignment editor and analysis workbench. *Bioinformatics*, 25(9), pp.1189–1191.

Webb, R.L., Zhou, M.-N. & McCartney, B.M., 2009. A novel role for an APC2-Diaphanous complex in regulating actin organization in Drosophila. *Development*, 136(8), pp.1283–1293.

Welte, M.A., 2015. As the fat flies: The dynamic lipid droplets of Drosophila embryos. *Biochimica et Biophysica Acta*, 1851(9), pp.1156–1185.

Wenzl, C. et al., 2010. Localization of RhoGEF2 during Drosophila cellularization is developmentally controlled by Slam. *Mechanisms of development*, 127(7-8), pp.371–84.

Whitney, A.J. et al., 1995. Cytoplasmic coat proteins involved in endosome function. *Cell*, 83(5), pp.703–713.

Whyte, J. et al., 2008. Phosphorylation regulates targeting of cytoplasmic dynein to kinetochores during mitosis. *The Journal of cell biology*, 183(5), pp.819–34.

Wilkie, G.S. & Davis, I., 2001. Drosophila wingless and pair-rule transcripts localize apically by dynein-mediated transport of RNA particles. *Cell*, 105(2), pp.209–219.

Winkler, F. et al., 2015. Fluctuation Analysis of Centrosomes Reveals a Cortical Function of Kinesin-1. *Biophysical Journal*, 109(5), pp.856–868.

Wong, R. et al., 2007. Phospholipase C and myosin light chain kinase inhibition define a common step in actin regulation during cytokinesis. *BMC cell biology*, 8(15).

Wong, R. et al., 2005. PIP2 hydrolysis and calcium release are required for cytokinesis in Drosophila spermatocytes. *Current Biology*, 15(15), pp.1401–1406.

Xi, X. et al., 2014. Expression pattern of class i phosphoinositide 3-kinase and distribution of its product, phosphatidylinositol-3,4,5-trisphosphate, during Drosophila embryogenesis. *Gene Expression Patterns*, 15(2), pp.88–95.

Xiong, H. et al., 2004. Interaction of TRAF6 with MAST205 regulates NF-kappaB activation and MAST205 stability. *The Journal of biological chemistry*, 279(42), pp.43675–83.

Yan, S. et al., 2013. The F-BAR protein Cip4/Toca-1 antagonizes the formin Diaphanous in membrane stabilization and compartmentalization. *Journal of cell science*, 126(8), pp.1796–805.

Yang, Z., Vadlamudi, R.K. & Kumar, R., 2005. Dynein light chain 1 phosphorylation controls macropinocytosis. *The Journal of biological chemistry*, 280(1), pp.654–9.

Yano, R. et al., 2003. SAST124, a novel splice variant of syntrophin-associated serine/threonine kinase (SAST), is specifically localized in the restricted brain regions. *Neuroscience*, 117(2), pp.373–381.

Ye, F. et al., 2013. Single molecule imaging reveals a major role for diffusion in the exploration of ciliary space by signaling receptors. *eLife*, 2, pp.1–16.

Yoon, Y. et al., 1998. A novel dynamin-like protein associates with cytoplasmic vesicles and tubules of the endoplasmic reticulum in mammalian cells. *Journal of Cell Biology*, 140(4), pp.779–793.

Yu, Z.W. & Quinn, P.J., 1994. Dimethyl sulphoxide: a review of its applications in cell biology. *Bioscience reports*, 14(6), pp.259–281.

Zallen, J.A. et al., 2002. SCAR is a primary regulator of Arp2/3-dependent morphological events in Drosophila. *Journal of Cell Biology*, 156(4), pp.689–701.

Zhang, C.X. et al., 2000. Discontinuous actin hexagon, a protein essential for cortical furrow formation in Drosophila, is membrane associated and hyperphosphorylated. *Molecular biology of the cell*, 11, pp.1011–1022.

Zhang, C.X. et al., 1996. Isolation and characterization of a Drosophila gene essential for early embryonic development and formation of cortical cleavage furrows. *The Journal of Cell Biology*, 134(4), pp.923–34.

Zhou, H. et al., 2004. Microtubule-Associated Serine/Threonine Kinase-205 kDa and Fc γ Receptor Control IL-12 p40 Synthesis and NF- B Activation. *The Journal of Immunology*, 172(4), pp.2559–2568.

Zuellig, R.A. et al., 2011. Tissue Expression and Actin Binding of a Novel N-Terminal Utrophin Isoform. *Journal of Biomedicine and Biotechnology*, pp.1–18.

6. Appendix

Dynamitin maternal overexpression egg phenotypes

To test if the fly stock carrying a UAS::(human)Dynamitin (Dmn) effector is clean, eggs deriving from females carrying this effector and a maternal α-tubulin Gal4 driver were analysed for dorsal appendage abnormalities (Fig.S1).

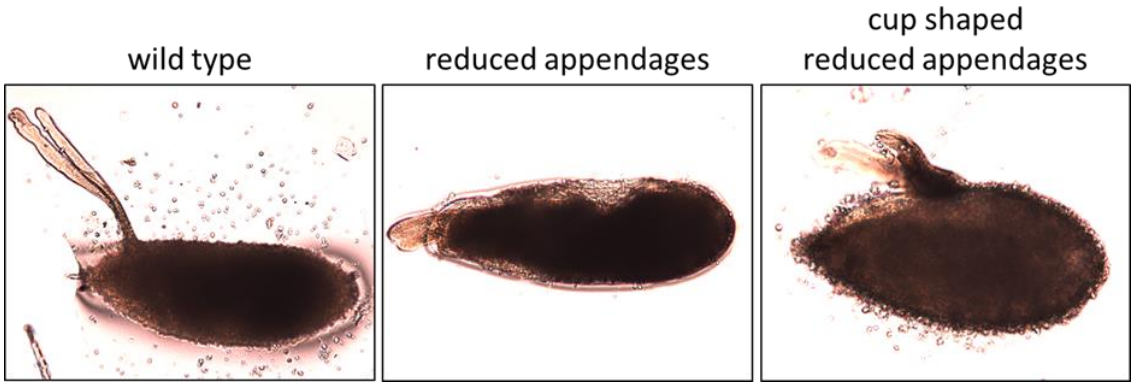

Figure S1 Eggs with a maternal overexpression of Dynamitin show a range of polarity and dorsal appendages defects. Eggs were collected from female flies carrying an α-tubulin Gal4 driver and a UAS::Dmn effector.

Eggs expressing Dynamitin maternally (Fig.S1) show a range of polarity and appendages defects that resemble the phenotypes reported in Januschke et al. (Januschke et al. 2002). In this publication, UAS::Dmn was driven also under the control of a maternal α-tubulin Gal4 driver. These data show that the fly stock is still intact and able to overexpress Dmn in the presence of Gal4.

Injection of Ciliobrevin D with Dextran-FITC

A molecule that can be used to visualise injections is FITC (Fluorescein isothiocyanate) coupled to Dextran. To test if this molecule is suitable to verify Ciliobrevin D injections, co-injections of Ciliobrevin D and Dextran-FITC in a 1:1 concentration were performed (Fig.S2).

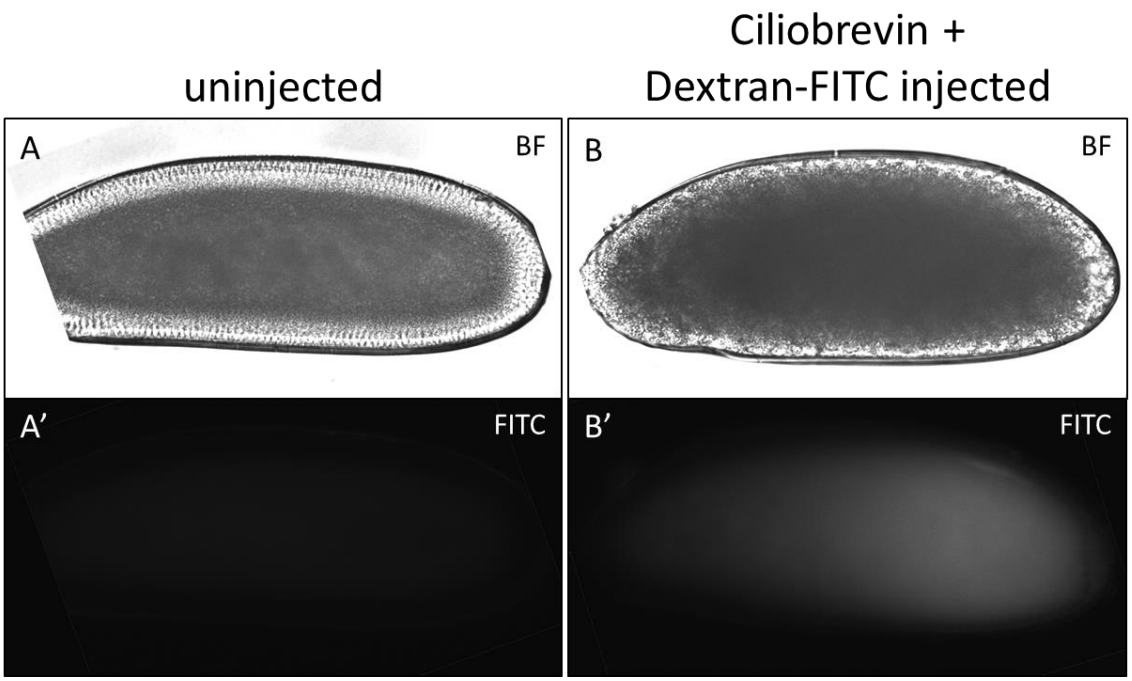

Figure S2 Injection of embryos can be verified by Fluorescein isothiocyanate molecules coupled to dextran. Embryos uninjected (A) or injected with Ciliobrevin D and Dextran-FITC (B) imaged with bright field (A, B) and GFP fluorescence filter channel imaging Dextran-FITC (A', B').

Imaging of uninjected and Dextran-FITC injected embryos with a GFP filter displayed a clear intensity difference between uninjected and injected embryos (Fig.S2 A', B'). Injected embryos show a gradient of fluorescence being strongest at the site of injection (posterior pole; right) (Fig.S2 B'). In contrast, uninjected embryos do not show fluorescence using the GFP filter (Fig.S2 A'). These data show that Dextran-FITC molecules are suitable to verify injections into early embryos in this system.

DlicGFP intensities

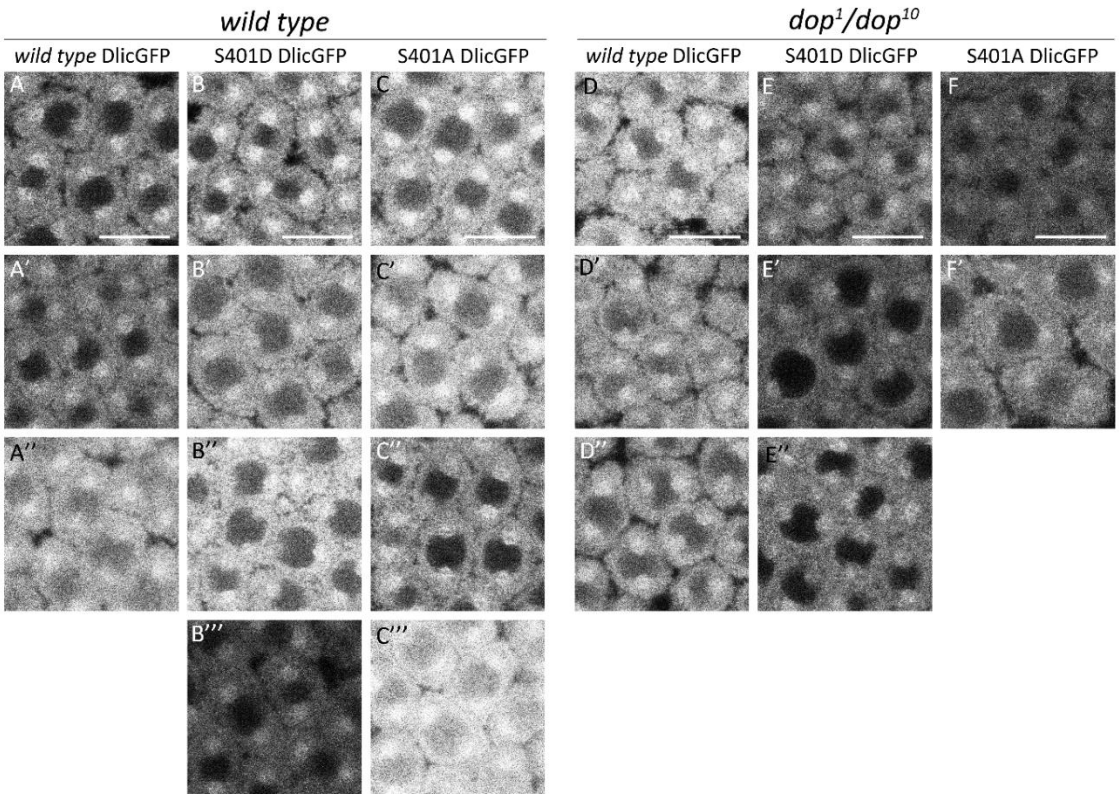

Figure S3 DlicGFP intensities vary strongly between embryos of the same genetic background expressing one and the same DlicGFP construct. Shown are examples of embryos expressing either phospho-mutant versions of Dlic S401 in either *dop*^{1}*/dop*^{10} mutant (D-F) or *wild type* (A-C) background during S-phase of syncytial cycle 13. Note the high intensity level differences between embryos expressing the same construct.

DlicGFP punctate accumulations

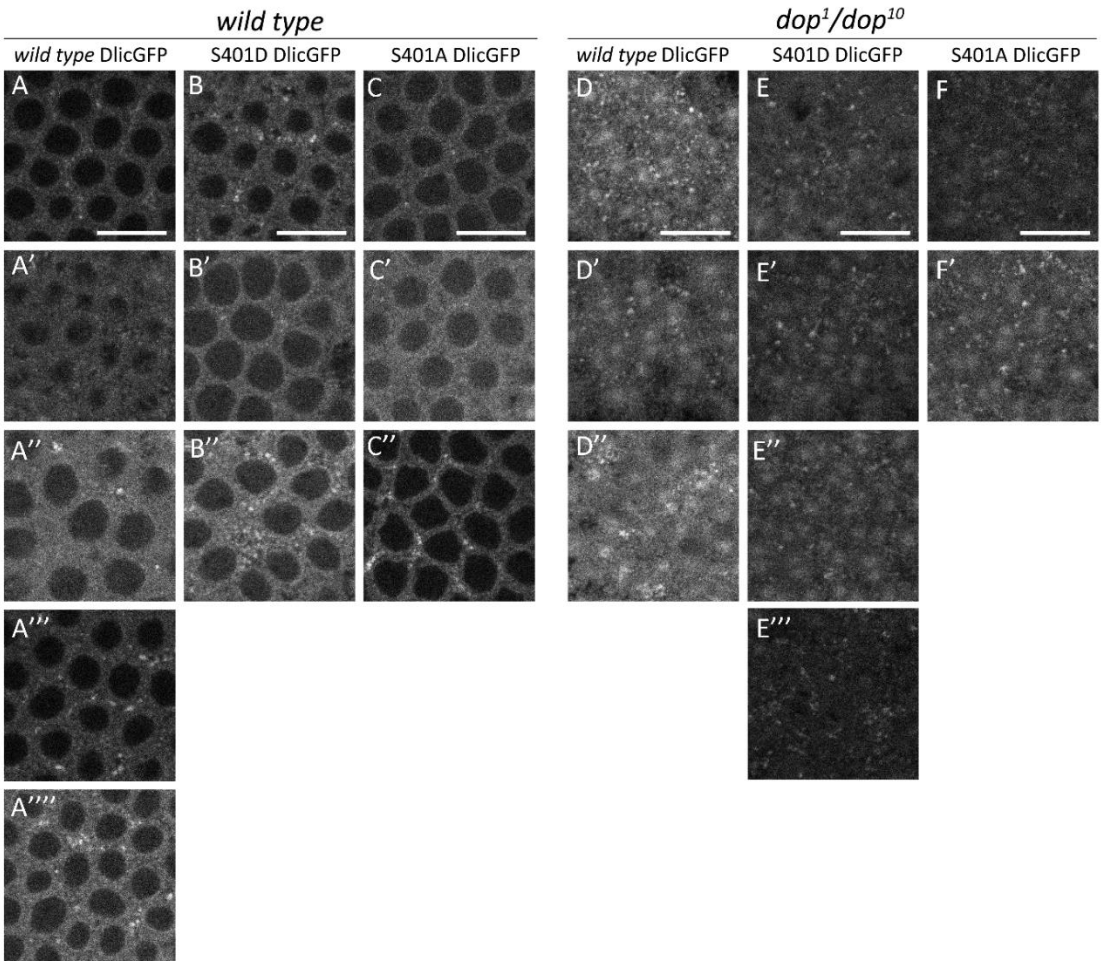

Figure S4 High variations can be seen in the number and intensity of punctate accumulations in embryos of the same genetic background expressing one and the same DlicGFP construct. Shown are examples of embryos expressing either phospho-mutant versions of Dlic S401 in either *dop*^{1}*/dop*^{10} mutant (D-F) or *wild type* (A-C) background during cellularisation. The presented z-levels have been chosen which show most and strongest signal accumulations of DlicGFP in each embryo. Note the high variation of numbers and intensities of the punctate structures between embryos expressing the same DlicGFP construct.

High variations in number and intensity levels of punctate accumulations in embryos expressing the same DlicGFP construct (Fig.S4) might be due to the small size of the accumulations and the comparatively low z-resolution (0.5 µm) due to the imaging settings. It is possible that not in every case the z-level with the most and brightest accumulations has been imaged.

DlicGFP nuclear drop-out phenotypes

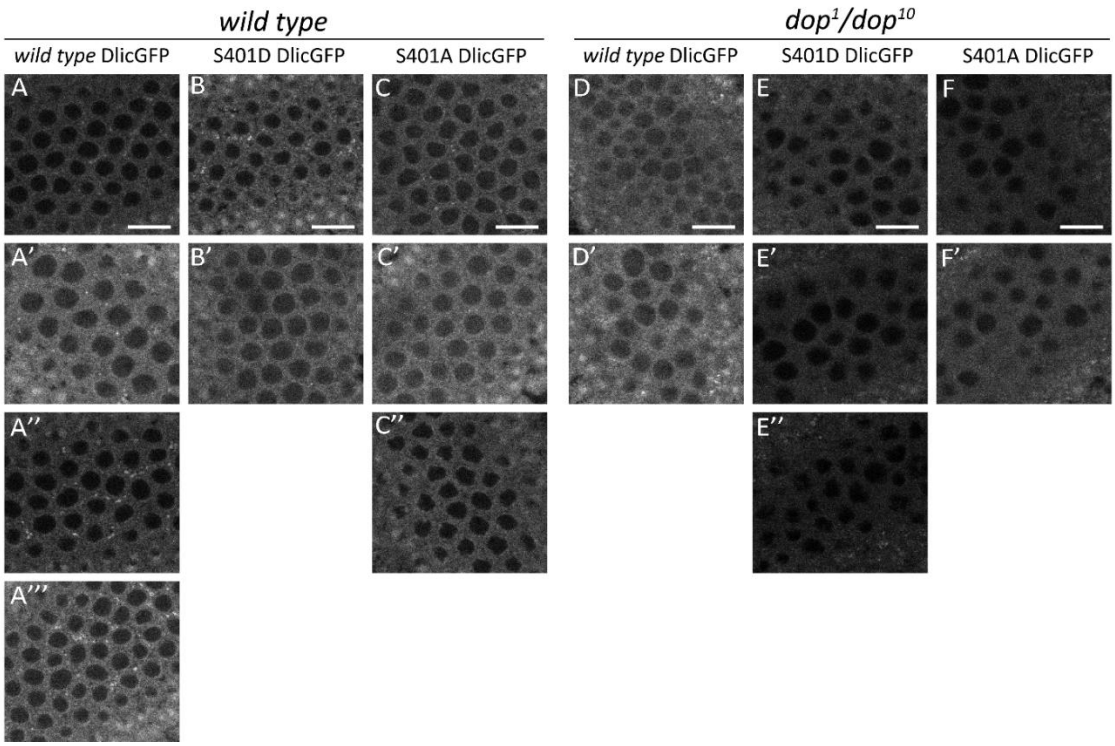

Figure S5 Nuclear drop-out can be seen in embryos with genetic *dop* mutant background expressing either of the DlicGFP constructs. Shown are examples of embryos expressing either phospho-mutant versions of Dlic S401 in either *dop*^{1}/*dop*^{10} mutant (D-F) or *wild type* (A-C) background during cellularisation. The presented z-levels have been chosen which show the nuclear drop-out phenotype.